

VOLUME 80

OCTOBER 21, 1976

/ NUMBER 22

JPCA<sub>x</sub>

---

THE JOURNAL OF  
PHYSICAL  
CHEMISTRY

---



PUBLISHED BIWEEKLY BY THE AMERICAN CHEMICAL SOCIETY

# THE JOURNAL OF PHYSICAL CHEMISTRY

BRYCE CRAWFORD, Jr., *Editor*  
STEPHEN PRAGER, *Associate Editor*  
ROBERT W. CARR, Jr., C. ALDEN MEAD, *Assistant Editors*

**EDITORIAL BOARD:** C. A. ANGELL (1973–1977), F. C. ANSON (1974–1978), V. A. BLOOMFIELD (1974–1978), J. R. BOLTON (1976–1980), L. M. DORFMAN (1974–1978), H. L. FRIEDMAN (1975–1979), H. L. FRISCH (1976–1980), W. A. GODDARD (1976–1980), E. J. HART (1975–1979), W. J. KAUZMANN (1974–1978), R. L. KAY (1972–1976), D. W. McCLURE (1974–1978), R. M. NOYES (1973–1977), W. B. PERSON (1976–1980), J. C. POLANYI (1976–1980), S. A. RICE (1976–1980), F. S. ROWLAND (1973–1977), R. L. SCOTT (1973–1977), W. A. STEELE (1976–1980), J. B. STOTHERS (1974–1978), W. A. ZISMAN (1972–1976)

Published by the  
**AMERICAN CHEMICAL SOCIETY**  
**BOOKS AND JOURNALS DIVISION**  
D. H. Michael Bowen, Director

Editorial Department: Charles R. Bertsch,  
Head; Marianne C. Brogan, Associate  
Head; Celia B. McFarland, Joseph E.  
Yurvati, Assistant Editors  
Graphics and Production Department:  
Bacil Guiley, Head  
Research and Development Department:  
Seldon W. Terrant, Head

Advertising Office: Centcom, Ltd., 50 W.  
State St., Westport, Conn. 06880.

© Copyright, 1976, by the American  
Chemical Society. No part of this publication  
may be reproduced in any form without  
permission in writing from the American  
Chemical Society.

Published biweekly by the American  
Chemical Society at 20th and Northampton  
Sts., Easton, Pennsylvania 18042. Second  
class postage paid at Washington, D.C. and  
at additional mailing offices.

## Editorial Information

**Instructions for authors** are printed in  
the first issue of each volume. Please conform  
to these instructions when submitting man-  
uscripts.

**Manuscripts for publication** should be  
submitted to *The Journal of Physical  
Chemistry*, Department of Chemistry, Uni-  
versity of Minnesota, Minneapolis, Minn.  
55455. Correspondence regarding **accepted  
papers and proofs** should be directed to the  
Editorial Department at the ACS Easton  
address.

**Page charges** of \$60.00 per page are as-  
sessed for papers published in this journal.  
Ability to pay does not affect acceptance or  
scheduling of papers.

**Bulk reprints or photocopies** of indi-  
vidual articles are available. For information  
write to Business Operations, Books and  
Journals Division at the ACS Washington  
address.

Requests for **permission to reprint**  
should be directed to Permissions, Books and  
Journals Division at the ACS Washington  
address. The American Chemical Society and  
its Editors assume no responsibility for the  
statements and opinions advanced by con-  
tributors.

## Subscription and Business Information

1976 Subscription rates—including surface  
postage

	U.S.	PUAS	Canada, Foreign
Member	\$24.00	\$29.75	\$30.25
Nonmember	96.00	101.75	102.25
Supplementary material	15.00	19.00	20.00

**Air mail and air freight** rates are avail-  
able from Membership & Subscription Ser-  
vices, at the ACS Columbus address.

**New and renewal subscriptions** should  
be sent with payment to the Office of the  
Controller at the ACS Washington address.

**Changes of address** must include both old  
and new addresses with ZIP code and a recent  
mailing label. Send all address changes to the  
ACS Columbus address. Please allow six  
weeks for change to become effective. **Claims**  
for missing numbers will not be allowed if loss  
was due to failure of notice of change of ad-  
dress to be received in the time specified; if

claim is dated (a) North America—more than  
90 days beyond issue date, (b) all other for-  
eign—more than 1 year beyond issue date; or  
if the reason given is “missing from files”.  
Hard copy claims are handled at the ACS  
Columbus address.

**Microfiche subscriptions** are available  
at the same rates but are mailed first class to  
U.S. subscribers, air mail to the rest of the  
world. Direct all inquiries to Business Oper-  
ations, Books and Journals Division, at the  
ACS Washington address or call (202) 872-  
4444. **Single issues** in hard copy and/or mi-  
crofiche are available from Special Issues  
Sales at the ACS Washington address. Cur-  
rent year \$4.75. Back issue rates available  
from Special Issues Sales. **Back volumes** are  
available in hard copy and/or microform.  
Write to Special Issues Sales at the ACS  
Washington address for further information.  
**Microfilm** editions of ACS periodical pub-  
lications are available from volume 1 to the  
present. For further information, contact  
Special Issues Sales at the ACS Washington  
address. **Supplementary material** must be  
ordered directly from Business Operations,  
Books and Journals Division, at the ACS  
Washington address.

	U.S.	PUAS, Canada	Other Foreign
Microfiche			
Photocopy	\$2.50	\$3.00	\$3.50
1–7 pages	4.00	5.50	7.00
8–20 pages	5.00	6.50	8.00

Orders over 20 pages are available only on  
microfiche, 4 × 6 in., 24X, negative, silver  
halide. Orders must state photocopy or mi-  
crofiche if both are available. Full bibliog-  
raphic citation including names of all au-  
thors and prepayment are required. Prices  
are subject to change.

American Chemical Society  
1155 16th Street, N.W.  
Washington, D.C. 20036  
(202) 872-4600

Member & Subscription Services  
American Chemical Society  
P.O. Box 3337  
Columbus, Ohio 43210  
(614) 421-7230

Editorial Department  
American Chemical Society  
20th and Northampton Sts.  
Easton, Pennsylvania 18042  
(215) 258-9111

THE JOURNAL OF  
PHYSICAL CHEMISTRY

---

Volume 80, Number 22 October 21, 1976

JPCA<sub>x</sub> 80(22) 2437-2530 (1976)

ISSN 0022-3654

Pyrolysis of Allene and Propyne behind Reflected Shocks . . . <b>Assa Lifshitz,* Michael Frenklach, and Alexander Burcat</b>	2437
Ordered and Disordered Phases in Mixed Dodecylammonium and Hexadecylammonium Tetrachloromanganate(II) . <b>Vincenzo Salerno, Andrea Grieco, and Michele Vacatello*</b>	2444
Infrared and Nuclear Magnetic Resonance Studies of Hydrogen Bonding in Aliphatic Alcohol Systems . . . . . <b>J. L. Kirsch* and D. R. Coffin</b>	2448
Enthalpy and Entropy of Transfer of Lithium Halides between Water and Long-Chain Alcohols . . . . . <b>Y. Marcus</b>	2451
Thermodynamics of the Anion Exchange of Cyanide and Thiocyanate on a Strong Base Anion Exchange . . . . . <b>M. Okamoto and Y. Marcus*</b>	2456
The Co-Association of Nucleosides and the Equilibrium Copolymerization of Nucleotides. Base Stacking Interactions and the Thermodynamics of Phosphodiester Bond Formation . . . . . <b>Leonard Peller</b>	2462
Krafft Points, Critical Micelle Concentrations, Surface Tension, and Solubilizing Power of Aqueous Solutions of Fluorinated Surfactants . . . . . <b>Hironobu Kunieda and Kozo Shinoda*</b>	2468
Hydrogen Profiles in Water-Oxidized Silicon . . . . . <b>D. J. Breed and R. H. Doremus*</b>	2471
Reaction of Amines with Haloalkanes. 4. Reaction at a Pyrex Surface . . . . . <b>Pierre A. Willermet and John G. Miller*</b>	2473
Raman Scattering of Pure Ammonia to High Pressures and Temperatures . . . . . <b>M. Buback* and K. R. Schulz</b>	2478
Ultraviolet Absorption Spectra of $e_{aq}^-$ , H, OH, D, and OD from Pulse Radiolysis of Aqueous Solutions . . . . . <b>S. O. Nielsen,* B. D. Michael, and E. J. Hart</b>	2482
Spectroscopic Evidence for Complex Formation of the Tributylammonium Cation with Hexamethylphosphoric Triamide in <i>o</i> -Dichlorobenzene and with Triphenylphosphine Oxide in 1,2-Dichloroethane . . . . . <b>W. R. Gilkerson</b>	2488
Spectra and Structure of Organophosphorous Compounds. 16. Infrared and Raman Spectra, Vibrational Assignment, and Conformational Analysis for Isopropylphosphine and Isopropylphosphine- $d_2$ . . . . . <b>J. R. Durig* and A. W. Cox, Jr.</b>	2493 ■
Efficiency of the Intersystem Crossing from the Lowest Spin-Allowed to the Lowest Spin- Forbidden Excited State of Some Chromium(III) and Ruthenium(II) Complexes . . . . . <b>F. Bolletta,* M. Maestri, and V. Balzani</b>	2499
Solvent Effect on the Electronic Transitions of the Triiodide Anion . . . . . <b>Christian Detellier and Pierre Laszlo*</b>	2503
Approximate Molecular Orbital Theory for Positrons and Positronium Atoms Bound to Molecules . . . . . <b>D. M. Schrader* and C. M. Wang</b>	2507

Electron Spin Resonance of the Triplet $\pi\pi^*$ State of Pyrene- $d_{10}$ in Benzophenone . . . . . <b>L. J. Noe*</b> and <b>L. F. Wojdac</b>	2519
Infrared Intensities, Polar Tensors, and Atomic Population Densities in Molecules . . . . . <b>W. T. King*</b> and <b>G. B. Mast</b>	2521
Dielectric Properties of Osmium-Fixed Hemoglobin and Its Water of Hydration . . . . . <b>G. T. Koide</b> and <b>E. L. Carstensen*</b>	2526

### COMMUNICATIONS TO THE EDITOR

Infrared and Far-Infrared Spectra of Ammonia Adsorbed on Calcium Chloride and Calcium Bromide . . . . . <b>O. Marcovitch, A. Lubezky, and Y. Kozirovski*</b>	2530
---	------

■ Supplementary and/or miniprint material for this paper is available separately (consult the masthead page for ordering information); it will also appear following the paper in the microfilm edition of this journal.

\* In papers with more than one author, the asterisk indicates the name of the author to whom inquiries about the paper should be addressed.

### AUTHOR INDEX

Balzani, V., 2499	Frenklach, M., 2437	Lifshitz, A., 2437	Peller, L., 2462
Bolletta, F., 2499	Gilkerson, W. R., 2488	Lubezky, A., 2530	
Breed, D. J., 2471	Grieco, A., 2444	Maestri, M., 2499	Salerno, V., 2444
Buback, M., 2478	Hart, E. J., 2482	Marcovitch, O., 2530	Schrader, D. M., 2507
Burcat, A., 2437	King, W. T., 2521	Marcus, Y., 2451, 2456	Schulz, K. R., 2478
Carstensen, E. L., 2526	Kirsch, J. L., 2448	Mast, G. B., 2521	Shinoda, K., 2468
Coffin, D. R., 2448	Koide, G. T., 2526	Michael, B. D., 2482	
Cox, A. W., Jr., 2493	Kozirovski, Y., 2530	Miller, J. G., 2473	Vacatello, M., 2444
Detellier, C., 2503	Kunieda, H., 2468	Nielsen, S. O., 2482	
Doremus, R. H., 2471	Laszlo, P., 2503	Noe, L. J., 2519	Wang, C. M., 2507
Durig, J. R., 2493		Okamoto, M., 2456	Willermet, P. A., 2473
			Wojdac, L. F., 2519

# THE JOURNAL OF PHYSICAL CHEMISTRY

Registered in U. S. Patent Office © Copyright, 1976, by the American Chemical Society

VOLUME 80, NUMBER 22 OCTOBER 21, 1976

## Pyrolysis of Allene and Propyne behind Reflected Shocks

Asa Lifshitz,\* Michael Frenklach,<sup>1a</sup>

*Department of Physical Chemistry, The Hebrew University, Jerusalem, Israel*

and Alexander Burcat

*Department of Aeronautical Engineering, Technion, Israel Institute of Technology, Haifa, Israel (Received April 12, 1976)*

The pyrolysis of allene and propyne was studied behind reflected shocks in a single pulse shock tube. The temperature range covered was 1040–1470 K and pressures ( $P_5$ ) varied between 1.2 and 6 atm. Over this temperature range more than five orders of magnitude in the rate of production of few of the products were observed.  $\text{CH}_4$ ,  $\text{C}_2\text{H}_2$ ,  $\text{C}_2\text{H}_4$ ,  $\text{C}_2\text{H}_6$ , and  $\text{H}_2$  (the latter in only one series of experiments) were detected and their rates of production were determined as a function of initial  $\text{C}_3\text{H}_4$  concentration, total density, and temperature. From the low temperature experiments, in which only a few percent isomerization took place, it was shown that  $\text{CH}_4$  is produced from propyne and  $\text{C}_2\text{H}_4$  from allene. No conclusion could be reached on the basis of the experimental results regarding the production pattern of the other reactions products. It is suggested however that  $\text{CH}_4$ ,  $\text{C}_2\text{H}_2$ , and  $\text{C}_2\text{H}_6$  are the result of  $\text{CH}_3\text{-CH=CH}$  decomposition. The latter is obtained by H atom addition to propyne.

### I. Introduction

We have recently published a detailed investigation of the structural isomerization allene = propyne<sup>1b</sup> and demonstrated that the reaction proceeds via a pure unimolecular reaction. It was also shown that the system reaches an equilibrium before less than 1% decomposition takes place.<sup>1b,2</sup> Allene and propyne are decomposition products of propane<sup>3</sup> and propylene<sup>4-7</sup> and are probably intermediate products in their combustion. Knowledge of the decomposition pattern of these two isomers is therefore highly important for the clarification of the pyrolysis of the  $\text{C}_3$  hydrocarbon system.

A detailed investigation of the pyrolysis of allene and propyne was conducted by Levush et al.<sup>8</sup> over the temperature range 900–1150 °C using a flow system. These authors have determined profiles of various decomposition products and determined first-order rate constants for their production. They have also demonstrated that the isomerization was by far faster than any decomposition process. They did not attempt however to offer a mechanism which describes the decomposition pattern of either isomer.

Wagner and Zellner<sup>9,10</sup> studied reactions of allene and propyne with hydrogen atoms using a flow system. They have discussed in detail a number of elementary reactions which participate in the overall scheme of the pyrolysis.

The understanding of the pyrolysis mechanism of propyne and allene is somewhat difficult relative to other hydrocarbons. As has been mentioned before, allene and propyne in-

terisomerize at a rate much faster than the pyrolysis itself. At a temperature where hardly 1% of the  $\text{C}_3\text{H}_4$  has decomposed, an isomerization equilibrium has almost been attained and the two isomers react, each at a different mechanism, to produce the observed reaction products. At this stage it is almost impossible to determine by experimental methods which substance is a reaction product of what isomer. Isotope labeling might help, but since the pyrolysis involves free radicals, isotope exchange takes place and makes the interpretation of the data rather complicated. However, if one can study the decomposition process at temperatures where only a few percent of the original isomer has isomerized, the sequence of events can then be determined. Since the isomerization is much faster than the decomposition, only a few hundredths of one percent decomposition products would appear under these conditions. The ability to conduct an investigation over such a range of conversions depends on the purity of the original materials and on the detection limits of the analytical methods. Fortunately the starting materials, allene and propyne, could be purified to the extent that only a few thousands of one percent of the pyrolysis products showed up as impurities. In addition, the analytical methods were sensitive enough to detect such quantities.

In this article, we present a detailed investigation of the pyrolysis of allene and propyne over five orders of magnitude in the decomposition rates. A discussion of the reaction mechanism is also presented.

## II. Experimental Section

A. *Apparatus.* The decomposition of allene and propyne was studied in a 2-in. i.d. single pulse shock tube. The tube's driven section was 13 ft long made of "double tough" Pyrex tubing, including an 11-in. stainless steel test section. The length of the driver section could be adjusted in small steps in order to achieve the best cooling conditions. A 36-l. dump tank was connected to the driven section near the diaphragm area to prevent reheating of the gas by doubly reflected shock waves. The driver was separated from the driven section by Mylar polyester films of various thickness. A full description of the tube and the mode of its operations has already been discussed in detail in previous publications.<sup>11</sup>

Before each run, the tube was pumped down to several hundredths of a micron. The leak and/or degassing rate was approximately  $2 \times 10^{-4}$  Torr/min.

Incident shock velocities were measured from which the reflected shock parameters were calculated. This was done with two miniature high-frequency pressure transducers the output of which was fed into a home-built period meter, accurate to 0.1  $\mu$ s. Dwell times could be determined from the oscilloscope traces to  $\pm 10\%$ . They were later corrected and averaged as has been discussed in a previous publication.<sup>12</sup>

B. *Materials.* Four reaction mixtures, two containing allene and two containing propyne (all diluted in argon), were prepared on a high-pressure line and were stored in stainless steel cylinders at approximately 150 psi. The cylinders were baked and pumped down to  $2 \times 10^{-5}$  Torr prior to the preparation of the mixtures. Six groups of experiments were run with these mixtures. The six groups and some additional information are listed in Table I.

The allene and the propyne used were obtained from the Matheson Gas Co. Before the preparation of the mixtures, a portion of the allene was transferred into a glass bulb for removal of lower molecular weight hydrocarbons. It was frozen in liquid N<sub>2</sub>, pumped on, and then thawed out. This was repeated several times. It was later frozen in a methylcyclohexane-liquid N<sub>2</sub> bath and pumped on for some time. In the final analysis the allene showed 0.000 22% CH<sub>4</sub>, no traces of C<sub>2</sub>H<sub>4</sub> or C<sub>2</sub>H<sub>6</sub>, 0.001% C<sub>2</sub>H<sub>2</sub>, and 0.10% propyne. Following the same procedure the propyne showed in the final analysis 0.0003% CH<sub>4</sub>, no traces of C<sub>2</sub>H<sub>4</sub> and C<sub>2</sub>H<sub>6</sub>, 3.9% C<sub>2</sub>H<sub>2</sub>, and 0.425% allene. We were unsuccessful in trying to reduce the acetylene level of impurities in the propyne.

The argon used was Matheson Grade, listed as 99.9995% pure.

C. *Analyses.* Samples were taken from the end block of the driven section and were analyzed for CH<sub>4</sub>, C<sub>2</sub>H<sub>2</sub>, C<sub>2</sub>H<sub>4</sub>, C<sub>2</sub>H<sub>6</sub>, CH<sub>2</sub>=C=CH<sub>2</sub> and CH<sub>3</sub>-C $\equiv$ CH on a Packard 800 series vapor phase chromatograph using a flame ionization detector. The initial column temperature (Porapak N) was 40 °C and was gradually raised to 85 °C with a Packard Model 846 temperature programmer. The hydrogen, in one series of experiments, was analyzed on a Molecular Sieve 5A column at room temperature using a thermal conductivity detector.

## III. Computations

A. *Reflected Shock Parameters.* The reflected shock parameters were calculated from the measured incident shock velocities using the three conservation equations and the ideal gas equation of state. The enthalpies of allene and propyne were taken from the American Petroleum Institute Project No. 44<sup>13</sup> and were presented as six-term polynomials whose coefficients were calculated by the least-squares method.

B. *Reaction Dwell Time.* The reaction dwell times were

TABLE I: Test Mixtures and the Experimental Conditions of the Six Groups of Experiments

Group	Composition	$p_1$ range, Torr	$T_5$ range, K	No. of shocks	Symbol used in figures
1A	0.25% allene	178-224	1085-1330	16	+
2A	1% allene	169-223	1065-1465	30	○
3A	1% allene	46-58	1040-1350	20	△
1P	0.25% propyne	190-210	1085-1300	13	□
2P	1% propyne	194-198	1040-1370	14	×
3P	1% propyne	49-55	1050-1160	9	◇

recorded by the pressure transducer located furthest from the end plate. The dwell time in this location is considerably shorter than the average one which must be considered in the evaluation of the rate constants. It has to be corrected for the following: (1) the variation of the dwell time along the test section and (2) the change in the location of the reacted mixture during the expansion. The equation which relates the corrected dwell time  $t_c$  with the measured one  $t_m$  is<sup>12</sup>

$$t_c = t_m + \left\{ b_m - \frac{1}{2} d_f (p_7/p_1) / (\rho_5/\rho_1) \right\} \left( \frac{1}{u_5} + \frac{1}{a_5} \right) \quad (I)$$

where  $b_m$  is the distance between the transducer by which  $t_m$  is recorded and the end plate,  $d_f$  is the length of the sampling zone,  $\rho_5/\rho_1$  is the compression ratio behind the reflected shock,  $u_5$  is the reflected shock velocity,  $a_5$  is the speed of sound at  $T_5$ , and  $p_7$  is the final equilibrium pressure in the tube.

## IV. Results

In order to determine the rate of production of the various decomposition products, their temperature dependence, and their dependence on the initial allene (or propyne) concentration, six groups of experiments were carried out, three starting from allene and three from propyne. The six groups and their experimental conditions are listed in Table I. In Table II, experimental details of five representative shocks from each group are shown. In view of the very high purity of the starting materials extents of reaction as low as a few thousandths of one percent could be determined quite accurately. In a few cases more than five orders of magnitude in the rate of production of the various products could be covered.

Figure 1 shows the product distribution for groups 2A (allene) and 2P (propyne) [Table I] over the entire temperature range following a reaction time of  $\sim 2$  ms. It can readily be seen that the isomerization product in both cases is of the highest concentration. Around 1400 K the two isomers reach an equilibrium; from this point and on their lines on both plots are parallel. Since the two isomers establish an equilibrium at the higher temperatures, the right end (high temperatures) of the two pictures are almost identical and the origin of the C<sub>3</sub>H<sub>4</sub> no more plays any role in the distribution. At the lower temperatures however, where only a few percent of the original C<sub>3</sub>H<sub>4</sub> has isomerized, the distribution represents the direct formation of the product from the starting isomer. Clearly, methane is formed mainly from propyne whereas ethylene is formed probably only from allene. It is interesting to note that the methane on the allene distribution plot and the ethylene on the propyne plot show a very steep temperature dependence, steeper than the one on the neighboring plot. This is clearly due to the isomerization process of the original isomer.

TABLE II: Details of Five Representative Shocks from the Six Groups of Experiments

Composition	$P_1$ , Torr	$T_5$ , K	$\rho_5/\rho_1$	[Product]/[C <sub>3</sub> H <sub>4</sub> ] <sub>0</sub>						Dwell time ( $t_c$ ), ms
				CH <sub>4</sub>	C <sub>2</sub> H <sub>4</sub>	C <sub>2</sub> H <sub>6</sub>	C <sub>2</sub> H <sub>2</sub>	CH <sub>2</sub> =C=CH <sub>2</sub>	CH <sub>3</sub> -C≡CH	
Allene 1%	194	1068	4.76	2.43E-5	2.04E-4	5.80E-5	9.55E-6	9.87E-1	1.25E-2	2.46
	203	1126	4.95	2.68E-4	7.24E-4	6.66E-5	1.28E-4	9.57E-1	4.27E-2	2.41
	197	1239	5.31	7.34E-3	4.25E-3	4.24E-4	7.97E-3	5.14E-1	4.75E-1	2.09
	205	1293	5.47	1.50E-2	4.93E-3	4.13E-4	1.71E-2	4.79E-1	5.01E-1	2.07
	190	1374	5.69	1.02E-1	2.12E-2	2.85E-3	1.65E-1	3.15E-1	5.25E-1	1.94
Allene 1%	50	1068	4.76	7.40E-5	1.48E-4	2.46E-5	1.04E-5	9.77E-1	2.32E-2	2.45
	57	1120	4.93	1.64E-4	3.26E-4	8.41E-5	1.09E-4	9.41E-1	5.84E-2	2.15
	52	1243	5.32	6.43E-3	2.38E-3	2.22E-4	8.87E-3	4.95E-1	4.95E-1	1.97
	50	1292	5.46	1.50E-2	3.51E-3	4.77E-4	1.89E-2	4.25E-1	5.54E-1	1.91
	50	1342	5.60	4.01E-2	6.70E-3	1.10E-3	5.83E-2	3.63E-1	5.80E-1	1.81
Allene 0.25%	207	1085	4.59	8.15E-5	1.79E-4	2.59E-4	1.88E-5	9.63E-1	3.67E-2	2.43
	200	1121	4.70	1.66E-4	3.24E-4	5.09E-4	9.09E-5	9.29E-1	7.02E-2	2.50
	195	1170	4.84	4.03E-4	6.06E-4	8.30E-4	4.19E-4	8.45E-1	1.54E-1	2.35
	179	1200	4.93	1.21E-3	1.03E-3	5.89E-4	1.59E-3	6.93E-1	3.05E-1	2.30
	148	1332	5.28	2.81E-2	5.86E-3	1.87E-3	5.10E-2	3.69E-1	5.82E-1	2.11
Propyne 1%	197	1039	4.65	1.15E-4	5.07E-6	1.66E-5		3.94E-3	9.97E-1	2.48
	194	1079	4.79	3.93E-4	9.38E-6			1.15E-2	9.88E-1	2.44
	217	1231	5.28	7.95E-3			1.68E-2	1.08E-1	8.87E-1	2.03
	219	1291	5.46	2.34E-2			2.83E-2	1.85E-1	7.96E-1	1.98
	221	1363	5.66	1.40E-1			2.26E-1	1.76E-1	6.19E-1	1.93
Propyne 1%	55	1051	4.70	1.48E-4	5.60E-6	1.34E-5		4.60E-3	1.00E+0	2.50
	54	1086	4.82	2.47E-4	1.21E-5	1.67E-5		7.26E-3	9.95E-1	2.57
	52	1117	4.92	6.14E-4	1.48E-5	5.29E-5		1.56E-2	9.90E-1	2.44
	49	1127	4.95	9.89E-4	3.15E-5	1.23E-4		2.80E-2	9.77E-1	2.34
	55	1160	5.06	1.61E-3	5.48E-5	2.20E-4		4.70E-2	9.55E-1	2.32
Propyne 0.25%	195	1083	4.58	3.30E-4		2.26E-4		1.28E-2	9.90E-1	2.37
	194	1116	4.68	6.40E-4	5.40E-5	4.73E-4		2.05E-2	9.82E-1	2.33
	197	1150	4.78	1.45E-3	8.60E-5	8.62E-4		4.77E-2	9.55E-1	2.41
	198	1258	5.09	9.96E-3	6.31E-4	3.53E-3	1.16E-2	1.53E-1	8.33E-1	2.23
	202	1299	5.19	2.82E-2	3.13E-3	5.89E-3	4.31E-2	2.51E-1	7.05E-1	2.15

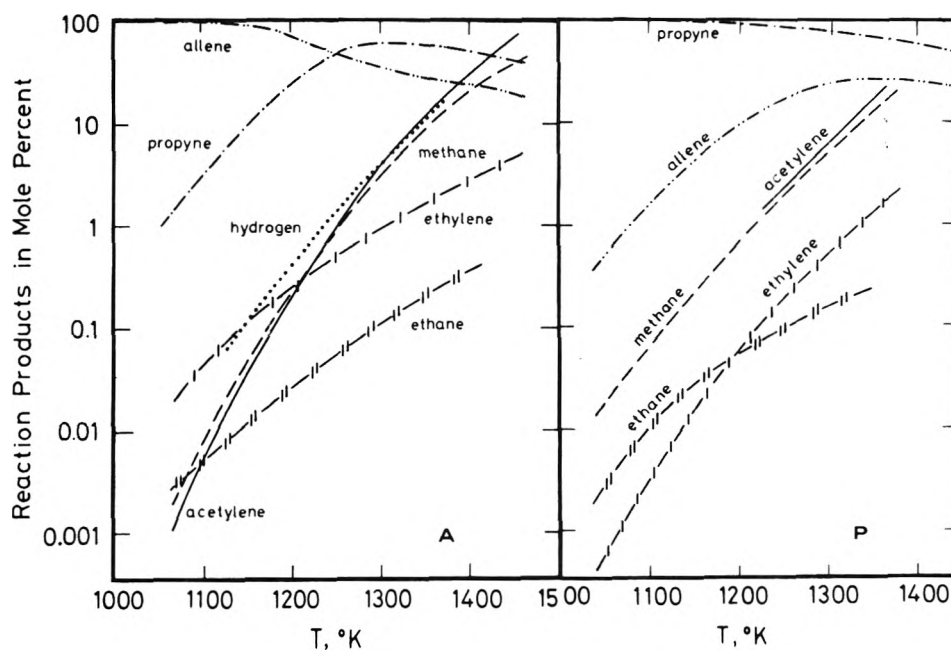
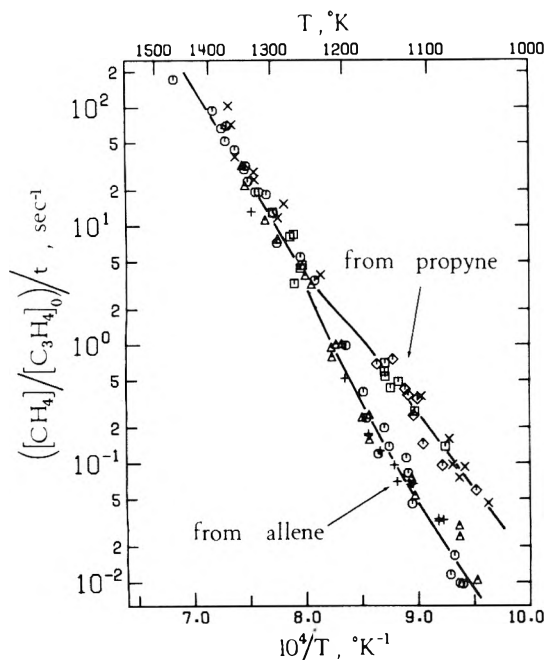


Figure 1. Product distribution of 1% C<sub>3</sub>H<sub>4</sub> in argon over the temperature range 1040–1470 K: (A) allene, (P) propyne. At high temperatures the two isomers reach an equilibrium and the distribution of reaction product is almost identical for both isomers. At low temperatures the picture is entirely different.

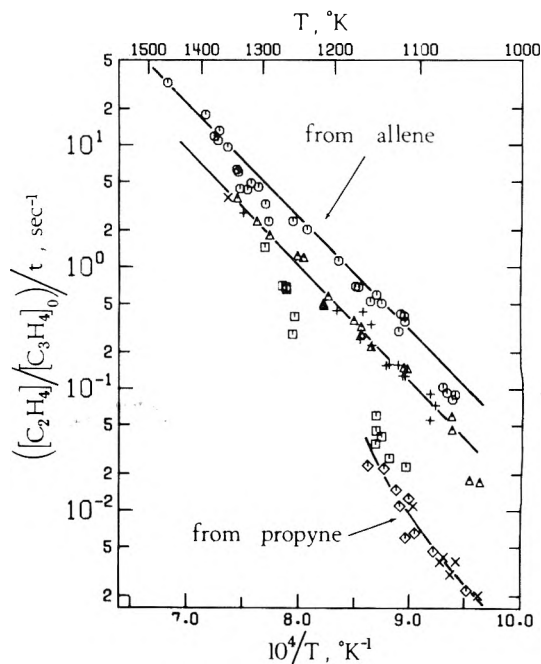


**Figure 2.** A plot of  $\{[CH_4]/[C_3H_4]_0\}/t$  vs.  $1/T$  for the six groups of experiments. The data points for each three groups (A or P) scatter along one line indicating a first-order dependence on  $C_3H_4$  and zero dependence on the argon density. Methane is formed faster from propyne than from allene.

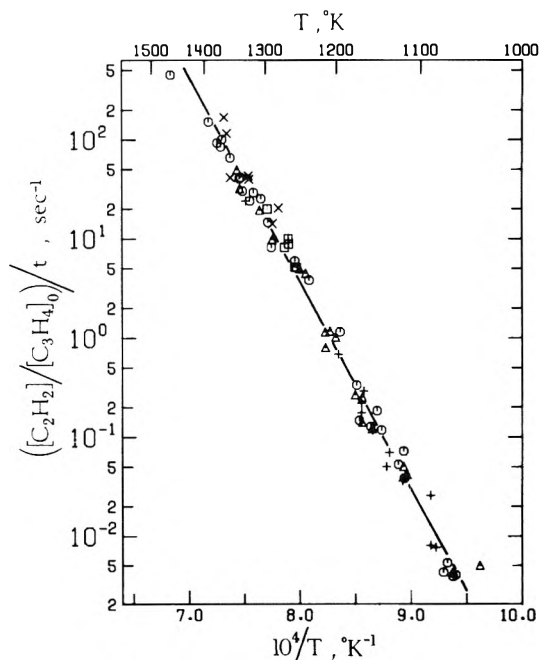
The three groups of experiments for each isomer listed in Table I were chosen in such a manner that information on the rate of production of each isomer, its dependence on the initial  $C_3H_4$  concentration and on the argon concentration could be directly obtained. In Figures 2-4, the rates of production of  $CH_4$ ,  $C_2H_4$ , and  $C_2H_2$  in units of  $s^{-1}$  (mole fraction/time) are plotted against the reciprocal temperature over the entire range covered by this investigation, for the six groups of experiments listed in Table I. It can readily be seen that the rate of production of methane (Figure 2) which is presented as  $[CH_4]_t/[C_3H_4]_0/t$  is identical for the three groups in series A (allene) and for the three groups in series P (propyne). Since this presentation is somewhat equivalent to that of a first-order rate constant, the results indicate that the production of methane is roughly first order with respect to the  $C_3H_4$ , allene, or propyne. There is also no dependence on the argon concentration. The low temperature points on Figure 2 clearly show that the production of methane from propyne is considerably faster than its production from allene. At higher temperatures on the other hand the two isomers reach an equilibrium and the system loses its original identity. At these temperatures the data points of all the six groups scatter along one line.

Figure 3 depicts an identical plot for the rate of production of ethylene shown again in a presentation equivalent to that of a first-order rate constant. However the picture is entirely different. The production of ethylene in 2A is faster (in  $s^{-1}$ ) than that in 1A and 3A, indicating a dependence on the initial allene concentration which is higher than unity. It is hard to decide whether series P shows the same behavior or not owing to the limited temperature range in which the isomer can retain its original identity.

In Figure 4,  $[C_2H_2]/[C_3H_4]_0/t$  is plotted against  $1/T$ . Because of the high level of acetylene impurity in the propyne (3.9%) we do not have data points at low temperatures when the starting isomer was propyne. The production of acetylene



**Figure 3.** A plot of  $\{[C_2H_4]/[C_3H_4]_0\}/t$  vs.  $1/T$  for the six groups of shocks. It can readily be seen that ethylene is formed mainly from allene. The rate of production of allene in units of  $s^{-1}$  depends on the initial allene concentration indicating a reaction order higher than unity.



**Figure 4.** A plot of  $\{[C_2H_2]/[C_3H_4]_0\}/t$  vs.  $1/T$  for the six groups of experiments. Data points for propyne at low temperatures are not available. The Arrhenius plot is linear over more than five orders of magnitude.

is roughly first order with respect to allene, and obeys an Arrhenius type dependence over five orders of its magnitude.

Figure 5 shows a similar plot for hydrogen. The hydrogen was analyzed on a thermal conductivity detector which is over two orders of magnitude less sensitive than the flame ionization detector. Data are therefore available only at high temperatures where the concentrations are above the detection limit.

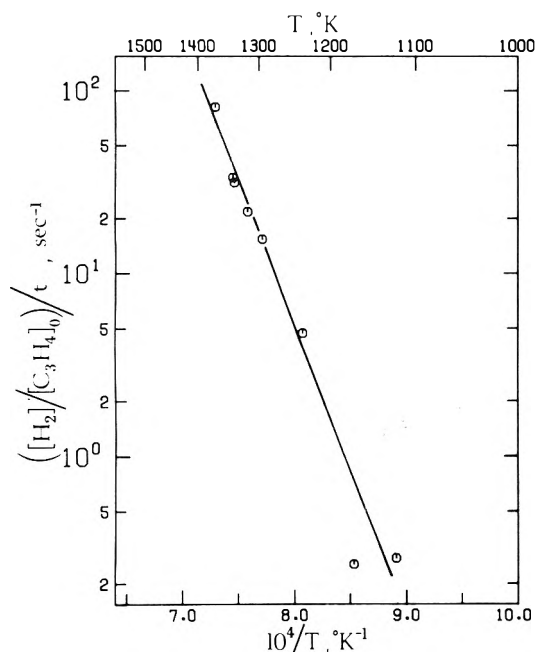
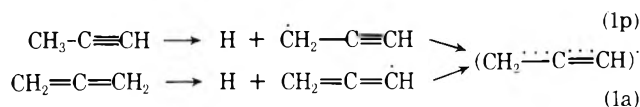


Figure 5. A plot of  $\{[H_2]/[C_3H_4]_0\}/t$  vs.  $1/T$  for group of runs 2A. Molecular hydrogen is formed by the abstraction of hydrogen atoms from the  $C_3H_4$  by hydrogen atoms.

## V. Discussion

The distribution of bond strengths in a molecule determines the initiation step through which a pyrolysis process begins. When one deals with propane, for example,  $C-CH_3$  is the weakest bond ( $\sim 85$  kcal/mol)<sup>14</sup> and the loss of a methyl group is the first among a scheme of elementary reactions which determine the nature of the pyrolysis. The  $C-CH_3$  bond in propyne is strong, approximately 117 kcal/mol.<sup>15</sup> The initiation step involves, therefore, the loss of the hydrogen atom  $CH=C-CH_2-H$  which requires only 80–90 kcal/mol.<sup>16,17</sup> Allene has only carbon-carbon double bonds and will also start to decompose by the rupture of a C-H bond.

The loss of a hydrogen atom leaves the radical  $C_3H_3\cdot$  in both allene and propyne.



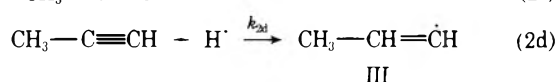
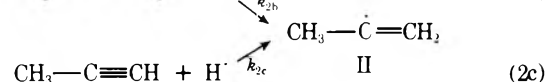
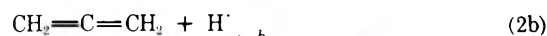
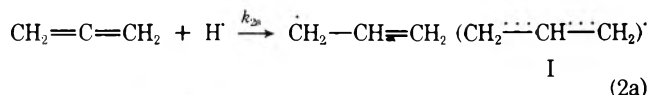
Since the  $C_3H_3\cdot$  is the same species regardless whether it arrives from allene or from propyne its consecutive reactions cannot account for any difference in the behavior of the two isomers. Also, owing to the strong C-C as well as C-H bonds, the  $C_3H_3\cdot$  radical cannot easily undergo decomposition or disproportionation and is thus a very poor chain carrier. We shall discuss its possible fate at a later stage. It is believed that the pyrolysis chain is carried by the reaction of the hydrogen atoms produced in reaction 1 with allene and propyne.

Wagner and Zellner<sup>9,10</sup> have investigated the reactions of H atoms with both allene and propyne in a flow system over the temperature range 273–470 K. They found the addition reactions as the predominant ones and reported rate constants for the addition of hydrogen to the terminal and nonterminal positions of allene and propyne to produce the various  $C_3H_5\cdot$  species. These species are believed to determine the general character of the system and account for the differences in the allene and propyne behavior.

At the temperature range covered in this study abstraction

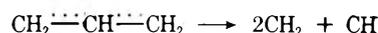
as well as addition of hydrogen atoms takes place. The abstraction will result in the production of molecular hydrogen which was observed in this study (Figures 1 and 5). It will also leave the unreactive  $C_3H_3\cdot$  radical which does not contribute much to the propagation reactions through which methane, ethane, and acetylene are being formed.

The four possible addition reactions are as follows:



They produce three  $C_3H_5\cdot$  isomers which do not isomerize.<sup>9,10</sup> Reactions 2b and 2c produce an identical isomer. Reactions 2a and 2d give additional two radicals which differ considerably from one another and from the one produced by reactions 2b and 2c. The behavior of the system as a whole should be examined on the basis of the relative reactivity of these three free radicals. By reactivity we mean rupture of a carbon-carbon bond rather than a C-H bond since the latter might only lead to interisomerization for which the unimolecular channel has been shown to be considerably faster.

The species obtained in reaction 2a is a symmetrical species having two equivalent carbon-carbon bonds of the order of 3/2. To evaluate their strength one can use the reaction



where  $D(C\cdots C) = \frac{1}{2}\{\Delta H_f^\circ(CH) + 2\Delta H_f^\circ(CH_2) - \Delta H_f^\circ(CH_2-CH-CH_2)\} \sim 137$  kcal/mol.<sup>18</sup> This is a strong bond and it is very unlikely that this radical will be an effective chain carrier. It will probably lose a hydrogen to yield back either allene or propyne.

One should now compare the reactivity of species II and III. Again, species II,  $CH_3-\dot{C}=CH_2$ , is obtained from both allene and propyne at almost equal rates.<sup>9,10</sup> One cannot expect, therefore, that this free radical will characterize in its reactions the specific behavior of allene or propyne. Also, by its decomposition it leaves two free radicals  $CH_3\cdot$  and  $\dot{C}=CH_2$ , the latter is an unstable biradical rather than the stable acetylene molecule. This requires a considerable amount of energy. In fact Wagner and Zellner have shown<sup>9,10</sup> that the decomposition of  $CH_3-\dot{C}=CH_2$  to acetylene and methane (via  $\dot{C}H_3$ ) does not occur. It is believed therefore that only the  $CH_3-CH=\dot{C}H$  radical which is the product of hydrogen atom addition to propyne is an active radical and it is the main supplier of methane and acetylene. The  $CH_3-C$  bond energy in this species is only 32 kcal/mol.<sup>15</sup> Indeed, Figure 2 shows that at the low temperature range (before appreciable isomerization occurs) the production of methane from propyne is an order of magnitude faster than its production from allene. Moreover, if  $CH_3-CH=\dot{C}H$  is indeed responsible for most of the methane and acetylene formed in this pyrolysis then these two substances should have equal concentrations since  $\dot{C}H_3$  will produce methane by an abstraction of H atom from  $C_3H_4$ . The fact that this is indeed the situation is shown in Figure 6 over more than three orders of magnitude in concentrations. At the higher temperature end, the concentration of acetylene exceeds that of methane. Here, more than 10% of the original material has already decomposed, and the decomposition

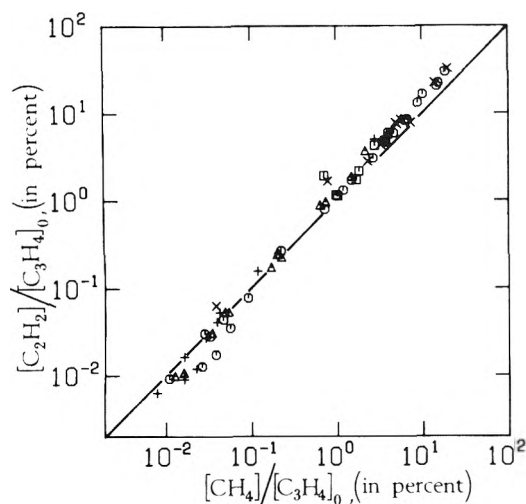


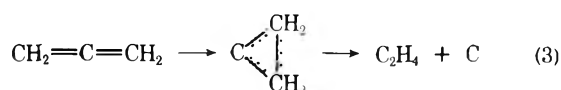
**Figure 6.** A comparison plot of the methane and acetylene concentrations. They are equal except for the high temperature end, verifying the assumption that they both are the result of  $\text{CH}_3\text{-CH=CH}$  decomposition.

products  $\text{CH}_4$ ,  $\text{C}_2\text{H}_4$ , and  $\text{C}_2\text{H}_6$  are known to form acetylene at high temperatures.

In fact one should have compared the acetylene concentration to  $\{[\text{CH}_4] + 2[\text{C}_2\text{H}_6]\}$  rather than  $\text{CH}_4$  alone since ethane is probably formed by recombination of methyl radicals. The concentration of the latter, however, is very small (see Figure 1) and does not change the picture. The reason for leaving out the ethane data points in this article is their *extremely high scatter*. This scatter was far beyond what one would have expected due to bad separation or other analytical problems. It remains an unsolved puzzle.

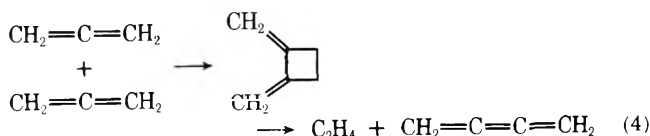
Levush et al.<sup>8</sup> reported in their flow system experiments production of large quantities of brown polymers which accumulated on the walls of the flow apparatus. Analysis showed that the polymers were of the type  $\text{C}_n\text{H}_n$ . In view of the very low reactivity of the  $\text{C}_3\text{H}_3\cdot$  radical it is believed that it forms long polymers by successive recombinations. At higher temperatures this polymer can decompose to yield acetylene molecules or hydrogen atoms, toward the production of carbon richer polymers. Some indication for such a decomposition is shown in Figure 6. At higher temperatures acetylene concentration exceeds that of methane indicating an additional source of acetylene molecules over the  $\text{CH}_3\text{-CH=CH}$  decomposition.

Whereas methane, ethane, and acetylene are believed to be mainly the result of  $\text{CH}_3\text{-CH=CH}$  decomposition, it is hard to explain the production of ethylene from any of the  $\text{C}_3\text{H}_5\cdot$  species. Figure 3 shows that ethylene comes mainly (if not only) from allene, neither  $\text{C}_3\text{H}_3\cdot$  nor  $\text{C}_3\text{H}_5\cdot$  (either  $\text{CH}_2\text{-CH=CH}_2$  or  $\text{CH}_3\text{-C=CH}_2$ ) can be its precursor. A unimolecular rearrangement of allene to yield ethylene:



can be ruled out on the basis of the reaction thermochemistry. Such a process requires 138.5 kcal/mol<sup>13</sup> and can hardly take place at temperatures where ethylene has been observed.

The only way that the production of ethylene from allene can be rationalized is by a bimolecular reaction between two allene molecules via the formation of dimethylenecyclobutane as an intermediate:



The formation of dimethylenecyclobutane by allene dimerization has been reported in the literature<sup>19</sup> and cyclobutanes are known to undergo ring cleavage to form ethylenes.<sup>20</sup> Dimethylenecyclobutane can either decompose back to two allene molecules or to form ethylene and cummulene.

Supporting evidence for a bimolecular reaction is found in the dependence of the production rate of ethylene on the initial allene concentration. Figure 3 shows a power dependence greater than unity. A least-squares analysis of the ethylene data to fit a rate law of the type

$$\Delta[\text{C}_2\text{H}_4]/\Delta t = k_b[\text{CH}_2=\text{C}=\text{CH}_2]^\alpha \quad (\text{II})$$

gives  $\alpha = 1.56$ . The rate constants  $k_b$  were evaluated taking into account the extent of isomerization of allene to propyne.

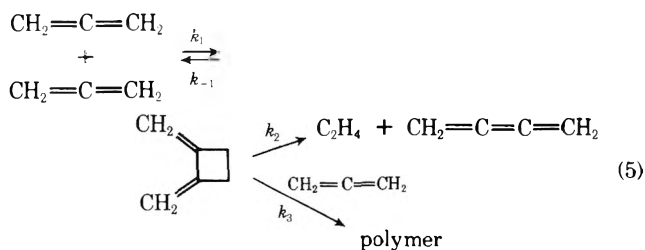
Figure 7 shows a plot of  $\log k_b$  vs.  $1/T$  in which all the data points lie on a single line. The fact that the line is not a straight line and the reaction order is not exactly two indicates that the formation of ethylene from allene molecules is more complicated than just a simple bimolecular reaction. Levush et al.<sup>8</sup> have also reported an increased rate of ethylene production at high conversions indicating an additional path for its formation.

A rate law of the type

$$\Delta[\text{C}_2\text{H}_4]/\Delta t = k_1[\text{CH}_2=\text{C}=\text{CH}_2] + k_2[\text{CH}_2=\text{C}=\text{CH}_2]^2 \quad (\text{III})$$

can account for the experimental results, but it is very hard to rationalize a mechanism which does not involve two allene molecules.

Another way to explain a reaction order between one and two is by the assumption that polymerization takes place by a fast reaction between the dimer and another allene molecule or any other molecule whose concentration is proportional to the allene concentration.



In this case if one assumes a steady state for the dimer (whatever it may be) one obtains

$$\frac{\Delta[\text{C}_2\text{H}_4]}{\Delta t} = \frac{k_1 k_2 [\text{CH}_2=\text{C}=\text{CH}_2]^2}{k_{-1} + k_2 + k_3 [\text{CH}_2=\text{C}=\text{CH}_2]} \approx k_b [\text{CH}_2=\text{C}=\text{CH}_2]^{1.5 \leq \alpha \leq 2} \quad (\text{IV})$$

One should add however that these are only ways to rationalize the observed data and not to determine the reaction mechanism. The exact formation of ethylene is still not completely understood but probably involves a bimolecular reaction in one of the steps.

## VI. Summary

Whereas the pyrolysis of molecules such as propane and

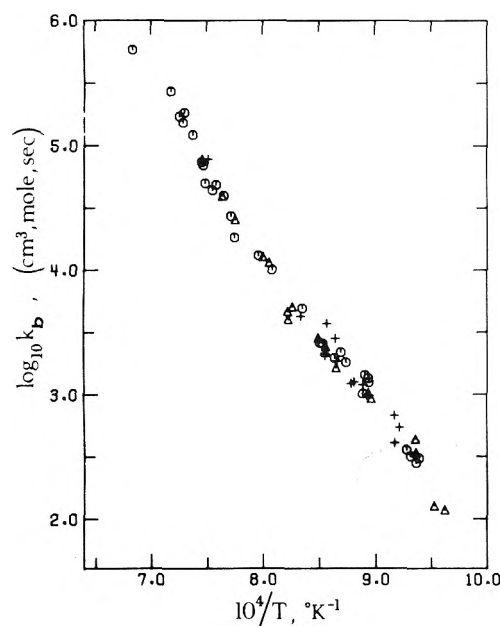
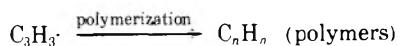
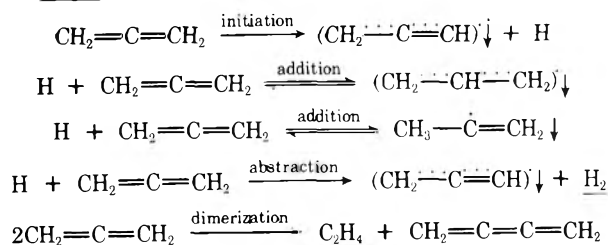


**Figure 7.** A plot of  $\log k_b$  vs.  $1/T$  (see eq II). The data points of all three groups coincide to a single line. They do not form a straight line indicating a rather involved reaction scheme for the production of ethylene from allene.

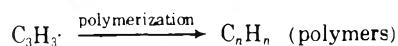
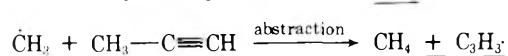
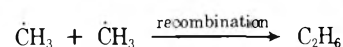
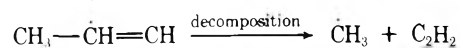
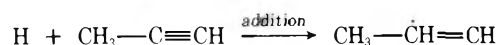
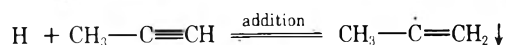
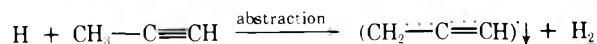
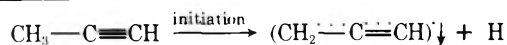
propylene can be considered as typical free radical chain reactions, the pyrolysis of both allene and propyne can hardly be considered as such. The free radical  $C_3H_3$ , which is formed in the initiation step is unreactive and prevents the propagation of long chains. It polymerizes, and only at very high temperatures releases hydrogen atoms.

The mechanism of the production of the various products from allene and propyne can be described by the following scheme, where an arrow ( $\downarrow$ ) means an unreactive species and the stable reaction products are underlined.

(1) allene



(2) propyne



*Acknowledgment.* The authors wish to thank Professor Z. Rappoport for valuable discussions.

## References and Notes

- (1) (a) In partial fulfillment for the requirement for a Ph.D Degree. (b) A. Lifshitz, M. Frenklach, and A. Burcat, *J. Phys. Chem.*, **79**, 1148 (1975).
- (2) J. N. Bradley and K. O. West, *J. Chem. Soc., Faraday Trans.*, **71**, 967 (1975).
- (3) A. Lifshitz, K. Scheller, and A. Burcat in "Recent Developments in Shock Tube Research", Stanford University Press, Stanford, Calif., 1973, p 690.
- (4) A. Burcat, *Fuel*, **54**, 87 (1975).
- (5) Y. Sakakibara, *Bull. Chem. Soc. Jpn.*, **37**, 1262 (1964).
- (6) Y. Sakakibara, *Bull. Chem. Soc. Jpn.*, **37**, 1268 (1964).
- (7) J. N. Bradley, private communication.
- (8) S. S. Levush, S. S. Abadzhev, and V. U. Shvechuk, *Neftechimia*, **9**, 215 (1969).
- (9) H. Gg. Wagner and R. Zellner, *Ber. Bunsenges. Phys. Chem.*, **76**, 518 (1972).
- (10) H. Gg. Wagner and R. Zellner, *Ber. Bunsenges. Phys. Chem.*, **76**, 667 (1972).
- (11) A. Bar-Nun and A. Lifshitz, *J. Chem. Phys.*, **47**, 2878 (1967).
- (12) A. Lifshitz and P. Schechner, *Isr. J. Chem.*, **12**, 729 (1974).
- (13) F. D. Rossini et al., "Selected Values of Physical and Thermodynamic Properties of Hydrocarbons and Related Compounds", Carnegie Press, Pittsburgh, Pa., 1953.
- (14) D. A. Leathard and J. H. Purnell, *Proc. R. Soc. London, Ser. A*, **305**, 517 (1968).
- (15) S. W. Benson, *J. Chem. Educ.*, **42**, 502 (1965).
- (16) J. Collin and F. P. Lossing, *J. Am. Chem. Soc.*, **79**, 5848 (1957).
- (17) W. Tsang, *Int. J. Chem. Kinet.*, **2**, 23 (1970).
- (18) D. R. Stull and H. Prophet, *Natl. Stand. Ref. Data Ser., Natl. Bur. Stand.*, **No. 37** (1971).
- (19) H. Fisher in "The Chemistry of Alkenes", Interscience, S. Patai, Ed., New York, N.Y., 1964, p 1078.
- (20) P. J. Robinson and K. A. Holbrook, "Unimolecular Reactions", Wiley-Interscience, New York, N.Y., 1972, p 195.

## Ordered and Disordered Phases in Mixed Dodecylammonium and Hexadecylammonium Tetrachloromanganate(II)

Vincenzo Salerno, Andrea Grieco, and Michele Vacatello\*

Istituto Chimico dell'Università, Via Mezzocannone, 4-Naples, Italy (Received February 23, 1976)

Publication costs assisted by the National Research Council (CNR) of Italy

We studied the solid–solid order–disorder phase transitions in mixed tetrachloromanganate(II)'s of dodecyl- and hexadecylammonium. The low temperature crystal structure of the pure salts results from the piling of sandwiches in which a two-dimensional macroanion  $\text{MnCl}_4^{2-}$  is sandwiched between two alkylammonium layers. These latter become conformationally disordered in the high temperature phases. The crystallization products from ethanolic solutions of mixtures of the amines are heterogeneous materials containing the new mixed salt  $(n\text{-C}_{12}\text{H}_{25}\text{NH}_3)(n\text{-C}_{16}\text{H}_{33}\text{NH}_3)\text{MnCl}_4$  and the excess pure salt in their ordered phases. Heating these materials results in mixtures of conformationally disordered phases which mix giving conformationally disordered solid solutions in which alkylammonium ions of different length are randomly arranged on the macroanion's surfaces. These give on cooling conformationally ordered solid solutions in which the positional randomness is congealed.

### Introduction

We have recently shown that long chain alkylammonium tetrachloromanganate(II)'s, with the alkyl group greater than  $n\text{-C}_{10}\text{H}_{21}$ , exist at room temperature as a crystalline phase ( $\alpha$  phase) characterized by the presence of two-dimensional macroanions each sandwiched between two alkylammonium layers.<sup>1,2</sup> The overall crystal structure results from the piling of successive sandwiches (Figure 1).<sup>3</sup> All the compounds show solid–solid order–disorder phase transitions below 373 K, the high temperature form ( $\beta$  phase) being stable over very large temperature ranges.

The transition temperature decreases with decreasing chain length, so that the phase stable at room temperature for the nonylammonium salt is the  $\beta$  phase. The macroanions remain practically unchanged in the transitions, while the alkylammonium chains possess in the  $\beta$  phase a conformational freedom comparable with that possessed by  $n$ -alkane molecules in the melt.<sup>1,2,4</sup> The  $\beta$  phase is thus characterized by two-dimensional macroanions each sandwiched between two "liquidlike" alkylammonium layers.

Since we are interested in the study of the properties of these unusual disordered crystalline solids, we have investigated the products obtained from mixtures of different amines. We show in this work the results of a calorimetric and structural investigation of the products obtained from mixtures of varying amounts of dodecylamine and hexadecylamine.

### Experimental Section

Products were obtained by allowing hot ethanolic solutions of mixtures of the amines to react with the stoichiometric amount of concentrated  $\text{HCl}(\text{aq})$  and adding hot ethanolic solutions of  $\text{MnCl}_2 \cdot 6\text{H}_2\text{O}$ . The resulting solutions were concentrated by boiling and then allowed to cool to room temperature. The pink-white precipitates were filtered and dried in vacuo. Yields were practically quantitative.

The thermal behavior of the products was investigated by differential scanning calorimetry with a Perkin-Elmer DSC-1 apparatus at a scanning rate of  $16 \text{ K min}^{-1}$  in a  $\text{N}_2$  atmosphere. The temperature scale was calibrated by using pure

reference compounds. The transition enthalpies were obtained using as a reference standard a sample of pure indium ( $\Delta h = 28.5 \text{ J g}^{-1}$ ). X-ray diffraction patterns on compacted samples of the powders were taken by reflection and transmission with a Philips diffractometer using the  $\text{Fe K}\alpha$  radiation. High temperature powder diffraction patterns were taken with an oil-heated apparatus whose details will be described elsewhere.

### Results

Products were prepared as described in the previous section from mixtures of amines containing various mole fractions of hexadecylamine ( $x_{16}$ ). All the products show solid–solid phase transitions in the temperature range 310–370 K. Figure 2 shows some typical heating thermograms. Thermograms of the pure dodecylammonium and hexadecylammonium salts are also shown. These are always reproducible, both in temperature and enthalpy, after heating and cooling cycles throughout the transition points. This is not the case for the mixed products. Figure 3 shows some typical reheating thermograms. No further variations are observed after a second heating and cooling cycle. We report in Table I transition temperatures, enthalpies, and entropies (values per mole of metal atoms) as obtained from heating (a) and reheating (b) scans.

X-ray diffraction patterns were taken by reflection and transmission at room temperature both for freshly prepared products and for products heated above the transition point and then cooled. As already observed<sup>1,2</sup> the platelike crystallites are predominantly oriented in such a way as to have the planes of the macroanions parallel to the surface of the sample holder. The prominent feature of the resulting x-ray diffraction patterns obtained by reflection is a series of reflections from planes which are parallel to the macroanion surfaces ( $00l$  reflections). The maxima observed in the diffraction patterns of thermally treated products are associated to a unique interplanar spacing, while in the diffraction patterns of freshly prepared products two distinct sets of  $00l$  reflections can be generally observed. In the case of the product containing equimolar amounts of the two amines a unique series of  $00l$  reflections is observed also for the freshly pre-

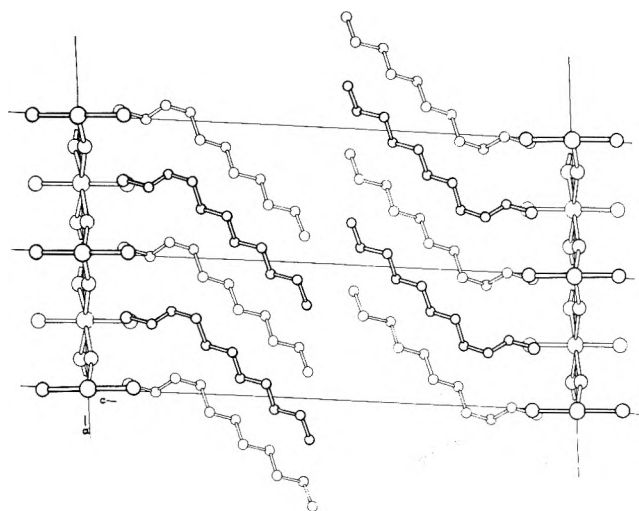


Figure 1. View of the layer structure of  $(n\text{-C}_n\text{H}_{2n+1}\text{NH}_3)_2\text{MnCl}_4$  with  $n = 10$  in the  $\alpha$  phase.

pared product. Table II shows the interplanar spacings deduced from the diffraction patterns taken by reflection of the freshly prepared products ( $c$ ) and of the thermally treated products ( $c'$ ).

X-ray diffraction patterns were also taken by reflection and transmission at a temperature of 383 K. Also in this case series of  $00l$  reflections associated to a unique interplanar spacing can be observed by reflection. Table II lists the interplanar spacings ( $c''$ ) deduced from these patterns. Figures 4 and 5 show typical diffraction patterns obtained by reflection and transmission at room temperature and 383 K when  $x_{16} = 0$ ,  $x_{16} = 0.5$ , and  $x_{16} = 1$ .

### Discussion

Table II shows that the crystallization product from ethanolic solutions containing various mole fractions of the amines is a heterogeneous material, except when  $x_{16} = 0.5$ . In this latter case the product is the mixed compound  $(n\text{-C}_{12}\text{H}_{25}\text{NH}_3)(n\text{-C}_{16}\text{H}_{33}\text{NH}_3)\text{MnCl}_4$ . The crystallization products obtained when  $x_{16} < 0.5$  are mixtures of crystals of this mixed salt and of the pure  $\alpha$  phase dodecylammonium salt, while the products obtained when  $x_{16} > 0.5$  are mixtures of the mixed salt and of the pure  $\alpha$  phase hexadecylammonium salt. The interplanar spacing characteristic of the mixed salt

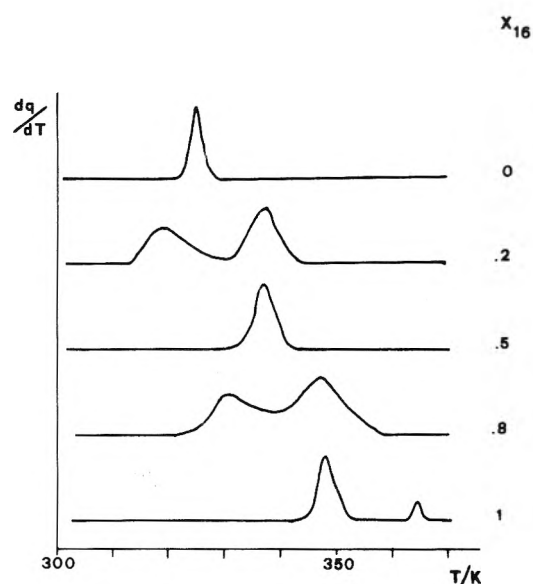


Figure 2. Typical heating thermograms of freshly prepared products with various  $x_{16}$ .

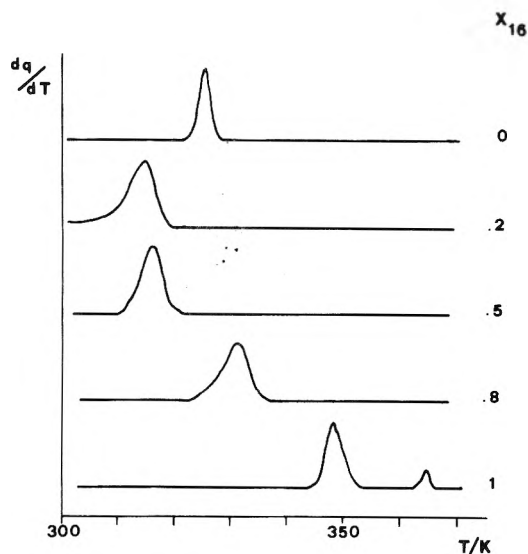


Figure 3. Typical heating thermograms of thermally treated products with various  $x_{16}$ .

TABLE I: Transition Temperatures, Enthalpies, and Entropies of Freshly Prepared Products (a) and Thermally Treated Products (b) per Mole of Metal Atom <sup>a</sup>

$x_{16}$	(a)			(b)		
	$T/\text{K}$	$\Delta H/\text{kJ mol}^{-1}$	$\Delta S/\text{J K}^{-1} \text{mol}^{-1}$	$T/\text{K}$	$\Delta H/\text{kJ mol}^{-1}$	$\Delta S/\text{J K}^{-1} \text{mol}^{-1}$
0	324	41	127	324	41	127
0.1	318-334	38	119	313	33	105
0.2	318-336	45	134	313	31	102
0.3	318-337	48	143	312	38	122
0.4	315-335	48	143	314	43	137
0.5	337	46	136	313	40	127
0.6	335-344	51	152	314	35	111
0.7	335-344	53	158	313	47	137
0.8	331-347	53	158	341	46	135
0.9	332-347	64	183	341	52	153
1	348	69	198	348	69	198

<sup>a</sup> Evaluated error on enthalpy and entropy values was 5%.

TABLE II: Interlayer Distances as Obtained from X-Ray Powder Diffraction Patterns Taken by Reflection<sup>a</sup>

$x_{16}$	$c/\text{\AA}$	$c'/\text{\AA}$	$c''/\text{\AA}$
0	30.28(5)	30.28(5)	33.4(1)
0.1	30.3(1)	30.3(1)	33.7(2)
0.2	30.3(1) 33.3(2)	33.3(2)	35.0(2)
0.3	30.3(2) 33.3(1)	33.5(3)	36.2(3)
0.4	30.3(2) 33.3(1)	33.3(2)	36.8(2)
0.5	33.3(1)	33.7(2)	37.2(2)
0.6	33.3(1) 36.7(2)	34.8(2)	37.9(2)
0.7	33.3(2) 36.7(2)	36.7(3)	39.2(3)
0.8	33.3(3) 36.7(1)	37.2(3)	40.2(2)
0.9	36.7(1)	36.7(2)	40.9(2)
1	36.71(5)	36.71(5)	41.8(1)

<sup>a</sup> Evaluated error on the last digit in parentheses. Room temperature data for freshly prepared ( $c$ ) and thermally treated ( $c'$ ) products and high temperature ( $T = 383$  K) data ( $c''$ ).

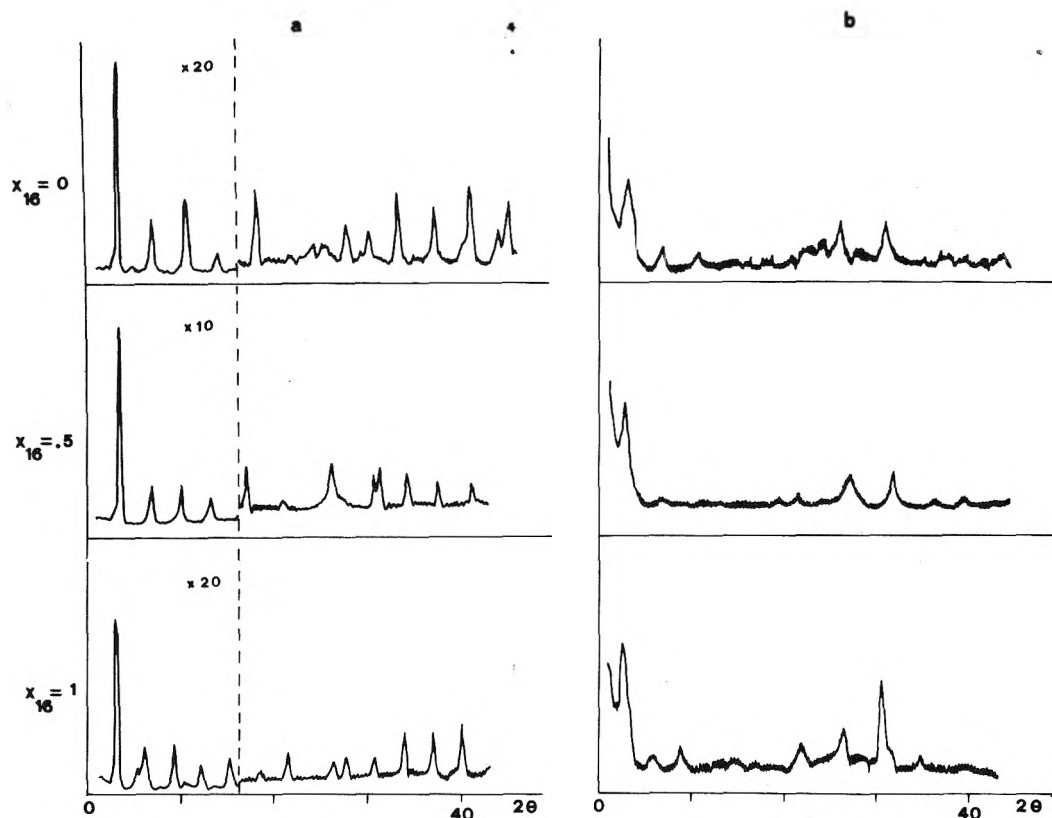


Figure 4. Room temperature reflection (a) and transmission (b) x-ray powder diffraction patterns obtained when  $x_{16} = 0$ ,  $x_{16} = 0.5$  (freshly prepared product), and  $x_{16} = 1$ . Fe  $K\alpha$  radiation, Mn filter.

is 33.3 Å, intermediate between the spacings of the pure salts in their  $\alpha$  phases. The analysis of the reflection intensities shows that the relative amount of the mixed salt increases with increasing  $x_{16}$  when  $x_{16} < 0.5$ . The reverse is true when  $x_{16} > 0.5$ . These observations show that no solid solution among alkylammonium chains of different length can be obtained directly by crystallization.

Heating the crystallization mixtures results in solid–solid phase transitions which are associated with very large entropic effects, intermediate between those observed for the order–disorder solid–solid phase transitions of the pure dodecylammonium and hexadecylammonium salts (Table I). The entropy change increases with increasing  $x_{16}$ , that is with increasing mean number of conformationally flexible chain

bonds. These facts, and the presence of a typical amorphous halo<sup>4</sup> in the high-temperature x-ray diffraction patterns taken by transmission (Figure 5), show that also in this case the transitions observed are of the order–disorder kind, with the alkyl chains in a “liquidlike” state in the  $\beta$  disordered forms. Table II shows moreover that the phase transitions are also associated with the formation of a true solid solution among chains of different length on the macroanion’s surfaces. In fact a unique interplanar spacing  $c''$ , always uniformly increasing with increasing  $x_{16}$ , can be observed.

A further support in favor of this hypothesis is found in the fact that cooling the disordered phase results at room temperature in a new phase. This new  $\alpha'$  phase is essentially ordered from the conformational point of view, as is shown by

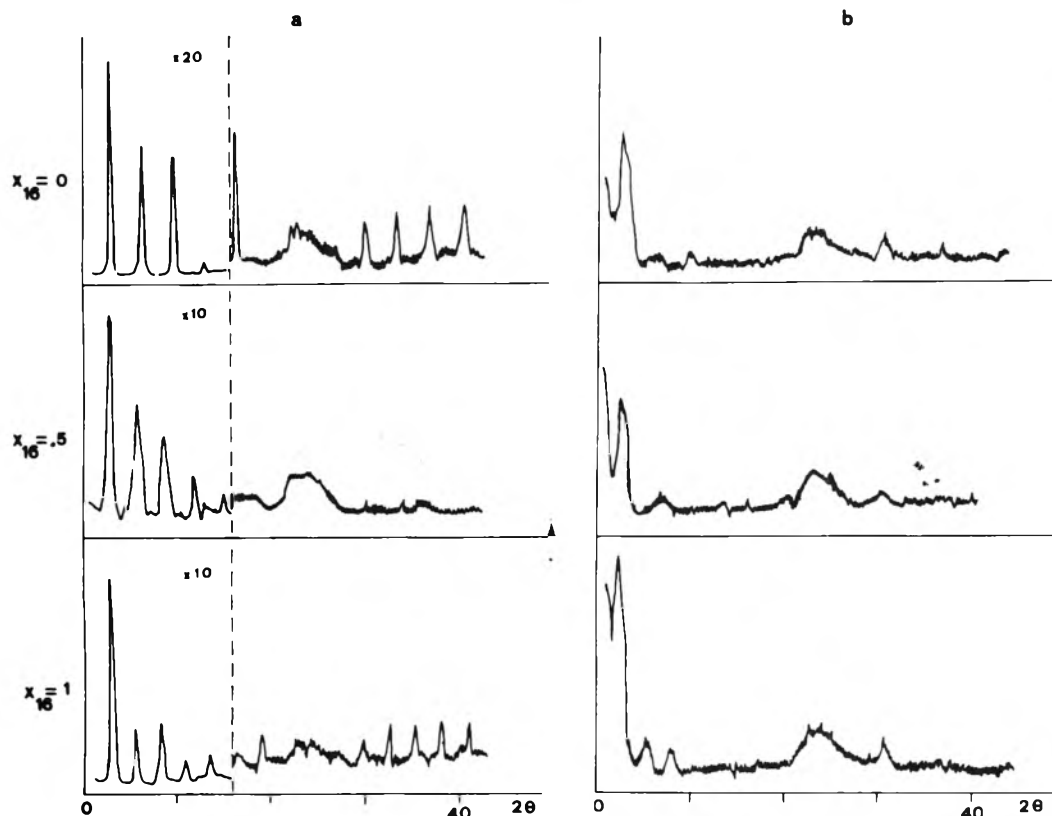


Figure 5. Reflection (a) and transmission (b) x-ray powder diffraction patterns obtained at 383 K when  $x_{16} = 0$ ,  $x_{16} = 0.5$ , and  $x_{16} = 1$ . Fe  $K\alpha$  radiation, Mn filter.

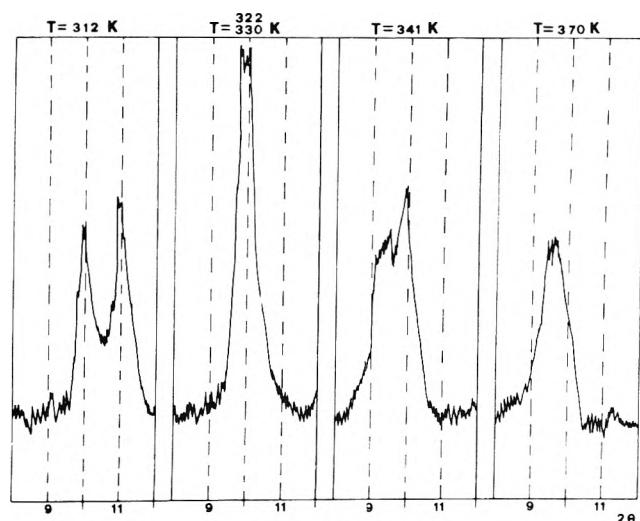


Figure 6. Part of the x-ray powder diffraction pattern obtained by reflection when  $x_{16} = 0.2$  (freshly prepared product), taken at various increasing temperatures, showing the temperature behavior of the 003 reflection. Fe  $K\alpha$  radiation, Mn filter. Mean heating rate:  $0.6 \text{ K min}^{-1}$ .

the high entropy changes of Table I (last column), which increase with increasing  $x_{16}$ . However, a unique interplanar spacing  $c'$ , roughly increasing with increasing  $x_{16}$ , is observed also in this case. A possible explanation of these facts may be found in the assumption that cooling the disordered solid solution results in the "freezing in" of the positional disorder, yielding the  $\alpha'$  phase, which is essentially ordered from the conformational point of view, but positionally disordered.

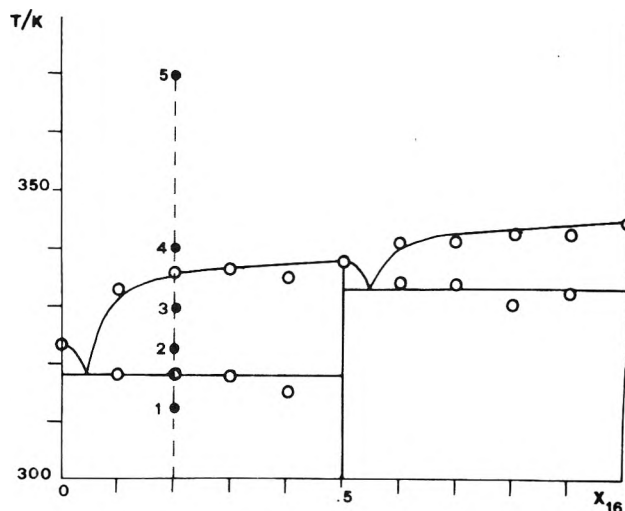


Figure 7. Approximate phase diagram of the system  $(n\text{-C}_{12}\text{H}_{25}\text{-NH}_2)_2\text{MnCl}_4\text{-(}n\text{-C}_{16}\text{H}_{33}\text{NH}_2)_2\text{MnCl}_4$ .

Figure 7 shows an approximate phase diagram derived from the data of Table Ia in the hypothesis that the thermograms describe equilibrium situations. This is, however, not the case. In fact an examination of Figure 6 shows that the thermograms do not really describe equilibrium situations, the mixing rate among alkylammonium ions from  $\beta$  phases of different composition being slow. Figure 6 can be rationalized as follows. At temperatures lower than the eutectic point the system contains the pure dodecylammonium salt and the mixed salt in their  $\alpha$  phase (point 1 of Figure 7). At temperatures intermediate between the eutectic point and the transition point

of the mixed salt the system contains a  $\beta$  phase very similar to the pure dodecylammonium salt and the mixed salt in its  $\alpha$  phase, with a slow dissolution rate of the latter in the first (points 2 and 3 of Figure 7). At temperatures beyond the transition point of the mixed salt the system contains two  $\beta$  phases of different composition which mix at a rate increasing with increasing temperature (point 4 of Figure 7). Figure 6 shows in fact in the latter case two different maxima whose separation tends to vanish, so that at temperatures beyond 370 K (point 5 of Figure 7) a unique intermediate reflection maximum can be observed. A slow mixing rate among alkylammonium ions from different solid phases is, however, not surprising.

In conclusion, we can try to justify the data shown in the previous sections as follows. The crystallization product from ethanolic solutions when  $x_{16} \neq 0.5$  is a heterogeneous material containing the mixed salt and the excess pure salt in their  $\alpha$  phases. Heating these products results at first in a mixture of two  $\beta$  phases of different composition. If enough time is allowed or the temperature is raised, the  $\beta$  phases can mix

thoroughly giving a true conformationally disordered solid solution in which chains of different length are randomly arranged on the macroanion's surfaces. Cooling this disordered solid solution results in the  $\alpha'$  phase, in which the positional randomness is congealed. The  $\alpha'$  phase is thus a conformationally ordered solid solution. When  $x_{16} = 0.5$  only the mixed salt is obtained by crystallization. Also in this case, however, heating results in a disordered solid solution which gives on cooling the corresponding  $\alpha'$  phase.

*Acknowledgment.* We thank Professor Paolo Corradini for many helpful discussions. We are grateful to the C.N.R. of Italy for financial assistance.

## References and Notes

- (1) M. Vacatello and P. Corradini, *Gazz. Chim. Ital.*, **103**, 1027 (1973).
- (2) M. Vacatello and P. Corradini, *Gazz. Chim. Ital.*, **104**, 773 (1974).
- (3) M. R. Ciajolo, P. Corradini, and V. Pavone, *Gazz. Chim. Ital.*, in press.
- (4) C. Carfagna, M. Vacatello, and P. Corradini, to be submitted for publication.

## Infrared and Nuclear Magnetic Resonance Studies of Hydrogen Bonding in Aliphatic Alcohol Systems

J. L. Kirsch\* and D. R. Coffin<sup>1</sup>

Department of Chemistry, Butler University, Indianapolis, Indiana 46208 (Received April 6, 1976)

Publication costs assisted by the Department of Chemistry, Butler University

In this study the concentration dependence of NMR chemical shifts of hydroxyl protons and ir absorption area ratios of the hydroxyl vibration are related to the molecular geometry at the hydroxyl site and the extent of the hydrogen bonding in the system.

### Introduction

Hydrogen bonding is an important factor in determining physical and chemical properties of many classes of compounds. The extent of hydrogen bonding which exists in a given system depends on many molecular parameters. Molecular geometry at the hydrogen bonding site can be a major contribution to the hydrogen bonding for many classes of compounds.

Infrared and nuclear magnetic resonance spectroscopy can be used to study the hydrogen bonding phenomenon. Little quantitative correlation between data obtained from these spectroscopic techniques and the extent of hydrogen bonding in a series of similar compounds has been reported.<sup>2-6</sup>

In this study the concentration dependence of NMR chemical shifts of hydroxyl protons and ir absorption area ratios of the hydroxyl vibration are related to the molecular geometry at the hydroxyl site and the extent of the hydrogen bonding in the system. This study is carried out on a series of aliphatic alcohols.

### Experimental Section

*Infrared Spectroscopy.* Carbon tetrachloride solutions of selected alcohols were prepared in a concentration range of

0.3 to 3.2 mass %. Spectra were obtained at room temperature on a Perkin-Elmer 567 infrared spectrometer using the x5 abscissa expansion over the range of 3700 to 3000  $\text{cm}^{-1}$ . A variable path length cell was used to adjust the percent transmission to minimum or 10%, whichever was largest. The appropriate base lines were chosen and the areas under the absorption peaks were determined with a compensating polar planimeter.

*NMR Spectroscopy.* Carbon tetrachloride solutions of selected alcohols were prepared in a concentration range of 0.3 to 3.2 mass % with 3% TMS internal standard. Spectra were obtained on a Perkin-Elmer R32 NMR spectrometer at 35 °C using the internal lock mode. The chemical shifts of the hydroxyl protons were measured using a 300-Hz sweep range. Assignment of the hydroxyl proton line was made by shaking with  $\text{D}_2\text{O}$ .

### Discussion and Results

Alcohols in the pure state exist in a high degree of association. This association is caused by hydrogen bonding at the hydroxyl site. If an alcohol is placed in a noninteracting solvent such as carbon tetrachloride, the extent of hydrogen bonding is concentration dependent. At low concentrations

TABLE I

2-Methyl-2-propanol		2-Methyl-2-butanol		3-Methyl-3-pentanol		3-Ethyl-3-pentanol		1-Butanol	
$\rho$	Concn	$\rho$	Concn	$\rho$	Concn	$\rho$	Concn	$\rho$	Concn
10.30	2.03 <sup>a</sup>	9.47	3.09 <sup>a</sup>	5.16	2.96	3.06	3.06	15.20	2.00 <sup>a</sup>
9.50	1.61 <sup>a</sup>	8.60	2.59 <sup>a</sup>	4.49	2.54	2.44	2.53	13.69	1.63
6.58	1.00	7.48	2.07	3.61	2.08	1.91	2.02	8.98	1.04
5.02	0.733	5.83	1.52	2.43	1.53	1.25	1.46	3.87	0.564
2.32	0.505	3.06	1.04	1.52	0.973	0.805	1.05	1.15	0.327
1.45	0.332	1.16	0.510	0.582	0.522	0.284	0.505		
		0.445	0.287	0.353	0.355	0.204	0.312		

3,5,5-Trimethyl-1-hexanol		2-Ethyl-1-hexanol		4-Methyl-2-pentanol		3-Pentanol		2-Methyl-3-pentanol	
$\rho$	Concn	$\rho$	Concn	$\rho$	Concn	$\rho$	Concn	$\rho$	Concn
11.81	3.00	9.94	3.00	12.46	3.06 <sup>a</sup>	8.99	3.01	5.56	2.98
9.48	2.53	9.16	2.75	10.96	2.56	7.52	2.56	4.49	2.54
7.84	2.02	8.33	2.57	8.42	2.00	6.07	1.94	3.31	1.99
5.94	1.56	6.92	2.11	6.41	1.53	4.56	1.45	2.16	1.48
3.21	1.21	4.66	1.57	3.45	0.965	2.62	0.965	1.18	1.04
0.520	0.502	2.70	1.13	0.968	0.503	0.704	0.460	0.482	0.530 <sup>a</sup>
0.383	0.342 <sup>a</sup>	0.593	0.516	0.486	0.376	0.334	0.285	0.211	0.309 <sup>a</sup>
		0.360	0.354						

<sup>a</sup> These data are not in the linear portion of the sigmoid curve and are not used to compute the least-squares slope.

TABLE II

2-Methyl-2-propanol		2-Methyl-2-butanol		3-Methyl-3-pentanol		3-Ethyl-3-pentanol		1-Butanol	
$\Upsilon$	Concn	$\Upsilon$	Concn	$\Upsilon$	Concn	$\Upsilon$	Concn	$\Upsilon$	Concn
7.92	2.06	8.16	3.28 <sup>a</sup>	8.77	3.08	9.07	2.95	7.18	2.39 <sup>a</sup>
8.17	1.77	8.36	2.61	8.87	2.57	9.11	2.56	7.42	1.94 <sup>a</sup>
8.31	1.45	8.58	2.04	8.89	2.05	9.18	2.06	7.69	1.59
8.66	0.961	8.79	1.48	9.08	1.52	9.24	1.49	8.01	1.26
9.01	0.488	8.98	1.05	9.19	0.972	9.29	1.00	8.24	1.03
9.07	0.380	9.17	0.541	9.26	0.562	9.34	0.511	8.92	0.508
		9.24	0.301 <sup>a</sup>	9.31	0.304			9.11	0.327

3,5,5-Trimethyl-1-hexanol		2-Ethyl-1-hexanol		4-Methyl-2-pentanol		3-Pentanol		2-Methyl-3-pentanol	
$\Upsilon$	Concn	$\Upsilon$	Concn	$\Upsilon$	Concn	$\Upsilon$	Concn	$\Upsilon$	Concn
7.92	3.01	8.02	3.03	7.89	2.98 <sup>a</sup>	8.00	3.03	8.42	3.04
8.16	2.49	8.20	2.58	8.07	2.53	8.16	2.60	8.56	2.58
8.39	2.03	8.48	1.98	8.30	2.05	8.37	2.04	8.68	2.06
8.74	1.41	8.72	1.50	8.59	1.49	8.63	1.45	8.82	1.45
8.94	1.08	8.98	1.01	8.85	1.03	8.84	0.941	8.92	1.04
9.21	0.495	9.18	0.506	9.18	0.301	8.92	0.504 <sup>a</sup>	9.02	0.501
9.26	0.342 <sup>a</sup>	9.24	0.322			8.93	0.334 <sup>a</sup>		

<sup>a</sup> These data are not in the linear portion of the sigmoid curve and are not used to compute the least-squares slope.

little hydrogen bonding exist. The exact nature of the molecular species in the solution has been discussed in a number of papers in the literature.<sup>7-9</sup>

The major contribution to the extent of hydrogen bonding in aliphatic alcohols is the molecular geometry at the hydroxyl site. The extent of hydrogen bonding at a given concentration decreases as the steric hindrance at the hydroxyl site increases. The extent of the hydrogen bonding and its dependence on molecular geometry in a series of aliphatic alcohols can be

demonstrated quantitatively by concentration dependence studies.

The concentration dependence of the extent of hydrogen bonding depends on the accessibility of the hydroxyl group to interacting with the hydroxyl group on other neighboring solute molecules. As the steric hindrance at the hydroxyl site increases, the interaction with other solute molecules and the sensitivity to changes in the molecular environment of the solute molecule decreases. These effects cause the concen-

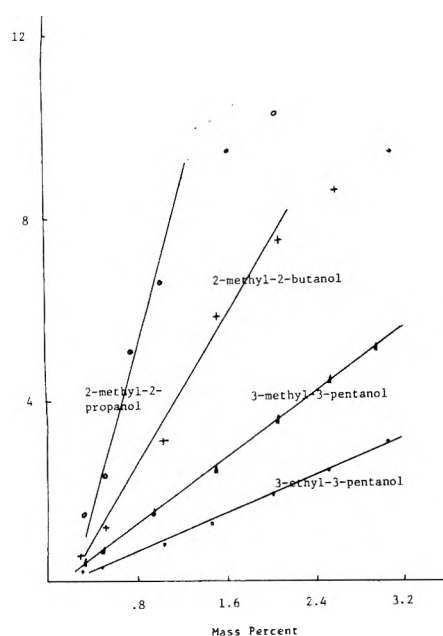


Figure 1.

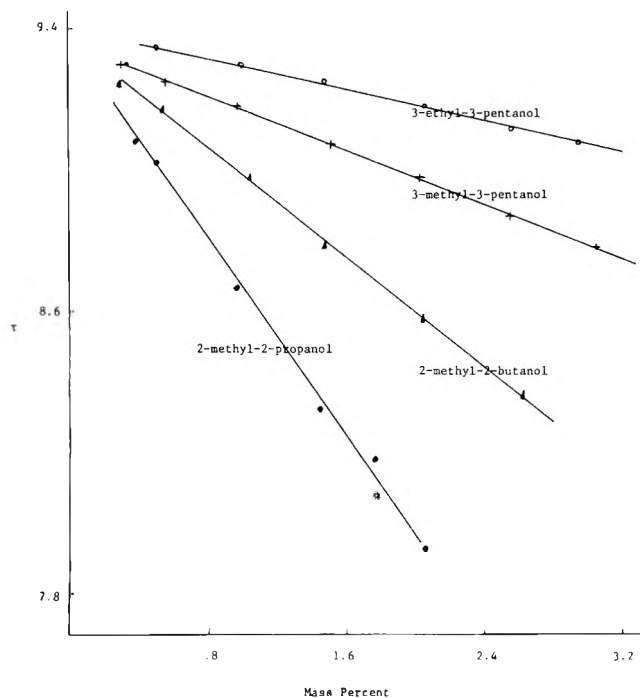


Figure 2.

tration dependence of the extent of the hydrogen bonding to decrease as the steric hindrance of the hydroxyl site increases. The extent of hydrogen bonding effects the nature of both the infrared and NMR spectrum of the alcohol solutions.

The infrared spectrum of aliphatic alcohols in noninteracting solvents at low concentrations contains a sharp peak near  $3600\text{ cm}^{-1}$  and a broad peak at near  $3300\text{ cm}^{-1}$ . The broad peak is associated with a hydroxyl stretching vibration in a hydrogen bonding environment (polymer band). The sharp peak originates from a hydroxyl stretching vibration in a nonhydrogen bonding environment (monomer band). The ratio of the intensities of these two bands is a quantitative measure of the extent of hydrogen bonding in the solution.

TABLE III

	Slope	( $\rho$ vs. %)	Slope	( $\Upsilon$ vs. %)
<b>Tertiary alcohols</b>				
2-Methyl-2-propanol	8.11	(0.988) <sup>a</sup>	-0.678	(0.998)
2-Methyl-2-butanol	4.11	(0.995)	-0.393	(0.999)
3-Methyl-3-pentanol	1.88	(0.999)	-0.195	(1.000)
3-Ethyl-3-pentanol	1.06	(0.998)	-0.112	(0.999)
<b>Secondary alcohols</b>				
4-Methyl-2-pentanol	4.85	(0.999)	-0.505	(0.999)
3-Pentanol	3.21	(0.997)	-0.404	(0.999)
2-Methyl-3-pentanol	2.24	(1.000)	-0.235	(0.998)
<b>Primary alcohols</b>				
1-Butanol	9.62	(0.996)	-1.15	(0.998)
3,5,5-Trimethyl-1-hexanol	4.54	(0.995)	-0.524	(0.999)
2-Ethyl-1-hexanol	3.74	(0.999)	-0.463	(0.999)

<sup>a</sup> Correlation coefficient.

Table I gives the ratios ( $\rho$ ) of the polymer band to the monomer band as a function of concentration for each alcohol. Selected plots of  $\rho$  vs. concentration are given in Figure 1. These plots show the general nature of  $\rho$  vs. concentration for all the alcohols studied.

The NMR spectrum of the aliphatic alcohols in noninteracting solvents is characterized by one hydroxyl proton line whose chemical shift is concentration dependent. The one line results from the rapid molecular exchange of the hydroxyl protons between all of the various hydrogen bonded species in the solution. The value of the chemical shift of the hydroxyl proton is a mole fraction weighted function of the chemical shift of each hydrogen bonded species

$$\delta_{\text{OH}} = \sum_i \chi_i \delta_i \quad i = \text{monomer, dimer, tetramer, } \dots$$

$$\Upsilon_{\text{OH}} = 10 - \delta_{\text{OH}}$$

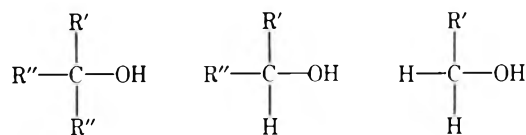
Table II gives the chemical shift of the hydroxyl proton as a function of concentration for each alcohol. Selected plots of  $\Upsilon$  vs. concentrations are given in Figure 2. These plots show the general dependence of  $\Upsilon$  on concentration for all the alcohols in this study.

A large value of  $\rho$  and a small value of  $\Upsilon_{\text{OH}}$  indicates a large extent of hydrogen bonding in the solution. As the concentration of the alcohol in the noninteracting solvent decreases, the extent of hydrogen bonding decreases,  $\rho$  decreases, and  $\Upsilon$  increases. The concentration dependence of  $\rho$  and  $\Upsilon$  over a large concentration is sigmoid in nature. The linear portion of the sigmoid curves (approximately 0.3–3.2%) is characteristic of a major transformation from associated alcohols to unassociated alcohols. In this study the slopes of the  $\rho$  vs. concentration and  $\Upsilon_{\text{OH}}$  vs. concentration in the linear portion of the sigmoid curves are used as the measure of the sensitivity of the alcohol molecule to changes in the hydrogen bonding environment. A small absolute value for these slopes indicates a small dependence of the extent of hydrogen bonding on concentration. These small values of the slopes are characteristic of alcohol molecules with the hydroxyl group in a sterically hindered site. A large steric hindrance at the hydroxyl site decreases the sensitivity of the hydroxyl group to the molecular environment and, therefore, changes in the molecular environment.

A least-squares computer program was used to compute the slope of the best straight line through the  $\rho$  and  $\Upsilon_{\text{OH}}$  vs. concentration data in the linear region. These slopes are listed for each alcohol in Table III. The absolute values of the correla-

tion coefficients for all computed slopes were 0.98 or greater.

The alcohols in this study are arranged in three groups in Table III (primary, secondary, and tertiary).



The tertiary series is characterized by variation of the three R groups (three methyls; two methyls, one ethyl; one methyl, two ethyls; and three ethyls). The primary and secondary series vary in the length and complexity of the R groups. Table III, Figure 1, and Figure 2 show that as the length and complexity of the R groups increase, the steric hindrance at the

hydroxyl site increases, the sensitivity to changes in the molecular environment of the alcohol decreases, and the absolute values of the slopes of the concentration dependencies of  $\rho$  and  $\Upsilon$  decreases.

## References and Notes

- (1) Submitted as partial fulfillment of the requirements for Master of Science Degree.
- (2) N. D. Coggeshall, *J. Am. Chem. Soc.*, **69**, 1620 (1947).
- (3) F. A. Smith and E. C. Creitz, *J. Res. Natl. Bur. Stand.*, **46** (2), 145 (1951).
- (4) V. I. Malyshev and M. V. Shiskina, *Zh. Eksp. Teor. Fiz.*, **20**, 297 (1950).
- (5) V. I. Malyshev and M. V. Shiskina, *Dokl. Akad. Nauk SSSR*, **66**, 833 (1949).
- (6) R. Konopka, B. Pedzisz, and M. Jurewicz, *Acta Phys. Polon.*, **40**, (6), 751 (1971).
- (7) H. C. Van Ness et al., *J. Phys. Chem.*, **71**, 1483 (1967).
- (8) E. D. Becker, U. Liddel, and J. N. Shoolery, *J. Mol. Spectrosc.*, **2**, 1 (1958).
- (9) W. L. Chandler and R. H. Dinius, *J. Phys. Chem.*, **73**, 1596 (1969).

## Enthalpy and Entropy of Transfer of Lithium Halides between Water and Long-Chain Alcohols

Y. Marcus

Department of Inorganic and Analytical Chemistry, The Hebrew University of Jerusalem, Jerusalem, Israel (Received March 16, 1976)

The thermodynamic functions of transfer of lithium halides between immiscible water and long-chain alcoholic solutions have been reconsidered in terms of an effective infinitely dilute standard state of the latter, where the solute is completely ion paired, but no further solute-solute interactions occur. A further consideration of the saturated solution standard state shows its advantages. The earlier conclusion that the transfer is entropy controlled is confirmed, and interpreted in terms of detailed enthalpy- and entropy-level diagrams, and the effects that lead to the various terms.

### Introduction

In recent papers<sup>1,2</sup> the thermodynamics of the extraction of lithium bromide from aqueous into 2-ethylhexanolic solutions and the molar volumes of lithium halides in alcohols were reported. The ion pairing of the lithium halide salts was found to be an important factor, and this permits now a more detailed interpretation of the distribution data and the heat effect. In particular, the approach<sup>3a</sup> found effective for the interpretation of the thermodynamics of the distribution equilibrium of dioxouranium(VI) nitrate between aqueous and tri-*n*-butylphosphate solutions can now be applied to the transfer of lithium halides from aqueous to long-chain alcoholic solutions.

One important consideration in the interpretation is that the distribution reaction<sup>1</sup>



is *entropy controlled*, that is, that the contribution of  $-T\Delta S^\circ$  to the standard Gibbs free energy of reaction 1 is considerably larger than that of  $\Delta H^\circ$ . The standard state here is that of infinite dilution, defined as usual for the aqueous phase by

$$\mu^\circ_{\text{LiX}(m)} = \lim_{(m \rightarrow 0)} (\mu_{\text{LiX}} - 2RT \ln m_{\text{LiX}}) \quad (2)$$

on the molal scale.

The standard state of infinite dilution in the alcohol cannot be approached practically, that is, no distribution data can be obtained at such low concentrations that the lithium salt is completely dissociated in the organic phase. Therefore an effective standard state is defined for the organic solutions (designated by superscript degree and prime), where the salt is completely ion paired, but where no solute-solute interaction occurs between these ion pairs. Operationally, this is defined by

$$\bar{\mu}^{\circ'}_{\text{LiX}(m)} = \lim_{(\bar{m} \rightarrow 0)} [\bar{\mu}_{\text{LiX}} - RT \ln \bar{m}] \quad (3)$$

and the corresponding Gibbs free energy of transfer, reaction 1, is  $\Delta G^{\circ'}_{\text{tr}(m)} = \bar{\mu}^{\circ'}_{\text{LiX}(m)} - \mu^\circ_{\text{LiX}(m)}$ . This can be transformed into the corresponding unitary quantity:

$$\Delta G^{\circ'}_{\text{tr}(x)} = \Delta G^{\circ'}_{\text{tr}(m)} - 2 \ln (\text{mol of water/kg}) + \ln (\text{mol of solvent/kg}) \quad (4)$$

The extrapolation to zero concentration leading via eq 2 and 3 to  $\Delta G^{\circ'}_{\text{tr}(x)}$  is considered more reliable than that made<sup>1</sup> leading to  $\Delta G^\circ_{\text{tr}(x)}$  (for complete dissociation at infinite dilution), since the linear dependence of  $\log \bar{m}_{\text{LiBr}}/m_{\text{LiBr}} \gamma_{\pm \text{LiBr}}$  on  $\bar{m}_{\text{LiBr}}$  observed in the range of measurements need not hold at the extremely low concentrations required for complete dissociation in the organic phase.

TABLE I: Solubility of Lithium Chloride in 1-Hexanol<sup>a</sup>

T, K	293.2	298.2	303.2	308.2	313.2	318.2	323.2	328.2
wt % LiCl	8.55 <sub>0</sub>	8.38 <sub>5</sub>	8.35 <sub>5</sub>	8.35 <sub>5</sub>	8.23 <sub>0</sub>	8.06 <sub>0</sub>	7.95 <sub>5</sub>	7.88 <sub>5</sub>
$\bar{m}_{\text{LiCl(satd)}}$	2.205	2.158	2.150	2.150	2.115	2.068	2.038	2.019

<sup>a</sup> Reference 4a.TABLE II: Concentrations in Aqueous and 2-Ethylhexanolic Solutions of Lithium Bromide in Equilibrium<sup>a</sup> Relative to the Saturated Solutions (*s* Scale) at 298.15 K

$m_{\text{LiBr}}$	$s\sigma_{\pm}$	$\bar{m}_{\text{LiBr}}$	$\log \bar{m}/s^2\sigma_{\pm}^2$	$\bar{s}$	$\bar{m}_{\text{H}_2\text{O}}$	$\bar{\sigma}$
9.98	0.0293	0.503	2.768	0.290	1.364	4017
10.11	0.0341	0.413	2.550	0.238	1.290	3613
11.23	0.0572	0.468	2.155	0.270	1.185	1132
11.31	0.0635	0.840	2.319	0.485	0.877	511
13.33	0.1728	0.990	1.521	0.571	0.727	59
15.41	0.3868	1.252	0.923	0.722	0.466	9.3
16.85	0.6132	1.538	0.612	0.888	0.181	2.8
(17.88)	(1.0000)	(1.73 ± 0.02)	(0.238)	(1.000)	(0.00)	(1.0)

<sup>a</sup> Reference 1.

Entropy control extends up to saturated solutions, where a new standard state can be defined, designated by superscript *s*, and where necessarily  $\Delta G_{\text{tr}}^s = 0$ , so that  $\Delta S_{\text{tr}}^s = \Delta H_{\text{tr}}^s/T$ . In this way the standard entropy change is obtained directly from heat change data, without the necessity for equilibrium data. The saturated solution as a reference state was already discussed by Milicevic,<sup>3b</sup> who pointed out the usefulness of this concept for partition equilibria. In the present case, a practical further advantage of the new standard state is the practical exclusion of water from the alcoholic solutions at saturation, so that the system becomes simpler.

The new concentration scale  $s = m_{\text{LiX}}/m_{\text{LiX(satd)}}$  is introduced, with its activity coefficient  $\sigma_{\pm} = \gamma_{\pm\text{LiX}}/\gamma_{\pm\text{LiX(satd)}}$ . The standard chemical potential on this scale is for the aqueous phase

$$\mu_{\text{LiX}}^s = \lim (s \rightarrow 1) [\mu_{\text{LiX}} - 2RT \ln s] \quad (5)$$

while for the organic phase, where complete association to ion-paired electrolyte occurs

$$\bar{\mu}_{\text{LiX}}^s = \lim (\bar{s} \rightarrow 1) [\bar{\mu}_{\text{LiX}} - RT \ln \bar{s}] \quad (6)$$

Obviously,  $\bar{\mu}_{\text{LiX}}^s - \mu_{\text{LiX}}^s = \Delta G_{\text{tr}}^s = 0$  and

$$K^s \equiv \bar{s}\bar{\sigma}/s^2\sigma_{\pm}^2 = 1 \quad (7)$$

which permits the evaluation of  $\bar{\sigma}$  from distribution data at high concentrations.

Some solubility measurements on lithium chloride and bromide in hexanol and 2-ethylhexanol were made in order to complement the thermodynamic information on these systems. Some information on the distribution of lithium chloride between water and 1-hexanol was also obtained.<sup>4b</sup>

### Experimental Section

Experiments were made<sup>4a</sup> to determine the solubility of lithium chloride and bromide in 1-hexanol and 2-ethylhexanol over a range of temperatures. Excess solid *anhydrous* salts were shaken with dry solvents in a bath regulated to  $\pm 0.2$  K for 1–3 days until consecutive sampling showed constant concentration (on a weight basis). The standard Mohr method was used for analysis of the chloride and the bromide, after mixing the alcoholic solutions with a large quantity of water, the accuracy being  $\pm 0.3\%$  for triplicate determinations. The

other results quoted in this paper are taken from ref 1, where the experimental procedures are described.

### Results

The solubility of lithium chloride in 1-hexanol was obtained at eight evenly spaced temperatures between 293.2 and 328.2 K, shown in Table I. The interpolated value for the standard temperature of 298.15 K,  $2.177 \pm 0.003 m$ , is more accurate than the direct determination at this single temperature.

Saturated solutions of lithium bromide in 1-hexanol and in 2-ethylhexanol are so viscous at room temperature that they are gellike, and no reliable solubility determinations could be made. Similarly, unsatisfactory results were obtained for lithium chloride in 2-ethylhexanol, and only a lower limit can be given for its solubility: at 298 K it is  $>0.82 m$ .

More information, however, can be obtained from the distribution and water content data reported earlier<sup>1</sup> concerning lithium bromide in 2-ethylhexanol. Table II shows  $\log \bar{m}_{\text{LiBr}}/s^2\sigma_{\pm}^2$  as a function of  $s\sigma_{\pm}$ . The aqueous solubility of lithium bromide was taken<sup>5</sup> as  $17.88 m$  at 298.15 K, contrary to the estimate<sup>1</sup>  $21.1 m$ , based on older literature. The necessary values of  $\gamma_{\pm\text{LiBr}}$  are obtained from the compilation of Gazith,<sup>6a</sup> with  $\gamma_{\pm\text{LiBr(satd)}} = 402$ . Extrapolation to  $s\sigma_{\pm} = 1$  should give, according to eq 4,  $\log \bar{m}_{\text{LiBr(satd)}}$ , since at the limit  $\bar{\sigma} = 1$ . In practice, it is necessary to assume a value of  $\bar{m}_{\text{LiBr(satd)}}$ , calculate  $\bar{s} = \bar{m}_{\text{LiBr}}/\bar{m}_{\text{LiBr(satd)}}$ , and extrapolate  $\log \bar{s}/s^2\sigma_{\pm}^2$  against  $\bar{s}$ , yielding zero at the limit  $\bar{s} = 1$  for the correct  $\bar{m}_{\text{LiBr(satd)}}$ . The last line in Table II thus includes the extrapolated data for saturated solutions. It is possible also to extrapolate the molality of water ( $\bar{m}_{\text{H}_2\text{O}}$ ) which decreases linearly with the molality of lithium bromide  $\bar{m}_{\text{LiBr}}$  in the 2-ethylhexanol, down to zero water content, to obtain<sup>1</sup> virtually the same saturation molality of  $\bar{m}_{\text{LiBr(satd)}} = 1.72$ . The values of  $\bar{\sigma}$  in Table II were calculated from eq 7.

The molal activity coefficient of saturated lithium bromide in 2-ethylhexanol is  $\bar{\gamma}_{\text{LiBr(satd)}} = m_{\text{LiBr(satd)}}^2 \gamma_{\pm\text{LiBr(satd)}}^2 \cdot M_{\text{H}_2\text{O}}^2 / \bar{m}_{\text{LiBr(satd)}} \bar{M}_{2\text{EtHexOH}} = 7.44 \times 10^4$ , the molar masses *M* being expressed in  $\text{kg mol}^{-1}$ . The solubility of lithium chloride in water<sup>6b</sup> is  $19.85 m$  at 298.15 K, and the activity coefficient is<sup>6a</sup> 61.3, hence for a saturated solution of lithium chloride in hexanol at this temperature  $\bar{\gamma}_{\text{LiCl(satd)}} = 2.16 \times 10^3$ , calculated as above with  $\bar{m}_{\text{LiCl(satd)}} = 2.177 m$  given earlier. These very high molal activity coefficients, pertaining to the

hypothetical ideal 1 *m* solution as the standard state, and obtained from the requirement that  $G_{\text{tr}}^{\text{S}} = 0$ , point to the strong solvation of the lithium salts by the alcohols.

For the distribution of lithium bromide between the two liquid phases, the equilibrium constant  $K'$  is defined by

$$\log K' = -\Delta G^{\circ'}_{\text{tr}(m)}/(\ln 10)RT = [\mu^{\circ'}_{\text{LiBr}(m)}$$

$$- \mu^{\circ}_{\text{LiBr}(m)}]/(\ln 10)RT = \lim_{(s \rightarrow 0)} \log (\bar{m}_{\text{LiBr}}/s^2 \sigma_{\pm}^2) - 2 \log (m_{\text{LiBr}(\text{satd})} \gamma_{\pm \text{LiBr}(\text{satd})}) \quad (8)$$

The value obtained on a short linear extrapolation is  $\log K' = -4.255 \pm 0.105$ , hence  $\Delta G^{\circ'}_{\text{tr}(m)} = +24.29 \pm 0.60 \text{ kJ mol}^{-1}$ . The corresponding unitary value is  $\Delta G^{\circ'}_{\text{tr}(x)} = +30.28 \pm 0.60 \text{ kJ mol}^{-1}$ . The heat of extraction found previously also corresponds to the effective standard state used here, as is evident from the range of concentrations used for the heats of dilution of the organic phase. Therefore it is not  $\Delta H^{\circ}_{\text{tr}}$  but the primed  $\Delta H^{\circ'}_{\text{tr}}$  that equals  $-7.69 \pm 0.21 \text{ kJ mol}^{-1}$ , and thus  $\Delta S^{\circ'}_{\text{tr}(x)} = (\Delta H^{\circ'}_{\text{tr}} - \Delta G^{\circ'}_{\text{tr}(x)})/T = -127.4 \pm 2.1 \text{ J K}^{-1} \text{ mol}^{-1}$ .

### Enthalpy and Entropy Diagrams

The enthalpy diagram in Figure 1 shows the various heat effects at 298.15 K between several states relevant to this study, based on crystalline anhydrous lithium bromide as an arbitrary zero of the enthalpy scale.

$\Delta H_1$  is the standard heat of solution to infinite dilution in water,<sup>7</sup>  $\Delta H^{\circ}_{\text{soln}} = -48.83 \pm 0.20 \text{ kJ mol}^{-1}$ .

$\Delta H_2$  is the heat of dilution from saturated aqueous to infinitely dilute aqueous lithium bromide,  $\Delta H^{\circ}_{\text{dil}(\text{satd} \rightarrow 0)} = -15.82 \text{ kJ mol}^{-1}$ , obtained by a short extrapolation of the reported<sup>7</sup> data.

$\Delta H_3$  is the standard heat of solution to a saturated aqueous solution,  $\Delta H^{\text{s}}_{\text{soln}} = \Delta H_1 - \Delta H_2 = -48.83 - (-15.82) = -33.01 \text{ kJ mol}^{-1}$ . This is the enthalpy level of the saturated aqueous solution.

$\Delta H_4$  is the lattice enthalpy of lithium bromide,  $\Delta H_{\text{latt}} = U_0 - \int_0^{298} C_p(\text{LiBr}, c) dT + 5RT$ , where  $U_0$  is the lattice energy at absolute zero, and  $C_p$  the molar heat capacity. For the present purpose, however, it is best to fix the level of the gaseous ions not via  $\Delta H_4$  but rather via  $\Delta H_5$ .

$\Delta H_5$  is the sum of the hydration enthalpies of lithium and bromide ions. These are obtained from standard compilations,<sup>8</sup> the sum being independent of any extrathermodynamic assumption concerning the hydration enthalpies of individual ions. Thus  $\Delta H_{\text{hyd}(\text{Li}^+)} + \Delta H_{\text{hyd}(\text{Br}^-)} = -849.4 \text{ kJ mol}^{-1}$ . The conventional heats of hydration (based<sup>8</sup> on  $\Delta H_{\text{hyd}(\text{H}^+)} = -1536.20 \text{ kJ mol}^{-1}$ ) are  $-959.9 \text{ kJ mol}^{-1}$  for  $\text{Li}^+$  and  $+110.5 \text{ kJ mol}^{-1}$  for  $\text{Br}^-$ . The absolute values (based<sup>9</sup> on  $\Delta H_{\text{hyd}(\text{H}^+)} = -1100 \pm 6 \text{ kJ mol}^{-1}$ ) are  $-524 \text{ kJ mol}^{-1}$  for  $\text{Li}^+$  and  $-325 \text{ kJ mol}^{-1}$  for  $\text{Br}^-$ . These values may be useful in the interpretation of the results. Since  $\text{Li}^+(\infty \text{H}_2\text{O}) + \text{Br}^-(\infty \text{H}_2\text{O})$  is at the level  $-48.8 \text{ kJ mol}^{-1}$  below the arbitrary zero, the hydration enthalpy brings  $\text{Li}^+(\text{g}) + \text{Br}^-(\text{g})$  to the level  $+800.6 \text{ kJ mol}^{-1}$  above it, and this is then also the value of  $\Delta H_4$ . This is consistent with the various estimates<sup>10</sup> of the lattice enthalpy ranging from 794 to 808  $\text{kJ mol}^{-1}$ .

$\Delta H_6$  is the experimental<sup>1</sup> enthalpy of transfer from the infinitely dilute aqueous solution to the effective standard state of infinitely dilute ion-paired electrolyte in 2-ethylhexanol,  $\Delta H^{\circ'}_{\text{tr}} = -7.69 \pm 0.21 \text{ kJ mol}^{-1}$ . This brings the level of  $\text{LiBr}(\infty 2\text{EtHxOH})$  down to  $-56.5 \text{ kJ mol}^{-1}$ .

$\Delta H_7$  is minus the heat of dilution of saturated lithium bromide to infinitely dilute, ion paired, salt in the alcohol

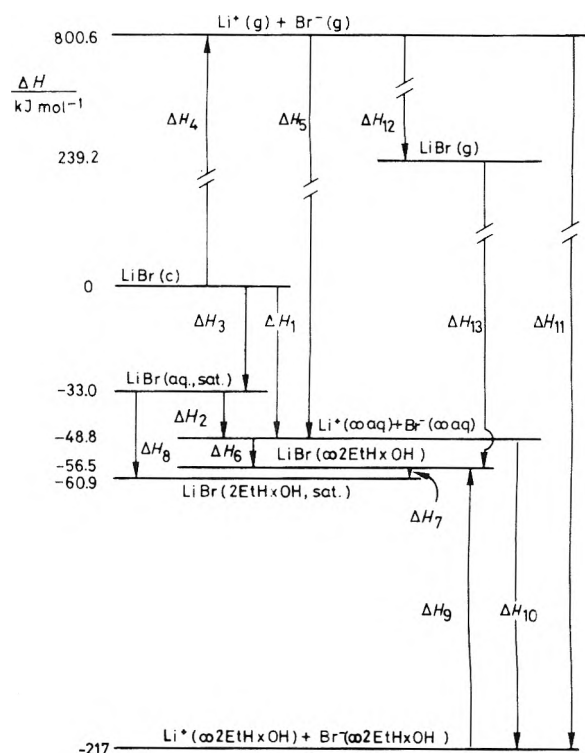


Figure 1. The enthalpy level diagram for lithium bromide in water and in 2-ethylhexanol, based on zero enthalpy for crystalline anhydrous lithium bromide as reference.

$-\Delta \bar{H}_{\text{dil}} = -(1.465 \pm 0.135) \times 1.73^2 = -4.4 \pm 0.4 \text{ kJ mol}^{-1}$ , where  $1.465 \bar{m}_{\text{LiBr}}^2$  is the integral heat of dilution<sup>1</sup> to infinite dilution, and  $1.73 m$  is the saturation solubility from Table II. This brings the level of  $\text{LiBr}(2\text{EtHxOH}, \text{satd})$  down to  $-60.9 \text{ kJ mol}^{-1}$ . The cumulative error from  $\Delta H_1$ ,  $\Delta H_6$ , and  $\Delta H_7$  is  $\pm 0.8 \text{ kJ mol}^{-1}$ .

$\Delta H_8$  is the heat of transfer of lithium bromide from its saturated solution in water to its saturated solution in 2-ethylhexanol,  $\Delta H^{\text{s}}_{\text{tr}} = \Delta H_2 + \Delta H_6 + \Delta H_7 = -27.9 \pm 0.8 \text{ kJ mol}^{-1}$ .

$\Delta H_9$  is the molar enthalpy of the ion pairing of lithium bromide in the alcohol, at infinite dilution. This may be estimated by differentiating an appropriate expression for the equilibrium constant with respect to the temperature. The Fuoss and Bjerrum expressions<sup>2,11a</sup>

$$K_{\text{F}(c)} = (400\pi N_A/3)a^3 \exp b \quad (9a)$$

$$K_{\text{B}(c)} = 4000\pi N_A a^3 b^2 Q(b) \simeq 4000 N_A a^3 b^{-1} \exp b \quad (9b)$$

which gives the equilibrium constant in liters/mole with *a* in meters, can be converted to the corresponding rational constant by division by the molar volume of the solvent. The enthalpy change is thus

$$\Delta H^{\circ}_{\text{F}(x)} = -RT[b(1 + T d \ln \epsilon/dT) + \alpha T] \quad (10a)$$

$$\Delta H^{\circ}_{\text{B}(x)} = -RT[(b-1)(1 + T d \ln \epsilon/dT) + \alpha T] \quad (10b)$$

where  $b = e^2/akT(4\pi\epsilon_0)\epsilon$ , with  $e^2/4k\pi\epsilon_0 = 1.67096 \times 10^{-5} \text{ m K}$ , and  $\alpha = d \ln v^{\circ}_{\text{soln}}/dT$ . The distance parameter *a*, assumed independent of temperature, may be taken<sup>11b</sup> as the sum of the ionic crystalline radii,  $2.55 \times 10^{-10} \text{ m}$ . The dielectric constant of the solvent and its temperature coefficient are<sup>12</sup>  $\epsilon = 7.58$  and  $d \ln \epsilon/dT = -0.01087 \text{ K}^{-1}$ , and the coefficient of thermal expansion is<sup>13</sup>  $\alpha = 0.000875 \text{ K}^{-1}$ . Equation 10a therefore gives  $\Delta H^{\circ}_{\text{F}(x)} = +160.3 \text{ kJ mol}^{-1}$  (the correction for

the  $\alpha$  term is quite small, only 0.62 kJ mol<sup>-1</sup>). Thus the enthalpy contribution to the ion pairing is very unfavorable.<sup>14</sup> The level of the state Li<sup>+</sup>(∞2EtHxOH) + Br<sup>-</sup>(∞2EtHxOH) is seen to be as low as -217 kJ mol<sup>-1</sup>.

$\Delta H_{10}$  is the standard enthalpy of transfer between the infinite dilute states in water and in alcohol,  $\Delta H_{10}^{\circ} = \Delta H_6 - \Delta H_9 = -168.0$  kJ mol<sup>-1</sup>. This very large quantity is not the observed heat  $\Delta H_{tr}^{\circ}$ , and its source requires interpretation; see the discussion below.

$\Delta H_{11}$  is the sum of the solvation enthalpies of the lithium and bromide ions in the alcohol,  $\Delta H_{11}^{\circ} = \Delta H_{11}^{\circ}(\text{Li}^+) + \Delta H_{11}^{\circ}(\text{Br}^-) = -1017.4$  kJ mol<sup>-1</sup>, larger than  $\Delta H_{11}^{\circ}(\text{Li}^+) + \Delta H_{11}^{\circ}(\text{Br}^-) = \Delta H_5$  by the amount  $\Delta H_{10}$ . According to the Born equation, the solvation enthalpy of a symmetrical  $z$  valent electrolyte is given by

$$\Delta H_{\text{soln}}^{\circ} = -(N_A z^2 e^2 / 4\pi\epsilon_0) [1 - \epsilon^{-1}(1 + T\partial \ln \epsilon / \partial T)](r_+^{-1} + r_-^{-1}) \quad (11)$$

The factor  $[1 - \epsilon^{-1}(1 + T\partial \ln \epsilon / \partial T)]$  is 1.004 65 for water and 1.296 for 2-ethylhexanol, and this difference can explain the difference between the hydration and solvation enthalpies, provided the ionic radii are assumed to be independent of the temperature and of the solvent.

$\Delta H_{12}$  is the enthalpy of ion pair formation in the gas phase. This is obtained from  $\Delta H_{\text{ip(g)}} = \Delta G_{\text{ip(g)}} + T\Delta S_{\text{ip(g)}}$ , where  $\Delta G_{\text{ip(g)}}$  is given by the electrical work  $-N_A e^2 / 4\pi\epsilon_0 a = -1.3893 \times 10^{-4} \text{ J m mol}^{-1} / 2.55 \times 10^{-10} \text{ m} = -544.8$  kJ mol<sup>-1</sup>, and  $T\Delta S_{\text{ip(g)}}$  is -16.6 kJ mol<sup>-1</sup> as calculated further below (cf.  $\Delta S_9$ ). Thus  $\Delta H_{\text{ip(g)}} = -544.8 - 16.6 = -561.4$  kJ mol<sup>-1</sup>, bringing the level of LiBr(g) to +239.2 kJ mol<sup>-1</sup>.

$\Delta H_{13}$ , finally, is the solvation enthalpy of the ion pairs, obtained from  $\Delta H_{\text{soln(ip)}}^{\circ} = \Delta H_5 + \Delta H_6 - \Delta H_{12} = -849.4 - 7.7 - (-561.4) = -283.7$  kJ mol<sup>-1</sup>. The solvation enthalpy of the dipolar ion pair is thus considerably less than that of the separate ions,  $\Delta H_{11}$ .

The entropy diagram in Figure 2 shows the various entropy changes at 298.15 K between the states shown in Figure 1 and described in detail in the text. The entropy differs from the enthalpy in two aspects: the zero of the scale is not arbitrary, but fixed by the third law of thermodynamics, and the standard solution state is not one of infinite dilution, but a hypothetical one of unit concentration on the scale used (the molal ( $m$ ) or the unitary ( $x$ )) with the ideal properties (absence of solute-solute interactions) of the infinitely dilute solution. On this basis, the reference level of the diagram is that of Li<sup>+</sup>(aq) + Br<sup>-</sup>(aq), where<sup>15</sup>  $S_{\text{aq}(m)}^{\circ} = +95.0$  J K<sup>-1</sup> mol<sup>-1</sup> and  $S_{\text{aq}(x)}^{\circ} = S_{\text{aq}(m)}^{\circ} + 2R \ln (\text{mol of H}_2\text{O/kg}) = 95.0 + 66.8 = 161.8$  J K<sup>-1</sup> mol<sup>-1</sup>. In the scheme of Figure 2, the unitary scale is used.

The conventional unitary individual ionic standard aqueous entropy of the lithium ion is 112.9 J K<sup>-1</sup> mol<sup>-1</sup>, that of the bromide ion 48.9 J K<sup>-1</sup> mol<sup>-1</sup> ( $S_{\text{aq}(x)\text{H}^+\text{conv}}^{\circ} = 98.7$  J K<sup>-1</sup> mol<sup>-1</sup>). The absolute values are obtained by setting<sup>9</sup>  $S_{\text{aq}(x)\text{H}^+\text{abs}}^{\circ} = 11.2 \pm 1.3$  J K<sup>-1</sup> mol<sup>-1</sup>, so that the values for lithium and bromide ions become 25.4 and 136.4 J K<sup>-1</sup> mol<sup>-1</sup>, respectively. The large positive value for the bromide ions is due to their water-structure-breaking properties.

$\Delta S_1$  is minus the entropy of dilution from saturated aqueous solutions to the dilute aqueous standard state, obtainable from the difference in the entropies of solution:  $\Delta S_{\text{dil}} = S_{\text{aq}(x)}^{\circ} - S_{\text{aq}(m)}^{\circ} = \Delta S_{\text{soln}(x)}^{\circ} - \Delta S_{\text{soln}(m)}^{\circ} = [\Delta H_{\text{soln}}^{\circ} - \Delta G_{\text{soln}(x)}^{\circ} - \Delta H_{\text{soln}}^{\circ}]/T$  since  $\Delta G_{\text{soln}}^{\circ} = 0$ . The values of  $\Delta H_{\text{soln}}^{\circ} = \Delta H_3 = -33.01$  kJ mol<sup>-1</sup>,  $\Delta H_{\text{soln}}^{\circ} = \Delta H_1 = -48.83$  kJ mol<sup>-1</sup> are taken from Figure 1, and<sup>5,6</sup>  $\Delta G_{\text{soln}(x)}^{\circ} = -2RT(\ln m_{\text{LiBr(satd)}} + \ln$

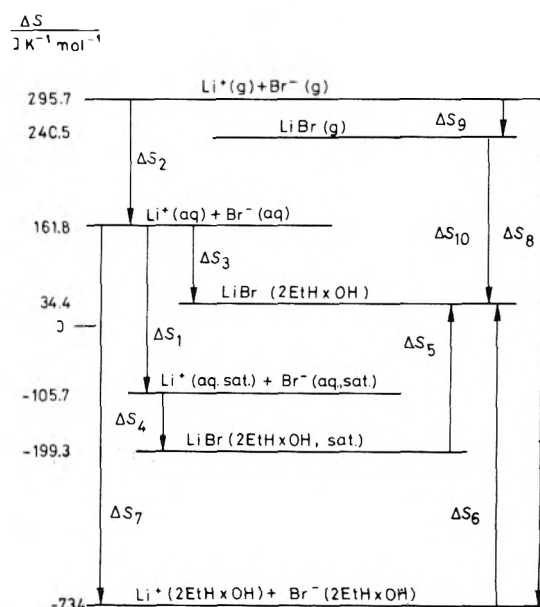


Figure 2. The entropy level diagram (unitary scale) for lithium bromide in water and in 2-ethylhexanol, based on third law entropies.

$\gamma_{\pm \text{LiBr(satd)}} - \ln (\text{mol of H}_2\text{O/kg}) = -63.94$  kJ mol<sup>-1</sup>. Hence  $\Delta S_{\text{dil}} = (-33.01 - (-63.94) - (-48.83))/0.29815 = +267.5$  J K<sup>-1</sup> mol<sup>-1</sup>. This brings the entropy level of the saturated solution down to -105.7 J K<sup>-1</sup> mol<sup>-1</sup>.

$\Delta S_2$  is the sum of the hydration entropies of the lithium and bromide ions. The standard entropy of a gaseous monatomic ion is<sup>16</sup>

$$S_{\text{oi}}^{\circ} = S_{\text{i(transl)}}^{\circ} / \text{J K}^{-1} \text{ mol}^{-1} = (3/2)R \ln M/\text{kg} + (5/2)R \ln T/\text{K} + 76.465 \quad (12)$$

where  $M$  is the molar mass, giving 132.3 and 163.4 J K<sup>-1</sup> mol<sup>-1</sup>, respectively, for the lithium and bromide ions, together 295.7 J K<sup>-1</sup> mol<sup>-1</sup>, which fixes the level of Li<sup>+</sup>(g) + Br<sup>-</sup>(g). The difference between that and the Li<sup>+</sup>(aq) + Br<sup>-</sup>(aq) level is  $\Delta S_{\text{hyd}(x)}^{\circ} = 161.8 - 295.7 = -133.9$  J K<sup>-1</sup> mol<sup>-1</sup>. This may be apportioned between the ions as  $\Delta S_{\text{hyd}(x)\text{Li}^+}^{\circ} = 132.3 - 25.4 = 106.9$  J K<sup>-1</sup> mol<sup>-1</sup> and  $\Delta S_{\text{hyd}(x)\text{Br}^-}^{\circ} = 163.4 - 136.4 = 27.0$  J K<sup>-1</sup> mol<sup>-1</sup>.

$\Delta S_3$  is the experimental standard entropy of transfer from the aqueous to the alcoholic phase,  $\Delta S_{\text{tr}(x)}^{\circ} = -127.4 \pm 2.1$  J K<sup>-1</sup> mol<sup>-1</sup>, established in this paper for the hypothetical standard state of ideal unit mole fraction of ion paired electrolyte in the organic phase. The entropy level of this state is, therefore, 161.8 - 127.4 = 34.4 J K<sup>-1</sup> mol<sup>-1</sup>.

$\Delta S_4$  is the standard entropy of transfer from a saturated aqueous solution to a saturated alcoholic solution, and is obtained from the corresponding enthalpy change  $\Delta H_8 = \Delta H_{\text{tr}}^{\circ}$ :  $\Delta S_{\text{tr}(x)}^{\circ} = \Delta H_{\text{tr}}^{\circ} / T = (-27.9 \pm 0.8) / 0.29815 = -93.6 \pm 2.7$  J K<sup>-1</sup> mol<sup>-1</sup>. The level of LiBr(2EtHxOH, satd) is therefore -105.7 - 93.6 = -199.3 J K<sup>-1</sup> mol<sup>-1</sup>.

$\Delta S_5$  is the entropy of dilution from the saturated alcoholic solution to the dilute standard state and is obtained from the difference in the entropy levels  $\Delta S_5 = \Delta S_3 - \Delta S_1 - \Delta S_4 = -127.4 \pm 2.1 - (-267.5) - (-93.6 \pm 2.7) = 233.7 \pm 3.4$  J K<sup>-1</sup> mol<sup>-1</sup>.

$\Delta S_6$  is the ion pairing entropy in the dilute alcoholic solutions. It may be obtained from differentiation of the association constant, eq 9, giving

$$\Delta S^\circ_{F(x)} = R[\ln K_{F(x)} - b(1 + T d \ln \epsilon/dT) - \alpha T] \quad (13a)$$

$$\Delta S^\circ_{B(x)} = R[\ln K_{B(x)} - (b-1)(1 + T d \ln \epsilon/dT) - \alpha T] \quad (13b)$$

The molar volume of the solvent is  $v^\circ = (0.1302 \text{ kg mol}^{-1}) / (829.1 \text{ kg m}^{-3}) = 1.570 \times 10^{-4} \text{ m}^3$ , so that with the values of  $a, b, \epsilon, d \ln \epsilon/dT$ , and  $\alpha$  used previously, the large positive value  $\Delta S^\circ_{F(x)} = 768 \text{ J K}^{-1} \text{ mol}^{-1}$  is obtained. The value of the Gibbs free energy for ion pairing,  $\Delta G^\circ_{F(x)} = \Delta H^\circ_{F(x)} - T\Delta S^\circ_{F(x)} = -RT \ln K_{F(x)} = -68.6 \text{ kJ mol}^{-1}$ , shows that this entropy change more than compensates<sup>14</sup> for the large positive enthalpy change. The entropy level of the dissociated alcoholic lithium bromide is fixed at  $161.8 + \Delta S_3 - \Delta S_6 = -734 \text{ J K}^{-1} \text{ mol}^{-1}$ .

$\Delta S_7$  is the just calculated standard entropy of transfer from the aqueous to the alcoholic solution,  $\Delta S^\circ_{tr(x)} = -896 \text{ J K}^{-1} \text{ mol}^{-1}$ . This is much more negative than the experimentally obtainable value,  $\Delta S^\circ_{tr(x)}$ .

$\Delta S_8$  is the corresponding entropy of solvation of the gaseous lithium and bromide ions to the dissociated state in the alcohol,  $\Delta S^\circ_{solv(Li^+)} + \Delta S^\circ_{solv(Br^-)} = \Delta S_2 + \Delta S_7 = -1029 \text{ J K}^{-1} \text{ mol}^{-1}$ . This may, again, be compared with the corresponding entropy of hydration,  $\Delta S_2 = -133.9 \text{ J K}^{-1} \text{ mol}^{-1}$ , the large difference being qualitatively explainable in terms of the Born equation, analogously to eq 11, where the relevant factor is now ( $\epsilon^{-1} d \ln \epsilon/dT$ ) which is  $0.583 \times 10^{-4} \text{ K}^{-1}$  for water and  $14.34 \times 10^{-4} \text{ K}^{-1}$  for 2-ethylhexanol.

$\Delta S_9$  is the entropy change for ion pairing in the gaseous phase, the difference between the entropy of the ion pair and the entropies of the ions, already evaluated for finding  $\Delta S_2$ . The ion pair has, in addition to the translational entropy according to eq 12, with  $M = M(\text{LiBr}) = 0.08686 \text{ kg}$ , also the rotational entropy

$$S^\circ_{LiBr(\text{rotn})} / \text{J K}^{-1} \text{ mol}^{-1} = R \ln T/K + R \ln I/\text{kg m}^2 + 1177.97 \quad (14)$$

where  $I/\text{kg m}^2 = (M_{LiBr}/\text{kg})N_A^{-1}(a/m)^2$  is the moment of inertia per ion pair. The vibrational entropy is assumed to be negligible, so that the total entropy is  $S^\circ_{LiBr(g)} = S^\circ_{LiBr(\text{transl})} + S^\circ_{LiBr(\text{rotn})} = 164.4 + 76.1 = 240.5 \text{ J K}^{-1} \text{ mol}^{-1}$ , which is the entropy level of the ion pair. Subtraction of the entropy of the ions yield  $\Delta S_{\text{ion pairing}(g)} = 240.5 - 295.7 = -55.2 \text{ J K}^{-1} \text{ mol}^{-1}$ .

$\Delta S_{10}$ , finally, is the entropy of solvation of the ion pair, obtained as  $\Delta S^\circ_{solv(ip)} = \Delta S_2 + \Delta S_3 - \Delta S_9 = -133.9 - 137.4 - (-55.2) = -206.1 \text{ J K}^{-1} \text{ mol}^{-1}$ .

## Discussion

The realization that the standard state of infinite dilution of the alcoholic solution that is attainable by the extrapolation of experimental data corresponds not to complete dissociation of the ions, but to an effective state of ion paired solute that is ideal with respect to solute-solute interactions, in no way affects the earlier conclusion<sup>1</sup> that the transfer is *entropy controlled* in the dilute solutions. On the contrary, the operational definition of the new standard state by eq 3, together with the usual definition of eq 2 for the aqueous phase, permits the estimation via eq 8 and  $\log K'$  of the Gibbs free energy of transfer and of the entropy of transfer  $\Delta S^\circ_{tr(x)} = -127.4 \pm 0.21 \text{ J K}^{-1} \text{ mol}^{-1}$ . The entropy effect  $T\Delta S^\circ_{tr(x)} = -37.97 \pm 0.63 \text{ kJ mol}^{-1}$  far outweighs the enthalpy effect,  $\Delta H^\circ_{tr} = -7.69 \pm 0.21 \text{ kJ mol}^{-1}$ .

The large entropy barrier to transfer from dilute solutions

is made up by: (a) loss of translational entropy  $S^\circ_{LiBr(\text{transl})} - S^\circ_{Li^+(\text{transl})} - S^\circ_{Br^-(\text{transl})} = 164.4 - 132.3 - 163.4 = -131.3 \text{ J K}^{-1} \text{ mol}^{-1}$ ; (b) hindered rotations of the ion pair in the alcohol compared to free ion pair; i.e., a part of  $-76.1 \text{ J K}^{-1} \text{ mol}^{-1}$ ; (c) binding of alcohol by solvation, which makes up the balance of  $\Delta S_{10}$ ; (d) reestablishment of water structure when the bromide ion leaves the aqueous phase ( $S^\circ_{aq(x)Br^-} = 136.4 \text{ J K}^{-1} \text{ mol}^{-1}$ ); (e) the opposing effect of a positive contribution when lithium ions relinquish their hydrating water molecules on transfer ( $S^\circ_{aq(x)Li^+} = 25.4 \text{ J K}^{-1} \text{ mol}^{-1}$ ). However, the compensating effect (e) may not be as large as thought, since the water found in the alcohol<sup>1</sup> at infinite dilution of salt may be effectively immobilized by hydrating the ion pair (or the lithium end of it). The effects (b) to (e) thus nearly balance out, making the barrier  $\Delta S_3$  effectively given by effect (a).

An independent estimate of  $\Delta S_3$  might be attempted via  $\Delta S_7 + \Delta S_6$  if a reliable estimate of  $\Delta S_7$  by the Born equation corrected for the difference in communal entropy<sup>3</sup> (compression from the molar volume of the gaseous ions at standard pressure to the molar volume of the solvent), i.e., via  $\Delta S_8 - \Delta S_2$ , were possible. However, this cannot be done, the Born equation being known not to produce correct quantitative results. Whereas  $\Delta S^\circ_{\text{hyd}(x)}$  is  $-231.4 \text{ J K}^{-1} \text{ mol}^{-1}$  according to this calculation compared with the correct value of  $-133.9 \text{ J K}^{-1} \text{ mol}^{-1}$ , for the alcoholic solution the discrepancy is much larger, the calculated  $\Delta S^\circ_{solv(x)}$  being  $-4409$ , depressing the level of the entropy of the solvated ions much below any reasonable estimate. Since the main factor in the Born equation leading to the discrepancy is  $\epsilon^{-1}$  (0.0113 for water, 0.1615 for 2-ethylhexanol), a small adjustment in  $d \ln \epsilon/dT$  due to the presence of water in the alcohol or in  $(r_+^{-1} + r_-^{-1})$  due to different sizes of cavities may not suffice to explain it. Regarding the solvents as dielectric continua, which is at the basis of the Born treatment, is inadequate, as has often been pointed out.

The same criticism may be raised against the alternative employed here, the calculation of the entropy level of the dissociated ions in the alcohol via the Fuoss or Bjerrum equations (9). For high  $b$  values (here  $b = 29.0$ ) the approximation shown in eq 9b,  $Q(b) \approx b^{-4} \exp b$  is admissible. This yields in (10b) and (13b) for the Bjerrum equations a factor  $(b-1)$  instead of the factor  $b$  in the Fuoss equations, a trivial difference indeed. It may be considered that perhaps an overly large importance is given the term  $T d \ln \epsilon/dT$  in eq 13, but its effect, describing the ability of the solvent to absorb energy by being partially released on ion pairing from alignment constraint,<sup>14</sup> should not be underestimated either. A similar large effect is observed for the molar volumes of the lithium salts on ion pairing,<sup>2</sup> which is ascribed to the corresponding factor  $d \ln \epsilon/dP$ .

The saturated solution standard state has the advantage that transfer occurs between practically binary solutions of the salt in the solvent, because of the negligible amounts of water in the alcoholic and of alcohol in the aqueous solutions. Furthermore, activity coefficients are much nearer unity than the commonly used ones: for 82% saturation in the aqueous phase (or 72% in the organic phase),  $\sigma_{\pm} = 0.449$  and  $\bar{\sigma} = 9.3$ , compared with  $\gamma_{\pm} = 1.67 \times 10^2$  and  $\bar{\gamma} = 4.96 \times 10^4$ . Since the purpose of an activity coefficient is to describe a deviation, rather than an entirely new situation,  $\sigma_{\pm}$  and  $\bar{\sigma}$  should be preferred.

The entropy change for transfer between the saturated solutions,  $\Delta S^\circ_{tr(x)} = \Delta S_4 = -93.6 \text{ J K}^{-1} \text{ mol}^{-1}$  is somewhat smaller than between the infinitely dilute solutions,  $\Delta S_3 = -127.4 \text{ J K}^{-1} \text{ mol}^{-1}$ . The same difference occurs, of course,

between the corresponding entropy changes of dilution,  $\Delta S_1$  and  $\Delta S_5$ . A major contribution to the decrease should be the disappearance of effect (d) from the entropy barrier to transfer, since in the concentrated solutions there is hardly any water structure left to break. All of the water participates in the hydration of the lithium ions, and above a concentration where even this is insufficient, ion pairing occurs also in the aqueous phase. If  $h_+ = 3.4$  molecules of water hydrate each lithium ion in concentrated solutions,<sup>17</sup> then above  $M_{\text{H}_2\text{O}}^{-1}/h_+ = 0.018\ 01^{-1}/3.4 = 16.3\ m$  ion pairing should be manifest. Thus also some of the translational entropy barrier to transfer, effect (a), is lowered.

On the other hand, the enthalpy change for transfer between the saturated solutions is much more favorable than that between the dilute solutions:  $\Delta H_8 = -27.9\ \text{kJ mol}^{-1}$  compared with  $\Delta H_6 = -7.7\ \text{kJ mol}^{-1}$ . A large part of the difference is accounted for by  $\Delta H_2 = 15.8\ \text{kJ mol}^{-1}$ , the enthalpy of dilution in the aqueous phase, which may be related to the loss<sup>17</sup> of  $\Delta h_+ = 2.2$  molecules of water of the hydration of the lithium ions and of  $\Delta h_- = 3.5$  molecules of water of the hydration of the bromide ions between the two standard states. In the saturated alcoholic solution there are  $M_{2\text{EtH}\times\text{OH}^{-1}}/\bar{m}_{\text{LiBr}}^{\text{(satd)}} = 0.1302^{-1}/1.73 = 4.44\ \text{mol}$  of solvent to solvate each ion pair, an apparently sufficient amount, but it may be necessary to invoke an electrostatic interaction between the dipoles of the ion pairs to counteract the loss of water of hydration (of the lithium end of the ion pair) as the solution is concentrated, to account for the negative heat  $\Delta H_7$ . The square dependence of  $\Delta H_7$  on  $\bar{m}_{\text{LiBr}}$  may point in this direction.

## References and Notes

- (1) Y. Marcus, *J. Chem. Eng. Data*, **20**, 141 (1975).
- (2) Y. Marcus, N. Ben-Zwi, and I. Shiloh, *J. Solution Chem.*, **5**, 86 (1976).
- (3) (a) Y. Marcus, *J. Inorg. Nucl. Chem.*, **37**, 493 (1975); (b) B. Milicevic, *Helv. Chim. Acta*, **46**, 1466 (1963).
- (4) (a) I. Shiloh provided the solubility data, M.Sc. Thesis, Hebrew University, Jerusalem, 1974. (b) J. M. Blinderman, M.Sc. Thesis, Hebrew University, Jerusalem, 1974, and unpublished data.
- (5) The caption of Figure 3 in the earlier paper<sup>1</sup> gave the aqueous solubility as 21.2 *m* (hence the alcohol solubility as 2.18 *m*), based on older solubility data (Seidell, 3d ed, also Blindin, *Zh. Obshch. Khim.*, **17**, 1590 (1947), and Huttig, *Z. Anorg. Chem.*, **137**, 155 (1924)). More recent determinations, A. F. Scott and E. J. Durham, *J. Phys. Chem.*, **34**, 532 (1930); L. Roger, *Ann. Chim. (11)*, **19**, 362 (1944); J. J. Kessiss, *Bull. Soc. Chim. Fr.*, **48** (1965); D. A. Boryta, *J. Chem. Eng. Data*, **15**, 142 (1970), show much better mutual consistency, and yield for 298.15 K a solubility of  $60.83 \pm 0.15\ \text{wt } \%$  or 17.88 *m* lithium bromide in water.
- (6) (a) M. Gazith, Israel Atomic Energy Commission Report IA-1004 (1964). (b) J. J. Kessiss, *Bull. Soc. Chim. Fr.*, 1503 (1961).
- (7) V. B. Parker, *Natl. Stand. Ref. Data Ser., Natl. Bur. Stand.*, **No. 2** (1965).
- (8) D. D. Wagman, W. H. Evans, V. B. Parker, I. Halow, S. M. Bailey, and R. H. Schumm, *Natl. Bur. Stand. Tech. Note*, **No. 270-3** (1968).
- (9) H. F. Halliwell and S. C. Nyburg, *Trans. Faraday Soc.*, **59**, 1126 (1963); D. F. C. Morris, *Struct. Bonding*, **4**, 63 (1968); J. E. Desnoyers and C. Jolicœur, *Mod. Aspects Electrochem.*, **5**, 1 (1969).
- (10) T. C. Waddington, *Adv. Inorg. Chem. Radiochem.*, **1**, 157 (1959).
- (11) (a) R. M. Fuoss, *J. Am. Chem. Soc.*, **80**, 5059 (1958); N. Bjerrum, *K. Dan. Vidensk. Selsk.*, **7**, No. 9 (1926). (b) The apparent molar volume change on ion pairing<sup>2</sup> strongly suggests that contact ion pairs are formed.
- (12) R. Wemelle, *C. R. Acad. Sci.*, **244**, 775 (1957). The value quoted by mistake in ref. 1 pertains to 1-octanol and should be replaced by the value given here.
- (13) C. Marsden and S. Mann, "Solvents Guide", 2d ed, Interscience, New York, N.Y., 1963.
- (14) J. E. Prue, *J. Chem. Educ.*, **46**, 12 (1969).
- (15) F. D. Rossini, *Natl. Bur. Stand. Circ.*, **No. 500** (1952).
- (16) K. S. Pitzer and L. Brewer, "Thermodynamics", 2d ed, McGraw-Hill, New York, N.Y., 1961, p. 421.
- (17) E. Högfeldt and L. Leifer, *Acta Chem. Scand.*, **17**, 338 (1963).

## Thermodynamics of the Anion Exchange of Cyanide and Thiocyanate on a Strong Base Anion Exchanger

M. Okamoto and Y. Marcus\*

Department of Inorganic and Analytical Chemistry, The Hebrew University of Jerusalem, Jerusalem, Israel, and Research Laboratory for Nuclear Reactors, Tokyo Institute of Technology, Ookayama, Meguro-ku, Tokyo, Japan (Received March 29, 1976)

Publication costs assisted by the Tokyo Institute of Technology

The equilibrium constant for the anion exchange reaction  $\overline{\text{RCN}} + \text{SCN}^- \rightleftharpoons \overline{\text{RSCN}} + \text{CN}^-$  with 0.1 M K(CN + SCN) solutions and Dowex-1X8 anion exchange resin was determined at 283, 298, and 313 K. The thermodynamic equilibrium constant at 298.15 K is  $K_{\text{CN,SCN}}^\circ = 23.2 \pm 3.0$ . The enthalpy change for the reaction was obtained calorimetrically at 298.15 K, being  $\Delta H_{\text{CN,SCN}}^\circ = -13.23 \pm 0.38\ \text{kJ mol}^{-1}$ , hence the calculated  $\Delta S_{\text{CN,SCN}}^\circ = -18.3 \pm 1.6\ \text{J K}^{-1}\ \text{mol}^{-1}$  and  $\Delta C_p^\circ = 21 \pm 13\ \text{J K}^{-1}\ \text{mol}^{-1}$ . Invasion of the thiocyanate form also releases heat  $66 \pm 9\ \text{kJ (mol of KSCN imbibed)}^{-1}$  and water  $6.0 \pm 1.5\ \text{mol of H}_2\text{O (mol of KSCN imbibed)}^{-1}$ . The exchange of cyanide form resin (total water content  $\bar{n}_w = 10.1\ \text{mol of H}_2\text{O equiv}^{-1}$ ) to thiocyanate form ( $\bar{n}_w = 5.3\ \text{mol of H}_2\text{O equiv}^{-1}$ ) is interpreted as release of free, not of hydration, water.

### Introduction

The thermodynamics of anion exchange reactions on anion exchange resins has not been as extensively studied as the

corresponding cation exchange reactions. The standard Gibbs energy, enthalpy, and entropy changes of the anion exchange reactions are not well documented.<sup>1</sup> These anion exchange reactions which have been studied are almost totally restricted to exchanges among the halide anions.<sup>2-7</sup> An important correlation has been found between composition and equilibrium constant data.<sup>7</sup> Both enthalpy and entropy changes (hence

\* Address correspondence to this author at the Department of Inorganic and Analytical Chemistry, The Hebrew University of Jerusalem.

also the logarithms of the equilibrium constants) were found to be proportional to the cross-linking, up to 4% divinylbenzene, and more significantly, to the change in water content of the swollen resin. However, the universality of this finding may be questioned in the light of other recent data. These<sup>8</sup> involve the exchange of nitrate, chloride, and bromide ions for hydroxide ions on 4 and 10% cross-linked resins. The integral enthalpies of the exchange can be estimated from the small scale figures presented of the differential enthalpies plotted against the ionic composition. The directly determined  $\Delta H_{\text{Cl,NO}_3}/\text{kJ mol}^{-1}$  are<sup>8</sup>  $-4.0$  (4% cross-linking) and  $-4.4$  (10% cross-linking) compared with values calculated by Hess's law via exchanges involving hydroxide ions:  $-3.3$  and  $-5.0$ , respectively. The Hess law  $\Delta H_{\text{Cl,Br}}/\text{kJ mol}^{-1}$  are  $-3.1$  and  $-4.7$  for 4 and 10% cross-linked resins, compared with the value obtained at trace bromide loading<sup>2</sup> on 10% cross-linked resin,  $-6.4$ , or with a 4% cross linked resin,<sup>6</sup>  $-9.6$  (from Hess's law). If the estimates<sup>8</sup> are accepted, their correlation with water content data also read from small scale figures<sup>8</sup> holds only very roughly for nitrate-chloride and bromide-chloride exchanges, but breaks down for exchanges involving the hydroxide ion. The latter show almost twice as high enthalpy changes as calculated from the changes in the water content.

It is of interest to test this correlation on further exchange reactions, of anions other than the halides, and to connect the changes in the water content of the swollen resin with the hydration properties of the ions. For this purpose, the exchange between the cyanide and thiocyanate anions has been studied.

This anion exchange reaction has not been studied before, although it is of considerable practical significance. Industrial wastes containing cyanide can be conveniently treated with anion exchangers for the removal and the recovery of heavy metals. Thiocyanate anions, however, which are likely to be present in these wastes, are known<sup>10</sup> to interfere with the sorption of the cyanide anions. It is therefore important to know the position of the equilibrium



To date, only indirect estimates of the equilibrium constant  $K_{\text{CN,SCN}}$  of reaction 1 can be made. Particularly lacking is information concerning the anion exchange properties of cyanide anions, which is known however to be slightly preferred over chloride anions.<sup>11,12</sup> A good estimate for the true equilibrium constant for the exchange reaction with chloride

$$K^{\circ}_{\text{Cl,CN}} = \int_0^1 K_{\text{Cl,CN}} d\bar{x}_{\text{CN}} \\ = \int_0^1 (\bar{x}_{\text{CN}} m_{\text{ClYCl}} / \bar{x}_{\text{Cl}} m_{\text{CN}^-\text{YCN}}) d\bar{x}_{\text{CN}} \quad (2)$$

is the equilibrium quotient at half-loading ( $\bar{x}_{\text{CN}} = 0.5$ ) which has been given as 1.6 for trimethylbenzylammonium (Dowex-1) type anion exchanger<sup>11,12</sup> and as 1.3<sup>11</sup> or 1.5<sup>12</sup> for 2-ethanoldimethylbenzylammonium (Dowex-2) type anion exchanger. More data on equilibrium constants for exchange reactions involving thiocyanate ions have been published, but these constants  $K_{\text{A,SCN}}$ , where A is an anion such as chloride, hydroxide, or nitrate, are very sensitive to  $\bar{x}_{\text{SCN}}$ , whereas insufficient data for evaluating  $K_{\text{A,SCN}}$  usually exist. Therefore very diverse estimates of this constant have been published, which for the purpose of comparison must still be converted to  $K^{\circ}_{\text{Cl,SCN}}$  by means of the better known  $K^{\circ}_{\text{Cl,A}}$  data. The value obtained by using  $\text{A}^- = \text{Au}(\text{CN})_2^-$ , on a Dowex-1 type (actually Amberlite IRA 400) anion exchange resin, is  $\log K^{\circ}_{\text{Cl,SCN}} = 1.86$ .<sup>13</sup> It is much higher than the value 0.44 ob-

tained by integration (albeit over only three values of  $\bar{x}_{\text{SCN}}$ : 0.05, 0.47, and 0.98) of chloride-thiocyanate exchange data for 8% cross-linked Dowex-2 resin,<sup>14</sup> the values 0.82–0.67 obtained<sup>6</sup> via  $\text{A}^- = \text{OH}^-$  on 2–10% cross-linked Dowex-1 resin with an unclear integration method, the value 1.19 obtained indirectly via  $\text{A}^- = \text{NO}_3^-$  on Wofatit SB,<sup>3</sup> or the value 1.02 obtained via  $\text{A}^- = \text{OH}^-$  without integration on Wofatit SBK (Dowex-2 type) resin.<sup>12</sup> The broad range of estimates permits one only to conclude that thiocyanate anions are considerably preferred over cyanide anions in the resin, so that equilibrium 1 should tend strongly to the right.

In the present work, the state of equilibrium 1 was determined on an 8% cross-linked Dowex-1 anion exchange resin at the three temperatures 283, 298, and 313 K as a function of the loading,  $\bar{x}_{\text{SCN}}$ . Also, the water contents of the totally and partly exchanged forms, and the invasion by potassium thiocyanate and its effect on the water content, were determined. Furthermore, the heat of exchange was determined calorimetrically at 298 K. From these data, insight into the anion exchange process, and the correlation of the enthalpy and the entropy of the exchange with the water content, could be gained.

## Experimental Section

**Materials.** The anion exchange resin used was an 8% (nominal) cross-linked poly(styrenemethylene) trimethylammonium (Dowex-1) of 100–200 mesh size. It was conditioned by the usual acid and base cycles, and converted to the cyanide or thiocyanate form by passing an excess of the 1 M potassium salts through resin packed in a column, until chloride could no longer be detected in the effluent. The resin was then washed with distilled water and air dried. No decomposition or hydrolysis of the cyanide resin was observed.

The other materials were analytical reagent grade salts and twice distilled water.

**Anion Exchange Equilibrium.** A quantity of resin in the cyanide form was packed in a small jacketed column, through the jacket of which water from a thermostat controlled to  $\pm 0.05$  K was circulated. A solution of a given composition,  $0.1002 \pm 0.002$  m (0.1000 M at 298 K) of  $\text{K}(\text{CN} + \text{SCN})$  was passed slowly through the column of resin until the effluent had the same composition as the influent. The anions of the column were then displaced and determined. The sum ( $\text{CN}^- + \text{SCN}^-$ ) was determined by potentiometric argentometry,  $\text{SCN}^-$  similarly after removal of HCN from another aliquot by addition of  $\text{H}_2\text{SO}_4$  and heating in a stream of  $\text{N}_2$  on a water bath, and  $\text{CN}^-$  by difference. The column was then treated with a new composition of the solution.

**Heat of Exchange.** The calorimetric setup has been described elsewhere,<sup>15</sup> and only small changes were required to convert it from liquid-liquid distribution to ion exchange operation. The dewar vessel had a volume of only ca. 200  $\text{cm}^3$ , and the heat capacity of the solution and resin was ca. 400 J  $\text{K}^{-1}$ , so that a precision of  $\pm 0.5$  J could be easily obtained. Magnetic stirring was substituted for stirring from above, and a goose-neck pipet in the vessel prevented premixing but permitted thermal preequilibration. A known quantity (2–5 g) cyanide form resin was placed along with a volume of 95  $\text{cm}^3$  of liquid, comprising 15–95  $\text{cm}^3$  of 0.1 M aqueous KCN, the rest being water in the dewar vessel, thermostated at 298.15  $\pm 0.08$  K. The thermally preequilibrated pipet contained 5  $\text{cm}^3$  of 0.1–1.7 M aqueous KSCN, calculated with the known weight of resin, amount of KCN solution, and the equilibrium position at 298 K to give a final solution of 0.100 M  $\text{K}(\text{CN} +$

SCN) and resin of desired ionic composition. The total heats of exchange measured were corrected for the heats of mixing of the aqueous solution, measured in separate experiments without resin. This procedure obviated the problem of a much larger correction for heat of swelling required, if the dry resin would have been added to the solution, instead of using a preswollen resin as here.

**Salt Invasion.** Known weights (2 g) of resin in the SCN<sup>-</sup> form were placed in the dewar vessel of the calorimeter along with 94–98 cm<sup>3</sup> of water, and 2–6 cm<sup>3</sup> of 10.0–2.5 M aqueous KSCN were added from the pipet at 298 K. The heat evolved was corrected for the heat of dilution, measured in separate experiments. The resin was then collected quantitatively, separated from the solution by centrifugation in a standardized procedure. The resin was weighed and the excess salt washed out by water and determined.

**Water Content.** Resin (1–2 g) in the appropriate ionic form was kept at 298.2 ± 0.2 K for 1 h with excess 0.1 M potassium salt solution, then separated by a standardized centrifugation procedure (2000 rpm, 1 h at room temperature, ca. 300 K) which defined the state of the water containing resin. It was weighed, then dried for 20–24 h at 343 K in a vacuum oven at a pressure of 800–1300 Pa, and reweighed.

## Results

**Equilibrium Constants.** The equilibrium quotients

$$K'_{\text{CN,SCN}} = \bar{x}_{\text{SCN}} m_{\text{CN}} / \bar{x}_{\text{CN}} m_{\text{SCN}} \quad (3)$$

obtained at 283, 298, and 313 K with 0.1002 m (0.1 M) potassium cyanide–thiocyanate solutions are shown in Table I, as a function of the thiocyanate loading,  $\bar{x}_{\text{SCN}}$ . The data give with a least-squares fitting the analytical expressions

$$\begin{aligned} K'_{\text{CN,SCN}} &= 64 - 124\bar{x}_{\text{SCN}} + 100\bar{x}_{\text{SCN}}^2 \\ &\quad (\text{within } \pm 4) \text{ at } 283 \text{ K} \\ &= 41 - 71\bar{x}_{\text{SCN}} + 53\bar{x}_{\text{SCN}}^2 \\ &\quad (\text{within } \pm 3) \text{ at } 298 \text{ K} \\ &= 42 - 66\bar{x}_{\text{SCN}} + 66\bar{x}_{\text{SCN}}^2 - 22\bar{x}_{\text{SCN}}^3 \\ &\quad (\text{within } \pm 4) \text{ at } 313 \text{ K} \end{aligned} \quad (4)$$

No activity coefficients are available in mixed cyanide–thiocyanate solutions, but the corrected equilibrium quotient,  $K_{\text{CN,SCN}} = K'_{\text{CN,SCN}}(\gamma_{\pm\text{KCN}}/\gamma_{\pm\text{KSCN}})^2$  can be well approximated at 0.1 m external solution concentration by  $K'_{\text{CN,SCN}}(\gamma^{\circ}_{\pm\text{KCN}}/\gamma^{\circ}_{\pm\text{KSCN}})^2$ . The activity coefficients in the individual potassium salt solutions,  $\gamma^{\circ}_{\pm}$ , are however, not all well known. At 0.1 m and at 273 K the ratio  $\gamma^{\circ}_{\pm\text{KCN}}/\gamma^{\circ}_{\pm\text{KSCN}}$  is 0.979.<sup>16</sup> At 298 K, experimental data are available only for  $\gamma^{\circ}_{\pm\text{KSCN}}$ .<sup>17</sup> A value for  $\gamma^{\circ}_{\pm\text{KCN}}$  has been estimated according to Kielland's method,<sup>18</sup> yielding 0.979 for the ratio of activity coefficients also at this temperature. The equilibrium constant for reaction 1 is therefore

$$K^{\circ}_{\text{CN,SCN}} \simeq (\gamma^{\circ}_{\pm\text{KCN}}/\gamma^{\circ}_{\pm\text{KSCN}})^2 \int_0^1 K'_{\text{CN,SCN}} d\bar{x}_{\text{SCN}} \quad (5)$$

If the standard states are selected as usual as the pure resin forms in equilibrium with 0.1 m potassium salt solutions, and as the hypothetical ideal 1 m solution respectively for the two phases, the Gibbs energy change is

$$\begin{aligned} \Delta G^{\circ}_{\text{CN,SCN}} &= -RT \ln K^{\circ}_{\text{CN,SCN}} \\ &= -8.37 \pm 0.26 \text{ kJ/mol at } 283 \text{ K} \\ &= -7.79 \pm 0.30 \text{ kJ/mol at } 298 \text{ K} \\ &= -8.63 \pm 0.36 \text{ kJ/mol at } 313 \text{ K} \end{aligned} \quad (6)$$

**TABLE I: Equilibrium Quotients  $K'_{\text{CN,SCN}}$  as a Function of Thiocyanate Mole Fraction in the Exchanger,  $\bar{x}_{\text{SCN}}$ , at Three Temperatures**

283 K		298 K		313 K	
$\bar{x}_{\text{SCN}}$	$K'_{\text{CN,SCN}}$	$\bar{x}_{\text{SCN}}$	$K'_{\text{CN,SCN}}$	$\bar{x}_{\text{SCN}}$	$K'_{\text{CN,SCN}}$
0.055	56.8	0.033	32.9	0.040	40.0
0.197	56.8	0.155	35.8	0.180	44.4
0.383	29.7	0.300	24.8	0.328	23.8
0.622	30.0	0.500	17.5	0.537	21.7
0.869	26.6	0.8077	17.5	0.703	21.3
0.966	41.9	0.9357	20.9	0.767	18.8
0.9826	38.7	0.9650	21.1	0.842	21.0
				0.844	21.4
				0.9292	19.5
				0.9611	16.1

The activity coefficient term amounts to only +0.100, +0.105, and +0.109 kJ/mol at these temperatures at most, well within the random errors, and any inaccuracies in it are insignificant.

**Heat of Exchange.** There is no reason to doubt the irregular change of  $\Delta G^{\circ}_{\text{CN,SCN}}$  with temperature exhibited in eq 6, since the data for 313 K definitely fall between those for 283 and 298 K. Therefore the enthalpy change for equilibrium 1 is best obtained from direct calorimetric measurements. The differential heats of exchange  $\Delta H'_{\text{CN,SCN}}$  obtained at 298 K are shown in Figure 1 as a function of the thiocyanate loading  $\bar{x}_{\text{SCN}}$ . These data were all obtained starting with cyanide resin,  $\overline{\text{RCN}}$ , since the very large excess of cyanide solution that would have been required for starting with thiocyanate resin  $\overline{\text{RSCN}}$  could not be accommodated in the calorimeter. Since, however, the composition dependence of  $\Delta H'_{\text{CN,SCN}}$  is mild and linear, integration over the whole composition range seems to be possible. Using the equal chord area method<sup>9</sup> and the analytical expression

$$\Delta H'_{\text{CN,SCN}}/\text{kJ mol}^{-1} = -14.52 + 2.55\bar{x}_{\text{SCN}} \quad (\text{within } \pm 0.38) \quad (7)$$

yields on integration

$$\begin{aligned} \Delta H_{\text{CN,SCN}} &= \int_0^1 \Delta H'_{\text{CN,SCN}} d\bar{x}_{\text{SCN}} \\ &= -13.24 \pm 0.38 \text{ kJ mol}^{-1} \end{aligned} \quad (8)$$

This quantity must still be corrected for the change in the heat contents of the aqueous solutions on going from 0.1 m KSCN to 0.1 m KCN. Heat contents of 1:1 electrolytes have been reviewed by Parker et al.,<sup>19</sup> and the apparent molal heat  $\phi_L$  of potassium thiocyanate is given there for 298 K as a function of the molality. The heat content

$$L_{\text{KSCN}} = \phi_L(\text{KSCN}) + \frac{1}{2} m^{1/2} (\partial\phi_L(\text{KSCN})/\partial m^{1/2})_T \quad (9)$$

can be obtained from the data at and near 0.1 m to give  $L_{\text{KSCN}}(0.1 \text{ m}) = 158 \text{ J/mol}$ . For potassium cyanide, however, only estimates are given, and none specifically for 298 K and 0.1 m. Resource may be taken again to the theoretical estimate of the activity coefficient,<sup>18</sup> since

$$L_{\text{KCN}} - L_{\text{KSCN}} = -RT^2(\partial/\partial T)(\ln \gamma_{\text{CN}} - \ln \gamma_{\text{SCN}}) \quad (10)$$

The theoretically obtained derivatives<sup>20</sup> give for the difference  $L_{\text{KCN}} - L_{\text{KSCN}} = 14 \text{ J mol}^{-1}$  (i.e.,  $L_{\text{KCN}} = 172 \text{ J mol}^{-1}$  at 298 K and 0.1 m). The standard heat of exchange 1 then is

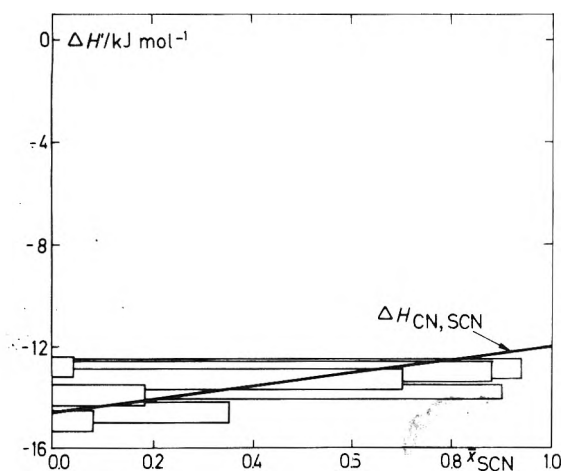


**Figure 1.** Differential heats of exchange  $\Delta H'/\text{kJ mol}^{-1}$  at 298 K for the exchange of thiocyanate for cyanide ions on Dowex-1 8% cross-linked anion exchanger as a function of the thiocyanate mole fraction on the exchanger,  $\bar{x}_{\text{SCN}}$ . The aqueous phase is 0.1 M  $\text{K}(\text{CN} + \text{SCN})$ . The rectangles enclose the initial and final resin compositions and indicate the experimental error of the heat evolved.

$$\Delta H^{\circ}_{\text{CN,SCN}} = \Delta H_{\text{CN,SCN}} + (L_{\text{KCN}} - L_{\text{KSCN}}) = -13.23 \pm 0.38 \text{ kJ mol}^{-1} \quad (11)$$

and it is seen that the correction is much smaller than the random experimental errors, hence immaterial.

**Electrolyte Invasion.** The quantity of electrolyte absorbed by the thiocyanate form of the resin in equilibrium with aqueous potassium thiocyanate solutions, and the corresponding heat effect, were measured at 298 K. The results are shown in Figure 2, along with some data obtained at higher concentrations on a similar resin by Zachariades et al.<sup>21</sup> Inherent inaccuracies in the water determinations in the resin make the presentation of the data as resin phase molalities inadvisable. Therefore, the primary data, i.e., the moles of electrolyte sorbed per equivalent of the anion exchange resin,  $\bar{n}_{\text{K}}$ , are shown, along with the heat effects  $\Delta q$  (actually  $\Delta q/66$  is plotted, see below), again per equivalent of resin. The ratio  $\Delta q/\bar{n}_{\text{K}}$  is seen to be approximately constant: about  $66 \pm 9 \text{ kJ}$  are released per mole of potassium thiocyanate imbibed. It is of interest to note also the change in the water content of the swollen resin when electrolyte is imbibed. According to Zachariades et al.,<sup>21</sup> considerable amounts of water are released when the electrolyte invades the resin. Since the water release is a small difference between relatively large numbers, inaccuracies in the latter strongly affect the values

$$\Delta \bar{n}_{\text{W}} = \bar{n}_{\text{W}}(\bar{n}_{\text{K}} = 0) - \bar{n}_{\text{W}}(\bar{n}_{\text{K}}) \quad (12)$$

It can be seen in Figure 2 that  $\Delta \bar{n}_{\text{W}}/\bar{n}_{\text{K}}$  is approximately constant at  $6.0 \pm 1.5$ . Hence, also  $\Delta q/\Delta \bar{n}_{\text{W}}$  is approximately constant, at ca.  $11 \text{ kJ/mol}$  of water released on electrolyte invasion.

**Water Contents.** The loss of weight on drying of resin samples swollen with 0.1 M solutions of the appropriate potassium salt were obtained. It is given as weight fractions of water in Table II, accurate to  $\pm 0.002$ . These primary data can be converted into  $\bar{n}_{\text{W}}$  values, moles of water per equivalent of resin, if accurate capacity data are available. The capacities of the chloride and thiocyanate forms (Table II) are mutually consistent within  $\pm 2\%$ , considering the change in the equivalent weight of the anion. The capacity of the cyanide resin, however, was low, signifying a considerable loss of cyanide (as HCN, leaving hydroxide behind) on drying. The values of  $\bar{n}_{\text{W}}$

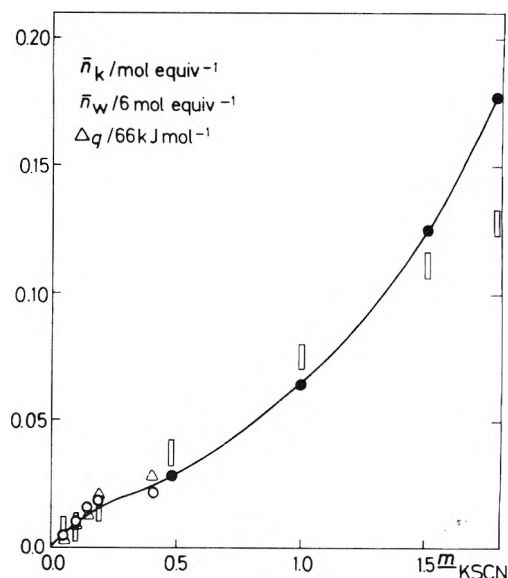


**Figure 2.** Invasion of resin thiocyanate with potassium thiocyanate from aqueous solutions as a function of the equilibrium molality of the latter: (circles)  $\bar{n}_{\text{K}}$ ; error bars:  $\Delta \bar{n}_{\text{W}}/6$  mol per equivalent of resin; (triangles) heat released on invasion,  $\Delta q/66 \text{ kJ/mol}$ ; open symbols, this work; filled symbols, from Zachariades et al.<sup>21</sup>

**TABLE II: Water Contents and Capacities of the Anion Exchanger in Various Ionic Forms**

Resin	Wt. fraction of water	Capacity, equiv/kg of dry resin		$\bar{n}_{\text{W}}$ , mol of $\text{H}_2\text{O}/\text{equiv}$ of resin
		Obsd	Calcd	
RCl	0.411	3.48	(3.48)	$11.1 \pm 0.2$
RSCN	0.242	3.34	3.28	$5.3 \pm 0.2$
RCN	0.400	2.78	3.66	$10.1 \pm 0.2$
R(0.496 CN + 0.504 SCN)	0.357		3.46	$8.9 \pm 0.2$

(Table II) are accurate to within  $\pm 0.2$ , assuming the capacity of the cyanide form, before drying, not to be impaired. A nonlinear decrease of  $\bar{n}_{\text{W}}$  as  $\bar{x}_{\text{SCN}}$  is increased is apparent; most of the water is lost only when the resin becomes rich in thiocyanate anions.

The water content found here for the chloride form RCl is consistent with values found previously for the same kind of exchanger,<sup>22</sup> the absolute value depending on the experimental procedure for defining the swollen resin. The value found here for the thiocyanate form RSCN is similarly in agreement with that calculated from the data of Zachariades et al.<sup>21</sup>

## Discussion

The equilibrium constant for the anion exchange of thiocyanate for cyanide on 8% cross-linked Dowex-1 at 298 K has been evaluated here as  $K^{\circ}_{\text{CN,SCN}} = 23.2 \pm 3.0$ . This permits now a selection of  $K^{\circ}_{\text{Cl,SCN}}$  based on  $K^{\circ}_{\text{Cl,CN}} = 1.60$ . The value for the logarithm of the equilibrium constant for exchanging chloride for thiocyanate on Dowex-1 is 1.57, much nearer the indirect estimate of 1.86<sup>13</sup> than the other estimates mentioned in the Introduction.

From the standard Gibbs energy change for equilibrium 1 at 298 K and the corresponding standard enthalpy change, eq 6 and 11, the standard entropy change is obtained as

$$\Delta H^\circ/T + R \ln K^\circ = \Delta S^\circ = -18.3 \pm 1.6 \text{ J/K mol} \quad (13)$$

Because of the irregular change of  $K^\circ$  with temperature, and the fact that  $\Delta H^\circ$  was determined at only one temperature, only a rough estimate of  $\Delta C_p^\circ$ ,  $21 \pm 13 \text{ J/K mol}$ , can be given.

These thermodynamic data may be compared with the few reliable determinations that have been published before.<sup>4-8,12</sup> These concern exchanges of the halide anions among themselves and with nitrate and hydroxide anions. Large negative enthalpies, as found here, eq 8, were obtained for exchanges involving the strongly held iodide ion:  $\Delta H^\circ_{F,I} = -21.0 \text{ kJ/mol}$  for 1% cross-linking,<sup>7</sup>  $\Delta H^\circ_{Cl,I} = -14.5 \text{ kJ/mol}$  for 1%<sup>7</sup> and  $-13.5 \text{ kJ/mol}$  for 0.5% cross-linking,<sup>6</sup> with Dowex-1 type exchangers. Large negative entropies,  $T\Delta S^\circ_{F,I} = -13.7$ ,  $T\Delta S^\circ_{Cl,I} = -9.6$  (1%) or  $-9.0$  (0.5%)  $\text{kJ/mol}$ , are also characteristic for these exchanges. The value found here,  $T\Delta S^\circ_{CN,SCN} = -5.4 \text{ kJ/mol}$ , is however not so large. The enthalpy and entropy changes for anion exchange reactions always agree in sign,<sup>2,4-8</sup> and the latter are approximately proportional to the former:  $T\Delta S^\circ \sim 0.6\Delta H^\circ$ , for various cross-linkings and resin types. The system studied at present, like the systems involving hydroxide anions,<sup>8</sup> do not conform to this relationship, the entropy changes not being as negative.

The situation in the literature concerning the standard heat capacity change of anion exchange is not at all clear. Some authors<sup>7,8</sup> conclude from their temperature dependence studies of the equilibrium constants that  $\Delta H^\circ$  is temperature independent, i.e.,  $\Delta C_p^\circ = 0$ . Others find appreciable values of  $\Delta C_p$ , albeit for tracer loadings of the preferred ion:  $\Delta C_{p,Cl,Br} = 21 \text{ J/K mol}$  on 10% cross-linked Dowex-1,<sup>2</sup> and  $\Delta C_{p,OH,Cl} = \Delta C_{p,OH,SCN} = 247 \text{ J/K mol}$ <sup>24</sup> on 2, 4, or 10% cross-linked Dowex-1. The calorimetric measurements on anion exchange reactions have always been made at one temperature only,<sup>4,5</sup> as in the present study. Still, the nonzero heat capacity change found here is considered to be significant. The statements<sup>7,8</sup> that  $\log K$  is linear with  $T^{-1}$  within experimental errors are considered valid only because of the not-so-small values of these errors.

The crucial point for the explanation of these data is the deswelling that occurs when the cyanide resin is converted into thiocyanate resin, together with changes in the hydration of the aqueous ions (changing from thiocyanate to cyanide) concomitant thereon. Ion exchange selectivities have already been correlated with changes in the equivalent swollen volume of the resins<sup>14</sup> and with the changes in water content.<sup>7</sup>

From the data in Table II,  $\Delta \bar{n}_w = \bar{n}_w(\text{RCN}) - \bar{n}_w(\text{RSCN}) = 10.1 \pm 0.2 - 5.3 \pm 0.2 = 4.8 \pm 0.3 \text{ mol of H}_2\text{O equiv}^{-1}$ . Therefore the enthalpy and entropy changes per unit change in water content per 1% of cross-linking are

$$\begin{aligned} \Delta H^\circ_{CN,SCN}/\Delta \bar{n}_w X &= (-13.23 \pm 0.38)/(4.8 \pm 0.3) \cdot 8 \\ &= -347 \pm 24 \text{ J}(\text{mol of H}_2\text{O})^{-1} (\% \text{ cross-link})^{-1} \end{aligned} \quad (14)$$

$$\begin{aligned} \Delta S^\circ_{CN,SCN}/\Delta \bar{n}_w X &= (-18.3 \pm 1.6)/(4.8 \pm 0.3) \cdot 8 \\ &= -0.48 \pm 0.05 \text{ J K}^{-1}(\text{mol of H}_2\text{O})^{-1} (\% \text{ cross-link})^{-1} \end{aligned} \quad (15)$$

The corresponding values for halide ion exchange on the same anion exchanger at 1-4% cross-linking is<sup>7</sup> ca.  $-240 \text{ J}(\text{mol of H}_2\text{O})^{-1}(\% \text{ cross-link})^{-1}$  for the enthalpy and ca.  $-0.50 \text{ J K}^{-1}(\text{mol of H}_2\text{O})^{-1}(\% \text{ cross-link})^{-1}$  for the entropy. The latter is in good agreement with the present value (for 8% cross-linked resin), but the enthalpy change found for the present system is about a factor of 1.5 more negative (see also the noncorrelation of enthalpy and entropy changes discussed above). The

higher cross-linking in the present study does not explain the discrepancy.<sup>7</sup> As noted in the Introduction, exchange of other ions (hydroxide) does not either conform to the generalization for the halide anions.

The exchange of the anions has the effect of removing thiocyanate anions from the aqueous solution and introducing there cyanide anions in their stead. The difference between the formation enthalpies of the aqueous ions in their standard state (assumed not to differ much from the 0.1 M solution employed here) is<sup>25</sup>  $\Delta H_f^\circ_{298}(\text{CN}^-, \text{aq}) - \Delta H_f^\circ_{298}(\text{SCN}^-, \text{aq}) = 74.2 \text{ kJ mol}^{-1}$  while the difference between the formation enthalpies of the gaseous ions is<sup>26</sup>  $\Delta H_f^\circ_{298}(\text{CN}^-, \text{g}) - \Delta H_f^\circ_{298}(\text{SCN}^-, \text{g}) = 137.7 \text{ kJ mol}^{-1}$ . Hence, the difference in the enthalpies of hydration is  $74.2 - 137.7 = -63.5 \text{ kJ mol}^{-1}$ . Since the enthalpy change of the ion exchange is only  $-13.2 \text{ kJ mol}^{-1}$ , either the ions are not completely dehydrated on entering the resin, or there exists some compensating endothermic effect. On the other hand, the difference between the standard entropies of the anions in the aqueous solution is<sup>25</sup>  $S^\circ_{298}(\text{CN}^-, \text{aq}) - S^\circ_{298}(\text{SCN}^-, \text{aq}) = -50.2 \text{ J K}^{-1} \text{ mol}^{-1}$ , while the difference in the gaseous standard entropies is<sup>27</sup>  $S^\circ_{298}(\text{CN}^-, \text{g}) - S^\circ_{298}(\text{SCN}^-, \text{g}) = -43.1 \text{ J K}^{-1} \text{ mol}^{-1}$ , so that the difference in the entropies of hydration is  $-50.2 - (-43.1) = -7.1 \text{ J K}^{-1} \text{ mol}^{-1}$ . This should be compared with the more negative entropy effect of the anion exchange,  $-18.3 \text{ J K}^{-1} \text{ mol}^{-1}$ . Either, again, the ions are not dehydrated, or a compensating ordering effect occurs that accounts for the discrepancy.

It turns out that the anions are hydrated to approximately the same extent in the aqueous solution,  $5.30 \pm 0.15 \text{ mol}$  of water per mole of anion. The volume of the hydrated ions can be calculated from<sup>28</sup>

$$V^\circ_{hi} = 2510(r_{hi}/\text{nm})^3 + 315(r_{hi}/\text{nm})^2 \text{ cm}^3 \text{ mol}^{-1} \quad (16)$$

where  $r_{hi}$ , the radius of the hydrated ions, is obtained according to Nightingale<sup>29</sup> from the Stokes radii  $r_{st} = 9.162 \times 10^{-4}/(\lambda^\circ_i/\Omega^{-1} \text{ m}^2 \text{ mol}^{-1}) \text{ nm}$ ,  $\lambda^\circ_i$  being the equivalent conductivity at infinite dilution. From the reported<sup>30</sup> values of  $\lambda^\circ_{\text{CN}^-} = 0.0078 \Omega^{-1} \text{ m}^2 \text{ equiv}^{-1}$  and  $\lambda^\circ_{\text{SCN}^-} = 0.00665 \Omega^{-1} \text{ m}^2 \text{ mol}^{-1}$  at 298 K, the Stokes radii  $r_{st(\text{CN}^-)} = 0.1175 \text{ nm}$  and  $r_{st(\text{SCN}^-)} = 0.1378 \text{ nm}$  are obtained, which interpolate in a large scale plot of Nightingale's data<sup>29</sup>  $r_{hi}(r_{st})$  to give  $r_{h\text{CN}^-} = 0.329 \text{ nm}$  and  $r_{h\text{SCN}^-} = 0.338 \text{ nm}$ . The volumes of the hydrated ions are, from (16)  $V^\circ_{h\text{CN}^-} = 123.48 \text{ cm}^3 \text{ mol}^{-1}$  and  $V^\circ_{h\text{SCN}^-} = 132.91 \text{ cm}^3 \text{ mol}^{-1}$ , the difference being  $9.43 \text{ cm}^3 \text{ mol}^{-1}$ . The partial molar volumes of the anions at infinite dilution are obtained from Millero<sup>31</sup> as  $\bar{V}^\circ_{\text{CN}^-} = 25.4 \text{ cm}^3 \text{ mol}^{-1}$  and  $\bar{V}^\circ_{\text{SCN}^-} = 40.1 \text{ cm}^3 \text{ mol}^{-1}$ , the difference being  $14.76 \text{ cm}^3 \text{ mol}^{-1}$ . From the relationships<sup>31,32</sup>

$$\begin{aligned} \bar{V}^\circ_i &= 4480(r_{ci}/\text{nm})^3 - 0.80(r_{ci}/\text{nm})^{-1} \\ &= V^\circ_{hi} - h_i V^\circ_w \text{ cm}^3 \text{ mol}^{-1} \end{aligned} \quad (17)$$

where  $r_{ci}$  is the crystal ionic radius,  $h_i$  the hydration number (defined operationally by eq 17), and  $V^\circ_w$  the molar volume of water,  $18.03 \text{ cm}^3 \text{ mol}^{-1}$  at 298.15 K, the hydration numbers  $h_{\text{CN}^-} = 5.44$  and  $h_{\text{SCN}^-} = 5.15$  are obtained, their difference being 0.29. A similar value is obtained from the electrostrictive term of (17),  $-0.80(r_{ci}/\text{nm})^{-1}$ , for the two anions, and the crystal ionic radii  $r_{\text{CN}^-} = 0.188 \text{ nm}$  and  $r_{\text{SCN}^-} = 0.214 \text{ nm}$  (which give with eq 17 the correct<sup>31</sup>  $\bar{V}^\circ_i$ ), compared with the value  $-2.1 \text{ cm}^3$  per mol of water of hydration:<sup>32</sup>  $[-0.80/0.188 - (-0.80/0.214)]/(-2.1) = 0.24$ . When thiocyanate anions replace cyanide anions on the exchanger, complete dehydration would release only these 0.24 to 0.29 mol of water per mol of anions exchanged to the aqueous phase, which is far from

the  $4.8 \pm 0.3$  mol of water actually released. These must then come from the "free" water, of which there exist hardly any in the thiocyanate form of the resin (compare  $\bar{n}_W = 5.3$  with  $h_{\text{SCN}^-} = 5.15$ ), but a large amount in the cyanide form (compare  $\bar{n}_W = 10.1$  with  $h_{\text{CN}^-} = 5.44$ ).

The conclusion from the enthalpy and entropy of hydration and from the hydration number considerations above is that the anions cyanide and thiocyanate remain hydrated in the resin, and that hydration–dehydration reactions are not primarily responsible for the observed thermodynamic quantities. The "free" water released can, however, contribute. It is this water that depends on the cross-linking, and its leaving the disordered state inside the resin and joining the ordered bulk water gives the decrease in entropy according to eq 15, in conformity with the interhalide exchanges. The additional hydrogen bonding permitted in the joining of the released water to the ordered bulk water is the contribution to the negative enthalpy change, eq 14. What remain unexplained are the discrepancy in  $\Delta H^\circ$  between the present system and interhalide exchanges, and the actual value of the "free" water content in the cyanide form of the anion exchange resin, the excess over the anion hydration. Site binding<sup>4,33</sup> of the preferred anion can be ruled out as a contributing cause, because there is no evidence of dehydration. Since the anions have nearly the same charges and hydrated radii,  $r_{\text{hi}}$ , no electrostatic contribution<sup>34</sup> should be important either. The excess, free, water in the cyanide form of the resin and excess negative enthalpy may perhaps be due to partial hydrolysis (the low capacity points that way), the polarized grouping  $\text{R}^+ \text{HO} \cdots \text{H} \cdots \text{CN}^-$  ( $\text{R}^+$  is the fixed ion of the resin) holding more water than the less polarized  $\text{R}^+(\text{H}_2\text{O})\text{SCN}^-$  grouping. When hydration water is released, as in the invasion of the thiocyanate form of the resin by potassium thiocyanate, much more heat is evolved  $(66 \pm 9)/(6.0 \pm 1.5) = 11 \pm 3$  kJ (mol of water)<sup>-1</sup> than when free water is released in the exchange  $(13.23 \pm 0.38)/(4.8 \pm 0.3) = 2.8 \pm 0.2$  kJ (mol of water)<sup>-1</sup>. The invasion must therefore provide a large source of enthalpy to compensate for the heat of hydration, probably through electrostatic interaction.

## References and Notes

- (1) Y. Marcus (with collaboration of D. G. Howery), "Ion Exchange Equilibrium Constants", IUPAC Additional Publication, Butterworths, London, 1975.
- (2) K. A. Kraus, R. J. R. Raridon, and D. L. Holcomb, *J. Chromatogr.*, **3**, 178 (1960).
- (3) K. Gartner, *Z. Phys. Chem. (Leipzig)*, **225**, 132 (1963).
- (4) F. Vaslow and G. E. Boyd, *J. Phys. Chem.*, **70**, 2507 (1966).
- (5) G. E. Boyd and A. Schwartz, *J. Phys. Chem.*, **71**, 1355 (1967).
- (6) T. L. Zalevskaya and G. L. Starobinets, *Zh. Anal. Khim.*, **24**, 721 (1969).
- (7) G. R. Choppin, G. Y. Markovits, and M. E. Clark, *J. Phys. Chem.*, **76**, 680 (1972).
- (8) V. S. Soldatov and V. I. Sokolova, *Zh. Fiz. Khim.*, **46**, 146 (1972).
- (9) No units for  $\Delta H$  are given in the paper,<sup>9</sup> but the order of magnitude suggests that the ordinates in the figures are in kcal/mol. Multiplied by 4.184 they give the values quoted here in kJ/mol.
- (10) There exists considerable patent literature on this subject. An example of a journal article is: I. D. Fridman, L. N. Kuznetsova, and B. L. Serebryanyi, *Zh. Priklad. Khim.*, **38**, 482 (1965).
- (11) R. M. Wheaton and W. C. Bauman, *Ind. Eng. Chem.*, **43**, 1088 (1951).
- (12) O. Gürtler, G. Müller, and H. Holzapfel, *Z. Naturforsch. B*, **23**, 1382 (1968); O. Gürtler and H. Holzapfel, *Angew. Makromol. Chem.*, **6**, 109 (1969).
- (13) J. Aveston, D. A. Everest, and R. A. Wells, *J. Chem. Soc.*, 231 (1958).
- (14) H. P. Gregor, J. Belle, and R. A. Marcus, *J. Am. Chem. Soc.*, **77**, 2713 (1955).
- (15) Y. Marcus and Z. Kolarik, *J. Chem. Eng. Data*, **18**, 155 (1973).
- (16) Landolt-Börnstein, 5th ed, Ecb. 11, Vol. 2, 1931, p 1120.
- (17) R. A. Robinson and R. H. Stokes, "Electrolyte Solutions", 2nd ed, Butterworths, London, 1959, p 494.
- (18) J. Kielland, *J. Am. Chem. Soc.*, **59**, 1675 (1937); N. Tanaka and T. Murayama, *Z. Phys. Chem. (Frankfurt am Main)*, **11**, 366 (1957).
- (19) V. Parker, *Natl. Stand. Ref. Data Ser., Nat. Bur. Stand.*, No. 2 (1965).
- (20) From the Debye–Hückel expression
 
$$\ln \gamma_- = -\sqrt{\mu}/(1 + Ba_-\sqrt{\mu})$$
 with  $a_-$  specific for a given anion, one obtains the derivative  $(\partial/\partial T)(\ln \gamma_{\text{CN}^-} - \ln \gamma_{\text{SCN}^-})_{\mu, T} = AB(a_{\text{CN}^-} - a_{\text{SCN}^-})\mu \{ [d \ln A/dT - B^2(d \ln B/dT)(a_{\text{CN}^-} a_{\text{SCN}^-}) \cdot \mu / (1 + B(a_{\text{CN}^-} + a_{\text{SCN}^-})\sqrt{\mu} + B^2 a_{\text{CN}^-} a_{\text{SCN}^-})] / [1 + B(a_{\text{CN}^-} + a_{\text{SCN}^-})\sqrt{\mu} + B^2 a_{\text{CN}^-} a_{\text{SCN}^-}] \}$ . For aqueous solutions at 298 K,  $A = 0.511$ ,  $B = 0.329$  (for  $a$  in  $10^{-10}$  m),  $d \ln A/dT = 0.001838$ ,  $d \ln B/dT = 0.000613$ . With the estimates<sup>17</sup>  $a_{\text{CN}^-} = 3.0 \times 10^{-10}$  m and  $a_{\text{SCN}^-} = 3.5 \times 10^{-10}$  m, and for  $\mu = 0.1$  m,  $(\partial/\partial T)(\ln \gamma_{\text{CN}^-} - \ln \gamma_{\text{SCN}^-}) = -1.945 \times 10^{-5} \text{ K}^{-1}$ .
- (21) G. Zachariades, W. H. Herrera, and C. J. Cummeisky, *J. Inorg. Nucl. Chem.*, **28**, 1707 (1966).
- (22) Y. Marcus and J. Naveh, *J. Phys. Chem.*, **73**, 591 (1969); G. E. Boyd and B. A. Soldano, *Z. Elektrochem.*, **57**, 162 (1953).
- (23) The thermodynamic quantities reported<sup>3</sup> concerning the  $\text{NO}_3^- \text{---} \text{SCN}^-$  exchange on Wofatit SB are considered unsatisfactory, because of there being no characterization of the resin, because of the unexplained low values for  $\Delta H$  reported for well documented exchanges (e.g.,  $\Delta H_{\text{Cl}^-/\text{Br}^-} = -1.0$  kJ/mol compared with values<sup>4,7,8</sup> ranging from  $-4.2$  to  $-5.7$ , depending on the cross-linking, for Dowex-1), and because of the disagreeing signs of  $\Delta H$  and  $\Delta S$ , contrary to their generally agreeing in other works.<sup>2,4-8</sup>
- (24) G. L. Starobinets and T. L. Zalevskaya, *Zh. Fiz. Khim.*, **41**, 989 (1967).
- (25) D. D. Wagman et al., *Natl. Bur. Stand. Tech. Note*, No. 270-3 (1968).
- (26) T. C. Waddington, *Adv. Inorg. Chem. Radiochem.*, **1**, 157 (1959).
- (27) A. P. Altschuler, *J. Chem. Phys.*, **28**, 1254 (1959).
- (28) E. Glueckauf, *Trans. Faraday Soc.*, **61**, 914 (1965); J. E. Desnoyers and B. E. Conway, *J. Phys. Chem.*, **70**, 3017 (1966).
- (29) E. R. Nightingale, Jr., *J. Phys. Chem.*, **63**, 1381 (1959).
- (30) H. Falkenhagen, G. Kelbg, and E. Schmutzer, Landolt-Börnstein, Vol. II/7, p 259.
- (31) F. J. Millero, *Limnol. Oceanogr.*, **14**, 376 (1969).
- (32) J. Padova, *J. Chem. Phys.*, **39**, 2599 (1963); **40**, 691 (1964).
- (33) G. E. Boyd, F. Vaslow, and S. Lindenbaum, *J. Phys. Chem.*, **68**, 590 (1964); S. Lindenbaum and G. E. Boyd, *ibid.*, **69**, 2374 (1965); K. E. Becker, S. Lindenbaum, and G. E. Boyd, *ibid.*, **70**, 3834 (1966); F. Vaslow and G. E. Boyd, *ibid.*, **70**, 2295 (1966).
- (34) D. S. Flett and P. Mears, *Trans. Faraday Soc.*, **62**, 1469 (1966).

# The Co-Association of Nucleosides and the Equilibrium Copolymerization of Nucleotides. Base Stacking Interactions and the Thermodynamics of Phosphodiester Bond Formation

Leonard Peller

Cardiovascular Research Institute, University of California, San Francisco, California 94143 (Received June 11, 1976)

Publication costs assisted by the Cardiovascular Research Institute, University of California, San Francisco

A matrix formulation of equilibrium copolymerization statistics has been applied to the co-association of nucleosides as studied by thermal osmometry and the enzyme-catalyzed copolymerization of nucleoside diphosphates. The former is examined in the limit of small extents of association while the latter is analyzed in the high molecular weight limit. With data drawn from both types of investigation an estimate is made of the equilibrium constant for polydeoxyadenylic acid formation from deoxyadenosine triphosphate. For linear polymers with phosphodiester linkages the thermodynamic influence of base stacking interactions is at least comparable to that of covalent bond formation. The contribution made by the hydrolysis of the pyrophosphate by-product in the polymerization of nucleoside triphosphates dwarfs all other factors and effectively abolishes any contingency of the thermodynamics of reaction on nucleotide sequence.

## Introduction

The energetics of the interaction of nucleotides in the polymers of which they are the monomeric elements has been the subject of a variety of investigations since the earliest characterization of the helix to coil transitions of the double stranded chains.<sup>1,2</sup> As specific purine-pyrimidine nucleotide base pairing is the predominant structural feature of these chains, the thermodynamic information obtained relates principally to this matching.<sup>2,3</sup>

Thermodynamic parameters for the interactions of these bases in single strand chains are less readily available. Application of simple models to the relatively diffuse thermal transitions in such chains has yielded some estimates of these quantities for polyadenylic acid.<sup>2,4</sup> Negative deviations of colligative properties of aqueous solutions of nucleosides such as osmotic coefficients from ideal solution behavior measured by the venerable physicochemical technique of thermal osmometry have been interpreted as arising from association equilibria.<sup>5-8</sup> These association equilibrium constants can in turn be used to establish a *scale* for base interactions.

Purine and pyrimidine interactions within single strands that are not of the canonical base pairing type may play a role in the determination of three-dimensional conformation of transfer RNA chains.<sup>9,10</sup> The calculations of the free energies of possible structures for RNA segments, where the principal driving force for the folding process resides in the establishment of base pairs, yields differences in stability of only a few kilocalories for alternative conformations.<sup>11</sup> Consequently inclusion of sequence dependent base stacking interactions in loops between bihelical regions may be of some significance in the assessment of the stabilizing free energies of single stranded nucleic acids.

The purpose of this communication is threefold: to extend the analysis of association equilibria as revealed by osmotic coefficient measurements to binary nucleoside systems, to examine the possibility of relating the extents of ribonucleoside diphosphate copolymerization yielding polyribonucleotides to the aforementioned interactions, and lastly to compare the free energy of this polymerization to that of deoxyribonucleoside triphosphates.

## Co-Association of Nucleosides

We begin with the assumption that in aqueous solution nucleoside association is principally by a base stacking mode for which there is considerable spectroscopic evidence.<sup>8,12</sup> Secondly it is assumed that the interaction is confined to neighboring pairs in such a linear array as has been customarily assumed in most studies with single nucleosides.<sup>5,8</sup>

Then a simple matrix treatment for linear copolymerization reactions can be utilized to treat this process.<sup>13-15</sup> For a binary system the mole fraction of *n*-meric species ( $P_n$ ) can be written as the matrix product

$$P_n = (\alpha_1 \alpha_2) \mathbf{P}^{n-1} (\omega_1 \omega_2)^T \quad (1)$$

In this expression  $\mathbf{P}$  is a  $2 \times 2$  matrix of transition or sequential probabilities. The row matrix  $(\alpha_1 \alpha_2)$  and the transposed row or column matrix  $(\omega_1 \omega_2)^T$  in eq 1 are composed of the probabilities of commencing and terminating a linear sequence respectively with the monomeric species indicated by the subscript. Because each sequence must commence with either one of these species  $\alpha_1 + \alpha_2 = 1$  while the condition that  $\sum_{n=1}^{\infty} P_n = 1$  is met by the definition  $(\omega_1 \omega_2)^T \equiv (\mathbf{1} - \mathbf{P}) (\mathbf{1} \mathbf{1})^T$ .

For the equilibrium linear association taken up here, it is possible to find a more specifically useful form for eq 1 inasmuch as the probabilities appearing in the expression can be related to the four equilibrium constants and the two concentrations of unassociated monomer ( $m_1$  and  $m_2$ ).<sup>15</sup> We can then write

$$\mathbf{P} = \Omega \mathbf{K} \mathbf{M} \Omega^{-1} \quad (2a)$$

where

$$\Omega \equiv \begin{pmatrix} \omega_1 & 0 \\ 0 & \omega_2 \end{pmatrix} \quad (2b)$$

$$\mathbf{M} \equiv \begin{pmatrix} m_1 & 0 \\ 0 & m_2 \end{pmatrix} \quad (2c)$$

and

$$\mathbf{K} \equiv \begin{pmatrix} K_{11} & K_{12} \\ K_{21} & K_{22} \end{pmatrix} \quad (2d)$$

with  $\Omega^{-1}$  the reciprocal of  $\Omega$ . Hence the total molar concen-

tration of  $n$ mer including all sequences and compositions of this designated length,  $m_n$ , is given by substitution of the expression for  $\mathbf{P}$  given by eq 2a into eq 1

$$m_n = mP_n = (m_1 m_2)(\mathbf{K M})^{n-1}(1 \ 1)^T \quad (3)$$

In eq 3  $m$  is the concentration of all chains, i.e.,  $m = \sum_{n=1}^{\infty} m_n$  while  $m_1 = m\alpha_1\omega_1$  and  $m_2 = m\alpha_2\omega_2$ .

The similarity transformation in eq 2a permits the passage from a formal Markov description of the association process to one obtained earlier by a direct mass action argument for the statistical weights of any chain.<sup>16</sup> For example, the concentration of a particular tetrameric chain 1 1 2 1 would be reading from left to right  $m_1(K_{11}m_1)(K_{12}m_2)(K_{21}m_1)$ , one of the sixteen such tetramers comprising  $m_4$  generated by performing the matrix multiplication in eq 3. (In both the defining equation for the mole fraction of  $n$ mer and in the above mass action formulation we have chosen to read from left to right rather than in the opposite semitic direction as in previous publications.)<sup>15,16</sup> With this transformation, only the diagonal matrix elements of  $\mathbf{K M}$ , i.e.,  $K_{11}m_1$  and  $K_{22}m_2$  retain their significance as probabilities.<sup>15</sup> Similarity transformations by diagonal matrices have often proven useful in polymer configuration statistics.<sup>17</sup>

The relation between the total concentration of chains ( $m$ ) and that of the unassociated monomers follows by summing all the  $n$ mer species equations like 3 above and noting that

$$\begin{aligned} \sum_{n=1}^{\infty} P_n &= 1 \\ m &= (m_1 m_2) \left[ \sum_{n=1}^{\infty} (\mathbf{K M})^{n-1} \right] (1 \ 1)^T \\ &= (m_1 m_2)(1 - \mathbf{K M})^{-1}(1 \ 1)^T \\ &\approx (m_1 m_2)(1 + \mathbf{K M})(1 \ 1)^T \\ &= m_1 + m_2 + K_{11}m_1^2 + K_{22}m_2^2 + (K_{12} + K_{21})(m_1 m_2) \end{aligned} \quad (4a)$$

The  $2 \times 2$  unit matrix is symbolized by  $\mathbf{1}$  and the approximate eq 4b obviously extends only as far as dimeric species (vide infra). Truncating the summation at the level of dimer is not equivalent to assuming that species of larger size cannot arise in the association for which there is much counterindicative evidence.<sup>6,8</sup>

The concentration of unassociated monomers ( $m_1$  and  $m_2$ ) appearing in eq 4a and 4b may be related to the total or ground molar concentration of monomers ( $m_1^0$  and  $m_2^0$ ) most readily by treating  $m$  like a partition function. Thus by differentiating it with respect to  $\ln m_1$  (and utilizing the matrix identity  $d\mathbf{A}^{-1}/d\mathbf{a} = -\mathbf{A}^{-1}(d\mathbf{A}^{-1}/d\mathbf{a})\mathbf{A}^{-1}$ ) we obtain

$$m_1^0 = m_1 \left( \frac{\partial m}{\partial m_1} \right) = (m_1 \ 0)(1 - \mathbf{K M})^{-1}(1 \ 1)^T + (m_1 m_2) \times (1 - \mathbf{K M})^{-1}\mathbf{K} \begin{pmatrix} m_1 & 0 \\ 0 & 0 \end{pmatrix} (1 - \mathbf{K M})^{-1}(1 \ 1)^T \quad (5a)$$

$$\begin{aligned} &\approx (m_1 \ 0)(1 + \mathbf{K M})(1 \ 1)^T + (m_1 m_2)(1) \mathbf{K} \begin{pmatrix} m_1 & 0 \\ 0 & 0 \end{pmatrix} (1)(1 \ 1)^T \\ &= m_1 + 2K_{11}m_1^2 + (K_{12} + K_{21})(m_1 m_2) \end{aligned} \quad (5b)$$

Again the approximate eq 5b extends only as far as dimerization. The symmetric expressions for  $m_2^0$  can be obtained from these equations by interchanging the subscripts 1 and 2.

We restate here the argument developed by Schellman<sup>18</sup> to relate the molal osmotic coefficients to the extent of asso-

ciation for a single interacting species in the context of this binary system. In terms of the osmotic pressure,  $\pi$ , this quantity can be defined by  $\pi/[RT(m_1^0 + m_2^0)] \equiv \phi$ . Now if the departures (negative) from ideality are ascribed solely to the existence of association reactions,  $\pi/RT = m$  where  $m$  is the total concentration of all such species, i.e., the system behaves ideally with respect to a concentration of  $m$  noninteracting entities. Equating these two expressions for  $\pi/RT$ , we have  $1/\phi = (m_1^0 + m_2^0)/m \equiv \langle n \rangle$  where  $\langle n \rangle$  is the number average degree of association in complete analogy to the single interacting component situation.

We have found it of value to construct the same function of  $\phi$  which yields a simple expression in  $m^0$  and in turn readily lends itself to a linear plot. Calculating  $\langle n \rangle$  and thus  $1/\phi$  from eq 4a, 5a and the equivalent expression for  $m_2^0$ , we can write

$$\begin{aligned} (1 - \phi)/[\phi^2(m_1^0 + m_2^0)] &= [(m_1 m_2)(1 - \mathbf{K M})^{-2}\mathbf{K M} (1 \ 1)^T] \\ &\times [(m_1 m_2)(1 - \mathbf{K M})^{-1} \begin{pmatrix} 1 & 1 \\ 1 & 1 \end{pmatrix} \mathbf{M}(1 - \mathbf{K M})^{-1}(1 \ 1)^T]^{-1} \end{aligned} \quad (6)$$

If all the association constants are equal,  $\mathbf{K} = K \begin{pmatrix} 1 & 1 \\ 1 & 1 \end{pmatrix}$  and eq 6 reduces to the earlier result<sup>18</sup>

$$(1 - \phi)/[\phi^2(m_1^0 + m_2^0)] = K \quad (7)$$

This is the only condition apart from the basal case of a single associating species that this simple linearity in total concentration is preserved in the binary case. However, if attention is confined to the limited association occurring at high dilutions the matrix products in eq 6 can be approximated as in eq 4b and 5b to yield the useful result

$$(1 - \phi)/(\phi^2 m^0) \approx [(f_1^0)^2 K_{11} + f_1^0 f_2^0 (K_{12} + K_{21}) + (f_2^0)^2 K_{22}] \quad (8)$$

where  $m^0 \equiv m_1^0 + m_2^0$  and  $f_1^0 \equiv m_1^0/m^0 = 1 - f_2^0$ . When  $f_1^0$  or  $f_2^0$  equals unity, the right-hand side of eq 8 becomes  $K_{11}$  or  $K_{22}$  which result holds for all degrees of association (vide supra). For  $f_1^0 = f_2^0 = 1/2$ , the apparent association constant from this approximate expression is the arithmetic average of the four elements of  $\mathbf{K}$ , i.e.,  $K_{1/2} \equiv (K_{11} + K_{12} + K_{21} + K_{22})/4$ .

A linear variation of  $(1 - \phi)/(\phi^2 m^0)$  with composition ( $f_1^0$  or  $f_2^0$ ) in eq 8 arises if  $K_{11} + K_{22} = K_{12} + K_{21}$ . This is not the customary condition for random association of high polymers which requires instead that  $\langle 11 \rangle \langle 22 \rangle / \langle 12 \rangle \langle 21 \rangle = K_{11}K_{22} / K_{12}K_{21}$  equal unity ( $\langle 11 \rangle = K_{11}(\partial m / \partial K_{11})$ , etc. are the average concentrations of various neighbor pairs).<sup>16</sup>

The quadratic course with composition of the apparent association constant is fixed by a determination of  $K_{11}$ ,  $K_{22}$ , and the average  $(K_{12} + K_{21})/2$ . In Figure 1 we have plotted the compositional dependence of this parameter for two cases of binary deoxyribonucleoside association from data of this type obtained by Solie and Schellman.<sup>8</sup> For one pair (thymidine (1) and deoxycytidine (2)) their results clearly display no dependence of the association on the initial proportions. Unlike the association of these two pyrimidines, the pyrimidine-purine pair (thymidine (1) and deoxyadenosine (2)) exhibit a mildly nonlinear variation with  $f_2^0$ . For this system their results for the various equilibria are  $K_{TT} = 0.91$  and  $K_{AA} = 12$  which combined with the equimolar mixture result of eq 8 leads to  $(K_{TA} + K_{AT})/2 = 5.5$ . Hence  $(AA)\langle TT \rangle / [(AT) + \langle TA \rangle]^2 = K_{AA}K_{TT} / [(K_{TA} + K_{AT})/2]^2 = 0.36$ . This could be construed as a tendency toward an alternating sequence

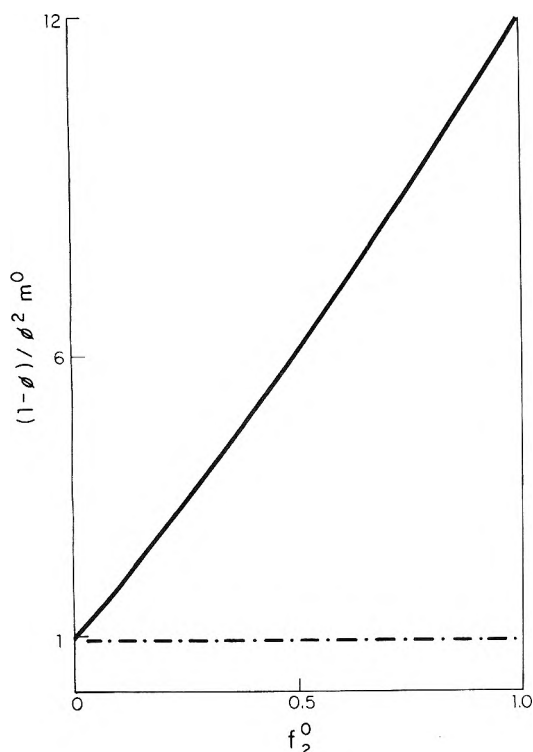


**Figure 1.** Plots of the apparent association constant  $(1 - \phi)/(\phi^2 m^0)$  against the mole fraction of component 2 for the systems uridine (1)-cytosine (2) (---) and uridine (1)-adenosine (2) (—). Data determining the two plots taken at 25 °C.

in the association reaction. (These authors<sup>8</sup> had previously suggested this if  $K_{1/2}$  were to be identified with  $(K_{TA}K_{AT})^{1/2}$ .) In view of the propensity for the enzymatic copolymerization of thymidine and deoxyadenosine triphosphates to yield rigidly alternating bihelical structures,<sup>19</sup> it is tempting to see this behavior mirrored in the association of the corresponding nucleosides. However, in the strictest sense such a conclusion would require  $\langle AA \rangle \langle TT \rangle / \langle AT \rangle \langle TA \rangle < 1$ , a deduction not warranted from an estimate of the arithmetic mean of the cross-association equilibrium constants. Also, it should be remarked that a tendency toward alternation appears to be widespread among synthetic copolymers far removed structurally and in mode of formation from polynucleotides.<sup>20,21</sup>

The matrix procedure used to analyze the association process is not restricted to equilibrium constants which do not change in magnitude with aggregate size though this seems a valid assumption. To incorporate such a variation<sup>22</sup> one simply introduces successively different  $\mathbf{K}$  matrices in the definition of  $m_n$ . However, we have shown that the simple functional dependence of the osmotic coefficient on total concentration of all species holds only in the limit of small extents of association for binary and hence higher multi-component mixtures. (In the experimental data cited here<sup>8</sup>  $\phi$  is never smaller than 0.67 and hence  $\langle n \rangle$  is less than 3/2.) Moreover, the existence of positive deviations from ideality which most likely arise from excluded volume effects are present in systems with a single associating component at higher concentrations and further argue for data extrapolations to regions where the attractive interactions appear to be predominant. The computation of such excluded volume effects as in the single associating species case<sup>23</sup> is substantially more complex for the case of multimonomeric mixtures.

### Copolymerization of Nucleoside Diphosphates

The linear equilibrium copolymerization of nucleotides is amenable to the same general treatment as the co-association reactions described above. Whether the resulting chains are held together by covalent linkages as in the former instance or by secondary forces as in the latter, variations in extents of reaction in either case will be affected by differing degrees of interaction of the nucleotide bases.

We begin by considering the copolymerization of nucleoside diphosphates which is a readily reversible reaction catalyzed by polyribonucleotide phosphorylase.<sup>24</sup> The formation of a phosphodiester bond between nucleotides is accompanied by the liberation of an orthophosphate ion. We presume that the polyribonucleotides all issue from a single primer oligomeric species.

Then the concentration of a primer species with a nucleotide arbitrarily designated as of type 1 at its 3'OH growing end and extended by the tetrameric sequence 1 1 2 1 is given by  $m_1(K_{11}^{(p)}m_1/m_p)(K_{11}^{(p)}m_1/m_p)(K_{12}^{(p)}m_2/m_p)(K_{21}^{(p)}m_1/m_p)$ . We have designated the concentration of unreacted primer or initiator as  $m_1$  and the superscript (p) distinguishes these equilibrium constants from those introduced in the previous section. Simple mass action considerations dictate that each reaction step is weighted by the ratio of the concentration of the appropriate nucleoside diphosphate ( $m_1$  and  $m_2$ ) to that of the orthophosphate product ( $m_p$ ). The generalization to the concentration of primer extended by  $n$  units ( $m_n$ ) is straightforward with

$$m_n = (m_1^0)(\mathbf{K}^{(p)}\mathbf{\Lambda})^{n-1}(1\ 1)^T \quad (9)$$

In eq 9  $\mathbf{\Lambda}$  is a diagonal matrix in the two concentration ratios  $\lambda_1 \equiv m_1/m_p$  and  $\lambda_2 \equiv m_2/m_p$ .<sup>25</sup>

This copolymerization has several constraints. The total concentration of chains is fixed by the initial concentration of primer  $m_1^0$ , i.e.

$$m_1^0 = \sum_{n=1}^{\infty} m_n = (m_1^0)(1 - \mathbf{K}^{(p)}\mathbf{\Lambda})^{-1}(1\ 1)^T \quad (10)$$

The concentration of orthophosphate produced is equal to the extent of conversion of both diphosphates into polyribonucleotide

$$m_p = (m_1^0 + m_2^0) - (m_1 + m_2) \quad (11)$$

where  $m_1^0$  and  $m_2^0$  are the initial concentrations of the two reactants. The parameter most experimentally accessible is the fractional extent of reaction as determined by the liberation of orthophosphate ( $F$ )

$$F \equiv (m_p)/(m_1^0 + m_2^0) = (1 + \lambda_1 + \lambda_2)^{-1} \quad (12)$$

where the second form for  $F$  follows from the definitions of the  $\lambda$ 's and the constraint embodied in eq 11.

The concentration of nucleotide 1 incorporated into polyribonucleotide product is obtained by differentiation of eq 10 with respect to  $\ln \lambda_1$

$$m_1^0 - m_1 = \lambda_1 \frac{\partial m_1^0}{\partial \lambda_1} = m_1^0 [\lambda_1 K_{11}^{(p)}(1 - \lambda_2 K_{22}^{(p)}) + \lambda_1 K_{12}^{(p)} \lambda_2 K_{21}^{(p)}] [1 - \mathbf{K}^{(p)}\mathbf{\Lambda}]^{-1} \quad (13a)$$

where the relation between  $m_1$  and  $m_1^0$  provided by eq 10 has also been utilized. The determinant of the matrix  $1 - \mathbf{K}^{(p)}\mathbf{\Lambda}$  is represented by  $|1 - \mathbf{K}^{(p)}\mathbf{\Lambda}|$ . The corresponding relation for the incorporation of nucleotide 2 is given by

$$m_2^0 - m_2 = m_1^0 \lambda_2 K_{12}^{(p)} [\lambda_1 K_{21}^{(p)} - (1 - \lambda_1 K_{11}^{(p)})] \\ \times [(1 - \lambda_2 K_{22}^{(p)}) + \lambda_2 K_{12}^{(p)}]^{-1} |1 - \mathbf{K}^{(p)} \mathbf{\Lambda}|^{-1} \quad (13b)$$

The difference in appearance of eq 13a and 13b arises from the arbitrary choice that the primer growing end commences with nucleotide 1. This difference disappears on extrapolation of the results to the high molecular weight limit.

The number average degree of extension of the polyribonucleotide chain is given by  $F(m_1^0 + m_2^0)/m_1^0$  which can be quite large even with only an incomplete conversion of nucleoside diphosphates into polymeric product provided that  $m_1^0 \ll m_1^0$  or  $m_2^0$ . The consequences of this condition have been previously explored for the homopolymeric situation.<sup>26</sup> For the case in hand this limit requires that

$$|1 - \mathbf{K}^{(p)} \mathbf{\Lambda}| = (1 - \lambda_1 K_{11}^{(p)})(1 - \lambda_2 K_{22}^{(p)}) \\ - \lambda_1 K_{21}^{(p)} \lambda_2 K_{12}^{(p)} \approx 0 \quad (14)$$

Equation 14 is recognizable as the generalization of the relationship providing an estimate of the homopolymeric equilibrium constant,  $\lambda_1 K_{11}^{(p)} \approx 1$ . We further note that in the high molecular weight limit the transition probability matrix  $\mathbf{P}$  becomes stochastic<sup>27</sup> or  $(1 - \mathbf{P})(1 \ 1)^T = (\omega_1 \ \omega_2)^T = (0 \ 0)^T$  which expresses the result that the row sums of  $\mathbf{P}$  are unity. The matrix  $\mathbf{K}^{(p)} \mathbf{\Lambda}$  is related to a probability matrix by a similarity transformation in the fashion described in the previous section. Consequently the less stringent requirement represented by eq 14 replaces the stochastic condition.

Employing the relation provided by eq 14 in the factors premultiplying  $|1 - \mathbf{K}^{(p)} \mathbf{\Lambda}|$  in eq 13a and 13b, we find that

$$m_1^0 - m_1 = m_1^0 (1 - \lambda_2 K_{22}^{(p)}) |1 - \mathbf{K}^{(p)} \mathbf{\Lambda}|^{-1} \quad (15a)$$

$$m_2^0 - m_2 = m_1^0 (1 - \lambda_1 K_{11}^{(p)}) |1 - \mathbf{K}^{(p)} \mathbf{\Lambda}|^{-1} \quad (15b)$$

With the restoration of symmetry in eq 15a and 15b any recollection of the chains emanation from an initiator with nucleotide 1 at the growing end has been expunged.

The final step to reduce these two conservation expressions to a useful form free of dependence on the initiator concentration, i.e., the independent of the degree of polymerization is achieved by adding eq 15a and 15b to obtain an expression for  $m_1^0 |1 - \mathbf{K}^{(p)} \mathbf{\Lambda}|^{-1}$ . On substitution of the result for this quantity into these equations coupled with utilization of the relation  $2 - \lambda_1 K_{11}^{(p)} - \lambda_2 K_{22}^{(p)} \approx 1 - \lambda_1 \lambda_2 (K_{11}^{(p)} K_{22}^{(p)} - K_{12}^{(p)} K_{21}^{(p)})$  from eq 14, we obtain

$$(f_1^0 + f_1^0 \lambda_2 - f_2^0 \lambda_1) [1 - \lambda_1 \lambda_2 K_{11}^{(p)} K_{12}^{(p)} (1 - \kappa^{-1})] \\ = 1 - \lambda_2 K_{22}^{(p)} \quad (16a)$$

$$(f_2^0 + f_2^0 \lambda_1 - f_1^0 \lambda_2) [1 - \lambda_1 \lambda_2 K_{11}^{(p)} K_{22}^{(p)} (1 - \kappa^{-1})] \\ = 1 - \lambda_1 K_{11}^{(p)} \quad (16b)$$

In the above  $\kappa \equiv K_{11}^{(p)} K_{22}^{(p)} / K_{12}^{(p)} K_{21}^{(p)}$  and is the customary index of copolymeric character alluded to earlier. Also  $f_1^0$  and  $f_2^0$  have the same meaning as previously. When, for example,  $f_2^0 = 0$ ,  $\lambda_2 = 0$  and  $\lambda_1^{-1} = K_{11}^{(p)}$ , the usual homopolymeric result cited above.

The character of the polymeric product can be further described in terms of the mole fraction of the species incorporated. For component 1, this quantity designated  $f_1$  is given by

$$f_1 \equiv (m_1^0 - m_1) / [(m_1^0 - m_1) + (m_2^0 - m_2)] \\ = f_1^0 + f_1^0 \lambda_2 - f_2^0 \lambda_1 \quad (17)$$

with an analogous expression for  $f_2$ . Hence it is  $f_1$  and  $f_2$  that are the first factors on the left side of eq 16a and 16b, respectively.

With simultaneous solution of these polynomial equations for  $\lambda_1$  and  $\lambda_2$  in terms of the initial composition and the respective equilibrium constants, we can calculate the experimental parameter  $F$ . A simple result for this quantity is obtained for  $\kappa = 1$ , the case of random copolymerization, when eq 16a and 16b become linear

$$F = [K_{11}^{(p)} K_{22}^{(p)} + f_1^0 K_{11}^{(p)} + f_2^0 K_{22}^{(p)}] \\ \times [(K_{11}^{(p)} + 1)(K_{22}^{(p)} + 1)]^{-1} \quad (18)$$

We note that a random copolymerization does not ensure the ratio of nucleotides in the polyribonucleotides is identical with that of the initial mixture. The latter condition requires  $f_1^0/f_2^0 = \lambda_1/\lambda_2$  which with  $\kappa = 1$  thus demands that  $K_{11}^{(p)} = K_{22}^{(p)}$ . Departures from this condition of equality of incorporation with "feed" are sometimes encountered in polyribonucleotide syntheses.<sup>28</sup>

Synthetic messenger RNA's prepared by the catalytic action of polyribonucleotide phosphorylase played a vital early role in determining the *composition* of the nucleotide triplets corresponding to the elements of the genetic code. The facile predictability of the frequency of triplets within the copolymers derived not merely from a random distribution of nucleotides within the macromolecule but to a near equivalence with the initial diphosphate "feed".<sup>29,30</sup> Of course, the character of polymers selected at early stages in the synthetic process will be governed principally by kinetic factors as well as the starting reactant composition rather than the thermodynamic considerations described here.

One might assert that it is within the catalytic capacity of the enzyme to synthesize *only* random copolymers having no well-developed secondary structures. However, there are counter arguments provided both by the nature of the synthesized homopolymers (vide infra) and by the ability of the enzyme to depolymerize or phosphorolyze a variety of single stranded RNA's having ramified bihelical regions.<sup>31</sup>

We take up here the results of one such study<sup>32</sup> where the final equilibrium extents of orthophosphate liberation for homopolymer synthesis correlate with nucleoside association. In Figure 2 we have plotted  $F$  vs.  $f_2^0$  for the exemplary binary system of uridine diphosphate (1) and adenosine diphosphate (2) for three values of  $\kappa$ . Only the intercepts  $K_{UU}^{(p)} / [K_{UU}^{(p)} + 1]$  and  $K_{AA}^{(p)} / [K_{AA}^{(p)} + 1]$  corresponding to  $K_{UU}^{(p)} = 1.5$  and  $K_{AA}^{(p)} = 3$  have been taken from experimental data.<sup>32</sup> The curves corresponding to  $\kappa = 1/3$  (alternating case suggested by nucleoside association data) and  $\kappa = 3$  (block tendency) have been approximately calculated from  $\lambda_1$  and  $\lambda_2$  as determined by the right-hand side of eq 16a and 16b by the method of successive substitution<sup>33</sup> using the random results for the left side. A well-defined plateau of  $F$  with increasing time was not generated for the copolymerization of an equimolar mixture of these two substrates. However, the apparent limiting value of  $F_{AU}$  appeared to be close to  $F_{UU}$  and more consistent with the bottom curve ( $\kappa = 3$ ) of Figure 2.

As the fundamental steps in the association and polymerization reactions involve different numbers of species, a direct comparison of the two types of equilibrium constants is not possible. The greater base stacking of dA than dT is consonant with the marginally more favorable thermodynamics of polymerization of ADP than UDP. In most instances, the equilibrium constants for polymerization are of the order of magnitude of unity for these readily reversible reactions (but see the next section).

There would seem to be a more significant parallel between these constants and the extent of secondary structure of the product than with the association constants for the nucleo-

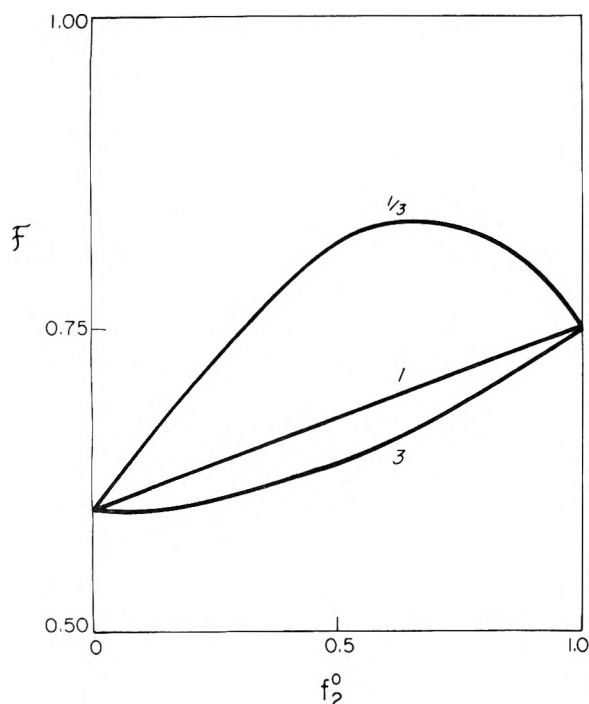
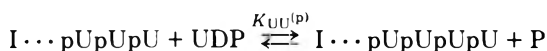


**Figure 2.** The limiting fractional extent of orthophosphate formation ( $F$ ) for the system UDP (1)–ADP (2) plotted against the mole fraction of the latter for three values of the copolymerization index  $\kappa$ . Data defining the two intercepts from measurements at 30 °C, pH  $\approx$  8, and  $10^{-2}$  M MgCl<sub>2</sub>.

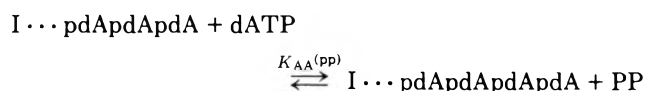
sides. For example, both cytidine (C) and deoxycytidine (dC) show a similar small disposition toward association.<sup>34</sup> Nonetheless, for the polymerization<sup>32</sup> of CDP we find  $K_{CC}^{(p)} = 4$ , which is comparable to  $K_{AA}^{(p)}$  with the product poly rC displaying a pronounced secondary structure<sup>4</sup> consistent with that of poly rA (for poly dC there is less evidence of secondary structure). Interestingly enough the same solubility problems which complicate studies of the association of guanosine (G)<sup>8</sup> plague the efforts to obtain polymers from GDP.

### Polymerization of Nucleoside Triphosphates

The prototypical homopolymeric reaction taken up in the previous section is given by

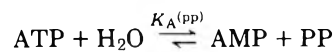


Uridine diphosphate (UDP) extends a polyuridylic acid chain commencing with a primer species designated I by one nucleotide unit with the splitting out of orthophosphate (P). By the generally applied spectroscopic criteria this polyribonucleotide chain manifests negligible base stacking and hence exhibits no secondary structure at room temperature.<sup>4</sup> We have previously related the free energy changes of a number of reactions of nucleic acids to  $\Delta G^{\circ}$  for this reaction of approximately zero.<sup>35</sup> We wish to compare the thermodynamics of this reaction to one catalyzed by deoxynucleotidyl transferase<sup>36,37</sup> in which



Deoxyadenosine triphosphate (dATP) extends a primer initiated polydeoxyadenylic acid chain by one deoxynucleotide unit with the liberation of pyrophosphate (PP).

First focusing on the difference between the nature of the by-product phosphate species, we will expect that the free energy difference between the second and first reaction should contain one term coming from the difference of the two hydrolytic reactions.



To a good approximation we would anticipate the hydrolysis free energies to be little influenced by whether we are dealing with a deoxy or a ribose nucleotide. The magnitude of the differences in free energy of these two reactions we take to be  $-1$  kcal so  $K_A^{(pp)}/K_A^{(p)} = 5.3$  at 25 °C.<sup>38</sup>

The fact that polydeoxydeoxyadenylic acid exhibits much more secondary structure than polyuridylic we correct for by introducing the factor  $K_{dAdA}/K_{UU} = 12/0.7 \approx 17.1$ .  $K_{UU}$  appears to be slightly smaller than  $K_{TT}$  quoted above.<sup>34</sup>

Combining these two factors we estimate that

$$K_{dAdA}^{(pp)} = K_{UU}^{(p)} [K_A^{(pp)}/K_A^{(p)}] [K_{dAdA}/K_{UU}] \\ = (1.5)(5.3)(12/0.7) \approx 140$$

We can perform the same calculation but employ as the reference polymerization reaction the synthesis of polyriboadenylic acid from adenosine diphosphate ( $K_{AA}^{(p)} \approx 3$ ) and the appropriate base stacking factor for this ribopolynucleotide<sup>34</sup> ( $K_{dAdA}/K_{AA} \approx 12/4.5 \approx 2.7$ ). The derived value for  $K_{dAdA}^{(pp)}$  is then approximately 40. These two estimates bracket that inferred from the equilibrium ratio of pyrophosphate to deoxyadenosine triphosphate ( $\sim 100$ ) obtained from the enzymatic synthesis.<sup>39</sup>

As the above estimates have involved data from polymerizations studied under different solution conditions than the associations (see the figure captions), the agreement may be more than a little fortuitous. However, the conclusion that base stacking interactions in polymerization reactions are at least as significant contributors to the thermodynamics of the reaction as covalent bond formation seems to be reasonably secure.

### Conclusion

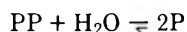
We have developed an argument for the equilibrium polymerization of nucleoside phosphates reflecting the extents of interaction of purine and pyrimidine bases in the chains. The presence of high molecular weight species in these systems owes little to the slightly thermodynamically favored synthetic step. Chain growth from a low concentration of oligonucleotide primers as described in the above analysis is the vital factor.

It has long been known that polymer synthesis proceeding from a fixed concentration of initiator species must lead to a narrow Poisson distribution of chain sizes<sup>40</sup> not the broad most probable equilibrium size distribution represented by eq 9. However, for a reversible synthetic reaction the system will ultimately pass from the former to the latter. Most importantly for the substance of this communication the equilibrium concentration of monomer (in this case the equilibrium ratio of nucleoside diphosphate to orthophosphate) is anticipated to be attained at a much earlier time than the complete collection of chains assumes its equilibrium character.<sup>41</sup> Consequently, it is the equilibrium value of  $F$  related to the  $\lambda$ 's which we have stressed here.

From the foregoing arguments we would expect the ther-

modynamics of the synthesis of single stranded nucleic acids to be effectively conditional on the sequence as well as the composition of the product chains. This proposition holds equally for the reaction of nucleoside triphosphates yielding pyrophosphate as a side product. Moreover, a similar situation applies to the synthesis of their double stranded counterparts.<sup>35</sup> This phenomenon is of doubtful desirability in vivo. Plainly it is a factitious consequence of the customary mode of in vitro study of these syntheses.

The action of inorganic pyrophosphatase intracellularly in catalyzing the highly irreversibly reaction



transforms the synthesis of polynucleotide utilizing nucleoside triphosphates from mildly to overwhelmingly favorable thermodynamically. The hydrolyses of phosphoanhydrides involve standard free energy changes in the range of  $-7$  to  $-10$  kcal.<sup>38</sup> In practical terms coupling this hydrolysis of pyrophosphate to the synthesis leads to an effective augmentation of the equilibrium constant for the addition of a nucleotide to a growing chain by a factor of approximately the ratio of the hydrolysis constant ( $\sim 10^5$ ) to that of the monomer concentration<sup>42,43</sup> ( $\sim 10^{-4}$  M) of  $10^9$ . By comparison fluctuations due to different extents of base stacking interactions are of negligible importance.

This consequence of uniting nucleic acid synthesis to the hydrolysis of the pyrophosphate by-product is an incidental benefit to be added to two other more striking accruals. They are (1) the raising by several orders of magnitude of the thermodynamic ceiling for the molecular weight of de novo synthesized polynucleotide chains<sup>42,43</sup> and (2) the extension also by orders of magnitude of the time scale on which a narrow range of chain sizes passes over to the broad distribution characteristic of a complete equilibrium.<sup>44</sup>

*Acknowledgment.* Research supported by the Samuel R. Neider Heart Research Fund.

## References and Notes

- (1) R. F. Steiner and R. F. Beers, Jr., "Polynucleotides", Elsevier, Amsterdam, 1961, Chapter 8.
- (2) G. Felsenfeld and H. T. Miles, *Annu. Rev. Biochem.*, **36** (II), 414 (1967).
- (3) V. A. Bloomfield, D. M. Crothers, and I. Tinoco, Jr., "Physical Chemistry of Nucleic Acids", Harper and Row, New York, N.Y., 1974, Chapter 6.
- (4) Reference 3, Chapter 3.
- (5) P. O. P. Ts'o, I. S. Melvin, and A. C. Olson, *J. Am. Chem. Soc.*, **85**, 1289 (1963).
- (6) P. O. P. Ts'o and S. I. Chan, *J. Am. Chem. Soc.*, **86**, 4176 (1964).
- (7) S. J. Gill, M. Downing, and G. F. Sheats, *Biochemistry*, **6**, 272 (1967).
- (8) T. N. Solle and J. A. Schelman, *J. Mol. Biol.*, **33**, 61 (1968).
- (9) S. H. Kim, F. L. Suddath, G. J. Quigley, A. McPherson, J. L. Sussman, A. H. J. Wang, N. C. Seeman, and A. Rich, *Science*, **185**, 435 (1974).
- (10) J. E. Ladner, A. Jack, J. D. Robertus, R. A. Brown, D. Rhodes, R. F. C. Clark, and A. Klug, *Proc. Natl. Acad. Sci. U.S.A.*, **72**, 4414 (1975).
- (11) I. Tinoco, Jr., P. N. Borer, B. Dengler, M. D. Levine, O. C. Uhlenbeck, D. M. Crothers, and J. Gralla, *Nature (London) New Biol.*, **246**, 40 (1973).
- (12) S. I. Chan, M. P. Schweizer, P. O. P. Ts'o, and G. K. Hemkamp, *J. Am. Chem. Soc.*, **86**, 4182 (1964).
- (13) H. K. Frensdorff and R. Pariser, *J. Chem. Phys.*, **39**, 2303 (1963).
- (14) J. Hijmans, *Physica* **29**, 1, 819 (1963).
- (15) L. Peller, *J. Chem. Phys.*, **43**, 2355 (1965).
- (16) L. Peller, *J. Chem. Phys.*, **36**, 2976 (1962).
- (17) P. J. Flory, "Statistical Mechanics of Chain Molecules", Interscience, New York, N.Y., 1969, p 65.
- (18) J. A. Schellman, *C. R. Trav. Lab. Carlsberg, Ser. Chim.*, **29**, 223 (1955).
- (19) H. K. Schachman, J. Adler, C. M. Radding, I. R. Lehman, and A. Kornberg, *J. Biol. Chem.*, **235**, 3242 (1960).
- (20) T. Alfrey, Jr., J. J. Bohrer, and H. Mark, "Copolymerization", Interscience, New York, N.Y., 1952.
- (21) P. J. Flory, "Principles of Polymer Chemistry", Cornell University Press, Ithaca, N.Y., 1953, Chapter V.
- (22) R. F. Steiner, *Biochemistry*, **7**, 2201 (1968).
- (23) T. L. Hill and Y-D. Chen, *Biopolymers*, **12**, 1285 (1973).
- (24) M. Grunberg-Manago and S. Ochoa, *J. Am. Chem. Soc.*, **77**, 3165 (1955).
- (25) L. Peller, *J. Phys. Chem.*, **66**, 685 (1962).
- (26) L. Peller and L. Barnett, *J. Phys. Chem.*, **66**, 680 (1962).
- (27) F. P. Price, *J. Chem. Phys.*, **36**, 209 (1962).
- (28) M. Grunberg-Manago, *Prog. Nucleic Acid Res. Mol. Biol.*, **1**, 93 (1963).
- (29) M. W. Nirenberg, O. W. Jones, P. Leder, B. F. C. Clark, W. S. Sly, and S. Pestka, *Cold Spring Harbor Symp.*, **28**, 549 (1963).
- (30) J. F. Speyer, P. Lengyel, C. Basilio, A. J. Wahba, R. S. Gardner, and S. Ochoa, *Cold Spring Harbor Symp.*, **28**, 559 (1963).
- (31) T. Godefroy-Colburn and M. Grunberg-Manago in "The Enzymes", Vol. 7, P. D. Boyer, Ed., Academic Press, New York, N.Y., 1972, p 533.
- (32) M. Grunberg-Manago, *Prog. Biophys. Mol. Biol.*, **13**, 191 (1963).
- (33) F. B. Hildebrand, "Introduction to Numerical Analysis", McGraw-Hill, New York, N.Y., 1956, p 450.
- (34) P. O. P. Ts'o in "Molecular Associations in Biology", B. Pullman, Ed., Academic Press, New York, N.Y., 1968, p 39.
- (35) L. Peller, *Biochemistry*, **15**, 141 (1976).
- (36) J. S. Krakow, C. Coutsogeorgopoulos, and E. S. Cannellakis, *Biochem. Biophys. Res. Commun.*, **5**, 477 (1961).
- (37) F. J. Bollum, *J. Biol. Chem.*, **237**, 1945 (1962).
- (38) R. A. Alberty, *J. Biol. Chem.*, **244**, 3290 (1969).
- (39) K.-I. Kato, J. M. Goncalves, G. E. Houts, and F. J. Bollum, *J. Biol. Chem.*, **242**, 2780 (1967).
- (40) P. J. Flory, *J. Am. Chem. Soc.*, **62**, 1561 (1940).
- (41) A. Miyake and W. H. Stockmayer, *Makromol. Chem.*, **88**, 90 (1965).
- (42) L. Peller, *Proc. Natl. Acad. Sci. U.S.A.*, **55**, 1025 (1966).
- (43) L. Peller, *Biochem. Biophys. Res. Commun.*, **63**, 912 (1975).
- (44) L. Peller, to be submitted for publication.

# Krafft Points, Critical Micelle Concentrations, Surface Tension, and Solubilizing Power of Aqueous Solutions of Fluorinated Surfactants

Hironobu Kunieda and Kōzō Shinoda\*

Department of Chemistry, Faculty of Engineering, Yokohama National University, Ooka-2, Minami-ku, Yokohama, Japan (Received April 2, 1976)

Publication costs assisted by Yokohama National University

The Krafft points, critical micelle concentrations (cmc), surface tension above the cmc, and solubilizing power in aqueous solutions of perfluoroalkane carboxylates as functions of fluorocarbon chain length and the types of gegenions have been studied. The Krafft point, surface tension above the cmc, and solubilizing power differ markedly with the types of gegenions, but the cmc is mainly dependent on the fluorocarbon chain length and not on the types of gegenions of same valency.

## Introduction

The surface tension of fluorinated surfactant solutions is considerably lower than that of ordinary surfactants. Fluorinated surfactants are stable against acidic, alkaline, oxidative, and reducing reagents as well as elevated temperature. Because of these features, the fluorinated surfactants have special industrial uses.<sup>1</sup> The longer chain surfactants are expected to be more surface active<sup>2</sup> and show large solubilization at low concentration than shorter chain surfactants.<sup>3</sup> However, the Krafft point, above which ionic surfactants form micelles and dissolve well, is elevated with increasing hydrophobic chain length.<sup>4</sup> Thus, the longer chain surfactants cannot be used at room temperature. The chain length of fluorinated surfactants heretofore used were mainly limited to C<sub>7</sub>-C<sub>8</sub>.<sup>5-12</sup> It was shown in the preceding paper<sup>5</sup> that the kinds of gegenions markedly affect the Krafft point. In the present investigation, the effect of the kinds of gegenions and chain length of surfactant on the Krafft point, surface tension, cmc, and solubilizing power in aqueous solutions of perfluoroalkane carboxylates have been studied.

## Experimental Section

**Materials.** The respective perfluoroalkane carboxylic acids, C<sub>6</sub>F<sub>13</sub>COOH (mp 24-30 °C), C<sub>8</sub>F<sub>17</sub>COOH (mp 59.3-61.1 °C), C<sub>10</sub>F<sub>21</sub>COOH (mp 97.9-100.3 °C), and C<sub>12</sub>F<sub>25</sub>COOH (mp 117.5-122 °C), were synthesized and purified by fractional distillation and recrystallization from CCl<sub>4</sub> at the Asahi Glass Co. The respective salts were prepared by neutralizing the acids with aqueous alkaline hydroxide, ammonia, ethanalamine, and triethanolamine solutions, respectively. The electrical conductance of water used was 1.5 μΩ<sup>-1</sup> cm<sup>-1</sup> at 25 °C.

**Procedures. Krafft Point and Cmc Measurements.** The Krafft point was determined from the abrupt increase in the electrical conductivity as a function of temperature. Conductivity was measured after the solution equilibrium was attained at a given temperature in a thermostat controlled to within ±0.02 °C. Cmc was measured by the electrical conductivity-concentration curve at constant temperature.

**Surface Tension Measurements.** The procedures are described in the previous study.<sup>5</sup>

**Solubilization Measurements.** Various amounts of CCl<sub>2</sub>F-CClF<sub>2</sub> were added to a fixed volume of aqueous solutions of surfactant and sealed in ampoules. A series of am-

poules kept in a thermostat was well shaken and left at constant temperature, and the boundary of solubilization was determined.

## Results and Discussions

**Krafft Points of Perfluoroalkane Carboxylates.** The Krafft point is the melting point of hydrated solid surfactant.<sup>4</sup> Surfactants form micelles above the Krafft point and the solubility in water increases abruptly. Hence, solubilization occurs above the Krafft point. It is known that the longer chain surfactants are much more surface active and their cmc's are low, i.e., they are more efficient surfactants. There exists a rough parallel between the Krafft point and the melting point of an homologous series of surfactants. The Krafft points of fluorinated surfactants are generally high, so that less than C<sub>7</sub> or C<sub>8</sub> carbon chain compounds may be used at room temperature. In order to use longer chain surfactants, the effect of the kinds of gegenions on the Krafft point has been studied and is shown in Figure 1. In some cases, Krafft points were not observed i.e., lower than 0 °C. These results are listed in Table I. The Krafft points of carboxylates are generally lower than those of sulfonates.<sup>5</sup> However, perfluoroalkanesulfonates are more heat resistant than the carboxylates (sulfonates have shown no decomposition below 350 °C, whereas carboxylates decompose at about 175-250 °C).<sup>1</sup>

Krafft points may be affected by several factors such as the nature of the bond between the surface active ion and the gegenion, the structure of hydrated solid agents, or the degree of hydration. It is seen in Figure 1 that the more hydrated the gegenion is, the steeper the slope of Krafft point vs. chain length. For univalent gegenions the order of the slope is H<sup>+</sup> > Li<sup>+</sup> > Na<sup>+</sup> > K<sup>+</sup> ≈ NH<sub>4</sub><sup>+</sup> ≈ Rb<sup>+</sup>.

**Cmc of Perfluoroalkane Carboxylates.** The cmc values of potassium and sodium perfluoroalkane carboxylates are plotted in Figure 2. The change in cmc as a function of hydrophobic chain length is expressed by the following equation<sup>1,3</sup>

$$\ln \text{cmc} = -\frac{m\omega}{(1 + Kg)kT} + K \quad (1)$$

where *Kg* and *K* are the experimental constants, *m* the number of carbon atoms in fluorocarbon chain, and *ω* the free energy difference per -CF<sub>2</sub>- group (-CH<sub>2</sub>- group) between micellar state and singly dispersed state. The slope of the

TABLE I: Krafft Points and Cmc Values of Perfluoroalkane Carboxylates

Compound	Krafft point, °C	Cmc, M
<i>n</i> -C <sub>6</sub> F <sub>13</sub> COOLi	Below 0	0.098 at 30 °C
<i>n</i> -C <sub>6</sub> F <sub>13</sub> COONa	Below 0	0.171 at 30 °C
<i>n</i> -C <sub>6</sub> F <sub>13</sub> COOK	16.2	0.129 at 30 °C
<i>n</i> -C <sub>6</sub> F <sub>13</sub> COORb	49	
<i>n</i> -C <sub>7</sub> F <sub>15</sub> COOH <sup>a</sup>	20	0.009 0 at 20 °C
<i>n</i> -C <sub>7</sub> F <sub>15</sub> COOLi <sup>a</sup>	Below 0	
<i>n</i> -C <sub>7</sub> F <sub>15</sub> COONa <sup>a</sup>	8.6	0.036 at 8 °C
<i>n</i> -C <sub>7</sub> F <sub>15</sub> COOK <sup>a</sup>	25.6	0.027 at 25.6 °C
<i>n</i> -C <sub>7</sub> F <sub>15</sub> COONH <sub>4</sub> <sup>a</sup>	2.5	0.033 at 2.5 °C
<i>n</i> -C <sub>8</sub> F <sub>17</sub> COOH	48.3	0.002 8 at 60 °C
<i>n</i> -C <sub>8</sub> F <sub>17</sub> COOLi	Below 0	0.010 6 at 30 °C
<i>n</i> -C <sub>8</sub> F <sub>17</sub> COONa	24.6	0.009 1 at 30 °C
<i>n</i> -C <sub>8</sub> F <sub>17</sub> COOK	35.5	0.006 3 at 50 °C
<i>n</i> -C <sub>8</sub> F <sub>17</sub> COORb	69	
<i>n</i> -C <sub>8</sub> F <sub>17</sub> COONH <sub>4</sub>	10.6	0.006 7 at 30 °C
<i>n</i> -C <sub>8</sub> F <sub>17</sub> COONH <sub>3</sub> C <sub>2</sub> H <sub>4</sub> OH	Below 0	0.006 5 at 30 °C
<i>n</i> -C <sub>8</sub> F <sub>17</sub> COONH(C <sub>2</sub> H <sub>4</sub> OH) <sub>3</sub>	Below 0	0.006 1 at 30 °C
<i>n</i> -C <sub>10</sub> F <sub>21</sub> COOLi	Below 0	0.000 39 at 30 °C
<i>n</i> -C <sub>10</sub> F <sub>21</sub> COONa	58.3	0.000 43 at 60 °C
<i>n</i> -C <sub>10</sub> F <sub>21</sub> COOK	56.0	0.000 34 at 60 °C
<i>n</i> -C <sub>10</sub> F <sub>21</sub> COORb	93	
<i>n</i> -C <sub>10</sub> F <sub>21</sub> COONH <sub>4</sub>	33	0.000 48 at 50 °C
<i>n</i> -C <sub>10</sub> F <sub>21</sub> COONH <sub>3</sub> C <sub>2</sub> H <sub>4</sub> OH	18	
<i>n</i> -C <sub>10</sub> F <sub>21</sub> COONH(C <sub>2</sub> H <sub>4</sub> OH) <sub>3</sub>	20	0.000 54 at 50 °C
<i>n</i> -C <sub>12</sub> F <sub>25</sub> COOLi	42	
<i>n</i> -C <sub>12</sub> F <sub>25</sub> COONa	89	
<i>n</i> -C <sub>12</sub> F <sub>25</sub> COOK	75.5	

<sup>a</sup> Reference 5.

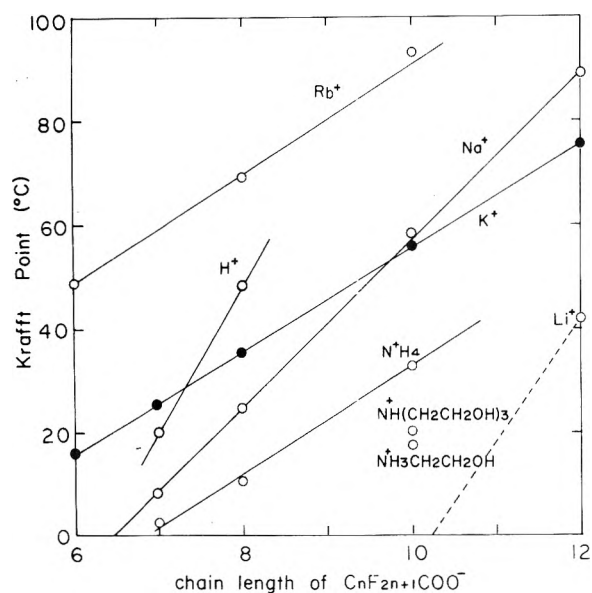


Figure 1. The relationship between the number of carbon atoms in fluorocarbon chain and the Krafft point of perfluoroalkane carboxylates.

logarithm of the cmc vs. the number of carbon atom in Figure 2 is equal to  $-m\omega/(1 + Kg)kT$ . Substituting  $Kg = 0.52$  (obtained in the case of *n*-C<sub>7</sub>F<sub>15</sub>COOK)<sup>14</sup> into eq 1, we obtain  $\omega = 2.21kT$ . This value is about twice that of the hydrocarbon surfactant ( $1.08kT$ )<sup>15</sup> so that the cmc of the perfluorinated surfactant is reduced to about  $\frac{1}{4}$  per  $-\text{CF}_2-$  group. The cmc values of C<sub>7</sub>~C<sub>8</sub> fluorinated surfactants are close to those of C<sub>11</sub>~C<sub>12</sub> hydrocarbon surfactants.<sup>5</sup> The cmc values of perfluoroalkane carboxylates are listed in Table I.

*Surface Tension of Perfluoroalkane Carboxylates.* The

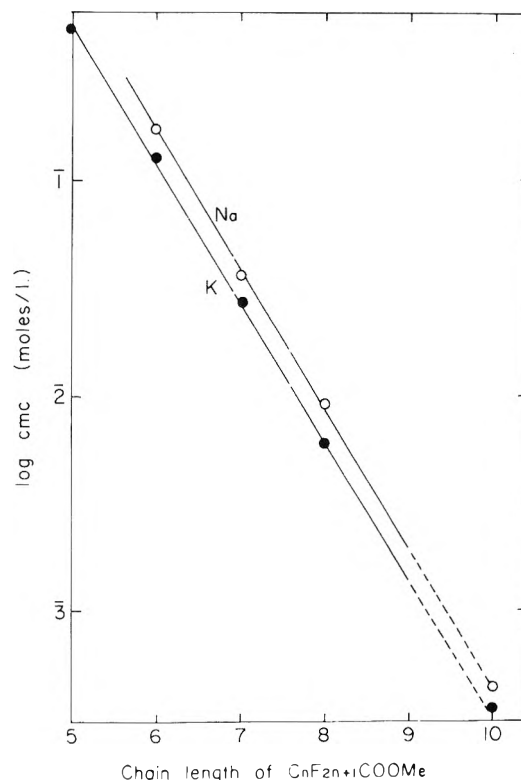


Figure 2. The relationship between the number of carbon atoms in fluorocarbon chain and the logarithm of the cmc of potassium (sodium) perfluoroalkane carboxylates.

surface tension of the fluorinated surfactant solution is lower than any other solutions. The minima of the surface tensions of ordinary surfactants are in the range 25–35 dyn/cm,

TABLE II: Surface Tension above the Cmc in Aqueous Solutions of Perfluoroalkane Carboxylates at 25 °C

Compound	Surface tension, dyn/cm
$n\text{-C}_6\text{F}_{13}\text{COOLi}$	27.8
$n\text{-C}_7\text{F}_{15}\text{COOH}^a$	15.2
$n\text{-C}_7\text{F}_{15}\text{COONa}^a$	24.6
$n\text{-C}_8\text{F}_{17}\text{COOLi}$	24.6
$n\text{-C}_8\text{F}_{17}\text{COONa}$	21.5
$n\text{-C}_8\text{F}_{17}\text{COOK}$	20.6
$n\text{-C}_8\text{F}_{17}\text{COONH}_4$	14.8
$n\text{-C}_8\text{F}_{17}\text{COONH}_3\text{C}_2\text{H}_4\text{OH}$	15.9
$n\text{-C}_8\text{F}_{17}\text{COONH}(\text{C}_2\text{H}_4\text{OH})_3$	21.9
$n\text{-C}_{10}\text{F}_{21}\text{COOLi}$	20.5
$n\text{-C}_{10}\text{F}_{21}\text{COONH}_3\text{C}_2\text{H}_4\text{OH}$	13.8
$n\text{-C}_{10}\text{F}_{21}\text{COONH}(\text{C}_2\text{H}_4\text{OH})_3$	16.9

<sup>a</sup> Reference 5.

whereas those of aqueous solutions of fluorinated surfactant are as low as 15–20 dyn/cm. The surface tension of aqueous solutions above the cmc which varies only slightly with concentration above the cmc are summarized in Table II. Surface tension above the cmc decreased with increasing fluorocarbon chain length in this experiment, but changes with the types of gengenions. For example, the surface tension is 24.6 dyn/cm in an aqueous solution of  $\text{C}_8\text{F}_{17}\text{COOLi}$ , 21.5 dyn/cm in the case of  $\text{C}_8\text{F}_{17}\text{COONa}$ , and 14.8 dyn/cm in a  $\text{C}_8\text{F}_{17}\text{COONH}_4$  solution.

**Solubilizing Power of Perfluoroalkane Carboxylates.** The solubilization of  $\text{CCl}_2\text{F}-\text{CClF}_2$  in aqueous solutions of perfluoroalkane carboxylates of different gengenions and fluorocarbon chain length is plotted in Figure 3. Fluorocarbons or chlorofluorocarbons which are nonpolar, saturated, and whose intermolecular force are mainly dispersion force may be used as typical solubilizates for fluorinated surfactants. Of these  $\text{CCl}_2\text{F}-\text{CClF}_2$  seems one of the most appropriate solubilizates to study, because it is liquid at room temperature and the molal volume is relatively small so that solubilization is relatively large. As the solubilization increases linearly with concentration of surfactant, above the cmc it is legitimate to draw a solubilization curve based on a few experimental points. The solubilization is larger when the fluorocarbon chain length is longer. However, the hydrophile-lipophile balance (HLB) of a surfactant, which is altered by the types of gengenions, was also markedly affected. It is known that

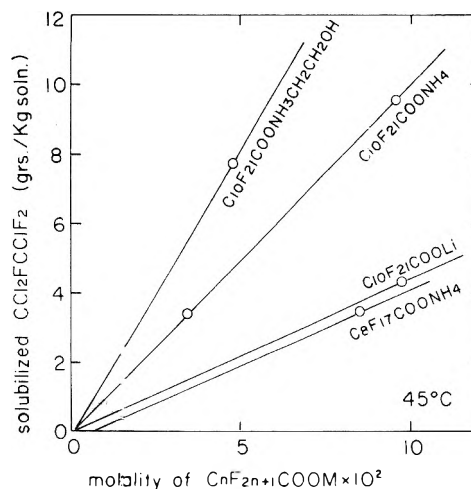


Figure 3. The effect of the gengenion and chain length of perfluoroalkane carboxylates on the solubilization of  $\text{CCl}_2\text{F}-\text{CClF}_2$  at 45 °C.

nonionic surfactants whose HLB's are well balanced form large micelles and solubilize more oil. A similar tendency may hold in the case of ionic surfactants. Lithium perfluoroalkancarboxylate ( $\gamma = 20.5$  dyn/cm) seems too hydrophilic to effect large solubilization, whereas the ethanolammonium salt which seems well balanced ( $\gamma = 13.8$  dyn/cm) showed four times greater solubilization.

**Acknowledgments.** The authors wish to thank the Asahi Glass Co. for the fluorinated compounds.

## References and Notes

- (1) J. H. Simons, Ed., "Fluorine Chemistry", Vol. 5, Academic Press, New York, N.Y., 1964, p 370
- (2) K. Shinoda and K. Mashio, *J. Phys. Chem.*, **64**, 54 (1960).
- (3) R. S. Stearns, H. Oppenheimer, E. Simon, and W. D. Harkins, *J. Chem. Phys.*, **15**, 496 (1947).
- (4) K. Shinoda, T. Nakagawa, B. Tamamushi, and T. Isemura, "Colloidal Surfactants", Academic Press, New York, N.Y., 1963, pp 7–9.
- (5) K. Shinoda, M. Hara, and T. Hayashi, *J. Phys. Chem.*, **76**, 909 (1972).
- (6) M. K. Bennett and W. A. Zisman, *J. Phys. Chem.*, **63**, 1911 (1959).
- (7) C. H. Arrington and G. D. Patterson, *J. Phys. Chem.*, **57**, 247 (1953).
- (8) H. M. Scholberg, F. A. Guenther, and R. I. Coon, *J. Phys. Chem.*, **57**, 923 (1953).
- (9) H. B. Klevens and M. Raison, *J. Chim. Phys.*, **51**, 1 (1954).
- (10) L. A. Schits, B/III, 143, 5th International Congress on Surface Active Substances, Barcelona, Spain, 1968.
- (11) K. Shinoda and H. Nakayama, *J. Colloid Sci.*, **18**, 705 (1963).
- (12) H. Nakayama and K. Shinoda, *Bull. Chem. Soc. Jpn.*, **40**, 1797 (1967).
- (13) Reference 4, pp 25–42.
- (14) K. Shinoda and K. Katsura, *J. Phys. Chem.*, **68**, 1568 (1964).
- (15) K. Shinoda, *Bull. Chem. Soc. Jpn.*, **26**, 101 (1953).

## Hydrogen Profiles in Water-Oxidized Silicon

D. J. Breed

Philips Research Laboratories, Eindhoven, Netherlands

and R. H. Doremus\*

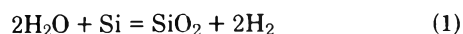
Rensselaer Polytechnic Institute, Materials Engineering Department, Troy, New York 12181 (Received April 5, 1976)

Publication costs assisted by Philips Research Laboratories

The profile of hydrogen in the silica layer on silicon oxidized by water is derived from a model of molecular diffusion of water and hydrogen in the silica. A minimum in the total hydrogen concentration in the layer, and a sharp increase in hydrogen concentration at the silicon-oxide interface are predicted by the model, and have been found experimentally, supporting the model of molecular diffusion in the silica.

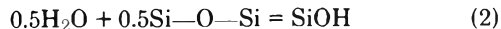
### Introduction

The rate of oxidation of silicon by water is controlled by molecular diffusion of water through the oxide layer, according to Doremus.<sup>1</sup> At the oxide-silicon interface the water reacts with the silicon, forming oxide and hydrogen



The molecular hydrogen produced in this reaction diffuses out of the silica in the direction opposite to that of the incoming water flux.

Both water<sup>2</sup> and hydrogen<sup>3,4</sup> can react with the silica to form hydroxyl groups



The profile of hydroxyl groups plus SiH groups (total reacted hydrogen) in silica on silicon oxidized by water was measured by Burkhardt<sup>5</sup> and by Beckmann and Harrick.<sup>6</sup> The latter authors presented spectroscopic evidence for the presence of SiH groups. In this paper these profiles are shown to agree with a model of molecular diffusion of water in and hydrogen out of the silica layer and their reaction with the silica by eq 2 and 3.

### Calculation of the Profile of Reacted Hydrogen

The concentration  $C$  of molecularly dissolved water as a function of the distance  $x$  from the outer surface of the silica layer is

$$C/C_i = 1 - x/X \quad (4)$$

as shown in the appendix of ref 1 when  $C_i \ll \rho$ .  $C_i$  is the concentration of water in the silica at the silica-gas interface in equilibrium with the ambient water vapor,  $X$  is the thickness of the silica layer, and  $\rho$  is the concentration of oxygen in the silica. The concentration  $S$  of hydroxyl groups formed by reaction of the molecularly dissolved water with the silica lattice (eq 2) is

$$S = K_1 C^{1/2} \quad (5)$$

From eq 4 and 5

$$S^2/S_i^2 = 1 - x/X \quad (6)$$

These concentration-distance profiles are shown schematically in Figure 1.

From eq 3 the concentration of molecularly dissolved hydrogen  $H$  in equilibrium with its reaction products is:

$$H = SR/K_2 \quad (7)$$

where  $R$  is the concentration of SiH groups. If  $H$  is much smaller than  $S$  and  $R$ , which in turn are much smaller than  $\rho$ , then, just as for the water profile,  $H$  is linearly dependent on  $x$ :

$$H/H_s = x/X \quad (8)$$

where  $H_s$  is the concentration of molecular hydrogen in the silica at the silica-silicon interface; the concentration of molecular hydrogen at the silica surface is zero, in equilibrium with an atmosphere containing negligible hydrogen.

The hydrogen concentration at the silica-silicon interface can be found by equating the flux of water to the interface ( $D_W C_i/X$ ), which results in both film growth and hydrogen production, to the flux of hydrogen away from the interface in the steady state ( $D_H[H_2]/X$ ), giving

$$H_s = C_i D_W / D_H$$

where  $D_W$  and  $D_H$  are the diffusion coefficients of molecular water and hydrogen, respectively. The ratio  $D_H/D_W$  is about 50 at 1000 °C,<sup>4,7</sup> so the effective hydrogen pressure at the silicon-silica interface should be about  $1/50$  of the water vapor pressure during oxidation.

When both hydrogen and water molecules are present in the silica, hydroxyl groups can be formed by both eq 2 and 3. Then the concentration  $R$  of SiH groups can be found from eq 5 and 7 to be

$$R = \frac{HK_2}{C^{1/2}K_1} \quad (9)$$

Thus  $R$  is proportional to  $H$  the concentration of molecularly dissolved hydrogen, and inversely proportional to  $C^{1/2}$ , where  $C$  is the concentration of molecular water.

The profile of  $R$  is found from eq 9 by introducing eq 4 and 8

$$R = \frac{\alpha x/X}{(1 - x/X)^{1/2}} \quad (10)$$

where

$$\alpha = \frac{H_s K_2}{S_i} = \frac{C_i K_2 D_W}{S_i D_H} \quad (11)$$

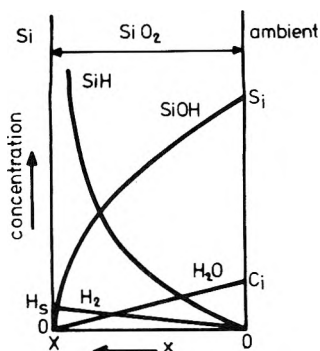


Figure 1. Calculated profiles of hydrogen-bearing species in silicon on wet-oxidized silicon.

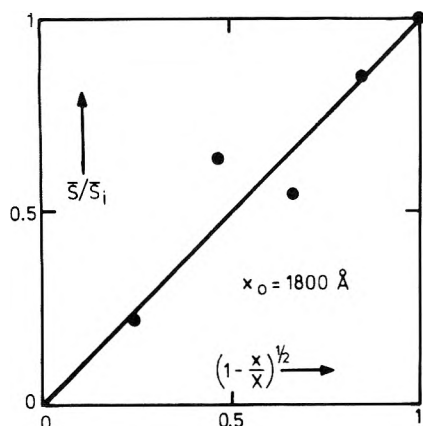


Figure 2. Average concentration  $\bar{S}$  of hydroxyl groups in a silica layer between  $x$  and  $X$ ; line from eq 15; points from ref 6.

The concentration profile of total hydrogen  $H_T$  is equal to  $S + R$ , neglecting the molecular water and hydrogen, or

$$H_T = S_i(1 - x/X)^{1/2} + \frac{\alpha x/X}{(1 - x/X)^{1/2}} \quad (12)$$

This equation gives a minimum in total hydrogen at

$$\frac{x}{X} = \frac{S_i - 2\alpha}{S_i - \alpha} \quad (13)$$

if  $2\alpha < S_i$ , and a sharp increase in the total hydrogen concentration as  $x \rightarrow X$  (at the silicon-oxide interface). For  $2\alpha \geq S_i$ ,  $H_T$  increases monotonically into the silica layer from  $S_i$  at the silica surface. For comparison with experiment, eq 12 can be written

$$H_T(1 - x/X)^{1/2} = (S_i - \alpha)(1 - x/X) + \alpha \quad (14)$$

Profiles of various species calculated from these equations are shown schematically in Figure 1.

### Comparison with Experimental Results

Beckmann and Harrick<sup>6</sup> measured the average hydroxyl concentration from the infrared absorption at  $2.7 \mu$  in a silica layer on wet-oxidized silicon that was successively etched. Integration of eq 6 to obtain the average hydroxyl concentration  $\bar{S}$  in a layer between  $x$  and  $X$  gives

$$\bar{S}/\bar{S}_i = (1 - x/X)^{1/2} \quad (15)$$

where  $\bar{S}_i$  is the initial average concentration and equals  $2S_i/3$ . In Figure 2 the experimental results of Beckmann and Harrick

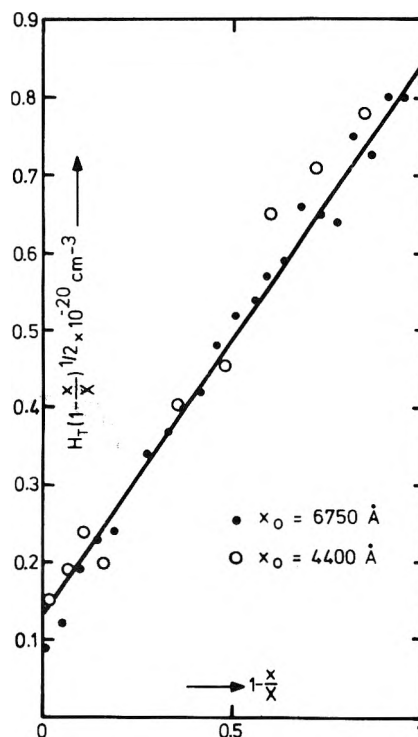


Figure 3. Total hydrogen concentration  $H_T$  in a silica layer on wet-oxidized silicon as a function of distance from the silicon-oxide interface; line from eq 14; points from ref 5.

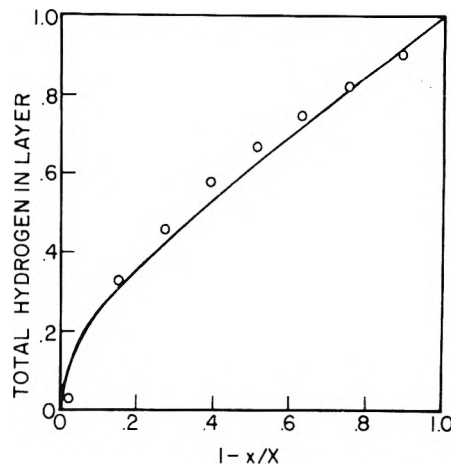


Figure 4. Tritium counts in a successively etched silica film initially  $820\text{-}\text{\AA}$  thick; points from Figure 2, ref 5; line from eq 16 with  $\alpha/S_i = 0.4$ .

are shown to agree reasonably well with eq 15; the agreement is poorer for a linear dependence of  $\bar{S}$  on distance, for example.

Burkhardt<sup>5</sup> measured the total hydrogen profile in silica layers of different thickness on wet-oxidized silicon. He found a minimum in the profile of total hydrogen concentration, and also an increase in hydrogen concentration near the silicon-oxide interface (Figure 5, ref 5). In one method Burkhardt measured the hydrogen profile by counting tritium in solutions progressively etched from the silica layer. Data from films of thickness 4400 and 6750  $\text{\AA}$  are plotted according to eq 14 in Figure 3. The experimental scatter was quite large, and the agreement with the equation is within this scatter. A second method of counting the tritium remaining in the silica

layer after progressive etching was more reliable for thinner films; for thicker films some of the tritium  $\beta$  rays were absorbed by the film. The profile expected from this kind of experiment is given by integrating eq 12

$$\int_x^X H_T dx = 2\alpha X(1 - x/X)^{1/2} + \frac{2X(S_i - \alpha)(1 - x/X)^{3/2}}{3} \quad (16)$$

A plot of this equation with  $\alpha/S_i \approx 0.4$  is compared to Burkhardt's data for residual counting of a film 820-Å thick (Figure 2, ref 5) in Figure 4. The agreement is within the experimental error of the measurements.

From  $H_T$  at  $x = X$  and at  $x = 0$  in Figure 3,  $\alpha = 1.3(10)^{19} \text{ cm}^{-3}$  and  $S_i = 8.5(10)^{19} \text{ cm}^{-3}$ , the latter value in good agreement with the result of  $6.9(10)^{19} \text{ cm}^{-3}$  measured by Moulson and Roberts.<sup>8</sup> This ratio of  $\alpha/S_i \approx 0.15$  gives a minimum at  $x/X = 0.82$ , in reasonable agreement with the minima in  $H_T$  for these films in Figure 5, ref 5. Although the calculated curve in Figure 4 is not very sensitive to values of  $\alpha/S_i$ , the data for the thinner film fit the curve for  $\alpha/S_i = 0.4$  better than curves for smaller values of  $\alpha/S_i$ , giving a minimum in  $H_T$  for this film at  $x/X \approx 0.3$ , consistent with Figure 2, ref 5. It is not clear why there are different values of  $\alpha/S_i$  for the thicker and thinner films, since this ratio should not be a function of film thick-

ness. From the value of  $\alpha$  and known values of  $S_i/C_i \approx 400$  and  $D_H/D_W = 527$  the value of  $K_2$  is about  $2.7(10)^{23} \text{ cm}^{-3}$ . This is about three orders of magnitude higher than the value of  $K_2$  calculated from the data of Bell et al.<sup>3</sup> on fused silica. The reason for this difference is not known.

Ota and Butler<sup>9</sup> found that addition of hydrogen to water vapor used for oxidizing silicon did not change the growth rate of the oxide. This result is consistent with the present point of view. Since hydrogen diffuses rapidly in the silica, an ambient pressure of hydrogen adds a constant additional uniform concentration of dissolved molecular hydrogen in the silica layer. This hydrogen reacts with the silica by eq 3 to give additional amounts of SiH groups. However, the presence of these groups does not influence the diffusion of molecular water, which is responsible for oxidizing the silicon.

## References and Notes

- (1) R. H. Doremus, to be published.
- (2) R. V. Adams and R. W. Douglas, *J. Soc. Glass Technol.*, **43**, 147 (1959).
- (3) T. Bell, G. Hetherington, and K. H. Jack, *Phys. Chem. Glasses*, **3**, 141 (1962).
- (4) R. W. Lee, *Phys. Chem. Glasses*, **5**, 35 (1964).
- (5) P. J. Burkhardt, *J. Electrochem. Soc.*, **114**, 196 (1967).
- (6) K. H. Beckmann and N. J. Harrick, *J. Electrochem. Soc.*, **118**, 614 (1971).
- (7) R. H. Doremus, "Reactivity of Solids", Wiley, New York, N.Y., 1969, p 667.
- (8) A. J. Moulson and J. P. Roberts, *Trans. Faraday Soc.*, **57**, 1208 (1961).
- (9) Y. Ota and S. R. Butler, *J. Electrochem. Soc.*, **121**, 1107 (1974).

## Reaction of Amines with Haloalkanes. 4. Reaction at a Pyrex Surface

Pierre A. Willermet and John G. Miller\*

Department of Chemistry and the Laboratory for Research on the Structure of Matter, University of Pennsylvania, Philadelphia, Pennsylvania 19174 (Received July 12, 1976)

Publication costs assisted by the Laboratory for Research on the Structure of Matter, University of Pennsylvania

The chain reaction of amines with haloalkanes is initiated by ultraviolet light, by a copper metal surface activated with oxygen, and by transition metal ions. We have discovered that it is also initiated at a Pyrex surface. The initiation requires oxygen and takes place at Lewis-acid sites provided by the alumina in the glass surface. A kinetic study of the process, using principally  $\text{CCl}_4$  and *n*-butylamine as reactants at 32 °C, has been made and a mechanism for the reaction is proposed. The reaction shows strong autoinhibition which appears to be due to free-radical trapping by substances formed in the reaction.

In earlier studies in this laboratory,<sup>1-3</sup> the chain reaction between amines and haloalkanes and the initiation of that reaction by ultraviolet light, by a copper metal surface activated with oxygen, and by cuprous and ferrous salts have been investigated. Hitherto undetected initiation at a Pyrex glass surface is described below. Since Pyrex vessels are used so frequently as containers for amine-haloalkane systems, this initiatory action is of obvious importance.

The initiation at a Pyrex surface requires oxygen and probably takes place at Lewis-acid sites provided by the alumina included in the Pyrex. The reaction shows strong autoinhibition which is probably due to radical scavenging by substances formed in the reaction. Kinetic study of both the

initiation and the inhibition was made using mainly  $\text{CCl}_4$  and *n*-butylamine as reactants and mechanisms are proposed for both processes.

## Experimental Section

**Materials.** Alumina was Ventron Corp., Alfa Inorganics, 99.99% pure, 1- $\mu$  nominal particle size. Cabosil L-5 silica had a BET surface area of  $50 \pm 10 \text{ m}^2 \text{ g}^{-1}$ .

The *n*-butylamine (Matheson Coleman and Bell) was refluxed and then distilled (77.0 °C) under nitrogen over Linde Type 4A molecular sieves in a Todd Scientific Co. fractionating still. The di-*n*-butylamine (Fisher) was distilled (158 °C) under nitrogen in the same way. Spectroquality  $\text{CCl}_4$  (Ma-

theson Coleman and Bell) was refluxed and distilled (76–77 °C) over molecular sieves, using the same still.

Prepurified nitrogen (Air Products, Inc.) was used as received for the reaction studies and as the carrier gas in gas chromatography. Linde oxygen (99.6% pure) was passed over Ascarite and Drierite before use.

*N*-Butylidenebutylamine ( $C_3H_7CH=NC_4H_9$ ) was prepared by the method of Day and Stein<sup>4</sup> (bp 141–143 °C, lit. 140–145 °C).

**Apparatus.** The reaction vessels were 250- or 500-ml round-bottom Pyrex flasks equipped with a Pyrex inlet tube to bubble gas under the surface of the liquid reaction mixtures, an adapter fitted with a septum for addition of reagents, and a Pyrex reflux condenser fitted with a cold finger. The outside of the entire apparatus was painted black to exclude light.

A similar apparatus was constructed entirely of General Electric 204 clear fused quartz. The impurities in the quartz were given as follows in ppm:  $Li_2O$ , 1; B, 0.5;  $ZrO_2$ , 1;  $K_2O$ , 4;  $Na_2O$ , 4;  $Al_2O_3$ , 50;  $Fe_2O_3$ , 5; CaO, 7;  $TiO_2$ , 2; MgO, 2.

All vessels and the solids added to produce additional surfaces were washed successively with *n*-butylamine in  $CCl_4$ ,  $CCl_4$ , acetone, and distilled water and were then dried at 110 °C before use.

Oxygen and nitrogen were passed through Matheson calibrated floating-ball flowmeters equipped with needle valves and were then combined in a single stream and passed into the gas inlet tube. Effluent gas was passed out through a tube at the top of the condenser and through a series of traps used to collect the volatile products.

Teflon-coated bar magnets were used to stir the reaction mixtures with a magnetic stirrer. All experiments were carried out with the apparatus in a water bath kept at  $32.00 \pm 0.03$  °C.

To measure the consumption of oxygen, the gas inlet was sealed off and the condenser was replaced by a manifold to which measured volumes of dibutylphthalate were added as needed to restore the pressure to the starting value.

**Procedures.**  $CCl_4$  (usually 200 ml) was introduced into the reaction flask and stirred by bubbling the gas through it at a rate of 2 ml/s. Vapors were refluxed by filling the condenser cold finger with a  $-23$  °C  $CCl_4$ -dry ice slush. After 1 h, amine was added by pipet or glass syringe. The volume of amine was varied to produce initial concentrations of from 0.05 to 0.92 M and the oxygen partial pressure was varied between 50 and 610 Torr by adjustment of the oxygen and nitrogen flow rates.

For measurement of oxygen uptake, the reaction vessel was first charged with  $CCl_4$  and was then degassed through three freeze-thaw cycles and attached to an evacuated manifold. Oxygen was admitted to the manifold and the stirred system was brought to equilibrium with the oxygen as judged by the dibutylphthalate-addition procedure described in the apparatus section.

Analyses were performed by extracting the reaction mixture with standard aqueous sulfuric acid. Aliquots of the extract were back-titrated with standard NaOH and the amount of acid consumed was designated "apparent amine", AA. Chloride ion was determined by Volhard titration. Butylidenebutylamine was measured by adding aliquots to a saturated solution of 2,4-dinitrophenylhydrazine in 2 N HCl. The resultant precipitate, butanal 2,4-dinitrophenylhydrazone, was either measured gravimetrically, or, when in small amount, dissolved in  $CCl_4$  and determined spectroscopically by its absorbance at 435 nm. Unextracted butylidenebutylamine remaining in the reaction mixture was determined by running

a second extraction with  $H_2SO_4$  or by adding the hydrazine to an aliquot of the reaction mixture and then evaporating the  $CCl_4$ , washing out the excess hydrazine with 2 N HCl, and redissolving the hydrazone in  $CCl_4$ . In this case, in order to remove the effect of colored polymeric products, the spectrum was run against a sample of the reaction mixture treated in the same manner except for addition of hydrazine.

*N,N'*-Di-*n*-butylurea was determined gravimetrically after evaporation of the  $CCl_4$  from an aliquot of the reaction system, redissolving in  $CCl_4$ , and precipitating by addition of diethyl ether. Ammonia was determined in the effluent gas stream by passing the stream through a dry ice-acetone trap into standard aqueous acid. Small amounts of chloroform were detected by gas chromatography and butyl isocyanide was detected by odor, but only a trace amount was shown by infrared absorption spectroscopy.

**Surfaces.** The Pyrex surface area was varied by adding 2-mm diameter Pyrex beads to the reaction vessel. The surface area of Pyrex was taken to be the surface area of the flask contacted by the liquid reaction solution plus the surface area of the added beads.

When fresh Pyrex glassware was used it was discovered that the reaction rate was relatively high. After two or three runs the rate declined to a fixed value and remained at that value thereafter. This passivating effect, which will be discussed below, was observed early in the study and all of the data reported here for Pyrex surfaces are based on use of Pyrex that had been preconditioned by that treatment.

In order to identify the types of sites responsible for the initiation of reaction, the Pyrex for some of the runs was leached with concentrated nitric acid at 60 °C to remove alumina selectively.<sup>6</sup> Quartz apparatus was also used and, in other tests, new surfaces were introduced by addition of particles of alumina or silica.

Separate experiments were carried out to determine the extent of autoxidation of *n*-butylamine in the absence of  $CCl_4$  and light. It was found that only 3% of the amine was oxidized in 6 days with an oxygen pressure of approximately 1 atm in a Pyrex vessel. When 1.10 g of alumina was added per 10 ml of amine the amount of oxidation was increased only to 5% in the same length of time.

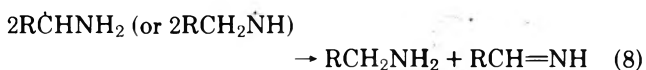
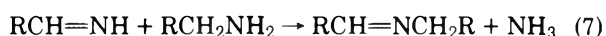
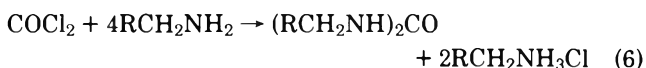
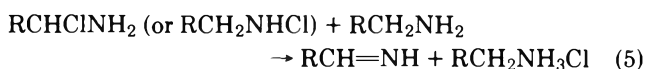
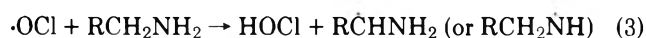
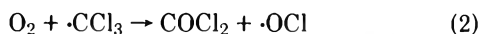
The known products of the reaction were tested as possible inhibitors by addition of measured amounts of them to the  $CCl_4$  before addition of amine. Ammonia added for this purpose was bubbled into the  $CCl_4$  and an aliquot was taken for analysis before addition of amine.

## Results and Discussion

**Reaction at a Pyrex Surface.** Some of the principal results of the studies of the  $CCl_4$ -*n*-butylamine reaction in Pyrex vessels, with and without added Pyrex beads, will be presented first as a basis for discussion of the other studies.

These results showed remarkably uniform product distribution over a wide range of initial amine concentration (0.05–0.92 M), oxygen pressures (50–610 Torr), and reaction times (up to 23 h). The major reaction products were *n*-butylamine hydrochloride, *N,N'*-di-*n*-butylurea,  $NH_3$ , butylidenebutylamine, and polymeric products due to amine oxidation.

The products may be accounted for on the basis of the chain reactions known<sup>1,7</sup> to occur in the haloalkane-amine systems in the presence of oxygen after an initiating process has produced a suitable free radical, which may be written simply as R·, without identification at this point:



Additional reactions probably take place, as will be discussed below. It is not implied that eq 8 is the terminating step.

Typical results are given in Table I to show the consumption of amine and oxygen and the distribution of identified products. The concentration of apparent amine reacted, [AAR], is equal to the initial amine concentration,  $[A]_0$ , minus the concentration of apparent amine, [AA], which is determined at any time from back-titration of the standard acid used to quench the reaction at that time. It should be noted that the AA value is given by the amount of unreacted amine present plus the amount of butylidenebutylamine formed. The other substances present do not consume the quenching acid and in the titration the butylidenebutylamine is hydrolyzed to form one molecule of amine and one of butyraldehyde. The ammonia passes out of the system during the reaction.

The values in Table I show that 89%  $([43.8 + 2(10.9) + 2(15.6)] / (93.0 + 15.6) = 0.89)$  of the amine consumed is accounted for by the identified products. The other products are assumed to be the polymeric substances observed.

The data may also be used to calculate the ratio  $[Cl^-]/[AAR]$  which we have found to be a useful index of the relative amount of polymeric products formed. The photochemically initiated reaction in the presence of oxygen<sup>1</sup> has a stoichiometry approaching the following relationship as the oxygen pressure approaches 1 atm:



Equation 9 predicts a  $[Cl^-]/[AAR]$  ratio of  $4/7 = 0.57$ . The data in Table I give the value  $43.8/93.0 = 0.47$  for that ratio and the average value for all of the determinations in Pyrex was  $0.45 \pm 0.01$ , the difference from 0.57 being ascribed mainly to polymer formation.

The amounts of chloride ion and urea shown in Table I are in the ratio required by eq 9 and the amounts of  $NH_3$  and butylidenebutylamine, which are formed simultaneously from the fleeting intermediate aldimine,  $RCH=NH$ , are closely equal, as expected, but are higher than predicted by eq 9. The amount of oxygen consumed is much greater than required by eq 9. These results indicate the formation of larger amounts of  $RCHNH_2$  than expected by the mechanism given above. This is not surprising in view of the great ease of production of  $RCHNH_2$  as the predominant initial process in the oxidation of aliphatic amines.<sup>8</sup> The high yield of butylidenebutylamine would also be expected to be accompanied by formation of polymers<sup>5</sup> and of other products in the presence of

TABLE I: Reactant Consumption and Product Distribution for a Typical Run in a Pyrex Vessel<sup>a</sup>

Apparent amine reacted [AAR]	93.0
O <sub>2</sub> consumed (separate run)	15.2
Chloride ion	43.8
<i>N,N'</i> -Di- <i>n</i> -butylurea	10.9
NH <sub>3</sub>	15.45
Butylidenebutylamine	15.6

<sup>a</sup> Initial amine concentration, 0.482 M. O<sub>2</sub> pressure, 610 Torr. Reaction time, 222 min. Concentrations are expressed in millimoles per liter.

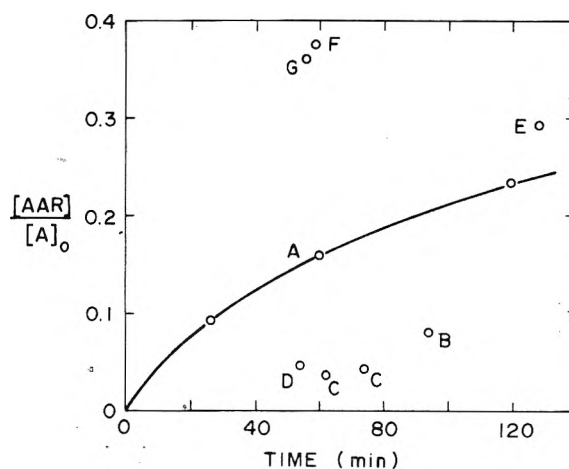


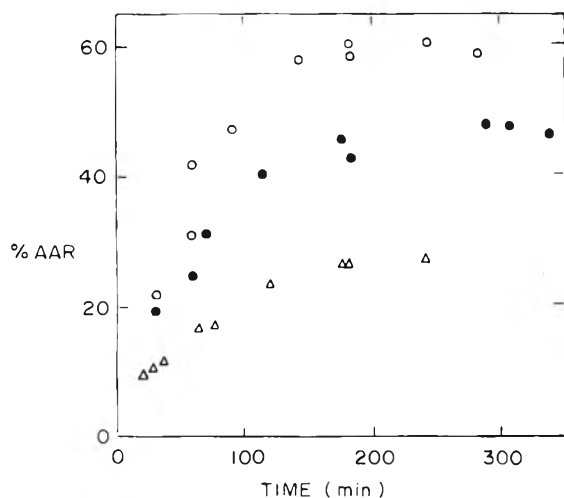
Figure 1. The effects of different surfaces on the rate of reaction. Curve A serves as reference and shows the rate of reaction in a Pyrex vessel ( $[A]_0 = 0.482$  M); B = quartz vessel; C = nitric acid-leached Pyrex vessel; D = 0.0741 g of Cabosil L-5 silica added to acid-leached vessel; E, F, G = 0.90, 1.79, and 4.08 g of alumina added to acid-leached vessel.

oxygen.<sup>8-10</sup> The  $CCl_4$  is able to compete with oxygen in reacting with the  $\alpha$ -aminoalkyl radicals (eq 4) because of its high concentration. The solubility of oxygen in  $CCl_4$  at 30 °C is only 0.0116 M at 1 atm.<sup>11</sup>

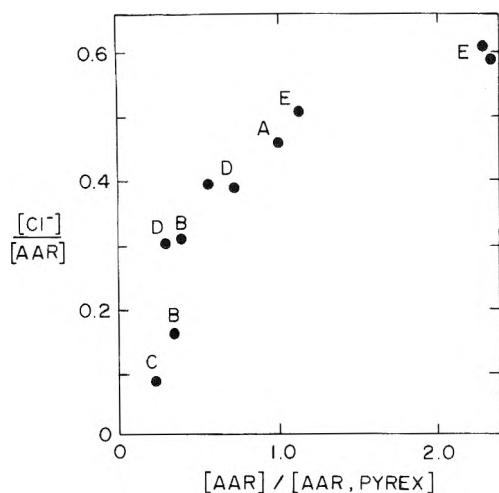
*Initiating Sites on the Glass Surface.* The higher reaction rate at a fresh Pyrex surface and the leveling off to a fixed lower rate after two or three runs has been noted in the Experimental Section. The leveling off is probably due to extraction of transition metal ions from the surface. When oxygen was carefully excluded, no detectable reaction was observed in the *n*-butylamine- $CCl_4$  system after 5 days in the usual preconditioned Pyrex vessels although transition metal ions readily initiate reaction in such systems. It was also found that di-*n*-butylamine and  $CCl_4$  reacted very slowly even in the presence of oxygen in the preconditioned Pyrex containers although they react very readily in the presence of transition metal ions. These observations show that initiation by transition metal ion impurities in the Pyrex surfaces was not significant in our procedure.

Figure 1 shows the effect of a quartz surface, the effect of leaching the Pyrex surface with nitric acid, and the effects of adding pure silica and alumina to the acid-leached vessels. The selective removal of the alumina from a Pyrex surface by the leaching<sup>6</sup> process produces a great reduction in rate and addition of alumina causes a great increase.

The quartz vessel surface is only slightly more active than the acid-leached Pyrex surface and the small difference may be due to the small concentration of transition metal ions in the quartz or, more probably, to the lack of proper annealing of the vessel. Cabosil silica also showed only a small effect.



**Figure 2.** Variation of the rate with the ratio of Pyrex surface area to volume of solution:  $\Delta$ ,  $0.615 \text{ cm}^{-1}$  (no beads added);  $\bullet$ ,  $1.75 \text{ cm}^{-1}$ ;  $\square$ ,  $2.91 \text{ cm}^{-1}$ .



**Figure 3.** Correlation between  $[\text{Cl}^-]/[\text{AAR}]$  and relative reaction rate: A, Pyrex vessel; B, butylidenebutylamine added to system in Pyrex vessel; C, acid-leached Pyrex vessel; D, quartz vessel; E, acid-leached Pyrex vessel with added alumina.

Silication of the Pyrex vessel surface with dichlorodimethylsilane to remove the Brönsted-acid sites resulted in no effect on the rate, but increase in the surface area by addition of Pyrex beads produced a proportionate increase (Figure 2).

It is clear that the active sites on the Pyrex surface are the alumina sites. Using infrared spectroscopy, Hirota and co-workers<sup>12</sup> have found that methylamine is strongly adsorbed on alumina. Morimoto, Imai, and Nagao<sup>13</sup> studied the infrared spectra of *n*-butylamine adsorbed on silica, on alumina, and on silica-alumina. They found that *n*-butylamine reacts weakly with protonic (Brönsted) acid sites on a silica surface that had been washed with water and dried at  $100^\circ\text{C}$ . Evacuation at  $100^\circ\text{C}$  for 4 h led to almost complete desorption of the amine. On alumina pretreated in the same way the spectra showed that the amine attached so strongly to the Lewis-acid sites that it was not desorbed in several hours at  $100^\circ\text{C}$ . Some of the Lewis-acid sites on the alumina had been converted into Brönsted-acid sites by the pretreatment and the amine reacted with those protonic sites. The pretreated silica-alumina adsorbents were dried only at  $500^\circ\text{C}$  and apparently had both Brönsted- and Lewis-acid sites. Although the strength of the protonic acid sites increased with decreasing amount of alumina, the amine was much more strongly adsorbed on

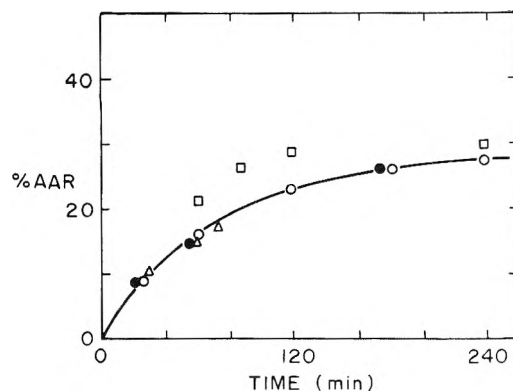


**Figure 4.** Effect of initial amine concentration on reaction rate at fixed ratio ( $r = 0.615 \text{ cm}^{-1}$ ) of Pyrex surface area to volume of solutions.  $[\text{A}]_0$ :  $\bullet$ ,  $0.127 \text{ M}$ ;  $\Delta$ ,  $0.247 \text{ M}$ ;  $\circ$ ,  $0.482 \text{ M}$ ;  $\square$ ,  $0.920 \text{ M}$ .

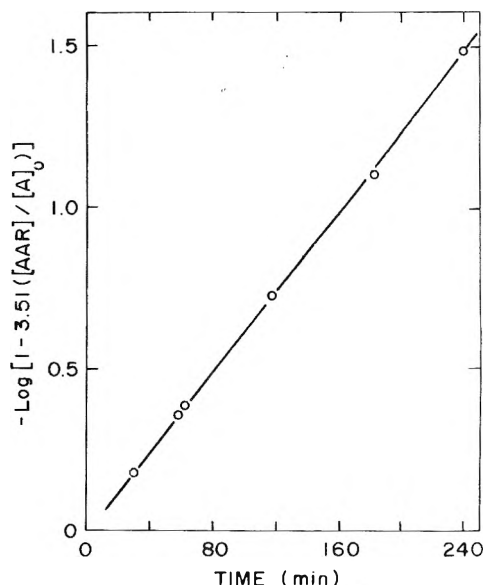


**Figure 5.** The empirical function for  $r = 0.615 \text{ cm}^{-1}$ ,  $[\text{A}]_0 = 0.482 \text{ M}$ .

the Lewis sites, which they believed were located about aluminum atoms in Si-O-Al bondings.

The product distribution was also affected by the nature of the surface. Figure 3 shows a correlation between the  $[\text{Cl}^-]/[\text{AAR}]$  values and the relative reaction rates expressed as the ratio of the  $[\text{AAR}]$  values in the different systems to those in a Pyrex vessel at the same reaction time. Quartz and acid-leached Pyrex produce higher yields of polymeric products and the alumina surface gives lower yields. Addition of butylidenebutylamine retards the rate and increases the yield of polymer. Thus, in all cases, decrease in reaction rate is accompanied by increase in polymer yield.

**Reaction Kinetics.** The rate of reaction at the Pyrex surface is independent of the oxygen pressure above approximately 100 Torr. The kinetic data with respect to other variables were collected at an oxygen pressure of 610 Torr. As shown in Figure 4, the rate is independent of initial amine concentration up to  $0.482 \text{ M}$ , but increases slightly at  $0.920 \text{ M}$ . The small increase may be due to the increased polarity of the medium caused by the increase in amine concentration.

The rate data were found to fit an empirical formulation

$$t = -k_1 \log [1 - (k_2 [\text{AAR}]/[\text{A}]_0)] \quad (10)$$

where  $t$  is the time and  $k_1$  and  $k_2$  are constants for a given ratio,  $r$ , of Pyrex surface area to solution volume (Figure 5).

**TABLE II: Correlation of Parameters Found for the Empirical Rate Expression (Eq 10)**

$r, \text{cm}^{-1}$	0.615	1.75	2.91
$k_1, \text{min}$	-158	-139	-139
$k_2$	3.51	2.07	1.61
$k_2^{-1}r^{-1/2}$	0.363	0.365	0.364

As shown in Table II,  $k_1$  was rather independent of  $r$ , while  $1/k_2$  was closely proportional to  $r^{1/2}$ . Differentiation of eq 10 yields the equation

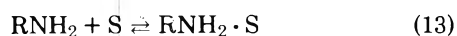
$$-d([\text{AA}]/[\text{A}]_0)/dt = 1/(k_1k_2) - (1/k_1)([\text{AAR}]/[\text{A}]_0) \quad (11)$$

where  $[\text{AA}]$  is the apparent amine concentration. The correlation shown in Table II allows rewriting eq 11 in the form

$$-d[\text{AA}]/dt = kr^{1/2}[\text{A}]_0 - k'[\text{AAR}] \quad (12)$$

A mechanistic interpretation of eq 12 may be given as follows:

The adsorption equilibrium



where S denotes an active site on the surface would be expected to lie far to the right so that the concentration of amine molecules adsorbed at activated sites would be proportional to  $r$ , i.e.,  $[\text{RNH}_2\text{S}] = ar$ . In turn, the rate of initiation (free radical formation) at the surface should be proportional to the concentration of those adsorbed molecules:

$$d[\text{R}\cdot]/dt = k_i ar \quad (14)$$

If the rate-determining propagation step is a reaction between amine and a free radical, the rate of reaction would be given by

$$-d[\text{AA}]/dt = k_r[\text{R}\cdot][\text{AA}] \quad (15)$$

Assuming second-order termination

$$-d[\text{R}\cdot]/dt = k_t[\text{R}\cdot]^2 \quad (16)$$

and employing the steady-state approximation

$$d[\text{R}\cdot]/dt = k_i ar - k_t[\text{R}\cdot]^2 = 0 \quad (17)$$

the concentration of free radicals is given by

$$[\text{R}\cdot] = (k_i ar/k_t)^{1/2}$$

which, on substitution in eq 15, yields

$$-d[\text{AA}]/dt = k_p(k_i ar/k_t)^{1/2}[\text{AA}] \quad (18)$$

which is in agreement with eq 12 for zero time when  $[\text{AA}] = [\text{A}]_0$  and  $[\text{AAR}] = 0$ , conditions for which the assumptions made in deriving eq 18 are most valid. Further interpretation of eq 12 will be made below.

While the mode of attachment of the amine to the active

alumina site is probably due to coordination of the lone electron pair of the nitrogen atom to an aluminum ion<sup>12,13</sup> and while oxygen participates in the initiating step, it is not possible at present to identify the free radical produced.

**Autoinhibition.** A striking feature of the reaction is the strong autoinhibition observed as the reaction progresses. In Pyrex vessels the reaction rate becomes virtually zero when only about one-third of the amine initially present has reacted, for all initial concentrations below 0.92 M. The empiric rate expression, eq 12, includes this behavior in the  $-k'[\text{AAR}]$  term.

The inhibition is not due primarily to the competitive adsorption of a product on the active sites. Addition of Pyrex beads to the reaction mixture at virtual termination resulted in no significant acceleration of the rate. It appears most likely that the reaction produces radical-trapping species that cause the inhibition. Earlier,<sup>1</sup> it was found that effective inhibition of the amine-haloalkane reaction can be caused by addition of radical scavengers.

Study of the inhibitory action of each of the major products of the reaction showed that the urea and amine hydrochloride had no effect. The slight inhibitory effect and the increase in polymer yield caused by butylidenebutylamine was noted above. Ammonia produced less inhibitory action and its effect may have been due to competitive adsorption, especially at sites recessed below the surface. The most likely inhibiting products are the polymeric materials, especially those conjugated unsaturated products<sup>8</sup> that may act as resonance-stabilized free radicals. When *n*-butylamine- $\text{CCl}_4\text{-O}_2$  systems are allowed to stand for extended periods, they acquire a progressively darker yellowish hue, indicating the presence of such substances.

**Acknowledgment.** This research was supported in part by the Advanced Research Projects Agency and by the National Science Foundation.

## References and Notes

- (1) W. J. Lautenberger, E. N. Jones, and J. G. Miller, *J. Am. Chem. Soc.*, **90**, 1110 (1968). References to earlier studies of the reaction are given in this article.
- (2) E. N. Jones, W. J. Lautenberger, P. A. Willermet, and J. G. Miller, *J. Am. Chem. Soc.*, **92**, 2946 (1970).
- (3) C. J. Biaselle and J. G. Miller, *J. Am. Chem. Soc.*, **96**, 3813 (1974).
- (4) A. R. Day and C. W. C. Stein, *J. Am. Chem. Soc.*, **64**, 2569 (1942).
- (5) W. S. Emerson, S. M. Hess, and F. C. Uhle, *J. Am. Chem. Soc.*, **63**, 872 (1941).
- (6) L. H. Little, H. E. Klauser, and C. H. Amberg, *Can. J. Chem.*, **39**, 42 (1961).
- (7) J. R. L. Smith and Z. A. Malik, *J. Chem. Soc. B*, 617, 920 (1970).
- (8) F. C. Schaefer and W. D. Zimmerman, *J. Org. Chem.*, **35**, 2165 (1970).
- (9) P. A. S. Smith, "Open-Chain Nitrogen Compounds", Vol. I, W. A. Benjamin, New York, N.Y., 1965, pp. 298-312.
- (10) G. Drefahl and G. Heublein, *J. Prakt. Chem.*, [4], **20**, 323 (1963).
- (11) J. Horiuti, *Sci. Papers Inst. Phys. Chem. Res. (Tokyo)*, **17**, 125 (1931).
- (12) K. Hirota, K. Fueki, and T. Sakai, *Bull. Chem. Soc. Jpn.*, **35**, 1545 (1962).
- (13) T. Morimoto, J. Imai, and M. Nagao, *J. Phys. Chem.*, **78**, 704 (1974).

# Raman Scattering of Pure Ammonia to High Pressures and Temperatures

M. Buback\* and K. R. Schulz

Institut für Physikalische Chemie und Elektrochemie, Universität Karlsruhe, D-75 Karlsruhe, West Germany (Received February 12, 1976)

Raman scattering of pure  $\text{NH}_3$  in the stretching fundamental region around  $3300\text{ cm}^{-1}$  was investigated at 21, 75, 200, and 225 °C to a maximum pressure of 2000 bars. The spectra obtained as the density was varied continuously between gaseous and liquidlike states at supercritical temperature ( $T_c = 132.5\text{ °C}$ ) enabled a definite assignment of the four vibrations  $\nu_1$ ,  $\nu_3$ ,  $2\nu_4^A$ , and  $2\nu_4^E$ . The degree of Fermi resonance between  $\nu_1$  and  $2\nu_4^A$  is determined from the density dependence of the Raman intensity of both vibrations. Quantitative determinations of the molar Raman scattering intensity indicate a maximum scattering intensity of the symmetric  $\nu_1$  stretching vibration at a moderately high density of  $0.40 \pm 0.05\text{ g/cm}^3$ . This result is compared to previously reported infrared data on pure  $\text{NH}_3$  where the  $\nu_1$  absorption intensity changes strongly with density. This was explained by assuming a variation of the  $\text{NH}_3$  molecular configuration as a function of density with a minimum in pyramidal height at about  $0.40\text{ g/cm}^3$  density.

## Introduction

There has been considerable interest in the study of polar liquids in recent years. By far most of the spectroscopic work in Raman, infrared, and near-infrared was performed on water<sup>1,2</sup> and on other simple liquids, e.g., hydrogen chloride<sup>3</sup> or ammonia.<sup>4</sup> Intermolecular interactions may be elucidated via spectroscopic techniques applied to high pressure systems. At temperatures above the critical point measurements can be made as a function of continuously varying density from gaseous to liquidlike densities. This technique was employed on both Raman<sup>5</sup> and infrared<sup>6</sup> spectra for water, in the infrared spectra for pure HCl,<sup>3</sup> and recently for pure  $\text{NH}_3$ .<sup>7,8</sup>

Measurements on ammonia seem to be of particular interest since  $\text{NH}_3$  is a simple molecule which may be compared to  $\text{H}_2\text{O}$ . Moreover, liquid ammonia is an important solvent system and special interest exists in the solutions of solvated electrons.<sup>9</sup> Furthermore, uncertainties exist in the literature on the assignment of bands occurring in the N-H stretching region at about  $3300\text{ cm}^{-1}$ . This region is composed of an overlap of four vibrations:  $\nu_1$  ( $A_1$ -type stretch),  $\nu_3$  (E-type stretch), and the  $A_1$ - and E-type overtones  $2\nu_4^A$  and  $2\nu_4^E$  and present a challenge for further spectroscopic effort.

The infrared results on pure  $\text{NH}_3$  over a wide temperature and pressure range contribute to the definite assignment of these vibrations.<sup>7,8</sup> They yield strong evidence of Fermi resonance between  $\nu_1$  and  $2\nu_4^A$  and between  $\nu_3$  and  $2\nu_4^E$ . Furthermore, the absorption of the symmetric  $\nu_1$  and  $2\nu_4^A$  vibrations decreases markedly with density. That the bands are of very low intensity at moderately high densities ( $0.4$  to  $0.5\text{ g/cm}^3$ ) seems to indicate a variation in the pyramidal height of  $\text{NH}_3$  as a function of density.

The study of  $\text{NH}_3$  Raman scattering over a wide range of densities seemed to be promising. The gradual change of spectral features with density at supercritical temperature ( $T_c = 132.5\text{ °C}$ ) allows the band assignments for the gaseous state to be applied to the more dense state. The Fermi resonance may be investigated in a more quantitative fashion by measuring the density dependence of the scattering intensity ratio of Fermi couples and of the frequency shift of the band maxima. Finally, the Raman scattering intensity must be sensitive to changes in the pyramidal height of the  $\text{NH}_3$  molecule and may support the infrared results.

Raman spectra of ammonia have frequently been studied in the liquid state at or below room temperature.<sup>10-18</sup> For

temperatures above  $T_c$  only one set of measurements at 225 °C exists.<sup>7</sup>

In the following section, Raman spectra of  $\text{NH}_3$  at 21, 75, 200, and 225 °C to maximum pressures of 2000 bars are reported. The experimental data are discussed with respect to band assignment, Fermi resonance, quantitative Raman scattering intensity data, and changes of the  $\text{NH}_3$  geometry.

## Experimental Section

Raman spectra were measured in a specially designed, high pressure, high temperature cell with three synthetic sapphire windows. The window geometry consisted of two 5-mm diameter windows for passage of the laser beam and a larger 12-mm diameter window (thickness 10 mm) at right angle for the observation of Raman scattered light. Details of the cell<sup>19</sup> will be published elsewhere.

The ammonia used in the experiments had a minimum purity of 99.98%.  $\text{NH}_3$  was distilled into a pressure generator maintained at 0 °C. The generator was connected to both the optical cell and a calibrated Heise-Bourdon gauge (accuracy at least  $\pm 3$  bars at the highest pressures). The temperature was determined with a sheathed thermocouple in the high pressure cell and was accurate to  $\pm 1\text{ °C}$ .

The excitation source was a Spectra Physics argon ion laser with 0.8-W intensity at 4880 Å. Scattered light was analyzed with a Jarrell-Ash double monochromator and a cooled photomultiplier. Photon counting rates were between  $10^4$  and  $10^5$  Hz at time constants from 0.3 to 3 s. The spectral bandwidth was  $5\text{ cm}^{-1}$  for all spectra.

In order to compare scattering intensities obtained from different high pressure, high temperature runs, Raman reference spectra at 21 °C and two pressures (200 and 800 bars) were determined before and after each series of experiments.

For a discussion of Raman scattering intensities at large density variations molar scattering intensities,  $I_m(\nu)$ , are calculated from observed intensities  $I(\nu)$  according to

$$I_m(\nu) = \frac{M}{\rho} I(\nu)$$

where  $M$  is the molecular weight of  $\text{NH}_3$  and  $\rho$  the experimental density of  $\text{NH}_3$ .  $\text{NH}_3$  molar scattering intensities  $I_m(\nu)$ , given in this paper, refer to the Raman intensity of

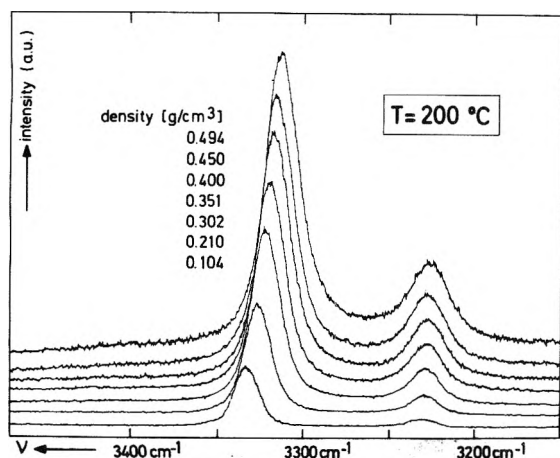


Figure 1. Raman scattering of ammonia for various densities between 0.494 and 0.104 g/cm<sup>3</sup> at 200 °C.

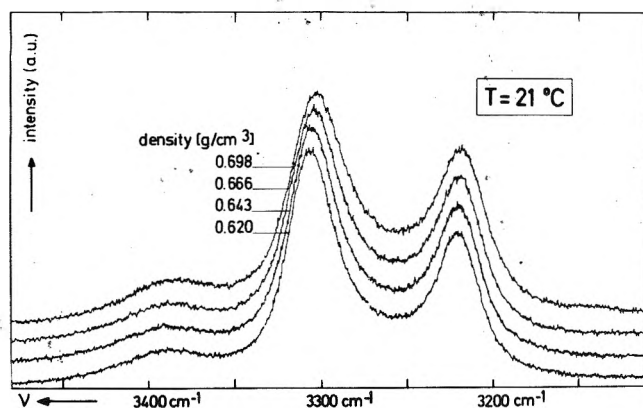


Figure 2. Raman scattering of ammonia for various densities between 0.698 and 0.620 g/cm<sup>3</sup> at 21 °C.

liquid NH<sub>3</sub> at 21 °C under its vapor pressure.  $I_m$  was set to 20 (in arbitrary intensity units) for the scattering maximum of the smaller band at 3221 cm<sup>-1</sup>. The ammonia densities are those reported by Davies.<sup>20</sup>

## Results

A set of experimental Raman bands at a constant supercritical temperature of 200 °C is shown in Figure 1. All spectra refer to the same parallel scattering geometry and have identical spectral bandwidth. The baseline has been shifted to avoid intersection of the individual curves. The pressure range 1040–155 bars corresponds to a density variation between 0.494 and 0.104 g/cm<sup>3</sup>, the critical density is 0.235 g/cm<sup>3</sup>. The experimental curves clearly show two domains of strong Raman scattering. The position of band maximum of the more intensive component at higher wavenumbers has a pronounced "red-shift" of about 20 cm<sup>-1</sup> in the pressure range under investigation (Figure 1), whereas the second component (3230 cm<sup>-1</sup>) shifts only 5 cm<sup>-1</sup>. A third band close to 3400 cm<sup>-1</sup>, which can hardly be detected even at the highest pressures in Figure 1, is clearly observed in the spectra at 21 °C and density variations between 0.698 (1500 bars) and 0.620 g/cm<sup>3</sup> (100 bars) (Figure 2). The Raman scattering intensity as in Figures 1 and 2 may be reduced to unit scattering particle density. This is achieved by calculating molar scattering intensities  $I_m(\nu)$  according to the formula given in the previous section. Results for 200 °C, as obtained from data in Figure 1, are shown in Figure 3. A remarkable result is that the scattering intensity in the maximum of the Raman band at

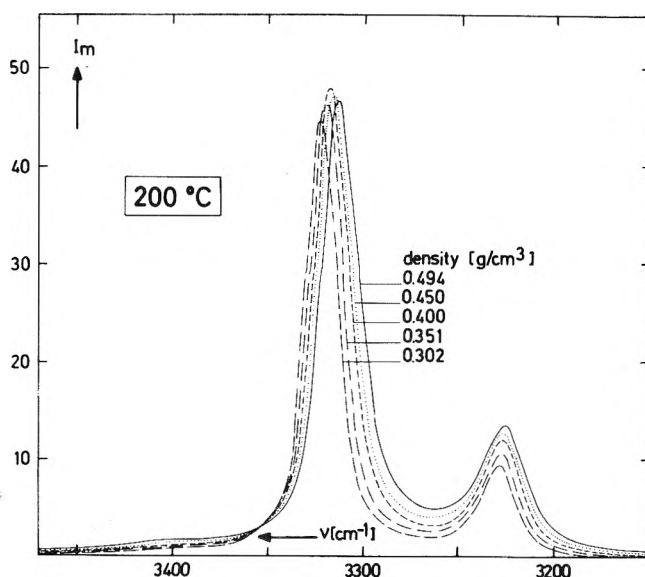


Figure 3. Molar Raman scattering intensity of ammonia for various densities between 0.494 and 0.302 g/cm<sup>3</sup> at 200 °C.

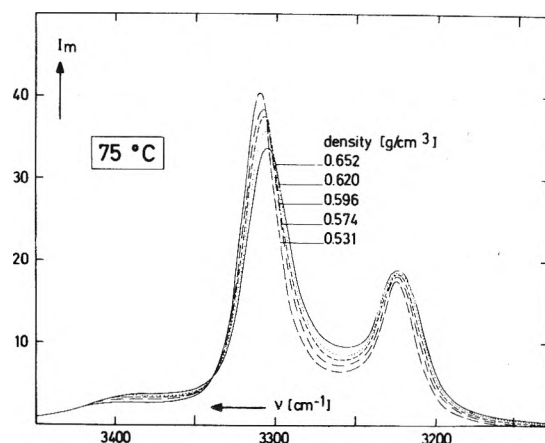
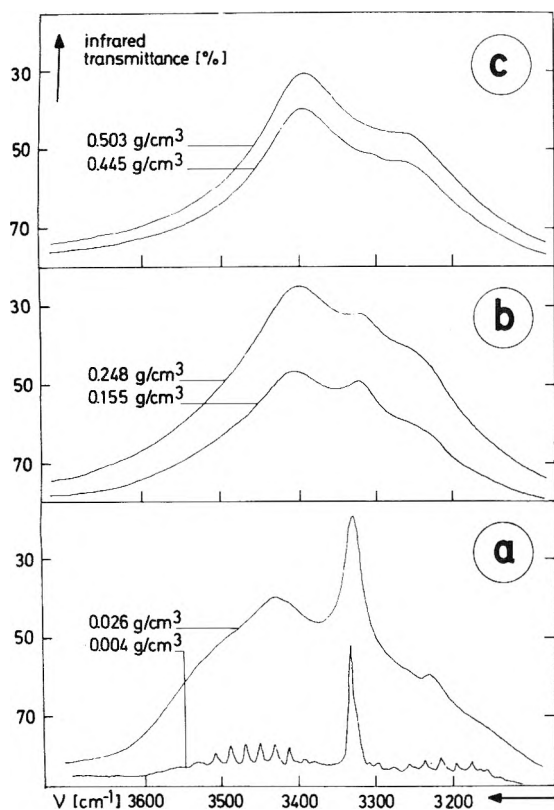


Figure 4. Molar Raman scattering intensity of ammonia for various densities between 0.652 and 0.531 g/cm<sup>3</sup> at 75 °C.

about 3315 cm<sup>-1</sup> passes through a maximum value at about 0.4 g/cm<sup>3</sup>, while the intensity of the low wavenumber band is steadily increasing with density as does the 3400-cm<sup>-1</sup> component. In liquid ammonia at 75 °C (Figure 4) the molar scattering intensity  $I_m$  of the intensive component decreases while it increases for the 3223-cm<sup>-1</sup> band.

## Discussion

The ammonia molecule of  $C_{3v}$  symmetry has four normal modes:  $\nu_1, \nu_2$  (A<sub>1</sub> type) and  $\nu_3, \nu_4$  (E type) with frequencies at 3336 ( $\nu_1$ ), 950 ( $\nu_2$ ), 3444 ( $\nu_3$ ), and 1626 cm<sup>-1</sup> ( $\nu_4$ ) in the gaseous state.<sup>4</sup> The band assignment in the 3300-cm<sup>-1</sup> region is complicated by the overlap of the stretching fundamentals  $\nu_1$  and  $\nu_3$  with the A<sub>1</sub>- and E-type overtones  $2\nu_4^A$  and  $2\nu_4^E$ . These four vibrations occur between 3200 and 3500 cm<sup>-1</sup>. In recent years numerous Raman<sup>12-18</sup> and infrared<sup>4,8,21,22</sup> investigations have been performed to clarify the assignments in this region. Nevertheless the interpretation of spectral features in the 3300-cm<sup>-1</sup> region is by no means clear. In this paper the band assignment problem will be discussed in two steps: (A) The observed bands are assigned either to A<sub>1</sub>-type ( $\nu_1, 2\nu_4^A$ ) or to E-type ( $\nu_3, 2\nu_4^E$ ) species. (B) An attempt is made to distinguish between species of the same symmetry which may interact via Fermi resonance.



**Figure 5.** Infrared spectra of ammonia. Experimental transmittance curves for various densities (in  $\text{g}/\text{cm}^3$ ) at  $225^\circ\text{C}$ . The optical layer thicknesses are 1.058 (a), 0.030 (b), and 0.005 mm (c).

(A) The assignment of bands to  $A_1$  or  $E$  types is of special importance for the ir spectra as is illustrated in Figure 5. The spectra are measured on pure  $\text{NH}_3$  at  $225^\circ\text{C}$ . The low density spectra (Figure 5a) show an intensive  $\nu_1$  absorption at about  $3330\text{ cm}^{-1}$ . The  $\nu_3$  absorption above  $3400\text{ cm}^{-1}$  is observed at high densities (Figure 5c) where, in addition, a shoulder at about  $3260\text{ cm}^{-1}$  occurs. The assignment of this component is not straightforward.

With application of high pressure, high temperature techniques spectroscopic investigations at intermediate densities become possible. They demonstrate (Figure 5b) that the intensity of  $\nu_1$  becomes less pronounced with increasing density. The low wavenumber component at  $3260\text{ cm}^{-1}$  (Figure 5c) should thus be a  $2\nu_4$  overtone. More precisely it is the  $2\nu_4^E$  component as the intensity seems to be increased by Fermi resonance with the  $\nu_3$  mode. The large band half-width which is typical for an  $E$  type supports this assignment. A comparison with the Raman data in Figures 1–4 where two nearly totally polarized  $A_1$ -type species<sup>15</sup> occur under comparable conditions at about  $3315$  and  $3227\text{ cm}^{-1}$  yields further support for the assignment of the  $3260\text{-cm}^{-1}$  ir band to  $2\nu_4^E$ .<sup>23</sup> The results may be summarized as follows:  $\nu_3$  and  $2\nu_4^E$  are positioned at about  $3400$  and  $3260\text{ cm}^{-1}$ . The  $\nu_1$  and  $2\nu_4^A$  modes occur at about  $3315$  and  $3225\text{ cm}^{-1}$ . The wavenumbers hold for supercritical temperatures.

(B) The existence of Fermi resonance between  $\nu_1$  and  $2\nu_4^A$  was clearly demonstrated by De Bettignies and Wallart.<sup>14</sup> Nevertheless some controversy exists concerning the assignment of the higher wavenumber band at about  $3300\text{ cm}^{-1}$  to  $\nu_1$ <sup>11,18</sup> or to  $2\nu_4^A$ .<sup>13,17</sup>

Inspection of the Raman spectra at  $200^\circ\text{C}$  (Figure 1) raises little doubt about the  $3312\text{--}3333\text{-cm}^{-1}$  component to be identified as  $\nu_1$ , since it shifts toward the well-established  $\nu_1$

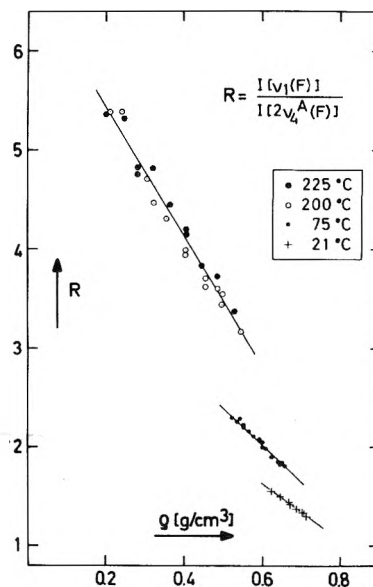


**Figure 6.** Density dependence of relative Raman scattering  $R = I[\nu_1(\text{F})]/I[2\nu_4^A(\text{F})]$  in the  $\nu_1(\text{F})$  and  $2\nu_4^A(\text{F})$  band maxima at 21, 75, 200, and  $225^\circ\text{C}$ .

gaseous frequency with decreasing density. The component at about  $3227\text{ cm}^{-1}$  seems to be exclusively due to  $2\nu_4^A$  as the position of maximum scattering remains almost constant with density variation. This behavior is well-known for bending modes. Closer inspection shows that a slight shift toward lower wavenumbers occurs with rising pressure (Figures 1–4). This red shift, however, is untypical for a bending component as can be seen from a comparison with the bending mode  $\nu_2$  in water or with the  $\nu_2$  bending fundamental of ammonia.<sup>24,25</sup> The observed shift of  $2\nu_4^A$  with density must thus be attributed to an enhanced  $\nu_1$  vibrational contribution to the  $3225\text{-cm}^{-1}$  component via Fermi resonance. For this reason the notations  $\nu_1(\text{F})$  and  $2\nu_4^A(\text{F})$  will be used in the subsequent text for the  $\nu_1\text{--}2\nu_4^A$  Fermi couple.  $\nu_1(\text{F})$  refers to the Raman band at about  $3315\text{ cm}^{-1}$  and  $2\nu_4^A(\text{F})$  to the scattering component in the  $3225\text{-cm}^{-1}$  region. Further evidence for Fermi resonance between  $\nu_1$  and  $2\nu_4^A$  is obtained from an investigation of the  $\nu_1(\text{F})$  and  $2\nu_4^A(\text{F})$  scattering intensities. The spectra in Figures 1–4 demonstrate an increasing contribution of  $2\nu_4^A(\text{F})$  compared to  $\nu_1(\text{F})$  Raman scattering with density. This may be seen more quantitatively from relative scattering intensities  $R$  calculated from the experimental spectra:

$$R = I[\nu_1(\text{F})]/I[2\nu_4^A(\text{F})]$$

$I[\nu_1(\text{F})]$  and  $I[2\nu_4^A(\text{F})]$  are the measured scattering intensities in the band maxima. Results for 225, 200, 75, and  $21^\circ\text{C}$  are shown in Figure 6. On increasing the density and lowering temperature the degree of Fermi resonance increases as is reflected in a decrease of  $R$ . The  $R$  values at  $21^\circ\text{C}$  are in excellent agreement with those calculated from published Raman spectra. Even at the lowest temperature of Figure 6 ( $21^\circ\text{C}$ ) the highest experimental densities are not sufficient to obtain the situation of ideal Fermi resonance ( $R = 1$ ). Extrapolation of the data in Figure 6, however, toward lower temperatures yields  $R = 1$  at about  $240\text{ K}$  in accordance with De Bettignies and Wallart.<sup>14</sup> The  $R$  values thus seem to be a reasonable measure of the degree of Fermi resonance coupling between  $\nu_1$  and  $2\nu_4^A$ . At 200 and  $225^\circ\text{C}$   $R$  is larger than 3 for all experimental densities. The stretching ( $\nu_1$ ) contribution to  $\nu_1(\text{F})$  as well as the bending ( $2\nu_4^A$ ) contribution to  $2\nu_4^A(\text{F})$

may thus be considered predominant in the experimental range under investigation.

An important conclusion may be drawn from Figure 6. As the band characteristics (frequency of band maximum and band half-width) of the  $\nu_1$  and  $2\nu_4^A$  modes in ammonia are temperature and density dependent, the observed Raman spectra seem to be one unique example for the degree of Fermi resonance to be varied continuously in a wide range by changing density and pressure. Most of the assignment problems in literature are thus not at all contradictory. They disappear when the different experimental conditions are taken into account.<sup>26</sup>

Another aspect of main interest in the  $\text{NH}_3$  Raman spectra centers around the density dependence of  $\nu_1(\text{F})$  Raman scattering. The  $\nu_1$  mode in infrared behaves rather peculiar on density variation as can be seen from Figure 5. The prominent  $\nu_1$  absorption disappears with increasing density. This has been explained by assuming that the height of the  $\text{NH}_3$  pyramid decreases with density.<sup>7,8</sup> In the limiting case of a planar molecule which, however, will not be obtained, the  $A_1$  type  $\nu_1$  mode would be infrared inactive. Though this is not the single explanation of the decrease of infrared intensity, we assume that a configurational change of this kind will be of primary importance. The phenomenon should have consequences for the explanation of other peculiarities of ammonia, too.

The assumption of a change in pyramidal height in dense  $\text{NH}_3$  is not unreasonable since, as is well-known, in gaseous  $\text{NH}_3$  the N atom may tunnel through the plane of the H atoms. With the  $\nu_2$ -bending mode zero-point energy taken into account the barrier to inversion amounts to about 4.5 kcal/mol.<sup>27,28</sup> Furthermore excited states of the ammonia molecule are definitely planar as was pointed out by Herzberg.<sup>29</sup> The decrease of pyramidal height with density may be understood as follows. The intermolecular interactions between the nitrogen lone pair electrons and hydrogen atoms of neighboring molecules give rise to some electron charge density transfer from the lone pair into the N-H bonds. The repulsion between the N-H bonds with electron densities enhanced at the expense of the lone pair then decreases the pyramidal height.

At very high densities a contradiction exists between this assumption, which indicates a minimum pyramidal height at maximum intermolecular interaction, and results from neutron scattering which definitely show that the molecule is clearly pyramidal.<sup>30</sup> The disagreement is ruled out by assuming that the density effect on the molecular configuration is reversed at high density. Thus ammonia should have a minimum pyramidal height at moderate high densities. The increase of pyramidal height at very high densities may be due to a better coordination of a more polar molecule: If the  $\text{NH}_3$  molecule has a facility of changing pyramidal height (and dipole moment!) the molecules will arrange on application of high pressure by attaining the most polar configuration which allows closest packing.

A variation of  $\text{NH}_3$  geometry with density should be reflected in the Raman spectra at supercritical conditions. A remarkable effect in the Raman data of Figure 3 is indeed the maximum value of  $I_m[\nu_1(\text{F})]$  at moderate high density. The decrease of  $I_m[\nu_1(\text{F})]$  at high densities is also clearly observed from the 75 °C data of Figure 4. The molar Raman scattering intensity is proportional to the square of the derivative of polarizability  $\alpha$  to vibrational normal coordinate  $Q$ . A variation of the polar character of  $\text{NH}_3$  associated with a change in pyramidal height will effect the scattering intensity  $I_m$ : Increasing polar character tends to decrease  $I_m$  since on charge separation the N-H bond electron density and thus  $d\alpha/dQ$

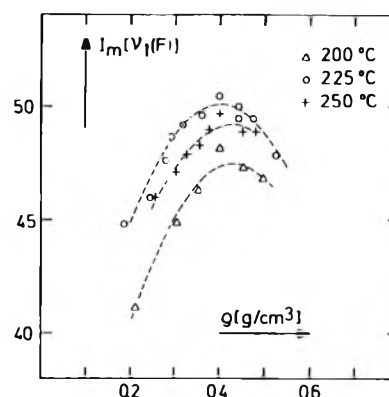


Figure 7. Density dependence of the molar Raman scattering  $I_m[\nu_1(\text{F})]$  in the  $\nu_1(\text{F})$  band maximum at 200, 225, and 250 °C.

for  $\nu_1$  diminish while decreasing polar character (and pyramidal height) enhances the N-H bond electron density and higher values of  $d\alpha/dQ$  cause the  $\nu_1(\text{F})$  scattering intensity to increase.

The results of Figure 3 are thus consistent with the assumption of decreasing pyramidal height starting from the gaseous state. The pyramidal height reaches a minimum at moderately high densities of about 0.4 g/cm<sup>3</sup> and increases again at very high density.

A maximum value of  $I_m[\nu_1(\text{F})]$  is also observed for isotherms at 225 and 250 °C (Figure 7). Each of the four isotherms in Figure 7 (two runs at 225 °C are reported) is measured within one experimental run. The internal accuracy of  $I_m[\nu_1(\text{F})]$  values at constant temperature is better than 2%, though the absolute value of  $I_m[\nu_1(\text{F})]$  may be less accurate. The isotherms are separately least-squares fitted to parabolas. The density at the maximum of  $I_m[\nu_1(\text{F})]$  is  $0.41 \pm 0.04$  g/cm<sup>3</sup>. We may conclude the following: The Raman data in the temperature region from 200 to 250 °C support the assumption of varying pyramidal height in  $\text{NH}_3$  with a minimum at about 0.4 g/cm<sup>3</sup>. It must be pointed out that the above argument contains some shortcomings as conclusions are drawn from scattering intensities in the band maximum and not from integrated band intensities. Furthermore, the  $\nu_1(\text{F})$  band under investigation is in Fermi resonance with  $2\nu_4^A(\text{F})$  which effects the component intensities. Since, however, no obvious reason explains a maximum in  $I_m[\nu_1(\text{F})]$  scattering at intermediate density via Fermi resonance, the statement of varying pyramidal height with a minimum value at about 0.4 g/cm<sup>3</sup> is considered to be reasonable. The result is supported further by previous  $\nu_2$  Raman scattering experiments which also indicate extreme scattering about 0.4 g/cm<sup>3</sup>. For  $\nu_2$  a minimum value of  $I_m[\nu_2]$  occurs as this mode would be Raman forbidden in the limiting case of a planar molecule.

A definite answer may be obtained from determinations of the static dielectric constant of ammonia measured recently between -70 and 220 °C to a maximum pressure of 2 kbar.<sup>31</sup> A first quantitative discussion of these new data shows a minimum dipole moment at densities around 0.4 g/cm<sup>3</sup>.

*Acknowledgment.* The authors wish to thank Professor Dr. E. U. Franck for valuable discussions and comments on the manuscript. Financial support by the "Fonds der Chemischen Industrie" is gratefully acknowledged.

## References and Notes

- (1) G. E. Walrafen, "Water—A Comprehensive Treatise", Vol. 1, F. Franks, Ed., Plenum Press, New York, N.Y., 1972

- (2) D. Eisenberg and W. Kauzmann, "The Structure and Properties of Water", Clarendon Press, Oxford, 1969.
- (3) M. Buback and E. U. Franck, *Ber. Bunsenges. Phys. Chem.*, **75**, 33 (1971).
- (4) J. Corset and J. Lascombe, *J. Chim. Phys.*, **64**, 665 (1967); J. Corset, Thesis, Bordeaux, 1967.
- (5) H. Lindner, Thesis, Karlsruhe, 1969.
- (6) E. U. Franck and K. Roth, *Discuss. Faraday Soc.*, **43**, 108 (1967).
- (7) M. Buback, *Ber. Bunsenges. Phys. Chem.*, **78**, 1230 (1974).
- (8) M. Buback and E. U. Franck, *J. Chim. Phys.*, **72**, 601 (1975).
- (9) J. Jortner and N. R. Kestner, Ed., "Electrons in Fluids", Springer-Verlag, Berlin, 1973.
- (10) S. Kinumaki and K. Aida, *Sci. Rep. Res. Inst. Tokoku Univ., Ser. A*, **6**, 186 (1954).
- (11) C. A. Plint, R. M. B. Small, and H. L. Welsh, *Can. J. Phys.*, **3**, 3653 (1954).
- (12) G. Seillier, M. Ceccaldi, and J. P. Leicknam, *Method. Phys. Anal.*, **4**, 388 (1968).
- (13) T. Birchall and J. Drummond, *J. Chem. Soc. A*, 1859 (1970).
- (14) B. De Bettignies and F. Wallart, *C. R. Acad. Sci.*, **271**, 640 (1970).
- (15) B. L. Smith and W. H. Koehler in ref 9.
- (16) M. G. de Backer, P. F. Rusch, B. De Bettignies, and G. Lepoutre, in ref 9.
- (17) M. Schwartz and C. H. Wang, *J. Chem. Phys.*, **59**, 5258 (1973).
- (18) A. T. Lemley, J. H. Roberts, K. R. Plowman, and J. J. Lagowski, *J. Phys. Chem.*, **77**, 2185 (1973).
- (19) K. R. Schulz, Thesis, Karlsruhe, 1974.
- (20) P. Davies, "Ammonia", in "Thermodynamic Functions of Gases", Vol. 1, F. Din, Ed., Butterworths, London, 1962.
- (21) I. V. Demidenkova and L. D. Sherba, *Izv. Akad. Nauk. SSSR, Ser. Fiz.*, **22**, 1122 (1958).
- (22) P. F. Rusch and J. J. Lagowski in ref 9.
- (23) Depolarized spectra would yield additional strong evidence. Unfortunately, due to the birefringence of sapphire, depolarization ratios can be determined only with poor precision under high pressure.
- (24) P. Datta and M. Barrow, *J. Am. Chem. Soc.*, **87**, 3053 (1965).
- (25) M. Buback and K. R. Schulz, to be submitted for publication.
- (26) This conclusion is fully consistent with very recent results derived by J. W. Lundeen and W. H. Koehler, (*J. Phys. Chem.*, **79**, 2957 (1975)) from Raman spectra measured at temperatures below 25 °C.
- (27) J. D. Swalen and J. A. Ibers, *J. Chem. Phys.*, **36**, 1914 (1962).
- (28) R. Ahlrichs, F. Driessler, H. Lischka, V. Staemmler, and W. Kutzelnigg, *J. Chem. Phys.*, **62**, 235 (1975).
- (29) G. Herzberg, "Molecular Spectra and Molecular Structure, III. Electronic Spectra and Electronic Structure of Polyatomic Molecules", Van Nostrand, Princeton, N.J., 1936.
- (30) J. W. Reed and P. M. Harris, *J. Chem. Phys.*, **35**, 1730 (1961).
- (31) M. Buback and W. D. Harder, to be submitted for publication.

## Ultraviolet Absorption Spectra of $e_{aq}^-$ , H, OH, D, and OD from Pulse Radiolysis of Aqueous Solutions<sup>1a</sup>

S. O. Nielsen,\*<sup>1b</sup>

Danish Atomic Energy Commission Research Establishment, Risø, 4000 Roskilde, Denmark

B. D. Michael,<sup>2</sup> and E. J. Hart

Chemistry Division, Argonne National Laboratory, Argonne, Illinois 60439 (Received October 28, 1975; Revised Manuscript Received April 16, 1976)

Publication costs assisted by Argonne National Laboratory, Danish Research Council, and Symplexor, Inc.

Previous pulse radiolytic measurements of the ultraviolet absorption spectra of aqueous solutions of H, OH, and  $e_{aq}^-$  at ambient temperatures have been extended down to 188 nm using two coupled grating monochromators, a solar-blind photomultiplier, and purging of the optical system with nitrogen. The measured spectra are in good agreement with the corresponding spectra measured earlier (down to 200 nm) using different experimental facilities. The onsets of new absorption bands for H, OH, and  $e_{aq}^-$  that were observed in the wavelength region immediately above 200 nm are continued in the region down to 188 nm. No absorption maxima are seen:  $\epsilon_H^{188} 1620 \text{ M}^{-1} \text{ cm}^{-1}$ ,  $\epsilon_{OH}^{188} 540 \text{ M}^{-1} \text{ cm}^{-1}$ , and  $\epsilon_{e_{aq}^-}^{188} 3000 \text{ M}^{-1} \text{ cm}^{-1}$ . We have also measured the ultraviolet absorption spectra of D and OD in aqueous solution down to 200 nm. Whereas the spectrum of OD in liquid D<sub>2</sub>O is identical with that of OH in liquid H<sub>2</sub>O within experimental error, there is a large blue isotope shift of the slope of the onset band for D in D<sub>2</sub>O when compared with H in H<sub>2</sub>O, which at 210 nm amounts to 9 nm (2000  $\text{cm}^{-1}$ ). The nature of the optical transitions involved in the ultraviolet absorption bands of H, OH, and  $e_{aq}^-$  in aqueous solution is discussed in the light of some proposals in the literature, and it is concluded that the bands are best interpreted in terms of a red shift of the first absorption band for water, normally found in the 180-nm region, for those water molecules adjacent to the solutes.

### Introduction

Ultraviolet absorption spectra down to 200 nm for the H and OH radicals<sup>3</sup> and for the hydrated electron<sup>4</sup> have been measured by pulse radiolysis of aqueous solutions at ambient temperatures. These spectra indicate that all three solutes have additional absorption bands with maxima below 200 nm. Confirming these ultraviolet spectra for H and OH in water are reports that they are in good agreement with flash photolysis experiments on H<sub>2</sub>O liquid<sup>5</sup> and ice.<sup>6</sup> In a search for the

maxima of the absorption bands of H, OH, and  $e_{aq}^-$  in H<sub>2</sub>O below 200 nm, we report here on the extension of the spectra for the three species down to 188 nm using an improved pulse radiolysis technique.

The absorption bands with indicated maxima below 200 nm for H, OH, and  $e_{aq}^-$  were originally interpreted<sup>3,4</sup> as originating from a red shift of the first absorption band for water, normally found in the 180-nm region, for those water molecules adjacent to the solutes. Recently several other proposals

have been published for these optical transitions.<sup>7-10</sup> In order to help decide among these proposals, we report here also on measurements of the ultraviolet spectra of D and OD dissolved in  $D_2O$ .

### Experimental Section

*Spectra of H, OH, and  $e_{aq}^-$ . Pulse Radiolysis Apparatus.* At wavelengths below 250 nm, kinetic spectrophotometry is difficult because in this region the intensities of the available analyzing light sources are low, and optical transmission losses are high. These adverse conditions lead to a high photodetector shot noise level, poor spectral purity due to scattering of the abundant longer-wavelength light through the monochromator, and interference from the intense Čerenkov light emitted in the uv region. To overcome these problems in the present work, an optical system was set up that provided optimum performance in the uv (Figure 1).

The light source used was an XBO 450 W/4 xenon arc lamp (Osram G.m.b.H., Germany) with a Suprasil envelope. The arc was intensified approximately 30-fold using a transistorized pulser designed to produce a flat-topped light pulse. By means of a Suprasil lens, the arc was imaged through the absorption cell onto the entrance slit of a pair of Bausch and Lomb high-intensity grating monochromators connected in series. One of the monochromator slits was removed and a coupling was introduced so that the monochromators fitted together with a single slit intermediate between them. This dual configuration is single dispersing, i.e., the dispersions of the two instruments are opposed, and the combined dispersive power is therefore equal to that of a single instrument.<sup>11</sup> Gratings were used with 2700 grooves/mm blazed for maximum efficiency at 250 nm. The entrance, intermediate, and exit slit widths were set to 3, 1.5, and 3 mm, respectively, giving a half-maximum intensity bandwidth of 4.8 nm. Stops were placed at the lenses and slits in order to constrict each aperture to no larger than its useful area, so minimizing the proportion of scattered light transmitted outside the selected wavelength band. The monochromators and a section of the light path between the light source and absorption cell were purged with nitrogen to improve transmission below 200 nm. The light emerging from the monochromator exit slit was reflected off a freshly aluminized mirror onto the photocathode of a solar-blind photomultiplier (R166, H.T.V. Co., Japan). This detector was relatively insensitive at wavelengths longer than 300 nm. Even at the shortest wavelengths studied, the effective proportion of scattered light was considerably less than 1%, and this low level was attributable to the solar-blind photomultiplier, the dual monochromators and the high uv transmission of the system. The system was capable of measuring transient absorptions down to 182 nm; however, with aqueous solutions, the onset of the water absorption bands prevented observation below 188 nm. The photomultiplier circuit response time constant was set between 80 and 300 ns according to the experimental conditions.

0.5- and 1.0- $\mu$ s electron pulses from the A.N.L. linac (Applied Radiation Co.) were used at the reduced energy of 7 MeV. This energy gave adequate penetration of the absorption cell, but produced less bremsstrahlung than the full 15-MeV energy. A lead shield further reduced the x-ray interference at the photomultiplier to an acceptable level. Pulse-to-pulse dose variations were monitored by a charge collection method. The doses delivered per pulse were approximately 3 and 7 krad. The dose per pulse was measured from the 600-nm absorption of  $e_{aq}^-$  in alkaline solution<sup>12</sup> using an RCA IP28 photomultiplier.

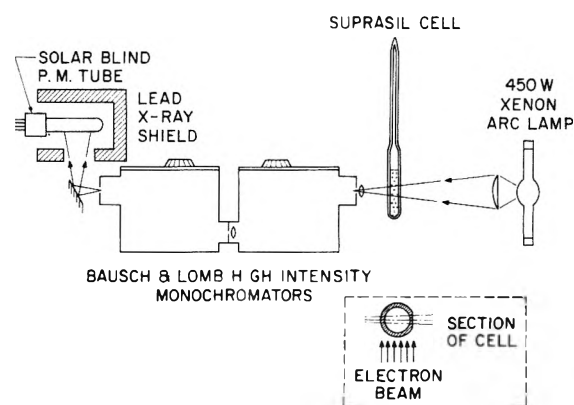


Figure 1. Optical system for pulse radiolysis in uv, showing dual monochromator arrangement and high pressure irradiation cell.

*Spectra of H, OH, and  $e_{aq}^-$ . Preparation of Solutions.* Solutions irradiated at atmospheric pressure were contained in a cylindrical cell of conventional design with Suprasil end windows and a path length of 1 cm. This cell was filled using the syringe technique.<sup>13</sup> For irradiation under high pressure, solutions were irradiated in a Suprasil tube of about 9 mm i.d. and 15 mm o.d., which was sealed at one end and joined to a smaller diameter filling tube at the other. The analyzing light beam passed at right angles to the axis of the Suprasil tube (see Figure 1). A flat face was ground and polished along one side of the Suprasil tube to reduce its refractive power. To fill the cell, the filling tube was first sealed onto a vacuum line, and the cell was evacuated and filled with argon. Degassed solutions were introduced into the cell with a syringe fitted with a fine capillary, which was inserted through an opening in the vacuum line. The vacuum line was then sealed off, and the solution evacuated to remove any traces of oxygen. The cell was immersed first in liquid nitrogen and then in liquid helium, and a measured volume of hydrogen was introduced through a palladium valve. The hydrogen condensed on top of the frozen solution. The filling tube was then sealed off, and the cell was removed from the vacuum line and plunged immediately into water at room temperature. In this way solutions were equilibrated with hydrogen at 30 atm pressure.

Solutions were prepared using water triply distilled in a silica system. The pH was adjusted using analytical grade  $HClO_4$  or  $NaOH$ .  $N_2O$  was purified by freezing to liquid nitrogen temperature and pumping off residual oxygen.

*Spectra of D and OD.* The Risø linac (Varian) was used. The pulse radiolysis apparatus and the methods used have already been described.<sup>3,14</sup> The optical bandwidth at 200 nm (the lowest wavelength obtainable) was 0.95 nm. The irradiation cell (length 2.55 cm, optical pathlength 5.1 cm) received a dose of ca.  $3 \times 10^{20}$  eV/l (5 krad) with each 1.0- $\mu$ s single pulse of 10–11-MeV electrons. Solutions of  $10^{-3}$  M  $DClO_4$  were made by diluting  $HClO_4$  (60% Merck analytical grade) with  $D_2O$  (analytical grade) and deaerating by bubbling argon through it. Solutions of  $3 \times 10^{-5}$  M  $DClO_4 + 2 \times 10^{-3}$  M  $N_2O$  in  $D_2O$  were made by dilution of the  $10^{-3}$  M  $DClO_4$  solution and a solution of  $D_2O$  saturated with purified  $N_2O$ . The temperature of the solutions was approximately 25 °C.

### Results

*Spectra of H, OH, and  $e_{aq}^-$ . Measurement of Transient Absorption Spectra.* Solutions A and B (Table I) were designed to yield H and  $e_{aq}^-$ , respectively; these solutions were irradiated in the sealed cells under approximately 30 atm

**TABLE I: Solutions and Irradiation Conditions Used to Obtain Corresponding Spectra, A, B, and C, at Time Delays  $t$  after the Pulse**

Solution	[NaOH], M	[HClO <sub>4</sub> ], M	[H <sub>2</sub> ], M	[N <sub>2</sub> O], M	[H <sub>2</sub> O <sub>2</sub> ], M	Pulse dose, krads	Pulse length, $\mu$ s	$t$ spectrum, $\mu$ s	Soln temp, $^{\circ}$ C	Soln path length, cm
A	0	$3.39 \times 10^{-4}$	$2.82 \times 10^{-2}$	0	$4.5 \times 10^{-5}$	3.3	1.0	1.0	34	0.95
B	$4.83 \times 10^{-5}$	0	$2.60 \times 10^{-2}$	0	$9.0 \times 10^{-6}$	2.9	1.0	1.0	34	0.97
C	$5.25 \times 10^{-5}$	0	0	$5.0 \times 10^{-4}$	0	6.6	0.5	0.8	29	1.00

pressure of hydrogen. Initially, the solutions were pulsed until a steady-state level of H<sub>2</sub>O<sub>2</sub> was produced, and these concentrations are shown in Table I. The value of [H<sub>2</sub>O<sub>2</sub>] shown for solution A was calculated using a water reaction kinetics computer program, WR20.<sup>15</sup> The computed steady-state [H<sub>2</sub>O<sub>2</sub>] in solution A was found to agree reasonably well with the H<sub>2</sub>O<sub>2</sub> concentration measured using the I<sub>3</sub><sup>-</sup> method.<sup>16</sup> In the alkaline solution B, the computed steady-state [H<sub>2</sub>O<sub>2</sub>] was approximately one-half of the measured value. This disagreement is in accord with an unexplained shortening of the chain length in the decomposition of H<sub>2</sub>O<sub>2</sub> by e<sub>aq</sub><sup>-</sup> in alkaline solution found in earlier work.<sup>17</sup> The value of [H<sub>2</sub>O<sub>2</sub>] shown in Table I for solution B was obtained by matching the computed decay of e<sub>aq</sub><sup>-</sup> with its decay observed at 600 nm. Solution C was designed to yield OH and was irradiated in the cell of conventional construction. This cell was emptied and refilled before each pulse.

Solutions A, B, and C were irradiated under the conditions shown in Table I, and the spectra recorded at the times indicated after the pulse. The pathlength of irradiated Suprasil traversed by the light beam was appreciable in the cases of solutions A and B. A similar piece of Suprasil was irradiated, and the resulting transient absorption spectrum is shown in Figure 2. This spectrum, scaled in proportion to dose and Suprasil path length, was then subtracted from the spectra obtained from solutions A and B to give the corrected absorption spectra, A and B, shown in Figure 3; also shown is spectrum C, which needed no correction because of the much shorter Suprasil pathlength. These spectra have also been corrected, where necessary, for the small contribution of Čerenkov emission; this correction was determined by recording the Čerenkov transient separately with the analyzing light shutter closed.

*Computation of Concentrations of Absorbing Species in Solutions of H, OH, and e<sub>aq</sub><sup>-</sup>.* To reduce the absorption spectra of H, e<sub>aq</sub><sup>-</sup>, and OH from spectra A, B, and C, it was necessary to determine the instantaneous concentrations of each of these species; also required were the instantaneous changes of concentration, relative to their values just before the pulse, of the absorbing solutes OH<sup>-</sup>, N<sub>2</sub>O, and H<sub>2</sub>O<sub>2</sub>. The reactions in each solution were simulated using the WR20 computer program.<sup>15</sup> Twenty-eight reactions of 12 stable and transient species were simulated using rate constants generally in agreement with values published by Hart and Anbar.<sup>18</sup> An important exception was the rate constant  $2k_{H+H}$ , where the value at 24  $^{\circ}$ C of  $1.55 \times 10^{10} \text{ M}^{-1} \text{ s}^{-1}$  was used.<sup>3</sup> Rates were adjusted to the irradiation temperatures shown in Table I using known or assumed activation energies, some of which have been reviewed.<sup>19</sup> The following yields were used:  $G(e_{aq}^-) = 2.80$ ,  $G(H^+) = 2.90$ ,  $G(OH^-) = 0.10$ ,  $G(OH) = 2.70$ ,  $G(H) = 0.48$ ,  $G(H_2) = 0.45$ ,  $G(H_2O_2) = 0.70$ ,  $G(HO_2) = 0.02$ . The electron pulse dose rate profile was determined by recording the Čerenkov emission pulse. The total dose per pulse was obtained by matching the computed e<sub>aq</sub><sup>-</sup> transient with that

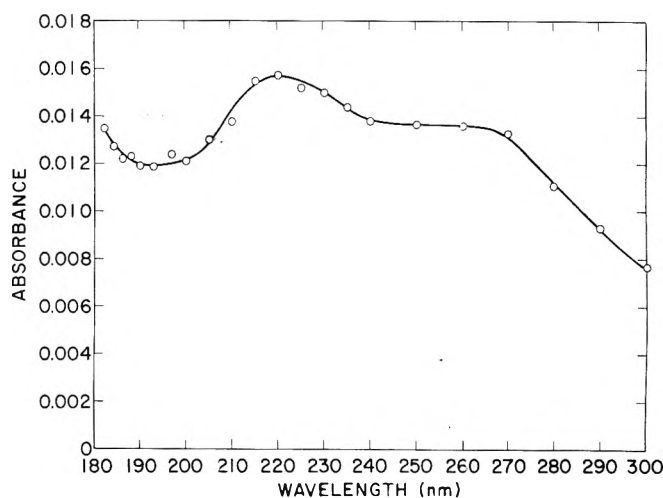


**Figure 2.** Transient absorption spectrum in irradiated Suprasil sample 1 cm thick. Measured immediately after 3- $\mu$ s electron pulse. Dose per pulse 24 krads, measured in water-equivalent dcsmeter.

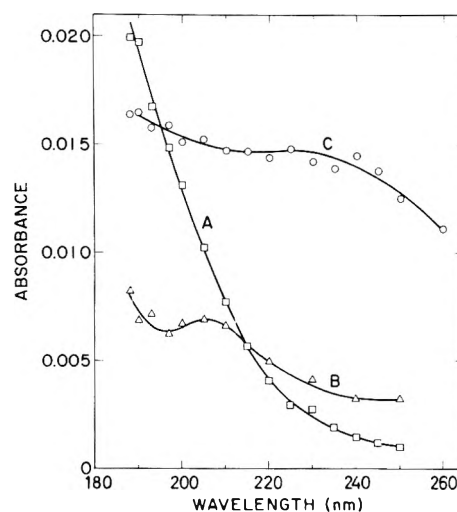


**Figure 3.** Transient absorption spectra obtained in solutions A, B, and C (see Table I).

observed at 600 nm using an alkaline solution. Concentrations of each of the absorbing species were computed for each solution at the times of the spectra shown in Table I. The concentrations of O<sub>2</sub><sup>-</sup>, HO<sub>2</sub>, and O<sub>2</sub> were calculated to be 10<sup>2</sup>-10<sup>3</sup> times lower than those of the major absorbing species, and their absorptions were, therefore, assumed to be insignificant.

*Determination of Absorption Spectra of e<sub>aq</sub><sup>-</sup>, H, and OH.* At each wavelength, the absorption spectra A, B, and C, shown in Figure 3, were adjusted to give spectra a, b, and c, respectively, by subtracting the contributions due to the absorbances

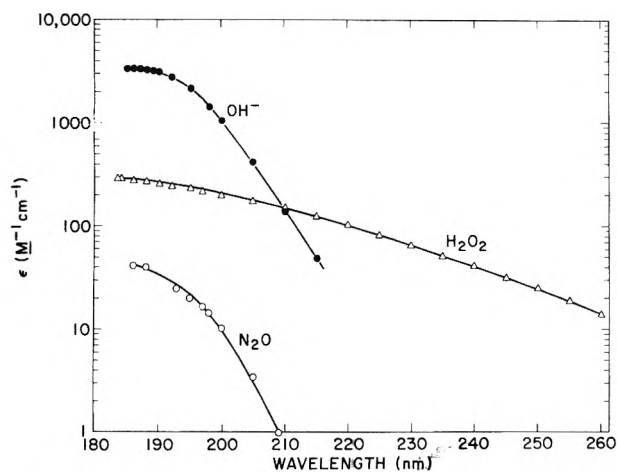


Figure 4. Measured absorption spectra of  $\text{OH}^-$ ,  $\text{H}_2\text{O}_2$ , and  $\text{N}_2\text{O}$  (see text).

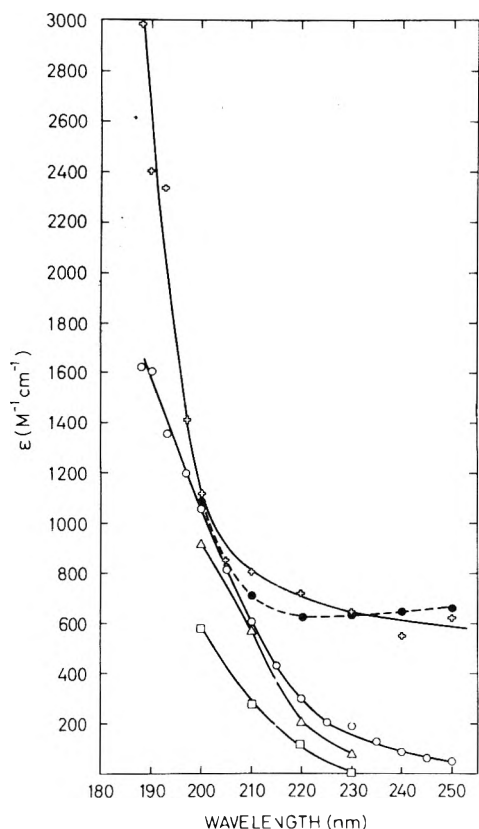


Figure 5. Absorption spectra of H, D, and  $e_{aq}^-$ : (O) H, this work, 34 °C; ( $\Delta$ ) H, ref 3, 23–25 °C; ( $\square$ ) D, this work, 25 °C; ( $\circ$ )  $e_{aq}^-$ , this work, 34 °C; ( $\bullet$ )  $e_{aq}^-$ , ref 4, 25 °C.

of  $\text{OH}^-$ ,  $\text{N}_2\text{O}$ , and  $\text{H}_2\text{O}_2$  using their computed concentration changes. The absorption spectra of these solutes were determined separately (Figure 4) using a Cary 14 spectrophotometer. All solutions were prepared in triple-distilled deaerated water. NaOH was added to produce  $[\text{OH}^-] = 403 \mu\text{M}$  as determined by pH measurement. Down to 200 nm  $\epsilon_{\text{OH}^-}$  agreed with published values,<sup>20</sup> but decreased to 10% lower values at 185 nm. At 190 nm our measurement of  $\epsilon_{\text{OH}^-}$  is about 15% higher than a previous determination.<sup>21</sup> The  $\text{H}_2\text{O}_2$  solution was prepared from 90% stabilizer-free  $\text{H}_2\text{O}_2$  (originally 98% from Becco Chemical Division, F.M.C., Buffalo, N.Y.) diluted unbuffered to 5.35 mM. This concentration was measured by

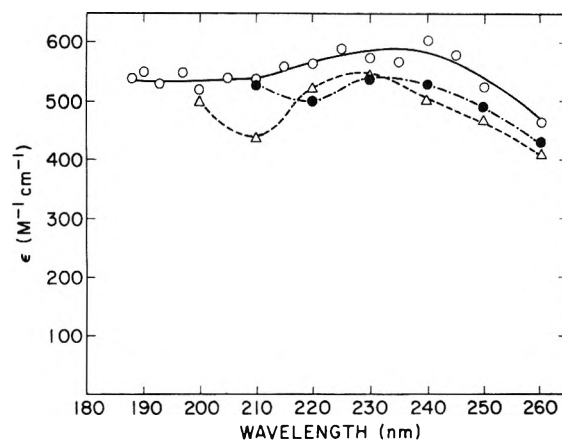


Figure 6. Absorption spectra of OH and OD: (O) OH, this work, 29 °C; ( $\Delta$ ) OH, ref 3, 23–25 °C; ( $\bullet$ ) OD, this work, 25 °C.

the  $\text{I}_3^-$  method.<sup>16</sup> The  $\text{H}_2\text{O}_2$  absorptivity was found to be about 20% higher than values previously reported between 200 and 270 nm,<sup>22</sup> but was in good agreement with values determined at 185 and 254 nm<sup>21</sup> and with published values between 210 and 260 nm.<sup>20</sup> The  $\text{N}_2\text{O}$  spectrum was measured from a saturated solution.

The most significant correction was that applied for  $\text{OH}^-$  in solution B. Here, at 1  $\mu\text{s}$  after the electron pulse, the depletion of  $\text{OH}^-$  was almost equal to the concentration of  $e_{aq}^-$ . The pulse-induced bleaching of the  $\text{OH}^-$  absorption has, therefore, considerably decreased the absorbance of spectrum B below 205 nm.

The residual absorption spectra a, b, and c with absorbances  $a$ ,  $b$ , and  $c$ , respectively, were each assumed to be composed of the unknown absorbances assigned to H,  $e_{aq}^-$ , and OH. Thus at each wavelength for solution A

$$a/l = [e_{aq}^-]\epsilon_{e_{aq}^-} + [\text{H}]\epsilon_{\text{H}} + [\text{OH}]\epsilon_{\text{OH}} \quad (1)$$

and similarly for solutions B and C.  $l$  is the optical pathlength. Values for the extinction coefficients  $\epsilon_{e_{aq}^-}$ ,  $\epsilon_{\text{H}}$ , and  $\epsilon_{\text{OH}}$  were solved by elimination from three equations at each wavelength giving the absorption spectra shown in Figures 5 and 6.

**Spectra of D and OD.** The optical absorption transients recorded with  $\text{D}_2\text{O}$  solutions of  $10^{-3}$  M  $\text{DClO}_4$  and of  $3 \times 10^{-5}$  M  $\text{DClO}_4 + 2 \times 10^{-3}$  M  $\text{N}_2\text{O}$  were extrapolated back to time zero at the end of the electron pulse (neglecting measured absorbances during the first 0.5  $\mu\text{s}$  after the pulse) giving "initial absorbances". From the monitored dose per pulse the corresponding concentrations of D, OD, and  $\text{D}_2\text{O}_2$  at time zero were calculated using values for the yields of  $G(\text{D}) = 0.44$ ,  $G(e_{aq}^-) = 2.90$ ,  $G(\text{OD}) = 2.90$ ,  $G(\text{D}_2\text{O}_2) = 0.62$ ,<sup>23</sup> and a small correction for radical recombination during the pulse.  $e_{aq}^-$  and  $\text{OD}^-$  did not contribute significantly to the extrapolated initial absorbances, having been transformed into D and  $\text{D}_2\text{O}$ , respectively. Corrections for the radiation-induced absorbance in the Suprasil windows and for the disappearance of  $\text{N}_2\text{O}$  were found to be negligible down to 200 nm. The Čerenkov emission did not affect the transients, which were measured using a fast clamping circuit.<sup>14</sup> The absorption spectra of D and OD, given as molar decadic absorptivity vs. wavelength, were calculated from equations analogous to eq 1 assuming  $\epsilon_{\text{D}_2\text{O}_2} = \epsilon_{\text{H}_2\text{O}_2}$ . The spectra are given in Figures 5 and 6.

## Discussion

In order to penetrate well into the spectral region below 200 nm it was necessary to take several precautions. A solar-blind

photomultiplier, a dual grating monochromator, and purging of the optical system with nitrogen were used to reduce the effective proportion of scattered light to considerably less than 1% even at 188 nm. The overall signal-to-noise ratio was improved by using a pulsed xenon arc lamp as a monitoring light source<sup>3</sup> and by increasing the spectral bandwidth at half-maximum intensity to 4.8 nm. Furthermore, to minimize the effect of the optical absorption edge of liquid H<sub>2</sub>O in the 180-nm region, optical pathlengths of only 9.5 and 10 mm were used.

For the measurements on D<sub>2</sub>O solutions in the region above 200 nm more conventional techniques were used.<sup>3</sup>

*H and e<sub>aq</sub><sup>-</sup>.* Figure 5 shows clearly that the hydrated electron, e<sub>aq</sub><sup>-</sup>, has a distinct optical absorption band with maximum below 188 nm, the long wavelength wing of which extends to at least 200 nm. Likewise, Figure 5 shows that H atoms dissolved in liquid H<sub>2</sub>O have a similar distinct absorption band with maximum below 188 nm and a long-wavelength slope that extends to at least 240 nm. At 188 nm the decadic molar absorptivity of e<sub>aq</sub><sup>-</sup> is  $\epsilon_{e_{aq}^{-188}}$  3000 M<sup>-1</sup> cm<sup>-1</sup>,<sup>24</sup> which is approximately 1.9 times that of  $\epsilon_H^{188}$  1620 M<sup>-1</sup> cm<sup>-1</sup>. If  $\epsilon_{e_{aq}^{-188}}$  is corrected for the contribution from the ultraviolet wing of the absorption band of e<sub>aq</sub><sup>-</sup> with a maximum around 700 nm obtained by extrapolation,  $\epsilon_{e_{aq}^{-188}}$  is lowered from 3000 to 2500 M<sup>-1</sup> cm<sup>-1</sup> compared with  $\epsilon_H^{188}$  of 1620 M<sup>-1</sup> cm<sup>-1</sup>, i.e., a ratio of only 2500/1620 = 1.55. The similarity as regards the apparent intensity and position of the two absorption bands for the structurally very different species, e<sub>aq</sub><sup>-</sup> and H, suggests a common origin of the observed optical transitions that is rooted in the aqueous solvent. We have assumed that the ultraviolet absorption spectrum of e<sub>aq</sub><sup>-</sup> is a superposition of two absorption bands, one that has a maximum below 188 nm and one very broad that has a maximum around 700 nm, which is due to the commonly accepted transition of e<sub>aq</sub><sup>-</sup> in the visible region.

Figure 5 also shows that the absorption spectra of H and e<sub>aq</sub><sup>-</sup>, as determined in the present investigation, are in fair agreement with the ultraviolet spectra for these same species determined earlier<sup>3,4</sup> using different experimental facilities. In the case of H it was possible at 200 nm and above to check the assignment of the spectrum, shown in Figure 5, to H by extensive kinetic and chemical tests.<sup>3</sup> In support of the assignment of the spectrum, shown in Figure 5, to e<sub>aq</sub><sup>-</sup> it was, furthermore, shown that the reaction e<sub>aq</sub><sup>-</sup> + H<sub>3</sub>O<sup>+</sup> → H + H<sub>2</sub>O, when monitored at 200 nm in dilute HClO<sub>4</sub>, is accompanied by only a relatively small change in absorbance.<sup>4</sup>

*OH and OD.* Figure 6 shows that OH has a broad absorption band with maximum around 230 nm, the long-wavelength slope of which extends beyond 320 nm.<sup>5</sup> Figure 6 also shows that OH is likely to have an additional very broad absorption band with almost constant absorptivity in the region 188–200 nm. The minimum in absorptivity at 210 nm, reported earlier,<sup>3</sup> is not observed in the present investigation. This discrepancy has not been resolved, but can be explained in part by the larger spectral bandwidth (4.8 nm) used in the present investigation compared with the smaller one (0.95 nm) used earlier.<sup>3</sup>

The 230-nm band observed with OH dissolved in liquid H<sub>2</sub>O is not found with OH in the gas phase, which only has absorption bands around 307 nm<sup>25</sup> that are shifted but slightly on dissolution of OH in a solid rare gas matrix.<sup>26</sup> In crystalline H<sub>2</sub>O ice-I two forms of OH are found. One that has an absorption spectrum in the region above 200 nm very much like OH dissolved in liquid H<sub>2</sub>O is believed to be OH in substitutional position<sup>6</sup> (hydrogen bonded), and the other that has an

absorption spectrum with maximum at 280 nm<sup>27</sup> is believed to be OH in interstitial positions. The observed large blue shift of the absorption spectrum of OH from 307 nm in the gas phase to 230 nm in H<sub>2</sub>O liquid solution (10 900 cm<sup>-1</sup>) may be compared with the blue shift of the uv spectrum of H<sub>2</sub>O on going from the vapor to ice-I, which amounts to approximately 10 000 cm<sup>-1</sup>.<sup>6</sup> The absorption in the optical spectrum of OH in the gas phase at 307 nm is caused by vibrational (0,0) transitions from the <sup>2</sup>Π ground state to the <sup>2</sup>Σ<sup>+</sup> excited state of OH.<sup>28</sup> Thus strong hydrogen bonding to the ground state of OH is capable of producing large blue shifts in the absorption spectrum of OH.<sup>29</sup> We conclude, therefore, that the optical transition behind the 230-nm absorption maximum for OH in H<sub>2</sub>O liquid solution is essentially a <sup>2</sup>Π → <sup>2</sup>Σ<sup>+</sup> transition in OH that is perturbed by various situations of hydrogen bonding to solvent H<sub>2</sub>O. The small isotope effect on the 230-nm band for OH in H<sub>2</sub>O on going to OD in D<sub>2</sub>O, shown in Figure 6, is in agreement with this interpretation. The spectra shown for OH and OD are identical within experimental error.

Although we are uncertain as to the nature of the almost constant absorptivity observed for OH in liquid H<sub>2</sub>O solution below 200 nm, we tentatively suggest that a new absorption band for OH is being observed in this region, which is similar to those of e<sub>aq</sub><sup>-</sup> and H in aqueous solution.

*D.* Whereas the 230-nm band of OH in H<sub>2</sub>O shows only a small isotope effect on going to OD in D<sub>2</sub>O, Figure 5 shows that the spectrum of D in D<sub>2</sub>O is shifted by ca. 9 nm (2000 cm<sup>-1</sup>) toward the blue relative to the spectrum of H in H<sub>2</sub>O. For comparison, the uv absorption edge of liquid D<sub>2</sub>O at 25 °C shows a large blue shift<sup>30</sup> (10 000 cm<sup>-1</sup>) relative to that of liquid H<sub>2</sub>O at 25 °C.

*Why do e<sub>aq</sub><sup>-</sup> and H have large absorptivities below 200 nm?*

Let us first turn to analogous systems for which quantitative interpretations have been made. In the case of electrons trapped in F centers in alkali crystals, so-called β bands are observed on or near the long-wavelength slope of the optical absorption edge of the crystal matrix. The β bands have been interpreted<sup>31</sup> as originating largely from excitation of the halide ions surrounding the F-center cavity. The excitation is, however, slightly perturbed by a partial negative charge transfer from the excited halide ions to the F-center cavity, which has an effective positive charge. The interaction that is believed to be responsible for the β bands is thus one in the excited state and not in the ground state.

In the case of interstitial H atoms in KI crystals, so-called U<sub>2</sub> bands are observed, which are analogous to the β bands in that they are observed on or near the long-wavelength slope of the optical absorption edge of the KI matrix, and in that they can be quantitatively interpreted as originating largely from excitation of the iodide ions surrounding the interstitial H atom, but perturbed by a partial negative charge transfer from I<sup>-</sup> to H.<sup>32</sup>

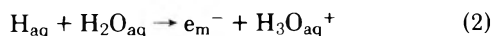
We believe that the spectrum of H and the main feature of the uv spectrum of e<sub>aq</sub><sup>-</sup> that we have measured can be interpreted along similar lines,<sup>3,4</sup> i.e., as a red shift of the first absorption band for water, normally found in the 180-nm region, for those water molecules adjacent to the solutes H and e<sub>aq</sub><sup>-</sup>. The relatively small red shift is caused by an interaction with the first excited state of the water molecule by way of a partial negative charge transfer to the solutes H or e<sub>aq</sub><sup>-</sup>. H has an electron affinity of 0.77 eV,<sup>33</sup> and the calculated charge distribution for e<sub>aq</sub><sup>-</sup> leaves it with a positively charged core<sup>34</sup> as in the case of the F centers. For H atoms dissolved in liquid water there is no compelling evidence for H<sub>3</sub>O formation and

persistence in the time range (microseconds) in which we are working. In particular, electron spin resonance measurements show that H atoms in aqueous solution have very nearly the same hyperfine splitting as do H atoms in the gas phase,<sup>35,36</sup> thus strongly suggesting that H atoms in H<sub>2</sub>O liquid solution interact with only thermal energies with any H<sub>2</sub>O solvent molecule in its ground state. In our interpretation of the ultraviolet absorption spectrum of H atoms, given in Figure 5, we have invoked a partial charge transfer interaction only between the dissolved H atoms and the surrounding optically excited water molecules, thus leaving the dissolved H atoms essentially free in the optical ground state of the system.

Our interpretation of the measured uv spectra of  $e_{aq}^-$  and H also yields a straightforward explanation of the large blue shift of the absorption spectrum of D in D<sub>2</sub>O relative to that of H in H<sub>2</sub>O when account is taken of the large blue shift of the absorption edge of liquid D<sub>2</sub>O relative to liquid H<sub>2</sub>O.<sup>30</sup>

No quantitative theory of the far-uv spectra of H and  $e_{aq}^-$  has been worked out, but several other interpretations have been proposed for the uv spectrum of H in addition to the original interpretation of the H spectrum,<sup>3</sup> which has been discussed above. Claxton and Symons<sup>7,8</sup> have proposed that the H spectrum is due to a distorted and hydrogen-bonded H<sub>3</sub>O configuration in which the hyperfine splitting of one proton by coincidental cancellation of terms assumes the characteristic value for free H atoms. In view of the lack of supporting evidence for the existence of H<sub>3</sub>O in aqueous solution, this proposal is, in our view, untenable.

Henglein<sup>9</sup> has proposed a model based on the observation that the standard free energy change in the reaction



where  $e_m^-$  is the thermal and mobile electron in water, is only ca. 1.9 eV, and that the ionization potential and the first excited singlet of H lie 13.6 and 10.2 eV, respectively, above the ground state. This led him to suggest that by gradually distorting the hydration shell of the proton in reaction 2 and simultaneously performing the same distortion of the "hydration shell" of H<sub>aq</sub> a point will be reached where reaction 2 can be driven photolytically by the 200-nm photon (6.2 eV) observed in the H spectrum.

Without going into the prohibitive energetics of the hydration shell distortions required by this mechanism, we wish to point out that the photolytically driven reaction 2 with distorted hydration shells of H<sub>3</sub>O<sub>aq</sub><sup>+</sup> and H<sub>aq</sub> depicts a bound-free transition for the electron, and consequently cannot account for the sharp onset of the H spectrum around 200 nm.

Treinin and Hayon<sup>10</sup> have proposed to interpret the 230-nm band of the OH spectrum and the H spectrum<sup>3</sup> in liquid H<sub>2</sub>O solution as charge transfer spectra with solvent H<sub>2</sub>O as the electron donor. In order to calculate the electronic transition energies of the proposed charge transfer spectra from the electron affinities of H and OH (1.33 eV) using the standard formulas of Person and Mulliken, they introduce a simple electrostatic model that considers the ions as point charges at the centers of solvent cavities in a continuous dielectric medium and make critical choices for the effective dielectric constant of the solvent and for the cavity parameters. Furthermore, they assume that the magnitudes of the resonance and overlap integrals, respectively, are the same for H in H<sub>2</sub>O and for OH in H<sub>2</sub>O. In this way they calculate that the charge transfer band for OH should fall at 5.1 eV, which they compare with the experimental value<sup>3</sup> of 5.40 eV (230 nm). A more reasonable comparison would have been not with the 230-nm

band of OH, which as discussed above is not a charge transfer band, but with the broad absorption band of OH below 200 nm (>6.2 eV), and this would have shown that their calculated value was off by more than 1 eV. The value that Treinin and Hayon calculate for the electronic transition energy for the H spectrum corresponds to a band maximum at  $\lambda_{max} \approx 190$  nm, which appears reasonable. This result is, however, obtained by allowing an ionic character H<sup>-</sup>...O<sup>+</sup>H<sub>2</sub> of 4% in the ground state of H atoms dissolved in water.<sup>37</sup> Such a large ionic content appears to be contradicted by ESR measurements that show that H atoms dissolved in aqueous solutions have very nearly the same hyperfine splitting as do H atoms in the gas phase.<sup>35,36</sup>

We conclude that until a quantitative treatment has been carried out for the spectra reported in this paper below 200 nm, these spectra appear to be best interpreted in terms of a red shift of the first absorption band for water, normally found in the 180-nm region, for those water molecules adjacent to the solutes.

*Acknowledgments.* The authors (E.J.H. and B.D.M.) wish to acknowledge the great help of Pat Walsh and Robert Clarke with the experiments and also of Benno Naderer with skilled operation of the A.N.L. linac. Klaus Schmidt provided much useful guidance in the use of his kinetics program, WR20. S.O.N. acknowledges valuable help with the experiments from Palle Pagsberg, Jytte Eriksen, Preben Genske, and the Risø linac staff and a productive discussion with Joseph Silverman.

## References and Notes

- (1) (a) Work performed under the auspices of the U.S. and Danish Atomic Energy Commissions. (b) Symploxor, Inc., Holte, DK-2840 Denmark.
- (2) Cancer Research Campaign, Gray Laboratory, Mount Vernon Hospital, Northwood, Middlesex, England.
- (3) P. Pagsberg, H. Christensen, J. Rabani, G. Nilsson, J. Fenger, and S. O. Nielsen, *J. Phys. Chem.*, **73**, 1029 (1969).
- (4) S. O. Nielsen, P. Pagsberg, E. J. Hart, H. Christensen, and G. Nilsson, *J. Phys. Chem.*, **73**, 3171 (1969).
- (5) J. W. Boyle, J. A. Ghormley, C. J. Hohanadel, and J. F. Riley, *J. Phys. Chem.*, **73**, 2886 (1969).
- (6) J. A. Ghormley and C. J. Hohanadel, *J. Phys. Chem.*, **75**, 40 (1971).
- (7) T. A. Claxton and M. C. R. Symons, *Chem. Commun.*, 379 (1970).
- (8) T. A. Claxton, I. S. Ginns, M. J. Godfrey, K. V. S. Rao, and M. C. R. Symons, *J. Chem. Soc., Faraday Trans. 2*, **69**, 217 (1973).
- (9) A. Henglein, *Ber. Bunsenges. Phys. Chem.*, **78**, 1078 (1974).
- (10) A. Treinin and E. Hayon, *J. Am. Chem. Soc.*, **97**, 1716 (1975).
- (11) R. L. Christensen and R. J. Fother, *Appl. Opt.*, **2**, 1049 (1963).
- (12) B. D. Michael, K. H. Schmidt, and E. J. Hart, *J. Phys. Chem.*, **75**, 2798 (1971).
- (13) C. B. Senvar and E. J. Hart, *Proc. U.N. Int. Conf. Peaceful Uses At. Energy*, **2nd**, **29**, 19 (1958).
- (14) H. Christensen, G. Nilsson, P. Pagsberg, and S. O. Nielsen, *Rev. Sci. Instrum.*, **40**, 786 (1969).
- (15) K. H. Schmidt, Argonne National Laboratory Report, ANL-7693, March 1970.
- (16) C. J. Hohanadel, *J. Phys. Chem.*, **56**, 587 (1952).
- (17) E. J. Hart and E. M. Fielden, *Adv. Chem. Ser.*, **No. 50**, 253 (1965).
- (18) E. J. Hart and M. Anbar, "The Hydrated Electron", Wiley-Interscience, New York, N.Y., 1970, Table X.E.1.
- (19) E. J. Hart and M. Anbar, ref 18, p 174.
- (20) Landolt-Börnstein Tables, 6th ed, Vol. 1, "Atomic and Molecular Physics", part 3, "Molecules II", Springer-Verlag, West Berlin, 1951, p 231.
- (21) J. L. Weeks, G. M. A. C. Meaburn, and S. Gordon, *Radiat. Res.*, **19**, 559 (1963).
- (22) J. Jortner and G. Stein, *Bull. Res. Council. Isr., Sect. A*, **6**, 239 (1957).
- (23) E. J. Hart and E. M. Fielden, *J. Phys. Chem.*, **72**, 577 (1968).
- (24) As measured with a half-maximum intensity optical band width of 4.8 nm.
- (25) G. H. Dieke and H. M. Crosswhite, *J. Quant. Spectrosc. Radiat. Transfer*, **2**, 97 (1962).
- (26) D. S. Tinti, *J. Chem. Phys.*, **48**, 1459 (1968).
- (27) I. A. Taub and K. Eiben, *J. Chem. Phys.*, **49**, 2499 (1968).
- (28) P. M. Solomon, *Nature (London)*, **217**, 334 (1968).
- (29) G. C. Pimentel, *J. Am. Chem. Soc.*, **79**, 3323 (1957).
- (30) M. F. Fox and E. Hayon, *J. Phys. Chem.*, **76**, 2703 (1972).

- (31) J. J. Markham, *Solid State Phys., Suppl.*, **8**, 1 (1966).  
 (32) B. C. Cavenett, J. V. Gee, W. Hayes, and M. C. M. O'Brien, *Solid State Commun.*, **6**, 697 (1968).  
 (33) J. D. Weisner and B. H. Armstrong, *Proc. Phys. Soc.*, **83**, 31 (1964).  
 (34) M. D. Newton, *J. Chem. Phys.*, **58**, 5833 (1973).  
 (35) B. Smaller, E. C. Avery, and J. R. Remko, *J. Chem. Phys.*, **55**, 2414 (1971).  
 (36) K. Eiben and R. W. Fessenden, *J. Phys. Chem.*, **75**, 1186 (1971).  
 (37) The ionic content in the ground state is not reported by Treinin and Hayon, ref 10, but can be calculated from their data.

## Spectroscopic Evidence for Complex Formation of the Tributylammonium Cation with Hexamethylphosphoric Triamide in *o*-Dichlorobenzene and with Triphenylphosphine Oxide in 1,2-Dichloroethane

W. R. Gilkerson

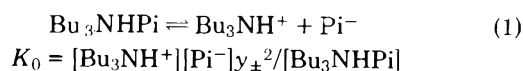
Department of Chemistry, University of South Carolina, Columbia, South Carolina 29208 (Received April 1, 1976)

Uv-visible spectra of  $10^{-5}$  M solutions of tri-*n*-butylammonium picrate in *o*-dichlorobenzene at 25 °C in the presence of added hexamethylphosphoric triamide, recorded as a function both of ligand and of salt concentration, show that a 1:1 complex is formed between the Lewis base, L, and the tertiary ammonium cation,  $\text{Bu}_3\text{NH}^+$ . Similar results are found with the salt in the presence of added triphenylphosphine oxide in 1,2-dichloroethane. Values of the equilibrium constants for the reaction  $\text{Bu}_3\text{NHPi} + \text{L} \rightleftharpoons \text{Bu}_3\text{NHL}^+ + \text{Pi}^-$  calculated from the spectroscopic data are found to be in good agreement with earlier results obtained using conductance measurements. These results confirm previous interpretations of the increases in electrical conductance of salt solutions in low dielectric solvents attending the addition of small quantities of certain Lewis bases as being due to the formation of 1:1 cation-ligand complexes.

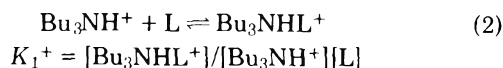
Solutions of salts of picric acid typically absorb strongly in the region 350 to 450 nm with molar extinction coefficients of the order of  $10^4 \text{ M}^{-1} \text{ cm}^{-1}$  or greater. Absorption maxima in the uv-visible spectra of picrate salts in the low dielectric solvents dioxane, chloroform, and 1,2-dichloroethane were found by von Halban and Szigeti<sup>1</sup> to be shifted toward shorter wavelength as the cation was varied from quaternary ammonium to tertiary ammonium to alkali metal cation. Similar shifts in the absorption maxima have been reported by Davis<sup>2</sup> for triethylammonium picrate when compared with tetraethylammonium picrate in benzene solvent. The tertiary amine salts are present in these solvents primarily as the hydrogen-bonded ion pairs<sup>3</sup> at the salt concentrations used ( $10^{-4}$  to  $10^{-5}$  M). Chantooni and Kolthoff<sup>4</sup> report that the absorption spectra of undissociated tertiary amine picrates in acetonitrile are shifted to shorter wavelengths as compared to that of picrate anion; the spectrum of the latter was taken to be that of tetra-*n*-butylammonium picrate in acetonitrile. No general shifts of this sort were observed for picrates in water.<sup>2</sup>

These results suggested that the absorption spectrum of the hydrogen bonded ion pair, tri-*n*-butylammonium picrate,  $\text{Bu}_3\text{NHPi}$ , might be different from that of the completely dissociated ions,  $\text{Bu}_3\text{NH}^+ + \text{Pi}^-$ , in a solvent such as 1,2-dichloroethane, DCE; the picrate hydrogen bonded to the tri-*n*-butylammonium cation would be expected to have a spectrum resembling that of triethylammonium picrate in benzene or of the undissociated salt in acetonitrile, while the spectrum of the free tri-*n*-butylammonium cation plus the picrate anion would be expected to resemble that of tetra-*n*-butylammonium picrate,  $\text{Bu}_4\text{NPi}$ , in acetonitrile where this salt is completely dissociated at low concentrations. Such environmental-dependent spectra of the picrate moiety

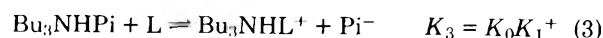
should prove useful in furnishing spectroscopic evidence for the series of reactions which have been postulated<sup>5-7</sup> to occur when a Lewis base such as triphenylphosphine oxide,  $\text{Ph}_3\text{PO}$ , is added to a solution of  $\text{Bu}_3\text{NHPi}$  in solvents such as DCE (dielectric constant  $\epsilon$  10.34).<sup>8</sup> Increases in electrical conductance accompanying the addition of Lewis bases to tertiary ammonium salt solutions in such solvents have been interpreted<sup>5-7</sup> as due to increased ion pair dissociation



as a result of mass action when the cation forms a cation-ligand complex



where L represents the Lewis base ligand. [A] represents the molar concentration of species A. The activity coefficients of uncharged species have been taken to be unity while the mean ionic activity coefficient  $\gamma_{\pm}$  is taken to be given by the Debye-Hückel limiting law. The activity coefficients of the cations  $\text{Bu}_3\text{NHL}^+$  and  $\text{Bu}_3\text{NH}^+$  present in the same solution are taken to be identical. Since the concentration of hydrogen bonded ion pairs,  $[\text{Bu}_3\text{NHPi}]$ , is much greater than the concentration of free cation,  $[\text{Bu}_3\text{NH}^+]$ , at the salt concentrations used, the principal reaction occurring in the solution as a result of adding the Lewis base  $\text{Ph}_3\text{PO}$  to the salt solution is postulated to be the sum of eq 1 and eq 2, yielding



The following investigation was undertaken to test the hypothesis that the spectra of solutions of  $\text{Bu}_3\text{NHPi}$  with and

without added ligand (the Lewis base) would afford evidence that eq 3 indeed describes the processes occurring in these systems. Earlier studies of the systems Bu<sub>3</sub>NHPi in DCE with added Ph<sub>3</sub>PO<sup>9</sup> and in *o*-dichlorobenzene (DCB) with added hexamethylphosphoric triamide (HMPT)<sup>5a</sup> indicated that these would be appropriate systems to use here. Uv-visible spectra of the salt in the two solvents with and without added Lewis bases were recorded. It is difficult to remove the last traces of water from organic solvents. To test the effects of added water on these systems solutions of the salt in each solvent with added known amounts of water were prepared and the spectra of these solutions with and without added bases were recorded.

### Experimental Section

*o*-Dichlorobenzene (Dow Chemical Co.) was purified as reported earlier.<sup>5b</sup> 1,2-Dichloroethane (Matheson Coleman and Bell, Spectrograde) was stored over molecular sieve (Linde Air Products Type 4A) for 2 days and distilled on a 35 × 2 cm column packed with glass helices under a dry nitrogen atmosphere, bp 83.5 °C. Tri-*n*-butylammonium picrate was prepared and purified as before,<sup>10</sup> as was tetra-*n*-butylammonium picrate.<sup>11</sup> Triphenylphosphine oxide (K and K Laboratories) was purified as before.<sup>12</sup> Hexamethylphosphoric triamide (Matheson Coleman and Bell) was purified as before.<sup>5a</sup> It should be noted that an incorrect boiling point was given in that report. The value observed here for a middle fraction, bp 105 °C (7 mm), is in agreement with values reported elsewhere.<sup>13</sup>

The salts and ligands were weighed in a nitrogen-filled drybox. The solutions were made up by weight and the molar concentrations were calculated taking the densities of the solutions to be the same as those<sup>10</sup> for the pure solvents.

Spectra were recorded on a Cary Model 14 spectrophotometer equipped with a thermostatted cell compartment. The latter was maintained at 25.0 °C. Solutions were placed in stoppered silica cells (1-cm path length except for the highest salt concentration in DCB, where a cell of 0.1-cm path length was used). All spectra were recorded with air in the reference beam. The absorbance of solvent alone in the cell was subtracted from those of the salt solutions at the wavelength of interest in arriving at the values of absorbance used in the calculations which follow. The changes in absorbance were estimated to have an uncertainty of ±0.002 absorbance units.

The concentration of water remaining in typical solvent samples and in typical salt solution preparations was determined by Karl Fischer titration; in DCE, [H<sub>2</sub>O] = 1.65 mM (24 ppm) and with a salt concentration of 7.2 × 10<sup>-5</sup> M, [H<sub>2</sub>O] = 1.78 mM; in DCB, [H<sub>2</sub>O] = 0.72 mM and with a salt concentration of 7.0 × 10<sup>-5</sup> M, [H<sub>2</sub>O] = 2.02 mM.

Water was added to these salt solutions by vapor equilibration; 100 ml of the salt solution in a 250-ml flask was connected by large bore pyrex tubing with another flask containing 100 ml of distilled water, both flasks being magnetically stirred, and the entire system was evacuated using a water pump, sealed off, and equilibrated at room temperature overnight. By these means the water concentration in the DCE salt solution was raised to 10.7 mM while that of the DCB salt solution was raised to 18.7 mM. Spectra of these solutions with added water were recorded with and without added ligand.

### Results

The spectra of 0.048 mM picric acid (HPi), tri-*n*-butylammonium picrate, and tetra-*n*-butylammonium picrate in

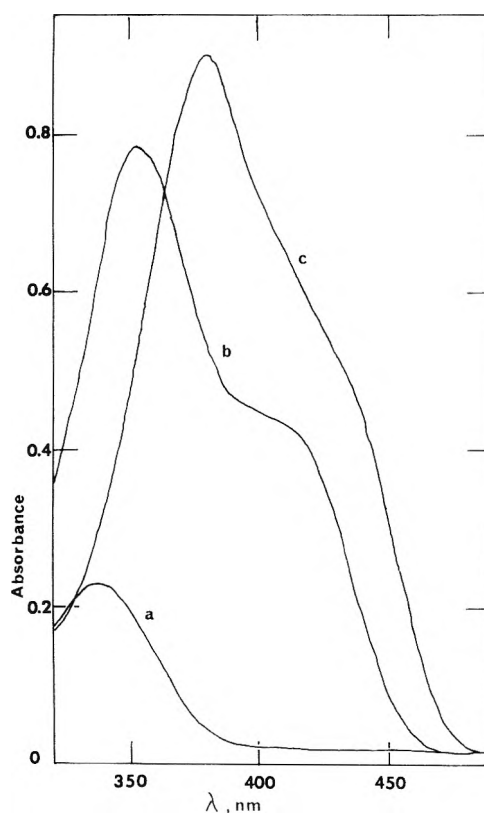


**Figure 1.** Salt spectra in 1,2-dichloroethane at 25 °C: curve a, 0.05 mM HPi; curve b, 0.048 mM Bu<sub>3</sub>NHPi; curve c, 0.048 mM Bu<sub>4</sub>NPI. Cell path length 1.0 cm. Addition of triphenylphosphine oxide (0.047 M) had no detectable effect on the spectrum of Bu<sub>4</sub>NPI.

DCE at 25 °C appear in Figure 1a–c, respectively. Spectra of these solutes in DCB are very similar in each case, and are similar for each solute to those already reported in acetonitrile,<sup>4</sup> dioxane,<sup>1</sup> and benzene solvents.<sup>2</sup>

Addition of triphenylphosphine oxide to dilute solutions of Bu<sub>3</sub>NHPi (ca. 0.05 mM) in DCE at 25 °C has decided effects on the spectrum, Figure 2. Spectrum a has no added Ph<sub>3</sub>PO while for spectra b–e, the [Ph<sub>3</sub>PO] increases from 0.0043 to 0.109 M. The maximum at 353 nm for Bu<sub>3</sub>NHPi alone appears to decrease in intensity while a new maximum near 380 nm grows in intensity. Note the isosbestic point at 362 nm. Comparison of these spectra of Bu<sub>3</sub>NHPi with added Ph<sub>3</sub>PO in DCE, Figure 2, with those of Bu<sub>3</sub>NHPi alone and Bu<sub>4</sub>NPI alone, Figure 1, yields the following: spectrum e in Figure 2, for Bu<sub>3</sub>NHPi at the highest [Ph<sub>3</sub>PO], resembles that of Bu<sub>4</sub>NPI, spectrum c in Figure 1, in regard to the wavelength at which the maximum occurs and the shape of the shoulder at around 420 nm. In addition, the wavelength, 363 nm, at which the spectral absorption curves of Bu<sub>3</sub>NHPi and Bu<sub>4</sub>NPI cross one another in the spectra in Figure 1 is almost identical with the wavelength at which the isosbestic point occurs in the spectra shown in Figure 2.

Addition of hexamethylphosphoric triamide to a 0.05 mM solution of Bu<sub>3</sub>NHPi in DCB at 25 °C has effects on the spectra, shown in Figure 3, similar to those observed in the case of addition of Ph<sub>3</sub>PO to the salt solutions in DCE noted above. The absorbance maximum for Bu<sub>3</sub>NHPi in DCB at 352 nm decreases as HMPT is added and a new maximum appears at 382 nm with an isosbestic point at 373 nm. Comparison of these spectra with those (at similar concentrations) of Bu<sub>3</sub>NHPi and Bu<sub>4</sub>NPI each alone in DCB at 25 °C shows (as with DCE solvent plus Ph<sub>3</sub>PO ligand) that the new maximum

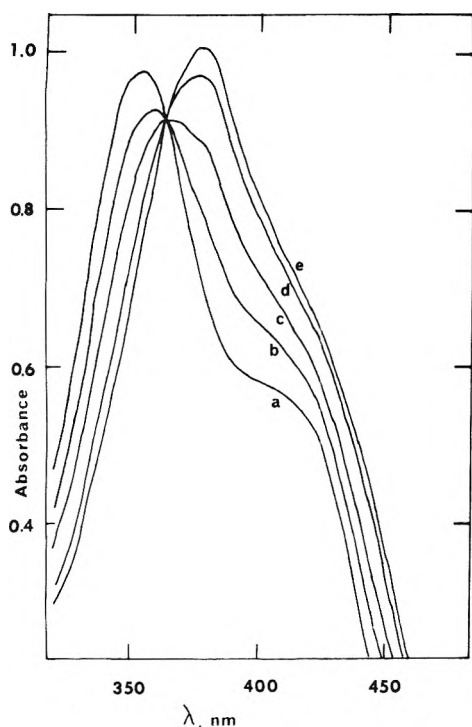


**Figure 2.** Spectra of 0.057 mM  $\text{Bu}_3\text{NHPi}$  in 1,2-dichloroethane at 25 °C with added triphenylphosphine oxide (the concentration of  $\text{Ph}_3\text{PO}$  follows the curve label): curve a, 0.0 M; curve b, 0.0043 M; curve c, 0.0206 M; curve d, 0.0638 M; curve e, 0.1094 M.

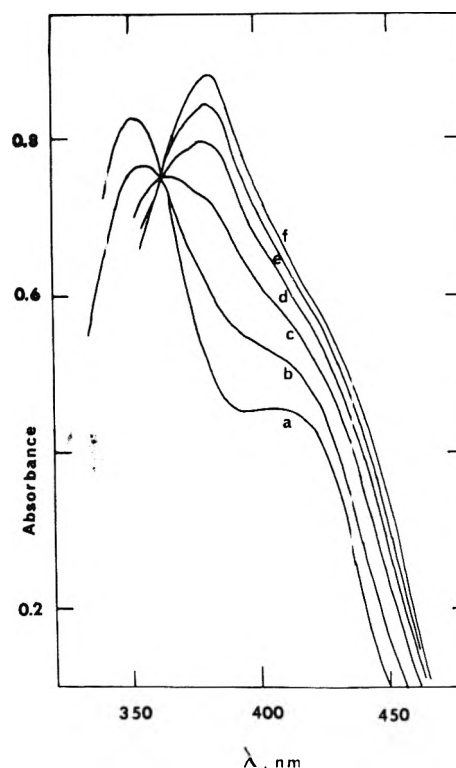


**Figure 3.** Spectra of 0.0506 mM  $\text{Bu}_3\text{NHPi}$  in *o*-dichlorobenzene at 25 °C with added hexamethylphosphoric triamide (the concentration of HMPT follows the curve label): curve a, 0.0 M; curve b, 0.0048 M; curve c, 0.0202 M; curve d, 0.0414 M; curve e, 0.0628 M; curve f, 0.0862 M.

in Figure 3 occurs at the same wavelength as the maximum of  $\text{Bu}_4\text{NHPi}$  (not shown) while the isosbestic point in Figure 3 occurs at the same wavelength as that at which the absorption curves (not shown) of  $\text{Bu}_3\text{NHPi}$  and  $\text{Bu}_4\text{NHPi}$  each alone in DCB cross one another. Let it be noted that neither  $\text{Ph}_3\text{PO}$  nor HMPT show any measurable absorption at the concentrations used in the spectral region from 330 to 500 nm.

A sixfold increase in water contaminant concentration in DCE had no detectable effect on the spectrum of the salt  $\text{Bu}_3\text{NHPi}$ . The added water had no significant effects on the spectra in the presence of  $\text{Ph}_3\text{PO}$  as will be shown below. The same observations can be made regarding the effect of a ninefold increase in water content on the spectrum of  $\text{Bu}_3\text{NHPi}$  in DCB with and without added HMPT.

## Discussion

The dissociation constant for  $\text{Bu}_3\text{NHPi}$  into free acid HPI and base  $\text{Bu}_3\text{N}$  has been previously found by conductance measurements<sup>10,14</sup> to be  $K_d = 7 \times 10^{-8}$  (on a molarity scale) while the dissociation constant for the salt into the free ions  $\text{Bu}_3\text{NH}^+$  and  $\text{Pi}^-$ , eq 1, has been found to be  $K_0 = 2 \times 10^{-8}$  in DCE, all at 25 °C. At the salt concentration used to obtain the spectra in Figure 1, this salt exists primarily as the hydrogen bonded ion pair  $\text{Bu}_3\text{NHPi}$ , with only a small fraction (2%) dissociated into free ions, and a slightly larger fraction (3.8%) dissociated into the free acid and base. It is clear that the spectrum of the tertiary ammonium salt, Figure 1b, is that of the picrate anion hydrogen bonded to the  $\text{Bu}_3\text{NH}^+$  cation, with a negligible contribution from the free acid, HPI. The spectra of  $\text{Bu}_3\text{NHPi}$  is similar to that of  $\text{Bu}_4\text{NHPi}$ , Figure 1c, but with a definite shift of the major features to shorter wavelength.

Tetra-*n*-butylammonium picrate has an ion pair dissociation constant<sup>15</sup> of  $2.28 \times 10^{-4}$  in DCE at 25 °C from which one can calculate that a large fraction (85%) of this salt is disso-

ciated into the free ions at a concentration of 0.048 mM. The spectrum in Figure 1c then is that primarily due to the dissociated picrate anion,  $\text{Pi}^-$ . All of this is to demonstrate that whatever the details of the nature of the interaction of the picrate moiety with the  $\text{Bu}_3\text{NH}^+$  moiety in the hydrogen bonded ion pair  $\text{Bu}_3\text{NHPi}$ , its spectrum is different both as to wavelength of the maximum and shape of the shoulder from that of free dissociated picrate anion as represented by that of  $\text{Bu}_4\text{NHPi}$ .

Similar arguments can be made regarding the relationship of the state of these salts to their spectra in the solvent DCB. This solvent has a dielectric constant<sup>8</sup> of 9.99 at 25 °C, almost isodielectric with DCE. The acid-base dissociation constant for  $\text{Bu}_3\text{NHPi}$  is  $9 \times 10^{-8}$  in DCB,<sup>10</sup> its ion pair dissociation constant is  $2.9 \times 10^{-10}$ , while the ion pair dissociation constant of  $\text{Bu}_4\text{NHPi}$  is  $1.92 \times 10^{-5}$ .<sup>11</sup>

The shifts in the spectra of  $\text{Bu}_3\text{NHPi}$  in DCE upon adding  $\text{Ph}_3\text{PO}$ , Figure 2, and in DCB upon adding HMPT, Figure 3, may be due to one or more of several possible reactions; (a) cation-ligand complex formation, eq 3,



or (c) ion pair-ligand complex formation,



where  $\text{Bu}_3\text{NHLPI}$  represents a hypothetical complex of the ligand with the ion pair  $\text{Bu}_3\text{NHPi}$  to form some kinetic entity. Equations 3 and 4 lead to relationships between the observed molar extinction coefficients  $\epsilon$  at a given wavelength, the stoichiometric salt concentration  $C$ , and the ligand concentration  $[\text{L}]$  which have the same form, with the exception of an ionic activity coefficient factor,  $\gamma_{\pm}^2$ , for eq 3. The relation between  $\epsilon$ ,  $C$ , and  $[\text{L}]$  for eq 5 is very different from those for

eq 3 or 4. First consider the latter two reactions to occur simultaneously.<sup>16</sup> Let  $\alpha_3$  represent the fraction  $[\text{Pi}^-]/C$ , and  $\alpha_4$  represent  $[\text{LHPi}]/C$ . For the ligands used here,  $[\text{Bu}_3\text{NH}^+]$  is very much less than  $[\text{Bu}_3\text{NHL}^+]$  at the lowest ligand concentration used so that the contribution to total  $[\text{Pi}^-]$  due to dissociation of  $\text{Bu}_3\text{NHPi}$  into uncomplexed cation and free  $\text{Pi}^-$  can be neglected in comparison to that furnished by reaction 3. Then the molar extinction coefficient observed at ligand concentration  $[\text{L}]$  is given by

$$\epsilon = \epsilon_0[\text{Bu}_3\text{NHPi}]/C + \epsilon_3[\text{Pi}^-]/C + \epsilon_4[\text{LHPi}]/C \quad (6)$$

where  $\epsilon_0$  is the molar extinction coefficient of  $\text{Bu}_3\text{NHPi}$ ,  $\epsilon_3$  is that of free  $\text{Pi}^-$ , and  $\epsilon_4$  is that of  $\text{LHPi}$ . It is assumed that these are the only absorbing species in these solutions at the wavelength of interest. The above expression can be rearranged into an equation for the change in molar extinction coefficient,  $\Delta\epsilon = \Delta\epsilon_3\alpha_3 + \Delta\epsilon_4\alpha_4$ , where  $\Delta\epsilon = \epsilon - \epsilon_0$ ,  $\Delta\epsilon_3 = \epsilon_3 - \epsilon_0$ , and  $\Delta\epsilon_4 = \epsilon_4 - \epsilon_0$ . The ratio  $\alpha_4/\alpha_3$  can be found by taking the ratio of the equilibrium constant expressions in terms of concentrations for eq 3 and 4;  $(K_4/K_3) = \alpha_4^2/\alpha_3^2 y_{\pm}^2$ , so that

$$\alpha_4/\alpha_3 = y_{\pm}(K_4/K_3)^{1/2}$$

Defining  $Q = y_{\pm}(K_4/K_3)^{1/2}$ , then  $\Delta\epsilon$  becomes  $\Delta\epsilon = (\Delta\epsilon_3 + Q\Delta\epsilon_4)\alpha_3 = \Delta\epsilon_c\alpha_3$ , defining the quantity  $\Delta\epsilon_c$ , or in terms of  $\alpha_4$ ,  $\Delta\epsilon = (\Delta\epsilon_3/Q + \Delta\epsilon_4)\alpha_4$ , or  $\Delta\epsilon = \Delta\epsilon_b\alpha_4$  where  $\Delta\epsilon_b = \Delta\epsilon_3/Q + \Delta\epsilon_4$ . The total fraction of salt which has reacted with ligand either in base exchange or to form cation–ligand complex is given by  $\alpha_3 + \alpha_4 = \Delta\epsilon(1/\Delta\epsilon_c + 1/\Delta\epsilon_b)$ . If these relations are used to substitute for the concentrations in the equilibrium constant expression for eq 3, rearrangement leads to

$$1/\Delta\epsilon = (1/\Delta\epsilon_c + 1/\Delta\epsilon_b) + (1/K_3\Delta\epsilon_c^2)(Cy_{\pm}^2\Delta\epsilon/[L]) \quad (7)$$

If instead the substitutions are made into  $K_4$ , the equilibrium constant expression for eq 4 then one obtains an expression identical with eq 7 except that the last term on the right-hand side of eq 7 is replaced by  $(1/K_4\Delta\epsilon_b^2)(C\Delta\epsilon/[L])$ . It can be shown that these two last terms are identical by making use of the expressions given above for  $\Delta\epsilon_c$  and  $\Delta\epsilon_b$ . Spectroscopic measurements alone will not allow an unambiguous determination of the four parameters involved in eq 7,  $\Delta\epsilon_3$ ,  $\Delta\epsilon_4$ ,  $K_3$ , and  $K_4$ . An estimate of the relative importance of base exchange compared to cation–ligand complex formation can be made using the following approach; earlier conductance measurements<sup>10</sup> yield values for the dissociation constants  $K_d$  of  $\text{Bu}_3\text{NHPi}$  into free picric acid,  $\text{HPi}$ , and tri-*n*-butylamine,  $\text{Bu}_3\text{N}$ , in DCB ( $K_d = 9 \times 10^{-8}$ ) and in DCE ( $K_d = 7 \times 10^{-8}$ ) while the formation constant  $K_f$  for the hydrogen bonded ion pair formed by  $\text{HPi}$  interacting with  $\text{Ph}_3\text{PO}$  has been determined spectrophotometrically<sup>9</sup> in DCB to be  $K_f = 35$ , all on a molarity scale at 25 °C. There is no value at hand for  $K_f$  for  $\text{HPi}$  with  $\text{HMPT}$  in DCB, but from what measures of basicity as are available<sup>17</sup> for the two compounds  $\text{Ph}_3\text{PO}$  and  $\text{HMPT}$  the latter is of comparable but slightly greater basicity than the former so that  $K_f$  for  $\text{HMPT}$  might be expected to be of the same order of magnitude as that for  $\text{Ph}_3\text{PO}$ . The equilibrium constant for eq 4 may be estimated as  $K_4 = K_f K_d \sim 2 \times 10^{-6}$  for  $\text{Ph}_3\text{PO}$  with  $\text{Bu}_3\text{NHPi}$  in DCB. The equilibrium constant for eq 3 for this system has been found by conductance measurements<sup>5,10</sup> to be  $K_3 = K_0 K_1^+ = 2.8 \times 10^{-10} \times 3.7 \times 10^5 = 1.0 \times 10^{-4}$ . The factor  $Q$  in this case would be 0.14. It is seen then that reaction 4 occurs to a small enough extent compared with reaction 3 that the major changes in molar extinction coefficient observed would be due to reaction 3. The intercept of a plot of eq 7,  $1/\Delta\epsilon$  vs.  $Cy_{\pm}^2\Delta\epsilon/[L]$ , would yield the quantity  $1/\Delta\epsilon_c + 1/\Delta\epsilon_b$  which is equal to  $(1 + Q)/\Delta\epsilon_c$ .

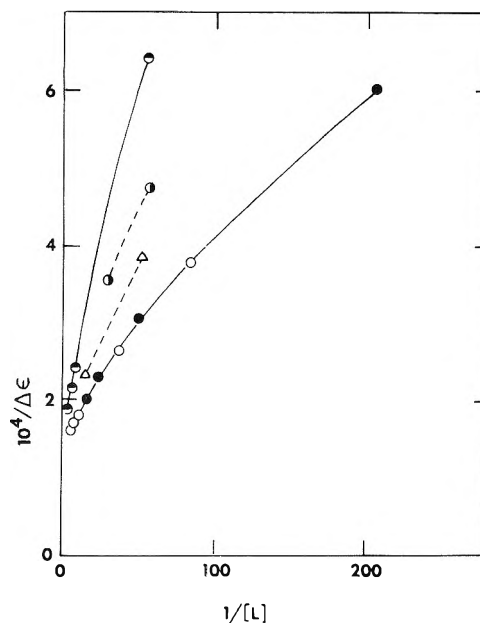


**Figure 4.** Plot of eq 8 for  $\text{Bu}_3\text{NHPi}$  in *o*-dichlorobenzene at 25 °C with added hexamethylphosphoric triamide: ●, 0.337 mM salt; ○, 0.171 mM salt; ○, 0.0509 mM salt; ●, 0.0506 mM salt; △, 0.0698 mM salt plus 18.7 mM  $\text{H}_2\text{O}$

This last quantity then is estimated to be only 10% different from  $1/\Delta\epsilon_c$ . Thus, the intercept can be used to calculate a reasonably accurate value of  $K_3$  from the slope of the plot of eq 7.

If the principal result of added ligand,  $\text{Ph}_3\text{PO}$  or  $\text{HMPT}$ , is the formation of ligand separated ion pairs, such as those formed by ammonium picrate and potassium picrate with certain crown ethers as reported by Smid,<sup>18</sup> then the overall reaction is given by eq 5 with a formation constant for the ion pair–ligand complex represented by  $K_p$ . Taking  $\epsilon_p$  to be the molar extinction coefficient of the ion pair–ligand complex  $\text{Bu}_3\text{NHLPi}$ , the relationship between  $\Delta\epsilon$  and  $[\text{L}]$  at a particular wavelength can be shown to be given by

$$1/\Delta\epsilon = 1/\Delta\epsilon_p + (1/K_p\Delta\epsilon_p)(1/[L]) \quad (8)$$

where  $\Delta\epsilon_p = \epsilon_p - \epsilon_0$ .

The different functional dependence of  $1/\Delta\epsilon$ , linear in  $Cy_{\pm}^2\Delta\epsilon/[L]$  for eq 3, and linear in  $1/[L]$  for eq 5, should allow a determination of which is being formed, a cation–ligand complex or an ion pair–ligand complex. Spectra for the system  $\text{Bu}_3\text{NHPi}$  in DCB at 25 °C as a function of added  $\text{HMPT}$  were recorded at three different salt concentrations, 0.0506, 0.171, and 0.337 mM, to test whether the changes in  $\epsilon$  were best represented by eq 7, implying cation–ligand complex formation or, by eq 8, implying ion pair–ligand complex formation. Values of  $\Delta\epsilon$  were read off at a wavelength of 400 nm. This wavelength was chosen for the analysis since  $\epsilon$  for the salt had the smallest rate of change with wavelength at this point. The data plotted according to eq 8 appear in Figure 4. The data plotted according to eq 7 appear in Figure 5 for both  $\text{HMPT}$  as ligand in DCB and  $\text{Ph}_3\text{PO}$  as ligand in DCE. Comparison of results for  $\text{HMPT}$  in Figures 4 and 5 clearly shows that the values of  $\Delta\epsilon$  observed at a given value of ligand concentration depend on the ratio of the product concentration (proportional to  $C\Delta\epsilon$ ) to the ligand concentration as required by eq 7, rather than being simply related to the ligand concentration as required by eq 8. It is concluded that ion pair–ligand complex formation is not important relative to cation–ligand complex formation in determining the spectral changes ob-

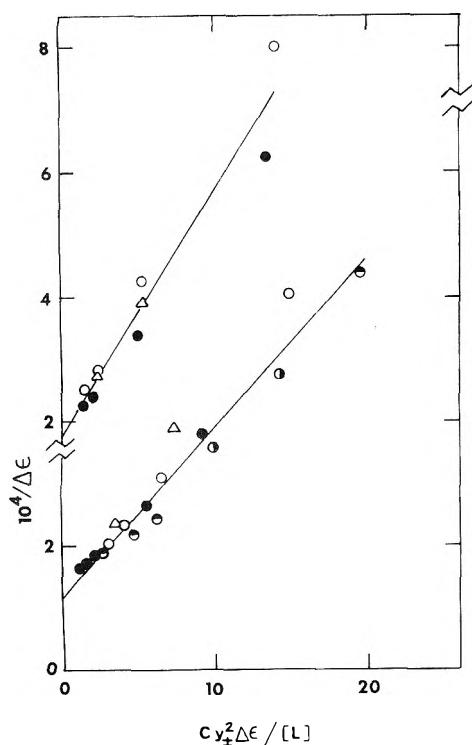


**Figure 5.** Plot of eq 7. Upper data set,  $\text{Bu}_3\text{NHPi}$  in 1,2-dichloroethane at 25 °C with added triphenylphosphine oxide: ●, 0.0555 mM in salt; ○, 0.0572 mM in salt; △, 0.0719 mM in salt plus 10.7 mM  $\text{H}_2\text{O}$ . Lower data set,  $\text{Bu}_3\text{NHPi}$  in *o*-dichlorobenzene at 25 °C with added hexamethylphosphoric triamide. The symbols for the data points are the same as in Figure 4.

served in the systems under study here, in agreement with the conclusions reached in the earlier conductance studies of these systems.<sup>5a,9</sup>

The slopes and intercepts of the lines (determined by least-squares treatment of the data) in Figure 5 yield for  $\text{Bu}_3\text{NHPi}$  with HMPT in DCB,  $\Delta\epsilon_c = 8950 \pm 300 \text{ M}^{-1} \text{ cm}^{-1}$  and  $K_3 = (4.51 \pm 0.85) \times 10^{-4}$ , and with  $\text{Ph}_3\text{PO}$  in DCE,  $\Delta\epsilon_c = 5740 \pm 610 \text{ M}^{-1} \text{ cm}^{-1}$  and  $K_3 = (7.7 \pm 2.1) \times 10^{-4}$ , all at 25 °C. The uncertainties are calculated from the standard deviations of the slopes and intercepts. These may be compared with the values of  $K_3$  calculated from the conductance results; for HMPT in DCB,<sup>5a</sup>  $K_3 = 6.3 \times 10^{-4}$ , and for  $\text{Ph}_3\text{PO}$  in DCE,<sup>9</sup>  $K_3 = 5.5 \times 10^{-4}$ . The uncertainty in these latter values may be estimated<sup>19</sup> as  $\pm 20\%$ . It is concluded that the spectrophotometric values of  $K_3$  are in agreement with those values determined conductometrically, within experimental error.

The agreement between these spectrophotometric results and the earlier conductance results is unequivocal evidence that the interpretations placed on the earlier conductance results as due to cation–ligand complex formation are correct. Extensive discussions of the important bearing these results have on our knowledge of specific ion–solvent interaction have

already been published<sup>5,9,10,12</sup> and will not be repeated here.

The effects of increases in water concentration on the values of  $\Delta\epsilon$  at two ligand concentrations are shown in Figure 5 as triangles; the water concentration in DCE was increased sixfold to 0.0107 M while that in DCB was increased ninefold to 0.0187 M. The data points in the presence of added water in DCE are almost coincident with the least-squares straight line representing the data in the absence of added water. One of the points in the presence of added water for HMPT in DCB falls very close to the least-squares line while the point at the lower ligand concentration is somewhat further from the least-squares line. It is felt that this deviation does not indicate any significant effect of added water on the system in DCB in view of the deviations of some of the data in the absence of added water in the system. In conclusion, it cannot be stated with certainty that water is not involved in the processes occurring in these solutions but if the concentration of water were an important factor, these changes in water concentration should have resulted in more significant differences between the values of  $\Delta\epsilon$  with and without added water than those shown in Figure 5.

*Acknowledgment.* Thanks are due Professor E. E. Mercer of this department for use of the Cary spectrophotometer. Thanks are also due the referees for several helpful suggestions.

## References and Notes

- (1) H. von Halban and B. Szigeti, *Helv. Chim. Acta.*, **20**, 746 (1937).
- (2) M. M. Davis, *Natl. Bur. Stand. (U.S.), Monogr. No.* **105**, 59 (1968).
- (3) Reference 2, p 41.
- (4) M. K. Chantoori and I. M. Kolthoff, *J. Am. Chem. Soc.*, **90**, 3005 (1968).
- (5) (a) H. W. Aitken and W. R. Gilkerson, *J. Am. Chem. Soc.*, **95**, 8551 (1973); (b) M. L. Junker and W. R. Gilkerson, *ibid.*, **97**, 493 (1975).
- (6) I. M. Kolthoff, D. Stocesoca, and T. S. Lee, *J. Am. Chem. Soc.*, **75**, 1834 (1953).
- (7) J. Macau, L. Lamberts, and P. Huyskens, *Bull. Soc. Chim. Fr.*, **7**, 2387 (1971).
- (8) A. D Aprano and R. M. Fuoss, *J. Solution, Chem.*, **4**, 175 (1975).
- (9) W. R. Gilkerson and J. B. Ezell, *J. Am. Chem. Soc.*, **89**, 808 (1967).
- (10) E. K. Ralph, III, and W. R. Gilkerson, *J. Am. Chem. Soc.*, **86**, 4783 (1964).
- (11) H. L. Curry and W. R. Gilkerson, *J. Am. Chem. Soc.*, **79**, 4021 (1957).
- (12) W. R. Gilkerson and J. B. Ezell, *J. Am. Chem. Soc.*, **87**, 3812 (1965).
- (13) L. Robert, *Chim. Ind.*, **97**, 337 (1967).
- (14) C. F. Witschonke and C. A. Kraus, *J. Am. Chem. Soc.*, **69**, 2472 (1947).
- (15) D. J. Mead, R. M. Fuoss, and C. A. Kraus, *Trans. Faraday Soc.*, **32**, 594 (1936).
- (16) Witschonke and Kraus<sup>14</sup> considered acid–base dissociation in addition to ion pair dissociation in the derivation of the conductance equation for a salt such as  $\text{Bu}_3\text{NHPi}$ .
- (17) E. M. Arnett, E. J. Mitchell, and T. S. S. R. Murty, *J. Am. Chem. Soc.*, **96**, 3875 (1974).
- (18) M. Bourgoin, K. H. Wong, J. Y. Hui, and J. Smid, *J. Am. Chem. Soc.*, **97**, 3462 (1975).
- (19) The reproducibility of these conductance values is  $5a \pm 10\%$ , but the uncertainty in absolute value of  $K_3$  is at least  $\pm 20\%$  due to approximations made in treating the data; the approximation yielding the largest uncertainty is that the ratio of the limiting equivalent conductance of the salt  $\text{Bu}_3\text{NHL}^+ + \text{Pi}^-$  to that of the salt  $\text{Bu}_3\text{NH}^+ + \text{Pi}^-$  is unity, while in fact<sup>20</sup> the former may be as much as 10% less than that of the latter. This ratio enters as its square in the data treatment.
- (20) J. B. Ezell and W. R. Gilkerson, *J. Phys. Chem.*, **72**, 144 (1968).

# Spectra and Structure of Organophosphorus Compounds. 16.<sup>1a</sup> Infrared and Raman Spectra, Vibrational Assignment, and Conformational Analysis for Isopropylphosphine and Isopropylphosphine-*d*<sub>2</sub>

J. R. Durig\* and A. W. Cox, Jr.<sup>1b</sup>

Department of Chemistry, University of South Carolina, Columbia, South Carolina 29208 (Received May 7, 1976)

Publication costs assisted by the University of South Carolina

The infrared spectra of gaseous (CH<sub>3</sub>)<sub>2</sub>CHPH<sub>2</sub> and (CH<sub>3</sub>)<sub>2</sub>CHPD<sub>2</sub> have been recorded from 80 to 3500 cm<sup>-1</sup>. The Raman spectra of gaseous and liquid (CH<sub>3</sub>)<sub>2</sub>CHPH<sub>2</sub> and (CH<sub>3</sub>)<sub>2</sub>CHPD<sub>2</sub> have been recorded from 100 to 3500 cm<sup>-1</sup>. The Raman spectrum from 100 to 3500 cm<sup>-1</sup> and the infrared spectrum from 450 to 3500 cm<sup>-1</sup> of solid (CH<sub>3</sub>)<sub>2</sub>CHPH<sub>2</sub> have been recorded. Both *gauche* and *trans* rotational isomers have been observed in the fluid phases. A vibrational assignment of the 33 normal modes has been made. Hot band transitions have been observed for the phosphino torsional mode. The average barrier to internal rotation of the methyl moiety was found to be 4.3 kcal/mol. The potential function for internal rotation around the C-P bond has been estimated. The *trans* conformation was found to be ~0.26 kcal/mol more stable than the *gauche* conformation using this estimated potential function.

## Introduction

Recently, we have published several spectroscopic studies on organophosphorous compounds<sup>2-5</sup> in which barriers to internal rotation have been determined or the most stable conformer elucidated. Vibrational assignments have also been presented for most of these molecules. As a continuation of these earlier studies, we have investigated the vibrational spectra of (CH<sub>3</sub>)<sub>2</sub>CHPH<sub>2</sub> and (CH<sub>3</sub>)<sub>2</sub>CHPD<sub>2</sub> where the possibility exists of two stable conformers, one with the PH<sub>2</sub> group *trans* to the methyl groups and another in a *gauche* configuration. We hoped to be able to compare the potential function governing internal rotation around the C-P bond of isopropylphosphine with that determined for the similar bond in ethylphosphine.<sup>3</sup> The results of this study are reported herein.

## Experimental Section

Infrared spectra were obtained using a Digilab FTS-15B Fourier transform interferometric spectrometer. A germanium beam splitter on a KBr substrate and glower source gave coverage of the 3800- to 400-cm<sup>-1</sup> region, while a mylar beam splitter and high pressure Hg arc lamp source were substituted for work in the 400- to 80-cm<sup>-1</sup> spectral region. Spectra of the gaseous phase were obtained by using a 10-cm cell with KBr windows and typically 4 Torr of sample pressure in the mid-infrared, or polyethylene windows, and ~300 Torr of sample pressure in the far-infrared.

Atmospheric water vapor was removed from the spectrometer housing by purging with dry nitrogen. Since the FTS system uses a He-Ne laser as a frequency reference of relatively high stability, calibration is achieved by adjusting a software parameter, the laser wavelength, to reproduce an observed vibrational transition of a suitable standard at its correct frequency. As a result, the accuracy of a measured frequency can be expected to be at least 0.1 cm<sup>-1</sup> throughout the spectrum. Both apodization function and resolution were varied for each sample to attain the best quality spectrum, but spectra of the gas phase were run at an effective resolution of better than 0.5 cm<sup>-1</sup> using a modified "boxcar" apodization

function for photometric accuracy. Spectra of the solid phase samples were obtained by condensing the compound into a Si plate maintained at ~15 K by a closed-cycle helium refrigerator.

Raman spectra were recorded to 4000 cm<sup>-1</sup> using a Cary 82 spectrometer equipped with either a Spectra Physics Model 171 or a Coherent Radiation Labs Model 53A argon ion laser operating on the 5145-Å line. Spectra of the gaseous phase were obtained using the Cary multipass accessory at sample pressures of 300 Torr. Spectra of the liquids were recorded from samples in sealed glass capillaries. Spectra of the solids were obtained by condensing the samples on a copper block maintained at ~88 K by boiling nitrogen or at ~15 K by a closed-cycle helium refrigerator. Polarization measurements were made using the standard Cary accessories. Frequencies measured for sharp, resolvable bands are expected to be accurate to at least ±2 cm<sup>-1</sup>.

In general, all sample preparations and manipulations were performed using standard high vacuum techniques where possible. This was done in view of the relative instability of trivalent phosphorus compounds with respect to oxidation as well as to minimize exposure to the compounds, which are probably quite toxic and undeniably unpleasant smelling. Sample purifications were performed using fractional condensation (trap-to-trap) methods or more generally a low temperature, low pressure fractionating column.

The sample of (CH<sub>3</sub>)<sub>2</sub>CHPH<sub>2</sub> was prepared by the reduction of (CH<sub>3</sub>)<sub>2</sub>CHPCl<sub>2</sub> with LiAlH<sub>4</sub> in di-*n*-butyl ether. (CH<sub>3</sub>)<sub>2</sub>CHPCl<sub>2</sub> was not commercially available and was prepared by the method of Reesor et al.<sup>7</sup> After low temperature distillation, the purity of the (CH<sub>3</sub>)<sub>2</sub>CHPH<sub>2</sub> was checked by mass spectrometry and <sup>1</sup>H, <sup>13</sup>C, and <sup>31</sup>P NMR. The deuterated derivative was prepared in a similar manner using LiAlD<sub>4</sub> instead of LiAlH<sub>4</sub>.

## Vibrational Assignment

The Raman spectra of gaseous, liquid, and solid isopropylphosphine-*d*<sub>0</sub> are shown in Figure 1, and the Raman spectra of gaseous and liquid isopropylphosphine-*d*<sub>2</sub> in Figure 2. The mid-infrared spectra of gaseous and solid isopropyl-

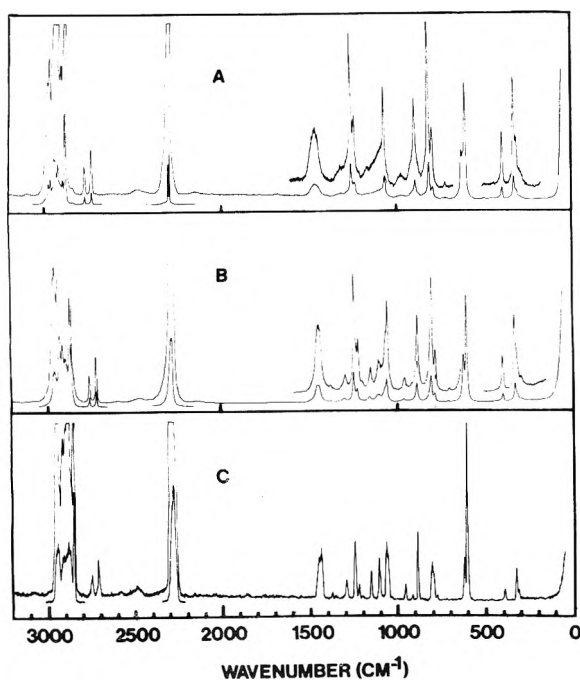


Figure 1. Raman spectra of  $(\text{CH}_3)_2\text{CHPH}_2$ : (A) gas; (B) liquid; (C) solid.

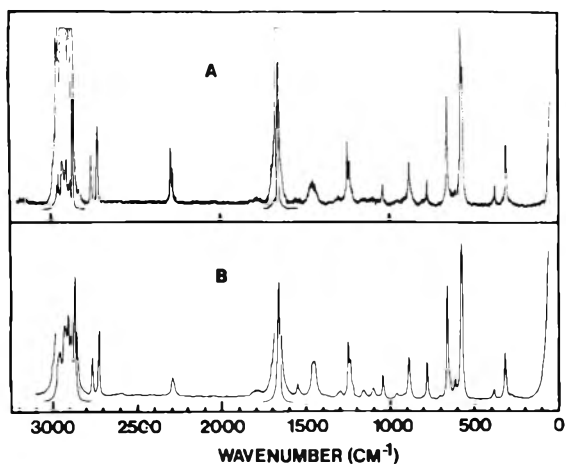


Figure 2. Raman spectra of  $(\text{CH}_3)_2\text{CHPD}_2$ : (A) gas; (B) liquid.

phosphine- $d_0$  and gaseous isopropylphosphine- $d_2$  are shown in Figure 3. While some portions of the spectra were easily analyzed, several complicating factors made the vibrational assignment somewhat difficult. If the energy difference between the two conformers is small, then both forms will exist at ambient temperatures and the spectra of both conformers will be observed in the fluid phases. While generally only one conformer will predominate in the well annealed solid, it was not found possible to form a good crystalline sample and the usual sharpening and splitting of peaks found in solid phase spectra were not observed. The melting point of the compound is below  $-160^\circ\text{C}$ , and the condensed samples merely formed glasses, even when cooled to 15 K. However, the group frequencies of the isopropyl moiety are well known,<sup>8</sup> and the frequency shifts upon deuteration of vibration modes associated with the hydrogens attached to the phosphorus atom made their identification straightforward. We feel the present assignment is reasonable in view of the available data, and

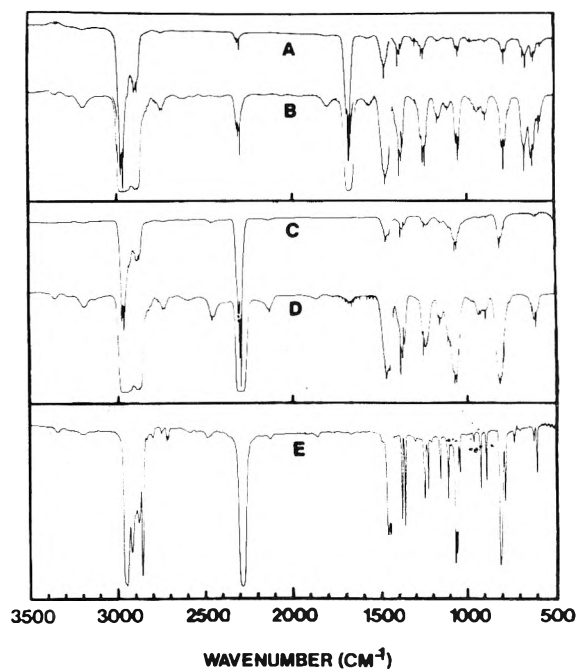


Figure 3. Mid-infrared spectra of  $(\text{CH}_3)_2\text{CHPH}_2$  and  $(\text{CH}_3)_2\text{CHPD}_2$ : (A) gas, isopropylphosphine- $d_2$ , approximately 2 Torr sample pressure; (B) gas, isopropylphosphine- $d_2$ , approximately 40 Torr sample pressure; (C) gas, isopropylphosphine- $d_0$ , approximately 2 Torr sample pressure; (D) gas, isopropylphosphine- $d_0$ , approximately 40 Torr sample pressure; (E) solid, isopropylphosphine- $d_0$ .

with regard to the vibrational modes of the phosphine moiety, most probably correct.

The observed frequencies and assignments for isopropylphosphine- $d_0$  and - $d_2$  are given in Tables I and II (miniprint, see paragraph at end of text regarding miniprint material). The vibrations are numbered relative to the trans conformer and the descriptions of the approximate normal modes associated with each vibration are given in Table III. The assignment of vibrational modes of the isopropyl moiety was guided by the assignment of Klabe<sup>8</sup> for a series of isopropyl halides. Several of these modes were identifiable by their characteristic infrared band contours, notably  $\nu_8$  and  $\nu_{25}$ . Only the methyl rocking modes,  $\nu_{10}$ ,  $\nu_{12}$ , and  $\nu_{28}$ , and the methyl torsions,  $\nu_{18}$  and  $\nu_{32}$ , seemed to be coupled with vibrational modes of the phosphine group, as evidenced by their relatively large shift upon deuteration of the phosphine moiety.

The assignment of the P-H stretching modes centered near  $2300\text{ cm}^{-1}$  and P-D stretches near  $1660\text{ cm}^{-1}$  is of prime importance, since it is here that the presence of two conformers is readily apparent. Relatively high resolution spectra of these regions are shown in Figure 4. Using a reasonable geometry for both gauche and trans isopropylphosphine, the expected band types for the P-H stretching modes were calculated. Both the symmetric and antisymmetric stretches of the gauche conformer are expected to be mixed A/B/C hybrids, while the symmetric stretch for the trans conformer is predominantly C type. The antisymmetric P-H stretch should be a pure B-type for the trans conformer. Three sharp  $Q$  branches, 2299, 2297, and  $2288\text{ cm}^{-1}$ , were observed in the infrared spectrum of gaseous isopropylphosphine- $d_0$ , the two highest in frequency exhibiting overlapped, but easily discernible  $P$  and  $R$  branch contours. The lowest band was clearly of C type contour. This pattern was repeated in the deuterated species. The Raman spectra of gaseous isopropylphosphine- $d_0$  and - $d_2$  also exhibited three strong, sharp

Table I. Vibrational Frequencies and Assignments for Isopropylphosphine- $d_0$ 

Infrared Int. gas	Infrared Int. Solid	Raman Int. gas	Raman Int. Liquid	Raman Int. Solid	Assignment
2972 vs. sh	2972 s, sh	2972 s, sh	2962 s, sh	2954 vs. sh	$\nu_1$
2969 vs	2956 vs, brd	2969 vs	2962 s, sh	2954 vs. sh	$\nu_{19}$
2960 vs, w, brd	2947 vs, brd	2959 vs	2952 s	2946 vs	$\nu_2$
2954 vs					$\nu_{20}$
2938 s, sh	2937 vs, sh	2937 vs, sh	2922 vs	2920 s, brd	$\nu_6$
2932 s	2930 s	2931 vs	2905 s	2914 s, sh	$\nu_3$
2916 s, brd	2868 s	2915 vs	2900 s	2885 s, brd	$\nu_6 + \nu_7$
2895 s, sh	2883 s	2893 vs	2885 s, sh	2888 s	$\nu_2$
2875 s, sh	2850 vs	2875 vs	2865 vs	2865 vs	$\nu_4$
					$\nu_8$
2799 vs, sh		2767 m	2760 m	2760 m	$\nu_4$
		2728 m	2720 m	2710 m	$\nu_6$
		2729 vs, sh			$\nu_{22}$
2727 vs, sh	2728 vs, brd	2727 vs, sh	2728 vs, brd	2728 vs, brd	$\nu_5$ gauche
2728 vs, sh		2728 vs, sh			$\nu_5$ trans
1471 m, sh					$\nu_6 + \nu_{23}$
1465 m, brd	1461 s	1465 m, brd	1453 m, brd	1457 m, brd	$\nu_6 + \nu_{23}$
1451 m, sh	1449 s	1450 m, brd	1386 vs	1381 vs	$\nu_7$
1389 m, sh	1381 s				$\nu_8$
1372 m, brd	1363 s				$\nu_9$
1302 m, sh	1290 m	1304 m	1301 m	1301 m	$\nu_{29} + \nu_{16}$
1276 m, sh	1250 m	1255 m	1252 m	1250 m	$\nu_9$
1237 m, sh					$\nu_9$
1231 m, sh	1229 m	1234 m	1231 m, sh	1229 m	$\nu_{26}$
1164 m, sh	1159 m				$\nu_{27}$
1114 m	1112 m				$\nu_{27}$
1072 s	1070 vs	1071 m	1070 vs	1070 vs	$\nu_{10}$
1066 s	1061 vs	1067 m	1062 m	1062 m, sh	$\nu_{11}$
1050 m	1044 m				$\nu_{12}$
974 m	973 m				$\nu_{28}$
892 m	890 m	892 m	891 m	889 m	$\nu_9$
813 s	809 vs	813 m	810 m	807 m	$\nu_{13}$
791 s		792 m	788 m	782 m, sh	$\nu_{14}$ gauche
699 m	783 m				$\nu_{14}$ trans
627 m	623 m	628 m, sh	622 m, sh	623 m, sh	$\nu_{30}$
606 m	606 m	606 s	605 s	607 s	$\nu_{15}$ gauche
588 <sup>b</sup> m	590	585 m	596 s	595 s	$\nu_{15}$ trans
325 <sup>b</sup> m, sh	327 <sup>b</sup> m	325 m	327 m	327 m	$\nu_{16}$
322 <sup>b</sup> m, sh	322 <sup>b</sup> m, sh	322 m, sh	317 m, sh	314 m, sh	$\nu_{17}$
289 <sup>b</sup> m	291 <sup>b</sup> m	309 vs, sh	290 m	293 m	$\nu_{31}$ gauche
266 <sup>b</sup> m, brd	263 <sup>b</sup> m				$\nu_{31}$ trans
163 <sup>b</sup> s	163 <sup>b</sup> s	163 s, brd	163 s		$\nu_{32}$

Abbreviations used: s, strong; m, medium; w, weak; v, very; sh, shoulder; b, from the far infrared spectrum

Table II. Vibrational Frequencies and Assignments for Isopropylphosphine- $d_2$ 

Infrared Int. gas	Infrared Int. Solid	Raman Int. gas	Raman Int. Liquid	Raman Int. Solid	Assignment
2973 vs, sh	2973 s, sh	2973 s, sh	2962 s, sh	2954 vs. sh	$\nu_1$
2969 vs	2960 vs	2969 vs	2962 s, sh	2954 vs. sh	$\nu_{19}$
2960 vs, brd	2947 vs, brd	2959 vs	2952 s	2946 vs	$\nu_2$
2954 vs					$\nu_{20}$
2938 s, sh	2937 vs, sh	2937 vs, sh	2922 vs	2920 s, brd	$\nu_6$
2932 s	2930 s	2931 vs	2905 s	2914 s, sh	$\nu_3$
2916 s, brd	2868 s	2915 vs	2900 s	2885 s, brd	$\nu_6 + \nu_7$
2895 s, sh	2883 s	2893 vs	2885 s, sh	2888 s	$\nu_2$
2875 s, sh	2850 vs	2875 vs	2865 vs	2865 vs	$\nu_4$
					$\nu_8$
2799 vs, sh		2767 m	2760 m	2760 m	$\nu_4$
		2728 m	2720 m	2710 m	$\nu_6$
2727 vs, sh	2728 vs, brd	2727 vs, sh	2728 vs, brd	2728 vs, brd	$\nu_5$ gauche
2728 vs, sh		2728 vs, sh			$\nu_5$ trans
1471 m, sh					$\nu_6 + \nu_{23}$
1465 m, brd	1461 s	1465 m, brd	1453 m, brd	1457 m, brd	$\nu_6 + \nu_{23}$
1451 m, sh	1449 s	1450 m, brd	1386 vs	1381 vs	$\nu_7$
1389 m, sh	1381 s				$\nu_8$
1372 m, brd	1363 s				$\nu_9$
1302 m, sh	1290 m	1304 m	1301 m	1301 m	$\nu_{29} + \nu_{16}$
1276 m, sh	1250 m	1255 m	1252 m	1250 m	$\nu_9$
1237 m, sh					$\nu_9$
1231 m, sh	1229 m	1234 m	1231 m, sh	1229 m	$\nu_{26}$
1164 m, sh	1159 m				$\nu_{27}$
1114 m	1112 m				$\nu_{27}$
1072 s	1070 vs	1071 m	1070 vs	1070 vs	$\nu_{10}$
1066 s	1061 vs	1067 m	1062 m	1062 m, sh	$\nu_{11}$
1050 m	1044 m				$\nu_{12}$
974 m	973 m				$\nu_{28}$
892 m	890 m	892 m	891 m	889 m	$\nu_9$
813 s	809 vs	813 m	810 m	807 m	$\nu_{13}$
791 s		792 m	788 m	782 m, sh	$\nu_{14}$ gauche
699 m	783 m				$\nu_{14}$ trans
627 m	623 m	628 m, sh	622 m, sh	623 m, sh	$\nu_{30}$
606 m	606 m	606 s	605 s	607 s	$\nu_{15}$ gauche
588 <sup>b</sup> m	590	585 m	596 s	595 s	$\nu_{15}$ trans
325 <sup>b</sup> m, sh	327 <sup>b</sup> m	325 m	327 m	327 m	$\nu_{16}$
322 <sup>b</sup> m, sh	322 <sup>b</sup> m, sh	322 m, sh	317 m, sh	314 m, sh	$\nu_{17}$
289 <sup>b</sup> m	291 <sup>b</sup> m	309 vs, sh	290 m	293 m	$\nu_{31}$ gauche
266 <sup>b</sup> m, brd	263 <sup>b</sup> m				$\nu_{31}$ trans
163 <sup>b</sup> s	163 <sup>b</sup> s	163 s, brd	163 s		$\nu_{32}$

Table III. (continued)

Infrared Int. gas	Infrared Int. Solid	Raman Int. gas	Raman Int. Liquid	Raman Int. Solid	Assignment
1448 m, sh	1447 m, brd				$\nu_7$
1399 m, sh					$\nu_8$
1372 m, sh					$\nu_{25}$
1233 m, sh	1234 m	1230 m	1228 m, sh	1228 m	$\nu_9$ in form resonance
1281 m, sh	1282 m, sh	1281 m, sh	1278 m, sh	1278 m	$\nu_9$ with $\nu_{17} + \nu_{29}$
1225 m, brd	1225 m, sh	1225 m, sh	1226 m, sh	1226 m	$\nu_8$
1163 m, sh	1160 m	1163 m	1160 m	1160 m	$\nu_{27}$
1103 m	1101 m				$\nu_{10}$
1046 s	1047 m				$\nu_{12}$
1038 s, sh		1047 m	1044 m	1044 m	$\nu_{28}$
934 m					$\nu_{29}$
888 m		888 m	889 m	889 m	$\nu_{13}$
783 s, sh		783 s, sh			$\nu_{13}$
782 s, sh		784 m	789 m	789 m	$\nu_{11}$
669 m	570 s, sh				$\nu_{14}$
569 m	(385) <sup>c</sup> 381 m				$\nu_{14}$
511 <sup>b</sup> m, sh	(319) <sup>c</sup> 314 m				$\nu_{30}$
278 <sup>b</sup> m	(283) <sup>c</sup> 278 m, sh				$\nu_{16}$
266 <sup>b</sup> m	(261) <sup>c</sup>				$\nu_{16}$
126 <sup>b</sup> s	(140) <sup>c</sup> 135 m				$\nu_{32}$

Abbreviations used: s, strong; m, medium; w, weak; v, very; sh, shoulder; b, from the far infrared spectrum; sp, sharp; c, from the far infrared spectrum of the solid

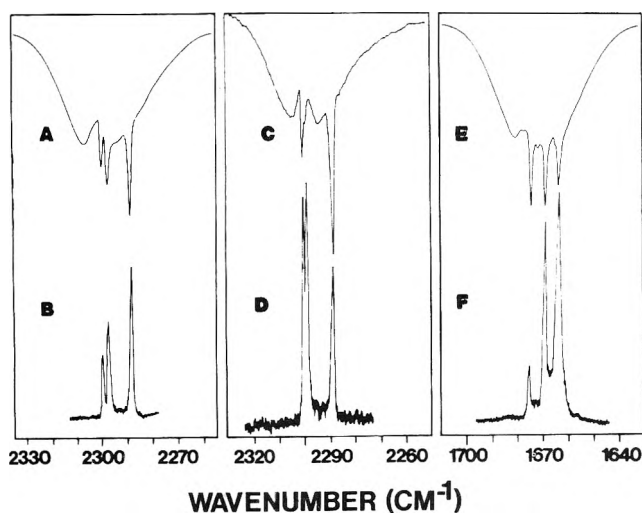


**Figure 4.** Mid-infrared and Raman spectra of the P-H and P-D stretching regions of gaseous  $(\text{CH}_3)_2\text{CHPH}_2$ ,  $(\text{CH}_3)_2\text{CHPHD}$ , and  $(\text{CH}_3)_2\text{CHPD}_2$ : (A) mid-infrared of isopropylphosphine- $d_0$ ,  $\text{PH}_2$  stretches; (B) Raman of isopropylphosphine- $d_0$ ,  $\text{PH}_2$  stretches; (C) mid-infrared of isopropylphosphine- $d_1$ ,  $\text{PH}$  stretches; (D) Raman of isopropylphosphine- $d_1$ ,  $\text{PH}$  stretches; (E) mid-infrared of isopropylphosphine- $d_2$ ,  $\text{PD}_2$  stretches; (F) Raman of isopropylphosphine- $d_2$ ,  $\text{PD}_2$  stretches.

bands in these regions with no evidence for a fourth band. From our previous studies,<sup>3</sup> we expected the trans antisymmetric stretch to be weak in the Raman spectra of the gas. Thus, the two higher  $Q$  branches can be assigned to  $\nu_{22}$  and  $\nu_5$ , respectively, of the gauche molecule, and the lower band

to  $\nu_5$  of the trans molecule. The B type of  $\nu_{22}$  for the trans species is apparently obscured by the other bands and has nominally been assigned as being degenerate with  $\nu_5$  of the trans species. Additional confirmation for this assignment can be seen in the P-H stretching region for isopropylphosphine- $d_1$ , present as an impurity in the  $d_2$  species. The two bands at 2300 and 2299  $\text{cm}^{-1}$  can be assigned to the two non-equivalent P-H stretches of the gauche molecule, and the band at 2288  $\text{cm}^{-1}$  to the P-H stretch for the trans molecule.

The strong infrared band at 1077  $\text{cm}^{-1}$  in the gas which shifts to 783  $\text{cm}^{-1}$  must be assigned as  $\nu_{11}$ , the  $\text{PH}_2$  scissoring mode. The double  $Q$  branch seen for this mode in the  $d_2$  species is probably attributable to different conformers. The two bands at 809 and 791  $\text{cm}^{-1}$  in the infrared spectrum of the gas which shifted to 615 and 661  $\text{cm}^{-1}$  can be assigned as  $\nu_{30}$ , the  $\text{PH}_2$  twisting mode, and  $\nu_{14}$ , the  $\text{PH}_2$  wagging mode, respectively. Considerable hot band structure was observed for  $\nu_{14}$  in both the  $d_0$  and  $d_2$  species.

The C-P stretching mode,  $\nu_{15}$ , which is quite strong in the Raman spectra and quite weak in the infrared spectra, has been assigned to the band to 606  $\text{cm}^{-1}$  in the spectra of the gas phase, shifting to 578  $\text{cm}^{-1}$  upon deuteration. An additional weaker feature near 627  $\text{cm}^{-1}$ , shifting to 569  $\text{cm}^{-1}$ , could be the C-P stretch of the conformer present in smaller abundance, but its assignment to the gauche conformer is unconfirmed. The C-C-C skeletal deformation,  $\nu_{16}$ , is assigned to the weak band at 388  $\text{cm}^{-1}$  in the far-infrared spectrum of the gas. The C-C-P in-plane and out-of-plane skeletal deformations,  $\nu_{17}$  and  $\nu_{31}$ , can be assigned to the bands at 325 and 322

TABLE III: Frequencies<sup>a</sup> (cm<sup>-1</sup>) and Approximate Descriptions of the Normal Modes of Isopropylphosphine

Description		(CH <sub>3</sub> ) <sub>2</sub> CHPH <sub>2</sub>	(CH <sub>3</sub> ) <sub>2</sub> CHPD <sub>2</sub>
A' ν <sub>1</sub>	CH <sub>3</sub> stretch antisymmetric, in-plane, in phase	2973	2973
ν <sub>2</sub>	CH <sub>3</sub> stretch antisymmetric, out-of-plane, in phase	2960	2960
ν <sub>3</sub>	CH stretch symmetric	2932	2932
ν <sub>4</sub>	CH <sub>3</sub> stretch symmetric, in phase	2875	2876
ν <sub>5</sub>	PH <sub>2</sub> stretch symmetric	2297 g 2288 t	1668 g 1663 t
ν <sub>6</sub>	CH <sub>3</sub> deformation antisymmetric, in-plane, in phase	1471	1468
ν <sub>7</sub>	CH <sub>3</sub> deformation antisymmetric, out-of-plane, in phase	1451	1448
ν <sub>8</sub>	CH <sub>3</sub> deformation symmetric, in phase	1389	1389
ν <sub>9</sub>	CH deformation, in plane	1256	≈ 1247
ν <sub>10</sub>	CH <sub>3</sub> rock in plane, in phase	1114	1103
ν <sub>11</sub>	PH <sub>2</sub> scissor	1077	784
ν <sub>12</sub>	CH <sub>3</sub> rock, out-of-plane, in phase	1066	1046
ν <sub>13</sub>	C-C stretch symmetric	892	888
ν <sub>14</sub>	PH <sub>2</sub> wag	813	661
ν <sub>15</sub>	C-P stretch	606	578
ν <sub>16</sub>	C-C-C deformation symmetric	388	380
ν <sub>17</sub>	C-C-P deformation, in plane	325	314
ν <sub>18</sub>	CH <sub>3</sub> torsion, in phase	287	278
A'' ν <sub>19</sub>	CH <sub>3</sub> stretch antisymmetric, in-plane, out of phase	2969	2869
ν <sub>20</sub>	CH <sub>3</sub> stretch antisymmetric, out-of-plane, out of phase	2954	2953
ν <sub>21</sub>	CH <sub>3</sub> stretch symmetric, out of phase	2895	2892
ν <sub>22</sub>	PH <sub>2</sub> stretch antisymmetric	2299 g 2288 t	1673.5 g 1663 t
ν <sub>23</sub>	CH <sub>3</sub> deformation antisymmetric, in-plane, out of phase	1471	1468
ν <sub>24</sub>	CH <sub>3</sub> deformation antisymmetric, out-of-plane, out of phase	1465	1462
ν <sub>25</sub>	CH <sub>3</sub> deformation symmetric, out of phase	1372	1372
ν <sub>26</sub>	CH deformation out of plane	1234	1225
ν <sub>27</sub>	C-C stretch antisymmetric	1164	1163
ν <sub>28</sub>	CH <sub>3</sub> rock, in plane, out of phase	1050	1038
ν <sub>29</sub>	CH <sub>3</sub> rock, in plane, out of phase	924	924
ν <sub>30</sub>	PH <sub>2</sub> twist	809	615
ν <sub>31</sub>	C-C-P deformation out of plane	322	314
ν <sub>32</sub>	CH <sub>3</sub> torsion out of phase	266	256
ν <sub>33</sub>	PH <sub>2</sub> torsion	163	125

<sup>a</sup> Frequencies given are taken from spectra of the gas phase, where possible.

cm<sup>-1</sup> in the far-infrared spectrum which shift to 314 cm<sup>-1</sup> upon deuteration.

#### Torsional Assignments and Barriers to Internal Rotation

The far-infrared spectra of gaseous isopropylphosphine-*d*<sub>0</sub> and -*d*<sub>2</sub> were examined carefully with the hope of observing bands assignable to the torsional modes of the methyl and phosphine groups. These spectra are shown in Figure 5. The two extremely weak bands centered at 287 and 266 cm<sup>-1</sup> in the *d*<sub>0</sub> species, and 278 and 256 cm<sup>-1</sup> in the *d*<sub>2</sub> species have been assigned as the a'' and a' methyl torsional vibrations, ν<sub>32</sub> and ν<sub>18</sub>, respectively. The band contours, an overlapped A/C hybrid and a B-type band, are consistent with such an assignment, especially if these motions tend to follow "local" C<sub>s</sub> symmetry in both conformers.

Möller and Andresen<sup>9</sup> have presented a theoretical treatment of the torsional vibrations in (CH<sub>3</sub>)<sub>2</sub>CHX type molecules and have expressed the potential function for such two-top molecules as a Fourier series in the two internal rotation angles α<sub>1</sub> and α<sub>2</sub>:

$$V(\alpha_1, \alpha_2) = (V_1/2)(1 - \cos 3\alpha_1) + (V_2/2)(1 - \cos 3\alpha_2) \\ + V_{12} \cos 3\alpha_1 \cos 3\alpha_2 + V_{12}' \sin 3\alpha_1 \sin 3\alpha_2 \\ + (V^*/2)(\cos 6\alpha_1 + \cos 6\alpha_2)$$

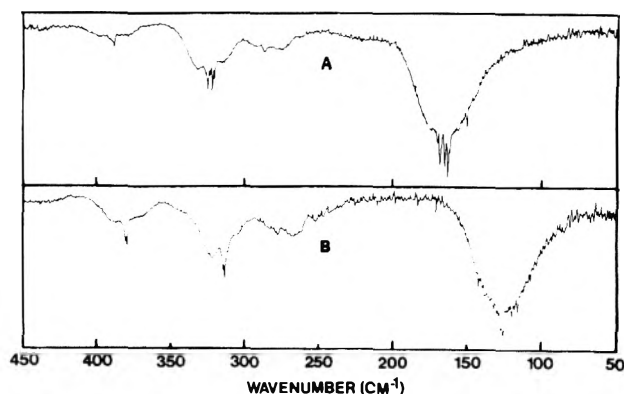


Figure 5. Far-infrared spectra of gaseous (CH<sub>3</sub>)<sub>2</sub>CHPH<sub>2</sub> and (CH<sub>3</sub>)<sub>2</sub>CHPD<sub>2</sub>: (A) isopropylphosphine-*d*<sub>0</sub>; (B) isopropylphosphine-*d*<sub>2</sub>.

If the two tops are symmetry equivalent, then it can be assumed that  $V_1$  is equal to  $V_2$  and the subscript dropped. Using the form of the energy Hamiltonian appropriate for the high barrier case and ignoring the  $V^*$  term, which is expected to be quite small, the following potential constant expressions may be evaluated in terms of the two 1 ← 0 torsional frequencies, ν<sub>+</sub> and ν<sub>-</sub>:

TABLE IV: Torsional Frequencies and Potential Constants for Isopropylphosphine- $d_0$  and - $d_2$ 

	$(\text{CH}_3)_2\text{CHPH}_2$	$(\text{CH}_3)_2\text{CHPD}_2$
$\nu_+(A')$ , $\text{cm}^{-1}$	287	278
$\nu_-(A'')$ , $\text{cm}^{-1}$	266	256
$F$ , $\text{cm}^{-1}$	5.418	5.410
$F'$ , $\text{cm}^{-1}$	-0.030	-0.026
$(V - 2V_{12})$ , kcal/mol	4.49	4.19
$V_{12}'$ , kcal/mol	0.16	0.18

TABLE V: Assumed Structure for Isopropylphosphine<sup>a,b</sup>

$r_{\text{P-H}}$	1.414 Å	$\angle\text{CCP}$	114°
$r_{\text{P-C}}$	1.863 Å	$\angle\text{HPH}$	93.5°
$r_{\text{C-C}}$	1.525 Å	$\angle\text{HCP}$	97.5°
$r_{\text{C-H}}$	1.093 Å	All other angles tetrahedral	

<sup>a</sup> The methyl groups are assumed to adopt a staggered configuration with respect to the methine hydrogen. <sup>b</sup> The  $\text{CH-PH}_2$  dihedral angle is taken as 0° for the trans conformer.

$$[V - 2V_{12}] = \frac{\nu_+^2}{18(F + F')} + \frac{\nu_-^2}{18(F - F')}$$

$$V_{12}' = \frac{\nu_+^2}{36(F + F')} - \frac{\nu_-^2}{36(F - F')}$$

where the symbols have their usual meanings.<sup>9,10</sup> In order to obtain an estimate of  $V$ , either of two simplifying assumptions may be used. In the first, the magnitude of  $V_{12}$  is assumed to be negligible with respect to  $V$  and is ignored. Another approach is to assume that the magnitude of  $V_{12}$  is approximately equal to  $V_{12}'$ . While there are no sound theoretical or experimental results to support either assumption, the first approach may be the best for the high barrier case.<sup>10</sup> The results of such calculations for the present system are given in Table IV.

The torsional mode associated with the phosphino group, however, did not lend itself to a straightforward analysis. While the band systems at 165 and 125  $\text{cm}^{-1}$  in the far-infrared spectra of the  $d_0$  and  $d_2$  species, respectively, are undoubtedly due to the  $\nu_{33}$  torsional vibration, several complications arise. The results of a calculation of the principal moments of inertia, using the structure shown in Table V, indicated that  $a''$  modes of the trans conformer are expected to have pure B-type contours, and therefore the band center for the torsional mode of this conformer would probably not be discernable when overlapped with its own hot band series and that of the gauche conformer. Similarly, in the Raman spectrum of the gas phase the trans torsion should show only a broad depolarized line. Thus, any sharp Q branches seen in either the Raman or infrared spectra assignable to the torsional mode can only belong to the gauche conformer.

The far-infrared spectrum of isopropylphosphine- $d_0$  exhibits at least four sharp peaks between 160 and 170  $\text{cm}^{-1}$  and several shoulders. If these bands are indeed the torsional hot band series, then the vibrational mode is only slightly anharmonic. On the basis of previous work,<sup>3</sup> we find this highly unlikely. The spectrum of the  $d_2$  species is considerably simpler and the  $\text{PD}_2$  torsional mode should be less coupled with other vibrations. Therefore an attempt was made to fit the data from the  $d_2$  species to a one-dimensional potential function similar to the one used for ethylphosphine.<sup>3</sup> From other work,<sup>10</sup> the trans conformer is expected to be slightly lower in energy than the gauche conformer and the  $1 \leftarrow 0$  torsional frequency of the trans conformer, therefore, slightly

TABLE VI: Observed Phosphino Torsional Frequencies, Assignments, and Potential Constants for Isopropylphosphine- $d_0$  and - $d_2$ 

Transition	$(\text{CH}_3)_2\text{CHPD}_2$		$(\text{CH}_3)_2\text{CHPH}_2$	
	Obsd	Calcd	Obsd	Calcd
Trans $1 \leftarrow 0$	132.5 <sup>a</sup>	132.5	173.0 <sup>a</sup>	173.0
Gauche $1 \leftarrow 0$	125.0	125.0	163.0	163.0
$2 \leftarrow 1$	119.5	119.5	156.0	156.0
Potential constant, $\text{cm}^{-1}$ <sup>b</sup>				
$V_2$	123		122	
$V_3$	826		861	
$V_6$	-12		-39	
$\Delta H$ , kcal/mol <sup>b</sup>	0.23		0.23	

<sup>a</sup> Estimated, see text. <sup>b</sup> Error estimates for the calculated potential constants obtained from the least-squares program are unreasonable in view of the number of approximations involved in the present problem.

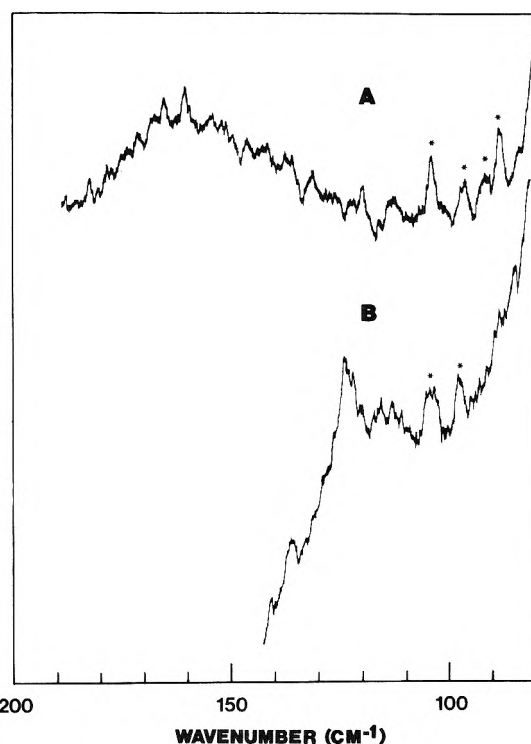


Figure 6. Raman spectra of gaseous  $(\text{CH}_3)_2\text{CHPH}_2$  and  $(\text{CH}_3)_2\text{CHPD}_2$  in the region of the phosphino torsional transitions (starred peaks are due to pure rotational transitions of  $\text{O}_2$  and  $\text{N}_2$ ): (A) isopropylphosphine- $d_0$ ; (B) isopropylphosphine- $d_2$ .

higher than the gauche frequency. A slight dip in the band contour at 132  $\text{cm}^{-1}$  was therefore estimated to be the center of the  $1 \leftarrow 0$  trans torsional vibration. The results of this calculation are shown in Table VI. Using this potential function to predict the  $d_0$  spectrum and taking the strongest band at 163  $\text{cm}^{-1}$  to be the gauche  $1 \leftarrow 0$ ; similar calculations gave the results also shown in Table VI. Once again, the center of the trans  $1 \leftarrow 0$  transition was estimated to be near 173  $\text{cm}^{-1}$ . Raman spectra of gaseous isopropylphosphine- $d_0$  and - $d_2$  in the region of the  $\text{PH}_2$  torsional vibration, shown in Figure 6, reinforce our assignment of the gauche transitions but do not yield any additional information. The extra bands seen in the spectra of isopropylphosphine- $d_0$  could be due to a perturbation imposed by potential or kinetic coupling of the phos-

phino torsional mode with other vibrations, notably the C-C-P skeletal bending modes near  $325\text{ cm}^{-1}$ . It should also be pointed out that difference bands between these bending modes and the torsional vibrations in the  $d_0$  species will fall directly in the  $\text{PH}_2$  torsional region. Two of the bands, at  $170$  and  $150\text{ cm}^{-1}$ , may be due to pure rotational transitions of water which were incompletely removed by the spectrometer system's "spectral subtraction" routines.

### Discussion

The vibrational assignment of molecules such as isopropylphosphine is of necessity somewhat ambiguous, in view of the large number of vibrational modes and the complexity introduced by the presence of two different molecular conformations. The low symmetry of the gauche conformer,  $C_{1s}$ , also prevented the use of Raman depolarization data as an aid in the assignment. Calculation of the Teller-Redlich product rule on the basis of  $C_s$  symmetry using the present assignment gave good results. The products for neither symmetry block exceeded the theoretical amount by more than 2%. The study of additional isotopic species, especially the  $(\text{CH}_3)_2\text{CDPH}_2$  compound, would be necessary to refine the vibrational assignment. The authors feel, however, that such an extension would probably not be valuable at this time.

The barriers to internal rotation of the methyl groups are in good agreement with those found by Durig et al.<sup>11</sup> in a series of isopropyl compounds and show the expected upward trend when compared to the methyl torsional barriers found in ethylphosphine.<sup>3</sup>

Clearly the problem of significant interest in this study is the determination of the more stable molecular conformation. The analysis of the P-H and P-D stretching vibrations clearly indicates that at least two conformations are present in the fluid phases. Furthermore, a consideration of the relative intensities of these bands would indicate that the relative abundances of the two conformations are not widely different. The results of the potential function determination for the phosphino torsional mode, while not definitive, indicate that the approximate energy difference between the two forms,  $0.26\text{ kcal/mol}$ , roughly cancels the statistical factor of two

which favors the gauche conformer, leading to a gauche to trans abundance ratio of about one. Krueger and Jan<sup>12</sup> determined the energy difference in  $(\text{CH}_3)_2\text{CDNH}_2$  between the gauche and trans forms to be  $0.12\text{ kcal/mol}$ . They attributed the increased stability of the trans form to partial electron overlap between the carbon  $\sigma^*$  orbital and the lone pair orbital, generating some double bond character in the C-N bond. Whether such an effect is present in isopropylphosphine, or that the stabilization of the trans form is due to electrostatic interactions between bond pairs and lone pairs, cannot be determined without further studies of similar molecules.

*Acknowledgment.* The authors gratefully acknowledge the financial support given this work by the National Aeronautics and Space Administration through Grant No. NGL-41-002-003. Acknowledgment is also given to the National Science Foundation for funds to purchase the Digilab FTS-15B interferometer by Grant No. MPS-75-06926.

*Miniprint Material Available:* Full-sized photocopies of the miniprinted material (Tables I and II, 4 pages). Ordering information is available on any current masthead page.

### References and Notes

- (1) For part 15, see J. R. Durig and A. W. Cox, Jr., *J. Chem. Phys.*, **64**, 1930 (1976); (b) Taken in part from the thesis of A. W. Cox, Jr., to be submitted to the Department of Chemistry in partial fulfillment of the requirements of the Ph.D. Degree.
- (2) J. R. Durig and J. E. Saunders, *J. Raman Spectrosc.*, **4**, 121 (1975).
- (3) J. R. Durig and A. W. Cox, Jr., *J. Chem. Phys.*, **64**, 1930 (1976).
- (4) J. R. Durig and J. E. Saunders, *J. Mol. Struct.*, **21**, 403 (1975).
- (5) J. R. Durig and A. W. Cox, Jr., *J. Chem. Phys.*, **63**, 2303 (1975).
- (6) J. R. Durig and R. W. MacNamee, *J. Mol. Struct.*, **17**, 426 (1973).
- (7) J. B. Reesor, B. J. Perry, and E. Sherlock, *Can. J. Chem.*, **38**, 1416 (1960).
- (8) P. Kläboe, *Spectrochim. Acta, Part A*, **26**, 87 (1970).
- (9) K. D. Möller and H. G. Andreson, *J. Chem. Phys.*, **37**, 1800 (1962); K. D. Möller, A. R. DeMeo, D. R. Smith, and L. H. London, *ibid.*, **47**, 2609 (1967).
- (10) J. R. Durig, S. M. Craven, and W. C. Harris, "Vibrational Spectra and Structure", Vol. 1, J. R. Durig, Ed., Marcel Dekker, New York, N.Y., 1972, Chapter 4, pp 73-179.
- (11) J. R. Durig, C. M. Player, Jr., Y. S. Li, J. Bragin, and C. W. Hawley, *J. Chem. Phys.*, **57**, 4544 (1972).
- (12) P. J. Krueger and J. Jan, *Can. J. Chem.*, **48**, 3229 (1970).

## Efficiency of the Intersystem Crossing from the Lowest Spin-Allowed to the Lowest Spin-Forbidden Excited State of Some Chromium(III) and Ruthenium(II) Complexes

F. Bolletta,\* M. Maestri, and V. Balzani

Istituto Chimico "G. Ciamician" dell'Università, 40126 Bologna, Italy (Received April 27, 1976)

The intersystem crossing efficiency ( $\eta_i$ ) from the lowest spin-allowed to the lowest spin-forbidden excited state of some Cr(III) and Ru(II) complexes has been obtained using a method based on the electronic energy transfer technique from an emitting donor to an emitting acceptor. The following donor/acceptor couples were studied in water and/or DMF solution at room temperature: Ru(phen)<sub>3</sub><sup>2+</sup>/t-Cr(en)<sub>2</sub>(NCS)<sub>2</sub><sup>+</sup>, Ru(bpy)<sub>3</sub><sup>2+</sup>/t-Cr(en)<sub>2</sub>(NCS)<sub>2</sub><sup>+</sup>, Ru(bpy)<sub>3</sub><sup>2+</sup>/Cr(CN)<sub>6</sub><sup>3-</sup>, Ru(bpy)<sub>2</sub>(CN)<sub>2</sub>/Cr(en)<sub>3</sub><sup>3+</sup>, Ru(bpy)<sub>2</sub>(CN)<sub>2</sub>/t-Cr(en)<sub>2</sub>(NCS)<sub>2</sub><sup>+</sup>, Cr(bpy)<sub>3</sub><sup>3+</sup>/Cr(CN)<sub>6</sub><sup>3-</sup>, Cr(phen)<sub>3</sub><sup>3+</sup>/Cr(CN)<sub>6</sub><sup>3-</sup>, t-Cr(en)<sub>2</sub>(NCS)<sub>2</sub><sup>+</sup>/Cr(CN)<sub>6</sub><sup>3-</sup>, and biacetyl/Cr(bpy)<sub>3</sub><sup>3+</sup>. For each one of these couples, energy transfer is energy and spin allowed and it does take place as is shown by the occurrence of a sensitized emission of the acceptor. Conversely, electron transfer is thermodynamically unfavorable except that for the couple involving biacetyl. Using Ru(bpy)<sub>3</sub><sup>2+</sup> ( $\eta_i = 1$ ) and biacetyl ( $\eta_i = 0.86$ ) as primary standard and assuming that the energy transfer efficiency is unity, the following values have been obtained for the intersystem crossing efficiency of the various complexes: Cr(CN)<sub>6</sub><sup>3-</sup>, 0.5; t-Cr(en)<sub>2</sub>(NCS)<sub>2</sub><sup>+</sup>, 0.4; Cr(phen)<sub>3</sub><sup>3+</sup>, 0.2; Cr(bpy)<sub>3</sub><sup>3+</sup>, 1.0; Cr(en)<sub>3</sub><sup>3+</sup>, 0.7; Ru(bpy)<sub>2</sub>(CN)<sub>2</sub>, 1.0; Ru(phen)<sub>3</sub><sup>2+</sup>, 0.65. The values obtained for the Cr(III) complexes are briefly discussed. A convenient experimental procedure for this type of experiments is reported.

### Introduction

The photochemical<sup>1-3</sup> and photophysical<sup>3-7</sup> properties of transition metal complexes have been the object of extensive investigations in the past decade. With a few exceptions, photophysical measurements have been made in rigid glasses at 77 K or in the solid state, i.e., under conditions which are completely different from those used for the photochemical investigations. Since temperature and environmental effects can strongly influence the rate of the nonradiative deactivation processes,<sup>4-7</sup> the results obtained from rigid glasses or solid samples cannot be used to infer photochemical mechanisms in fluid solution. Further progress in the photochemistry of transition metal complexes depends on the collection of photophysical data under photochemically important conditions. A particular important quantity for elucidating the photochemical behavior of a molecule is the intersystem crossing efficiency from the lowest spin-allowed to the lowest spin-forbidden excited state,  $\eta_i$ .<sup>8,9</sup> In fluid solution, this quantity has been measured for a number of organic molecules,<sup>10-13</sup> but only for a few transition metal complexes.<sup>14-16</sup> In this work, we have measured  $\eta_i$  for some luminescent Cr(III) and Ru(II) complexes in fluid solution at room temperature. The method used is based on the electronic energy transfer technique.

### Experimental Section

**Materials.** Tetra-*n*-butylammonium hexacyanochromate(III), (NBu<sub>4</sub>)<sub>3</sub>[Cr(CN)<sub>6</sub>], tris(ethylenediamine)chromium(III) chloride dihydrate, [Cr(en)<sub>3</sub>]Cl<sub>3</sub>·2H<sub>2</sub>O, *trans*-dithiocyanatobis(ethylenediamine)chromium(III) perchlorate, *trans*-[Cr(en)<sub>2</sub>(NCS)<sub>2</sub>](ClO<sub>4</sub>), tris(2,2'-bipyridine)chromium(III) perchlorate hemihydrate, [Cr(bpy)<sub>3</sub>](ClO<sub>4</sub>)<sub>3</sub>·0.5H<sub>2</sub>O, tris(1,10-phenanthroline)chromium(III) perchlorate dihydrate, [Cr(phen)<sub>3</sub>](ClO<sub>4</sub>)<sub>3</sub>·2H<sub>2</sub>O, tris(2,2'-bipyridine)ruthenium(II) chloride hexahydrate, [Ru(bpy)<sub>3</sub>]Cl<sub>2</sub>·6H<sub>2</sub>O, tris(1,10-phenanthroline)ruthenium(II) perchlorate, [Ru-

(phen)<sub>3</sub>](ClO<sub>4</sub>)<sub>2</sub>, and *cis*-dicyanobis(2,2'-bipyridine)ruthenium(II) dihydrate, *cis*-Ru(bpy)<sub>2</sub>(CN)<sub>2</sub>·2H<sub>2</sub>O, were prepared and purified as indicated in the literature. Biacetyl (Fluka puriss) was vacuum distilled before use. Dimethylformamide (DMF) Baker Instra-Analyzed was used. The other chemicals used were of reagent grade.

**Apparatus.** Emission intensity measurements were performed with a Perkin-Elmer MPF-3 spectrofluorimeter, using a R446 photomultiplier tube. Emission lifetime shorter than 1  $\mu$ s were measured by means of a modified Applied Photophysics apparatus which is based on the single photon counting technique. The solutions were irradiated at 337 nm with a thyratron gated air flash lamp (repetition rate 20 kHz). The pulses had a full-width at half-height of 3.0 ns. Both exciting and emitted light beams were filtered by means of grating monochromators. The performance of the single photon counting equipment was checked by measuring the emission lifetime of rhodamine B; the value of 3.3 ns measured with this apparatus is in good agreement with the literature value of 3.2 ns.<sup>17</sup> Approximate values of emission lifetimes longer than 1  $\mu$ s were obtained with an apparatus previously described.<sup>18</sup>

**Procedure.** All of the experiments were carried out at room temperature (~20 °C). When necessary, deaeration of the solution was obtained by bubbling pure nitrogen. Emission measurements were made with 1-cm cells. Right angle or frontal illumination were used, depending on the optical density of the solution. When necessary, the ionic strength was adjusted to 0.1 M with NH<sub>4</sub>Cl to avoid ion pair formation between donor and acceptor. For the experiments with Cr(en)<sub>3</sub><sup>3+</sup> and Cr(bpy)<sub>3</sub><sup>3+</sup> the solutions were slightly acidified (pH ~3) in order to minimize thermal aquation.<sup>19,20</sup>

### Results

Preliminary experiments showed that for each one of the donor-acceptor couples listed in Table I excitation of the donor caused a sensitized emission from the acceptor. No

TABLE I: Experimental Conditions and Results

Donor-acceptor	$\lambda_{\text{exc.}}^a$ nm	$\lambda_D^b$ nm	$\lambda_A^c$ nm	[D] <sup>d</sup>	[A] <sup>d</sup>	$\tau_D^e$ $\mu\text{s}$	Medium <sup>f</sup>	R <sup>g</sup>
Biacetyl-Cr(bpy) <sub>3</sub> <sup>3+</sup>	405	510	727	$2.0 \times 10^{-1}$ – $2.25 \times 10^{-1}$	$1.0 \times 10^{-4}$ – $2.0 \times 10^{-4}$	145 <sup>h</sup>	H <sub>2</sub> O <sup>i</sup>	1.1(4)
Ru(phen) <sub>3</sub> <sup>2+</sup> – Cr(en) <sub>2</sub> (NCS) <sub>2</sub> <sup>+</sup>	450	600	727	$1.4 \times 10^{-5}$	$5.9 \times 10^{-3}$	0.457	H <sub>2</sub> O	0.63(2)
Ru(bpy) <sub>3</sub> <sup>2+</sup> –Cr(en) <sub>2</sub> (NCS) <sub>2</sub> <sup>+</sup>	355	600	727	$6.75 \times 10^{-5}$	$7.5 \times 10^{-3}$	0.400	H <sub>2</sub> O	0.40(1)
Ru(bpy) <sub>3</sub> <sup>2+</sup> –Cr(en) <sub>2</sub> (NCS) <sub>2</sub> <sup>+</sup>	450	600	727	$1.3 \times 10^{-5}$ – $2.6 \times 10^{-5}$	$9.2 \times 10^{-3}$ – $1.2 \times 10^{-2}$	0.400	H <sub>2</sub> O	0.43(6)
Ru(bpy) <sub>3</sub> <sup>2+</sup> –Cr(en) <sub>2</sub> (NCS) <sub>2</sub> <sup>+</sup>	450	600	727	$1.3 \times 10^{-5}$ – $2.6 \times 10^{-5}$	$9.2 \times 10^{-3}$ – $1.2 \times 10^{-2}$	0.182	DMF	0.42(3)
Ru(bpy) <sub>3</sub> <sup>2+</sup> –Cr(CN) <sub>6</sub> <sup>3-</sup>	400	600	800	$3.9 \times 10^{-5}$	$1.0 \times 10^{-4}$	0.182	DMF <sup>j</sup>	0.56(4)
Ru(bpy) <sub>2</sub> (CN) <sub>2</sub> –Cr(en) <sub>3</sub> <sup>3+</sup>	400	600	670	$2.5 \times 10^{-5}$ – $5.0 \times 10^{-5}$	$2.0 \times 10^{-2}$ – $3.0 \times 10^{-2}$	0.175	H <sub>2</sub> O <sup>i</sup>	0.71(2)
Ru(bpy) <sub>2</sub> (CN) <sub>2</sub> – Cr(en) <sub>2</sub> (NCS) <sub>2</sub> <sup>+</sup>	430	600	727	$1.8 \times 10^{-5}$ – $2.8 \times 10^{-5}$	$6.2 \times 10^{-3}$ – $7.1 \times 10^{-3}$	0.175	H <sub>2</sub> O	0.43(3)
Ru(bpy) <sub>2</sub> (CN) <sub>2</sub> – Cr(en) <sub>2</sub> (NCS) <sub>2</sub> <sup>+</sup>	370	650	727	$4.7 \times 10^{-5}$ – $1.4 \times 10^{-4}$	$1.1 \times 10^{-2}$ – $1.6 \times 10^{-2}$	0.088	DMF	0.39(3)
Cr(bpy) <sub>3</sub> <sup>3+</sup> –Cr(CN) <sub>6</sub> <sup>3-</sup>	310	727	800	$4.0 \times 10^{-6}$ – $1.0 \times 10^{-5}$	$4.25 \times 10^{-3}$ – $6.8 \times 10^{-3}$	~10	H <sub>2</sub> O–DMF <sup>k</sup>	0.55(6)
Cr(phen) <sub>3</sub> <sup>3+</sup> –Cr(CN) <sub>6</sub> <sup>3-</sup>	310	727	800	$6.7 \times 10^{-6}$	$3.5 \times 10^{-3}$	~20	H <sub>2</sub> O–DMF <sup>k</sup>	2.5(3)
Cr(en) <sub>2</sub> (NCS) <sub>2</sub> <sup>+</sup> –Cr(CN) <sub>6</sub> <sup>3-</sup>	320	727	800	$8.1 \times 10^{-5}$	$1.5 \times 10^{-3}$	~10	DMF	1.2(4)

<sup>a</sup> Excitation wavelength. <sup>b</sup> Wavelength used for monitoring the donor emission. <sup>c</sup> Wavelength used for monitoring the acceptor emission. <sup>d</sup> Concentration (or range of concentrations) in the solution(s) containing both D and A. <sup>e</sup> Lifetime of the donor emitting state in air-equilibrated solution. <sup>f</sup> Natural pH and ionic strength, unless otherwise noted. <sup>g</sup> See eq 3; the value reported is the average obtained from different experiments whose number is shown in parentheses. <sup>h</sup> P. Bortolus and S. Dellonte, *J. Chem. Soc., Faraday Trans. 2*, 338 (1975); deaerated solution. <sup>i</sup> pH ~3. <sup>j</sup>  $\mu = 0.1$  adjusted with NH<sub>4</sub>Cl. <sup>k</sup> 1:3 v/v;  $\mu = 0.1$  adjusted with NH<sub>4</sub>Cl.

sensitized emission but spectral evidence of chemical interaction between donor and acceptor was obtained for biacetyl–Cr(CN)<sub>6</sub><sup>3-</sup> (in DMF), biacetyl–Cr(en)<sub>2</sub>(NCS)<sub>2</sub><sup>+</sup> (in water or DMF), and biacetyl–Ru(bpy)<sub>3</sub><sup>2+</sup> (in H<sub>2</sub>O); these couples were then discarded. The Ru(bpy)<sub>3</sub><sup>2+</sup>–Cr(bpy)<sub>3</sub><sup>3+</sup> couple was discarded because it is known to give an electron transfer reaction.<sup>21</sup> By analogy, the couples involving biacetyl as a donor and the Ru(II) complexes as acceptors, and the Ru(II) complexes as donors and Cr(bpy)<sub>3</sub><sup>3+</sup> or Cr(phen)<sub>3</sub><sup>3+</sup> as acceptors were also discarded.

For each experiment on a selected donor-acceptor couple, three different solutions were prepared which contained (i) the donor (D) alone, (ii) the acceptor (A) alone, and (iii) known concentrations of donor and acceptor. The optical densities of the three solutions, OD<sub>D</sub><sup>0</sup>, OD<sub>A</sub><sup>0</sup>, and OD<sub>DA</sub> = OD<sub>D</sub> + OD<sub>A</sub> were equal to one another at a selected wavelength (excitation wavelength,  $\lambda_{\text{exc}}$ ) and for solution (iii) the fraction of incident light absorbed by D and A was also known:<sup>22</sup>

$$\alpha_D = \frac{\text{OD}_D}{\text{OD}_D + \text{OD}_A} = \frac{\text{OD}_D}{\text{OD}_{D^0}} \quad (1)$$

$$\alpha_A = \frac{\text{OD}_A}{\text{OD}_D + \text{OD}_A} = \frac{\text{OD}_A}{\text{OD}_{A^0}} \quad (2)$$

The following quantities were then measured upon excitation at  $\lambda_{\text{exc}}$ :  $E_D^0$  = emission intensity of solution i (donor alone) at wavelength  $\lambda_D$  that corresponds to the emission maximum of the donor;  $E_A^0$  = emission intensity of solution ii (acceptor alone) at wavelength  $\lambda_A$  that corresponds to the emission maximum of the acceptor;  $E_{D'}$  = emission intensity of solution iii (donor plus acceptor) at  $\lambda_D$ ;  $E_{A'}$  = emission intensity of solution iii at  $\lambda_A$ . The excitation and emission wavelengths for the various donor-acceptor couples and the other experimental conditions are reported in Table I.

The values of  $E_D^0$ ,  $E_A^0$ ,  $E_{D'}$ ,  $E_{A'}$ ,  $\alpha_D$ , and  $\alpha_A$  obtained from each experiment were used to calculate  $R$  (see also eq 12):

$$R = \frac{E_{A^0}}{E_{A'} - \alpha_A E_{A^0}} \left( \alpha_D - \frac{E_{D'}}{E_{D^0}} \right) \quad (3)$$

The reproducibility of the  $R$  values was better than 10%.

It is known that static quenching can take place when the

donor and acceptor have opposite charge and the complex concentration is sufficiently high.<sup>3</sup> The comparison between lifetime and intensity quenching of the donor emission showed that no static quenching occurred under our experimental conditions.

## Discussion

*Method.* In order to discuss the results obtained, we will make reference to the scheme shown in Figure 1. In that scheme,  $k_1$  is the rate constant of the nonradiative deactivation of the spin-allowed (SA) excited state to the ground state (G),  $k_2$  and  $k_3$  are the rate constant of the radiative and non-radiative deactivation of the spin-forbidden (SF) excited state,  $k_i$  is the SA  $\rightarrow$  SF intersystem crossing rate constant,  $k_{et}$  is the rate constant of energy transfer from SF(D) to SF(A), and  $k_4$  is the rate constant of the quenching of SF(D) by the acceptor via mechanisms that do not involve the formation of an electronically excited acceptor. Quenching of the SA excited states is not taken into consideration since the lifetime of these states is known to be at least four orders of magnitude lower than the lifetime of the SF excited states.<sup>4–7,23–26</sup> Back intersystem crossing from SF to SA is not taken into consideration because, although it is not negligible for some of the complexes used, its occurrence does not modify the results of our treatment (see below). Finally, back electronic energy transfer<sup>27</sup> from the acceptor to the donor did not occur under our experimental conditions.<sup>28</sup>

Using the scheme shown in Figure 1, it can be shown<sup>3</sup> that the emission intensity  $E_A^0$  of the acceptor alone (solution ii) and the sensitized emission intensity  $E_{A^s}$  of the acceptor in solution iii are given by

$$E_A^0 \propto I_A^0 \eta_i^A \eta_2^A \quad (4)$$

$$E_{A^s} \propto I_D \eta_i^D \eta_{et}' \eta_2^A \quad (5)$$

where  $I_A^0$  is the light intensity absorbed by solution ii,  $I_D$  is the light intensity absorbed by the donor in solution iii,  $\eta_i^A = k_i^A / (k_i^A + k_1^A)$  and  $\eta_i^D = k_i^D / (k_i^D + k_1^D)$  are the efficiencies of the SA  $\rightarrow$  SF intersystem crossing steps in the acceptor and donor,  $\eta_2^A = k_2^A / (k_2^A + k_3^A)$  is the efficiency of the emission from the SF excited state of the acceptor, and  $\eta_{et}'$  is the energy

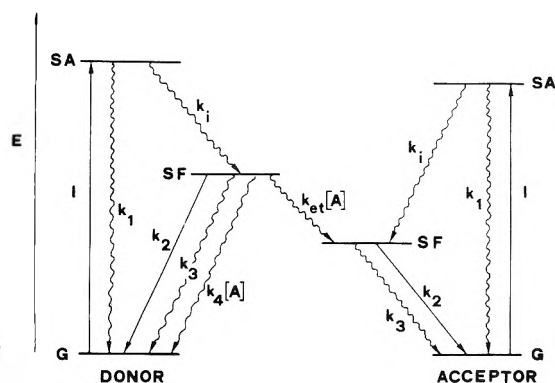


**Figure 1.** Schematic diagram showing the steps that are relevant to the discussion of electronic energy transfer from a donor to an acceptor: G = ground state; SA = lowest spin-allowed excited state; SF = lowest spin-forbidden excited state. For more details, see text.

transfer efficiency from the SF excited state of the donor to the SF excited state of the acceptor:

$$\eta_{et}' = \frac{k_{et}^D[A]}{k_2^D + k_3^D + (k_{et}^D + k_4^D)[A]} \quad (6)$$

Using the term  $k_q^D$  in place of  $k_{et}^D + k_4^D$ , the energy transfer efficiency can be expressed as follows:

$$\eta_{et}' = \frac{k_q^D[A]}{k_2^D + k_3^D + k_q^D[A]} \frac{k_{et}^D}{k_q^D} = \eta_q \eta_{et} \quad (7)$$

where  $\eta_q$  represents the quenching efficiency of SF(D) by ground state A, and  $\eta_{et}$  represents the (limiting) energy transfer efficiency, i.e., the fraction of quenching events that cause the formation of the excited acceptor.<sup>3</sup> As the emission intensity measurements were carried out under the same instrumental conditions, the proportionality constants in eq 4 and 5 are the same, so that we can write

$$\frac{E_A^0}{E_A^s} = \frac{I_A^0 \eta_i^A}{I_D \eta_i^D \eta_q \eta_{et}} \quad (8)$$

Now, it can be easily shown that

$$E_A^s = E_A' - \alpha_A E_A^0 \quad (9)$$

$$I_D = \alpha_D I_A^0 \quad (10)$$

$$\eta_q = \left(1 - \frac{E_D'}{\alpha_D E_D^0}\right) \quad (11)$$

It should be noted that eq 9 holds only when the donor emission is negligible at the wavelength used for measuring the acceptor emission ( $\lambda_A$ ). When this was not the case, the total emission at  $\lambda_A$  was corrected for the contribution from the donor. With regard to eq 11, it can be shown that if back intersystem crossing from SF(D) to SA(D) is not negligible, the formulation of  $\eta_q$  (see eq 7) changes but eq 11 is still valid. Upon substitution of eq 9, 10, and 11 into eq 8, one obtains

$$\frac{\eta_i^A}{\eta_i^D} \frac{1}{\eta_{et}} = \frac{E_A^0}{E_A' - \alpha_A E_A^0} \left(\alpha_D - \frac{E_D'}{E_D^0}\right) = R \quad (12)$$

As  $R$  is an experimentally measured quantity (Table I), the ratio  $\eta_i^A/\eta_i^D \eta_{et}$  can be obtained for each donor-acceptor couple.

It should be noted that eq 12 holds when the excitation leads to the lowest spin-allowed excited state (Figure 1), as it was the case for most of our experiments (see Table I and Figure 2). If upper excited states are populated upon excitation, the term  $\eta_i^A/\eta_i^D \eta_{et}$  in eq 12 has to be multiplied by the

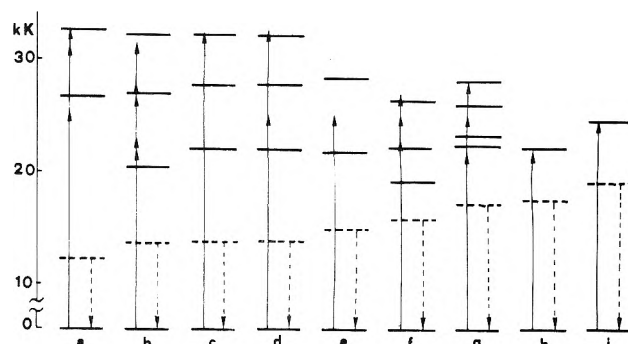


**Figure 2.** Schematic energy level diagram: a,  $\text{Cr}(\text{CN})_6^{3-}$ ; b,  $\text{Cr}(\text{en})_2(\text{NCS})_2^+$ ; c,  $\text{Cr}(\text{phen})_3^{3+}$ ; d,  $\text{Cr}(\text{bpy})_3^{3+}$ ; e,  $\text{Cr}(\text{en})_3^{3+}$ ; f,  $\text{Ru}(\text{bpy})_2(\text{CN})_2$ ; g,  $\text{Ru}(\text{bpy})_3^{2+}$ ; h,  $\text{Ru}(\text{phen})_3^{2+}$ ; i, biacetyl. Full lines = spin-allowed excited states; dashed lines = spin-forbidden excited states; full arrows = exciting light; dashed arrows = emitted light.

**TABLE II: Reduction Potentials<sup>a</sup>**

Complex <sup>b</sup>	A <sup>+</sup> /A	D <sup>+</sup> / <sup>*</sup> D <sup>c</sup>	A/A <sup>-</sup>	<sup>*</sup> D/D <sup>-c</sup>
$\text{Ru}(\text{phen})_3^{2+}$	$\sim +1.30^d$	$\sim -0.88^e$	$(-1.14)^f$	$(+1.04)^e$
$\text{Ru}(\text{bpy})_3^{2+}$	$+1.27^g$	$-0.83^h$	$-1.28^h$	$+0.84^h$
$\text{Ru}(\text{bpy})_2(\text{CN})_2$	$+1.09^i$	$\sim -0.87^j$	$-1.30^i$	$\sim +0.6^j$
$\text{Cr}(\text{en})_3^{3+}$	$(\gg +1)^k$		$\sim -1.1^l$	
$\text{Cr}(\text{bpy})_3^{3+}$	$(> +1.6)^m$	$(> -0.1)^n$	$-0.25^o$	$+1.46^{n,p}$
$\text{Cr}(\text{phen})_3^{3+}$	$(> +1.6)^k$	$(> -0.1)^n$	$-0.25^q$	$+1.46^n$
$\text{Cr}(\text{en})_2(\text{NCS})_2^+$	$(\gg +1)^k$	$(> -0.7)^r$	$(\sim -0.9)^s$	$(\sim +0.8)^r$
$\text{Cr}(\text{CN})_6^{3-}$	$(> +1.6)^m$		$-1.28^t$	

<sup>a</sup> In volts, relative to the NHE; in water at 25 °C unless otherwise noted. <sup>b</sup> In the other columns, each complex is indicated with A or D depending on whether it acts as an acceptor or donor in eq 14 and 15 of the text. <sup>c</sup> These values have been obtained by adding the excited state energy to the reduction potential of the corresponding couple involving the ground state. This assumption is reasonable when the excited state, as happens in our cases, is not very distorted compared with the ground state. <sup>d</sup> D. A. Buckingham and A. M. Sargeson in "Chelating Agents and Metal Chelates", F. P. Dwyer and D. P. Mellor, Ed., Academic Press, New York, N.Y., 1964, p 237. <sup>e</sup> Excited state energy = 2.18 eV, ref 32. <sup>f</sup> From the  $E_p$  value in acetonitrile: N. E. Tokel-Takvoryan, R. E. Hemingway, and A. J. Bard, *J. Am. Chem. Soc.*, **95**, 6582 (1973). <sup>g</sup> F. E. Lytle and D. M. Hercules, *Photochem. Photobiol.*, **13**, 123 (1971). <sup>h</sup> C. Creutz and N. Sutin, *Inorg. Chem.*, **15**, 496 (1976). <sup>i</sup> In DMF: S. Roffia and M. Ciano, *J. Electroanal. Chem.*, in press. <sup>j</sup> Excited state energy  $\sim 1.96$  eV, in DMF; in water the excited state energy is slightly higher ( $\sim 2.1$  eV); see also ref 32. <sup>k</sup> By analogy with  $\text{Cr}(\text{CN})_6^{3-}$  and  $\text{Cr}(\text{bpy})_3^{3+}$ . <sup>l</sup> J. E. Earley and R. D. Cannon, *Transition Metal Chem.*, **1**, 33 (1965). <sup>m</sup> Electroinactive up to the indicated potential at the platinum electrode in DMF. <sup>n</sup> Excited state energy = 1.71 eV; N. A. Kane-Maguire, J. Conway, and C. H. Langford, *J. Chem. Soc., Chem. Commun.*, 801 (1974). <sup>o</sup> R. D. Baker and D. Mehta, *Inorg. Chem.*, **4**, 848 (1965). <sup>p</sup> Reference 21. <sup>q</sup> D. M. Soignet and L. G. Hargis, *Inorg. Chem.*, **14**, 941 (1975). <sup>r</sup> Excited state energy = 1.70 eV, ref 4. <sup>s</sup>  $E_{1/2} \sim -0.93$  V in acetonitrile: Y. Sato and N. Tanaka, *Bull. Chem. Soc. Jpn.*, **42**, 1021 (1969). <sup>t</sup> "Stability Constants of Metal-Ion Complexes", *Chem. Soc. Spec. Publ.*, No. 17 (1964).

quantum yield of formation of the lowest spin-allowed excited state.<sup>9</sup> Photochemical or photophysical results show that this last quantity is unity for  $\text{Cr}(\text{CN})_6^{3-}$ ,<sup>1,2</sup>  $\text{Cr}(\text{en})_2(\text{NCS})_2^+$ ,<sup>30</sup>  $\text{Cr}(\text{bpy})_3^{3+}$ ,<sup>31</sup> and  $\text{Ru}(\text{bpy})_3^{2+}$ .<sup>32</sup> We assume that this is also true for the other two complexes,  $\text{Cr}(\text{phen})_3^{3+}$  and  $\text{Ru}(\text{bpy})_2(\text{CN})_2$ , for which the knowledge of this quantity is needed in our treatment. For biacetyl,  $\text{Cr}(\text{en})_3^{3+}$  and  $\text{Ru}(\text{phen})_3^{2+}$ , only the lowest spin-allowed excited state was

TABLE III: Intersystem Crossing Efficiencies

Complex	Standard		Med um	$\eta_i^a$
	Donor, $\eta_i^D$	Acceptor, $\eta_i^A$		
Cr(CN) $_6^{3-}$	Ru(bpy) $_3^{2+}$ , 1.0		DMF	0.56
	Cr(bpy) $_3^{3+}$ , 0.94		H $_2$ O-DMF $^b$	0.52
Cr(en) $_2$ (NCS) $_2^+$	Ru(bpy) $_3^{2+}$ , 1.0		H $_2$ O	0.41
	Ru(bpy) $_3^{2+}$ , 1.0		DMF	0.42
Cr(bpy) $_3^{3+}$	Biacetyl, 0.86	Cr(CN) $_6^{3-}$ , 0.56	DMF	0.47
			H $_2$ O	0.94
Cr(phen) $_3^{3+}$		Cr(CN) $_6^{3-}$ , 0.52	H $_2$ O-DMF $^b$	0.21
Cr(en) $_3^{3+}$	Ru(bpy) $_2$ (CN) $_2$ , 0.95		H $_2$ O	0.71
Ru(bpy) $_2$ (CN) $_2$		Cr(en) $_2$ (NCS) $_2^+$ , 0.41	H $_2$ O	0.95
Ru(phen) $_3^{2+}$		Cr(en) $_2$ (NCS) $_2^+$ , 0.42	DMF	1.08
		Cr(en) $_2$ (NCS) $_2^+$ , 0.41	H $_2$ O	0.65

$^a$  Relative to the indicated standard; in all cases,  $\eta_{et}$  has been assumed to be unity (see text).  $^b$  1:3 v/v.

populated by irradiation, so that there is no problem in this regard.

**Energy Transfer Efficiency.** Although energy transfer clearly takes place in each one of our donor-acceptor couples, as is shown by the occurrence of a sensitized emission of the acceptor, other mechanisms could play some role in the quenching of the donor emitting state. The difficulties encountered in establishing the actual contribution of a certain mechanism in the quenching process have been recently emphasized. $^3$  For each one of the donor-acceptor couples used in this work, energy transfer (eq 13) is thermodynamically (Figure 2) and spin $^3$  allowed:



Under such conditions, the sole quenching process which can compete with energy transfer is a thermodynamically allowed electron transfer: $^{3,33}$



The reduction potentials relevant to a discussion on the energetics of reactions 14 and 15 when both D and A are transition metal complexes are collected in Table II. Using these data, it can be easily shown that reactions 14 and 15 are thermodynamically *unfavorable* for each one of the donor-acceptor couples involving the complexes listed in Table II. Thus, for such couples energy transfer (reaction 13) is most likely the only quenching process and therefore the energy transfer efficiency ( $\eta_{et}$ ) is unity.

As the one electron reduction and oxidation potentials of biacetyl are not available, no inference can be drawn concerning the  $\eta_{et}$  value of the biacetyl-Cr(bpy) $_3^{3+}$  couple.

**Intersystem Crossing Efficiency.** As noted earlier, from our experiments we obtain  $R$ , which is the value of the  $\eta_i^A/\eta_i^D\eta_{et}$  ratio (eq 12). If two of the quantities contained in the ratio are known, the third one can be obtained. Our primary standards were Ru(bpy) $_3^{2+}$  and biacetyl, both of which were used as donors. For the experiments with Ru(bpy) $_3^{2+}$ ,  $\eta_{et}$  is most likely unity (see previous section). Much experimental evidence $^{23,32,34,35}$  indicates that  $\eta_i$  of Ru(bpy) $_3^{2+}$  is also unity. $^{36}$  As far as biacetyl is concerned,  $\eta_i$  is known to be  $0.86 \pm 0.07$  in aqueous solution at room temperature. $^{38}$  However, we do not know the value of  $\eta_{et}$  for the biacetyl-Cr(bpy) $_3^{3+}$  couple. As shown in Table III, the  $\eta_i$  value obtained for Cr(CN) $_6^{3-}$  from the Ru(bpy) $_3^{2+}$ /Cr(CN) $_6^{3-}$  couple using  $\eta_i$ (Ru(bpy) $_3^{2+}$ ) = 1 and  $\eta_{et} = 1$  is essentially equal to that obtained from the biacetyl-Cr(bpy) $_3^{3+}$ -Cr(CN) $_6^{3-}$  chain using  $\eta_i$ (biacetyl) =

0.86 and  $\eta_{et} = 1$ . This suggests that  $\eta_{et}$  of the biacetyl-Cr(bpy) $_3^{3+}$  couple is also unity.

**Remarks on the Various Complexes.** For Cr(CN) $_6^{3-}$ , the value  $\eta_i \sim 0.5$  we have obtained is in agreement with that previously reported in fluid solution. $^{16}$  For solid samples, Castelli and Forster $^{24}$  found that  $0.8 \leq \eta_i \leq 1$ . The difference between the value of  $\eta_i$  in the solid state and in solution is much higher than the quantum yield ( $\sim 0.1$ ) of the photosolvation reaction that takes place from the lowest spin-allowed excited state,  $^4T_{2g}$ . $^{39}$  This would indicate that internal conversion from  $^4T_{2g}$  to the ground state  $^4A_{1g}$  is an important deactivation path. However, it could also be that, as first suggested by Castelli and Forster, $^{24}$  the experimentally observed quantum yield of the photoreaction is lower than the primary quantum yield owing to cage recombination of the primary products. As cage recombination has recently been demonstrated to be important for Co(CN) $_6^{3-}$ , $^{40}$  there are good reasons to believe that it may also play an important role in Cr(CN) $_6^{3-}$ .

For Cr(en) $_2$ (NCS) $_2^+$ ,  $\eta_i \sim 0.4$  and the experimental quantum yield for the photoaquation reaction under comparable experimental condition is  $\sim 0.35$ . $^{41}$  Thus, even for this complex a nonnegligible fraction ( $\sim 25\%$ ) of the molecules which populate the lowest spin-allowed excited state either deactivate to the ground state via internal conversion or undergo a reversible photodissociation reaction (cage recombination). The intersystem crossing efficiency in the solid state is not known for this complex.

For Cr(bpy) $_3^{3+}$ ,  $\eta_i \sim 1$ . This value is compatible with the lack of appreciable photodissociation reaction from the  $^4T_{2g}$  excited state. $^{31}$  At present, we can offer no explanation for the low  $\eta_i$  value obtained for Cr(phen) $_3^{3+}$ . Also the  $\eta_i$  value in the solid state is not known for these complexes.

The value  $\eta_i \sim 0.7$  we have obtained for Cr(en) $_3^{3+}$  compares well with that ( $\sim 0.6$ ) estimated from a detailed analysis of the photochemical results. $^{42}$  The intersystem crossing efficiency of Cr(en) $_3^{3+}$  in the solid state is unity. $^{43}$  The quantum yield of the photoreaction coming from the lowest spin-allowed excited state is 0.15. $^{42}$  The possible explanations for the difference between fluid and solid media are the same as those discussed above for Cr(CN) $_6^{3-}$  and Cr(en) $_2$ (NCS) $_2^+$ .

Finally, our results indicate that  $\eta_i$  for Ru(bpy) $_2$ (CN) $_2$  is the same as that of Ru(bpy) $_3^{2+}$ , whereas the intersystem crossing efficiency of Ru(phen) $_3^{2+}$  is much lower. The fact that for both Cr(III) and Ru(II) the intersystem crossing efficiency of the tris-phen complexes is much lower than that of the tris-bpy complexes is puzzling. The lowest spin-forbidden excited state of these bipyridine and phenanthroline complexes is exten-

sively used in electron transfer processes<sup>44</sup> with the aim of converting solar energy into chemical energy.<sup>45</sup> Our results indicate that the bipyridine complexes have the advantage of a much higher quantum yield of formation of the reactive state. Further work is in progress with the aim of extending the results reported in this paper.

**Acknowledgment.** We thank Drs. S. Roffia and M. Ciano for the electrochemical measurements and the National Research Council of Italy for financial support.

## References and Notes

- V. Balzani and V. Carassiti, "Photochemistry of Coordination Compounds", Academic Press, London, 1970.
- A. W. Adamson and P. D. Fleischauer, Eds., "Concepts of Inorganic Photochemistry", Wiley, New York, N.Y., 1975.
- V. Balzani, L. Moggi, M. F. Manfrin, F. Bolletta, and G. S. Laurence, *Coord. Chem. Rev.*, **15**, 321 (1975).
- P. D. Fleischauer and P. Fleischauer, *Chem. Rev.*, **70**, 199 (1970).
- M. K. DeArmond, *Acc. Chem. Res.*, **7**, 309 (1974).
- G. A. Crosby, *Acc. Chem. Res.*, **8**, 231 (1975).
- L. S. Forster, *Adv. Chem. Ser.*, in press.
- The value of  $\eta_1$  coincides with the quantum yield of formation of the lowest spin-forbidden excited state upon irradiation in the lowest spin-allowed level.<sup>9</sup>
- G. B. Porter, V. Balzani, and L. Moggi, *Adv. Photochem.*, **9**, 147 (1974).
- A. A. Lamola, "Energy Transfer and Organic Photochemistry", A. A. Lamola and N. J. Turro, Eds., Interscience, New York, N.Y., 1969, p 17.
- C. A. Parker, "Photoluminescence of Solutions", Elsevier, Amsterdam, 1968.
- F. Wilkinson in "Organic Molecular Photophysics", Vol. 2, J. B. Birks, Ed., Wiley, New York, N.Y., 1975, p 95.
- B. Amand and R. Bensasson, *Chem. Phys. Lett.*, **34**, 44 (1975), and references therein.
- J. N. Demas and G. A. Crosby, *J. Am. Chem. Soc.*, **93**, 2841 (1971).
- E. L. Wehry and S. Sundararajan, *Chem. Commun.*, 456 (1971).
- N. Sabbatini, M. A. Scandola, and V. Balzani, *J. Phys. Chem.*, **78**, 541 (1974).
- I. B. Berlman, "Handbook of Fluorescence Spectra of Aromatic Molecules", Academic Press, New York, N.Y., 1971.
- A. Hutton, G. Giro, S. Dellonte, and A. Breccia, *Int. J. Radiat. Phys. Chem.*, **5**, 387 (1973).
- W. Geis and H. L. Schlafer, *Z. Phys. Chem. (Frankfurt am Main)*, **65**, 107 (1969).
- M. Maestri, F. Bolletta, N. Serpone, L. Moggi, and V. Balzani, *Inorg. Chem.*, in press.
- F. Bolletta, M. Maestri, L. Moggi, and V. Balzani, *J. Chem. Soc., Chem. Commun.*, 901 (1975).
- In order to obtain some very high values of optical density, the Lambert-Beer law was used. This is a reasonable assumption since even in the case of the highest optical density diluted solutions were used (see Table I). Moreover no static quenching was observed under our experimental conditions (see below), indicating the absence of ion pairs.
- F. Lytle and D. M. Hercules, *J. Am. Chem. Soc.*, **91**, 253 (1969).
- F. Castelli and L. S. Forster, *J. Phys. Chem.*, **78**, 2122 (1974).
- A. D. Kirk, P. E. Hoggard, G. B. Porter, M. C. Rockley, and M. M. Windsor, *Chem. Phys. Lett.*, **37**, 193 (1976).
- R. Bensasson, C. Salet, and V. Balzani, *J. Am. Chem. Soc.*, **98**, 3722 (1976).
- G. B. Porter, *Theor. Chim. Acta*, **24**, 265 (1972).
- For some donor-acceptor couples, the experimental conditions were actually dictated by the need to avoid back energy transfer. For example, for the  $Cr(bpy)_3^{3+}-Cr(CN)_6^{3-}$  couple, a water-DMF solvent mixture was chosen so as to have a sufficiently short lifetime of the SF excited state of the acceptor.<sup>29</sup>
- F. Wasgestian, unpublished results.
- C. Bifano and R. G. Linck, *Inorg. Chem.*, **13**, 609 (1974).
- M. Maestri, F. Bolletta, L. Moggi, V. Balzani, M. S. Henry, and M. Z. Hoffman, submitted for publication.
- J. N. Demas and G. A. Crosby, *J. Am. Chem. Soc.*, **93**, 2841 (1971).
- A. Juris, M. T. Gandolfi, M. F. Manfrin and V. Balzani, *J. Am. Chem. Soc.*, **98**, 1047 (1976), and references therein.
- M. Wrighton and J. Markham, *J. Phys. Chem.*, **77**, 3042 (1973).
- G. S. Laurence and V. Balzani, *Inorg. Chem.*, **13**, 2976 (1974).
- Laser flash experiments<sup>26</sup> show that the lower limiting value for  $\eta_1$  ( $Ru(bpy)_3^{2+}$ ) is 0.5 and seem also to indicate that this could be the actual value of  $\eta_1$  ( $Ru(bpy)_3^{2+}$ ). However, experiments based on the electron transfer techniques have confirmed that  $\eta_1$  ( $Ru(bpy)_3^{2+}$ ) is unity.<sup>37</sup>
- F. Bolletta et al., manuscript in preparation.
- M. Aimgren, *Mol. Photochem.*, **4**, 327 (1972).
- F. Wasgestian, *J. Phys. Chem.*, **76**, 1947 (1972).
- F. Scandola, M. A. Scandola, and C. Bartocci, *J. Am. Chem. Soc.*, **97**, 4757 (1975).
- This value is the sum of the quantum yields of the observed photoaquation reactions.<sup>30</sup> Whether these reactions come from the quartet or doublet states is unknown.
- R. Ballardini, G. Varani, H. F. Wasgestian, L. Moggi, and V. Balzani, *J. Phys. Chem.*, **77**, 2947 (1973).
- F. Castelli and L. S. Forster, *Chem. Phys. Lett.*, **30**, 465 (1975).
- See, for example, ref 21 and 33, and C. Creutz and N. Sutin, *Inorg. Chem.*, **15**, 496 (1976); R. C. Young, T. J. Meyer, and D. G. Whitten, *J. Am. Chem. Soc.*, **98**, 286 (1976), and references therein.
- C. Creutz and N. Sutin, *Proc. Natl. Acad. Sci. U.S.A.*, **70**, 1701 (1973); R. C. Young, T. J. Meyer, and D. G. Whitten, *J. Am. Chem. Soc.*, **97**, 4781 (1975); G. Sprintschnik, H. W. Sprintschnik, P. P. Kirsch, and D. G. Whitten, *ibid.*, **98**, 2337 (1976).

## Solvent Effect on the Electronic Transitions of the Triiodide Anion

Christian Detellier and Pierre Laszlo\*

Institut de Chimie, Université de Liège au Sart-Tilman, par 4000 Liège 1, Belgium (Received March 2, 1976)

The energy of the  $\sigma_g \rightarrow \sigma_u^*$  and  $\pi_g \rightarrow \sigma_u^*$  transitions is measured in 31 solvents and solvent mixtures, either protic or dipolar aprotic, for  $CsI_3$ ,  $(C_2H_5)_4NI_3$ , and  $(C_6H_5)_3AsII_3$ . The heat of transfer is determined between acetonitrile and dimethyl sulfoxide for the ammonium salt. The latter solvent appears to stabilize the  $\sigma_u^*$  excited state to a greater extent than the initial state ( $\sigma_g$  or  $\pi_g$ ).

## Introduction

The triiodide anion ( $I_3^-$ ) disperses its negative charge efficiently, which makes it a species with good internal stabilization. As a result, it interacts but weakly with the positive counterion or with the solvent. A significant feature, already noted by Parker,<sup>1</sup> is the similarity in the solvations of this large and polarizable anion and of the neutral iodine  $I_2$  molecule.

We studied two distinct electronic transitions: the  $\sigma_g \rightarrow \sigma_u^*$  and  $\pi_g \rightarrow \sigma_u^*$ .<sup>2</sup> This notation assumes  $D_{\infty h}$  symmetry, rather than the lower  $C_{2v}$  symmetry appropriate whenever  $I_3^-$  strongly interacts with the neighboring cation or solvent molecule.<sup>3</sup> The bonding scheme is that introduced by Pimentel<sup>4</sup> of a three-center four-electron bond. We decided to explore the influence of a change in solvent on the electronic transitions<sup>5</sup> for this unusual molecule. The cations chosen vary

TABLE I: Transition Energies for the Triiodide Anion ( $A = \pi_g \rightarrow \sigma_u^*$ ,  $B = \sigma_g \rightarrow \sigma_u^*$ ) ( $\pm 0.10$  kcal mol<sup>-1</sup>)

	Cs <sup>+</sup>		(C <sub>6</sub> H <sub>5</sub> ) <sub>3</sub> AsI <sup>+</sup>		Et <sub>4</sub> N <sup>+</sup>	
	A	B	A	B	A	B
1. Water	81.5 <sup>2</sup>	99.4 <sup>2</sup>	<i>a</i>	<i>a</i>	<i>a</i>	<i>a</i>
2. Methyl alcohol	79.6 <sup>2</sup>	98.2 <sup>2</sup>	79.7 <sup>6</sup>	98.2 <sup>4</sup>	79.6 <sup>5</sup>	98.1 <sup>6</sup>
3. Ethyl alcohol	79.4 <sup>3</sup>	98.0 <sup>2</sup>	79.5 <sup>4</sup>	98.0 <sup>6</sup>	79.6 <sup>0</sup>	98.0 <sup>9</sup>
4. <i>n</i> -Propyl alcohol	79.3 <sup>8</sup>	98.0 <sup>2</sup>	79.5 <sup>1</sup>	97.9 <sup>5</sup>	79.5 <sup>1</sup>	97.9 <sup>5</sup>
5. <i>n</i> -Butyl alcohol	79.4 <sup>0</sup>	97.7 <sup>9</sup>	<i>a</i>	<i>a</i>	79.4 <sup>3</sup>	97.7 <sup>9</sup>
6. <i>tert</i> -Amyl alcohol	79.4 <sup>0</sup>	97.6 <sup>9</sup>	<i>a</i>	<i>a</i>	<i>a</i>	<i>a</i>
7. Isopropyl alcohol	79.5 <sup>1</sup>	98.0 <sup>9</sup>	79.4 <sup>3</sup>	98.0 <sup>9</sup>	79.1 <sup>2</sup>	97.9 <sup>2</sup>
8. <i>tert</i> -Butyl alcohol	79.6 <sup>5</sup>	98.1 <sup>6</sup>	<i>a</i>	<i>a</i>	<i>a</i>	<i>a</i>
9. Isoamyl alcohol	79.8 <sup>7</sup>	97.8 <sup>5</sup>	<i>a</i>	<i>a</i>	<i>a</i>	<i>a</i>
10. Benzyl alcohol	78.6 <sup>6</sup>	<i>b</i>	78.8	<i>b</i>	78.5	<i>b</i>
11. Ethylene glycol	78.2 <sup>9</sup>	96.8 <sup>9</sup>	78.2 <sup>7</sup>	96.9 <sup>3</sup>	78.1 <sup>0</sup>	96.8 <sup>9</sup>
12. Methylcellosolve	77.8 <sup>1</sup>	96.7 <sup>6</sup>	77.7 <sup>8</sup>	96.8 <sup>6</sup>		
13. Chloroform	78.7 <sup>7</sup>	97.5 <sup>9</sup>	<i>c</i>	<i>c</i>	78.5 <sup>8</sup>	96.9 <sup>3</sup>
14. Dichloromethane	78.9 <sup>7</sup>	97.4 <sup>5</sup>	<i>c</i>	<i>c</i>		
15. Dimethylformamide	78.1 <sup>2</sup>	96.7 <sup>0</sup>			78.0 <sup>8</sup>	96.7 <sup>0</sup>
16. Dimethyl sulfoxide	78.0 <sup>7</sup>	96.2 <sup>4</sup>	77.8 <sup>9</sup>	96.2 <sup>7</sup>	77.9 <sup>3</sup>	96.1 <sup>4</sup>
17. Ethyl acetate	78.7 <sup>0</sup>	97.7 <sup>2</sup>	78.6 <sup>4</sup>	97.5 <sup>5</sup>	78.4 <sup>7</sup>	97.4 <sup>2</sup>
18. Dimethylacetamide	78.0 <sup>0</sup>	96.4 <sup>9</sup>	78.1 <sup>0</sup>	96.6 <sup>6</sup>	78.1 <sup>1</sup>	96.6 <sup>6</sup>
19. Acetone	78.4 <sup>7</sup>	<i>b</i>	78.3 <sup>8</sup>	<i>b</i>	78.3 <sup>2</sup>	<i>b</i>
20. Acetic anhydride	78.7 <sup>0</sup>	97.5 <sup>5</sup>	78.7 <sup>3</sup>	97.6 <sup>2</sup>	78.7 <sup>5</sup>	97.6 <sup>5</sup>
21. Tributyl phosphate	77.9 <sup>0</sup>	96.8 <sup>9</sup>	77.8 <sup>9</sup>	96.8 <sup>6</sup>	77.9 <sup>3</sup>	96.8 <sup>4</sup>
22. Hexamethylphosphoramide	77.6 <sup>4</sup>	96.2 <sup>7</sup>	77.7 <sup>0</sup>	96.3 <sup>7</sup>	77.8 <sup>0</sup>	96.4 <sup>7</sup>
23. Acetonitrile	79.0 <sup>1</sup>	98.0 <sup>2</sup>	78.9 <sup>2</sup>	97.8 <sup>9</sup>	78.9 <sup>6</sup>	97.9 <sup>2</sup>
24. Pyridine	77.6 <sup>9</sup>	<i>b</i>	77.6 <sup>9</sup>	<i>b</i>	77.6 <sup>6</sup>	<i>b</i>
25. 1,4-Dioxane	78.8 <sup>1</sup>	<i>d</i>	<i>c</i>	<i>c</i>		
26. Tetrahydrofuran	77.9 <sup>4</sup>	96.7 <sup>0</sup>	77.9 <sup>3</sup>	96.7 <sup>9</sup>	77.9 <sup>1</sup>	96.7 <sup>0</sup>
27. Diethyl ether	78.4 <sup>2</sup>	<i>d</i>	<i>c</i>	<i>c</i>	78.0 <sup>8</sup>	97.0 <sup>2</sup>
28. Dimethoxyethane	78.0 <sup>8</sup>	96.8 <sup>3</sup>				
29. Diglyme (dimethyl ether)	77.9 <sup>5</sup>	96.7 <sup>0</sup>	78.0 <sup>0</sup>	96.7 <sup>9</sup>	77.8 <sup>7</sup>	96.7 <sup>0</sup>
30. Triglyme	77.9 <sup>1</sup>	96.6 <sup>3</sup>	77.9 <sup>7</sup>	96.6 <sup>6</sup>	77.9 <sup>7</sup>	96.7 <sup>0</sup>
31. Diglyme (diethyl ether)	78.0 <sup>4</sup>	96.7 <sup>6</sup>	77.9 <sup>7</sup>	96.8 <sup>3</sup>	78.0 <sup>2</sup>	96.7 <sup>9</sup>

<sup>a</sup> Insoluble. <sup>b</sup> Absorption overlaps with solvent bond. <sup>c</sup> Triiodide anion unobservable. <sup>d</sup> The B transition was observed as a shoulder of the CTTS transition for the iodide anion.

from hard [<sup>+</sup>N(C<sub>2</sub>H<sub>5</sub>)<sub>4</sub>], to soft [Cs<sup>+</sup>], and very soft [IAs<sup>+</sup>(C<sub>6</sub>H<sub>5</sub>)<sub>3</sub>], according to the classification by Pearson.<sup>6</sup> In most solvents used, these salts are expected to form ion pairs of the solvent-separated or "loose" type.<sup>7</sup>

### Experimental Section

Cs<sup>+</sup>, I<sub>3</sub><sup>-</sup> was purchased from Alfa Inorganic. (C<sub>6</sub>H<sub>5</sub>)<sub>3</sub>AsI<sup>+</sup>, I<sub>3</sub><sup>-</sup> was prepared according to Beveridge and Harris<sup>8</sup> and recrystallized in acetonitrile. (C<sub>2</sub>H<sub>5</sub>)<sub>4</sub>N<sup>+</sup>, I<sub>3</sub><sup>-</sup> was prepared in ethanol solution by allowing bisublimed iodine (Carlo Erba) to react with the corresponding iodide (Merck, analytical purity); it was recrystallized twice from absolute ethanol.<sup>9</sup>

Spectra were recorded with a Cary 17 spectrometer on ~10<sup>-5</sup> M solutions at 25 °C. The two absorption bands overlap little, and deconvolution was not necessary to obtain accurate absorption maxima. All solvents used, of analytical quality whenever possible, were carefully dried and redistilled prior to use. Solutions are prepared in the dark. The invariance of I<sub>3</sub><sup>-</sup> absorbance with time<sup>10</sup> was carefully checked. Measurements of heats of solution were done on a LKB 8700-1 precision calorimeter, with a 100-ml reaction vessel, at a temperature of 25.00 ± 0.05 °C. The change in electrical resistance was calculated with the Dickinson extrapolation method.<sup>11</sup> The reproductibility was checked by measurement of the heat of solution of Tris [tris(hydroxymethyl)aminomethane] as a standard. In the solvent used, acetonitrile and dimethyl sulfoxide, dissolution of (C<sub>2</sub>H<sub>5</sub>)<sub>4</sub>N<sup>+</sup>I<sub>3</sub><sup>-</sup> was quasi-instantaneous, and in any case complete in less than 1 min.

The enthalpies of solution of (C<sub>2</sub>H<sub>5</sub>)<sub>4</sub>N<sup>+</sup>I<sub>3</sub><sup>-</sup> in acetonitrile and in dimethyl sulfoxide were measured at three concentrations, varying from 1.5 to 2.5 mM. The mean value was taken as equal to the heat of solution at infinite dilution,<sup>12</sup> and the experimental error was estimated from the spread:  $\Delta H_s = 6.02 \pm 0.02$  kcal mol<sup>-1</sup> (Me<sub>2</sub>SO) and  $6.88 \pm 0.06$  kcal mol<sup>-1</sup> (CH<sub>3</sub>CN). The former value is in the range expected on the basis of literature measurements for kindred salts in the same solvent: (C<sub>2</sub>H<sub>5</sub>)<sub>4</sub>NCl (2.42), (C<sub>2</sub>H<sub>5</sub>)<sub>4</sub>NBr (3.27), and (C<sub>2</sub>H<sub>5</sub>)<sub>4</sub>NI (4.86).<sup>13</sup>

### Discussion

The results are listed in Table I.

One notes the pronounced agreement of the transition energies for the three salts, within the combined experimental errors. The nature of the cation has indeed little influence on the position of the triiodide absorption maxima, with the exception of ether, in which the ammonium salt has little solubility, while the cesium salt undergoes the I<sub>3</sub><sup>-</sup> → I<sub>2</sub> + I<sup>-</sup> dissociation equilibrium; the discrepancies in isopropyl alcohol and in benzyl alcohol are barely outside the error limits; they may reflect contributions from "tight" ion pairs.

Correlating the energies of the two transition against one another (Figure 1) with a mean deviation of ±0.17 kcal mol<sup>-1</sup> distinguishes two solvent groups. Protic solvents give rise to experimental points centered about (79.5/98.0) kcal mol<sup>-1</sup>, while dipolar aprotic solvents correspond to a range around (78.3/96.9) kcal mol<sup>-1</sup>. The 0.85 slope [equal to 0.86 and 0.89

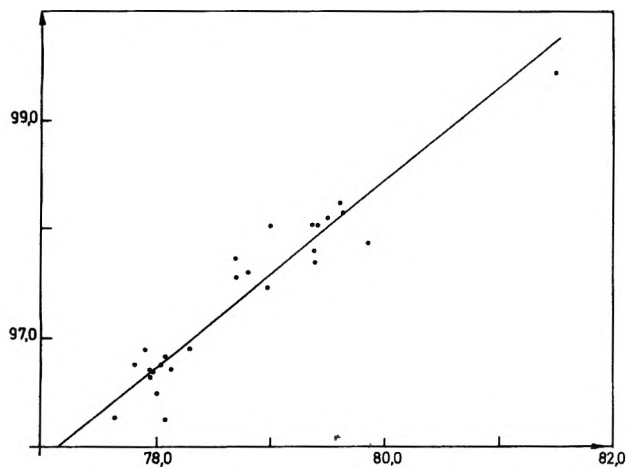


Figure 1. A plot of the energy for the B transition against that for the A transition of  $CsI_3$  ( $\text{kcal mol}^{-1}$ ).

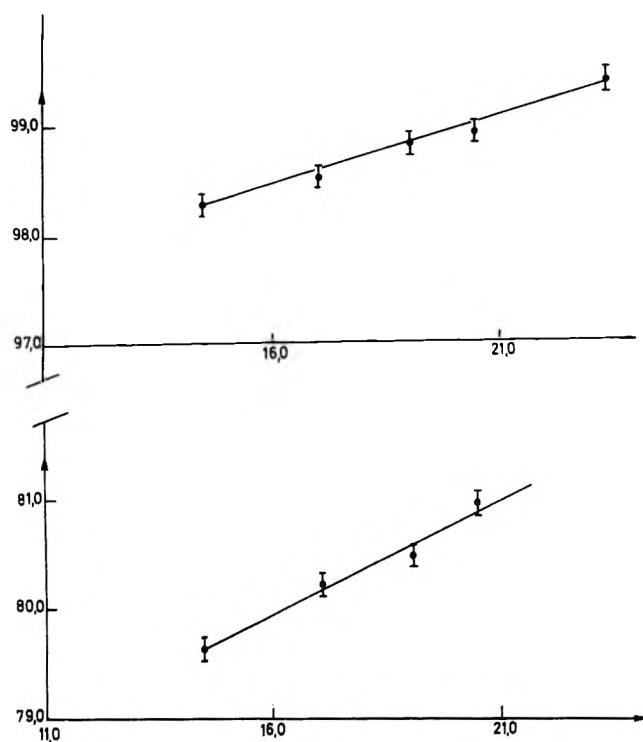


Figure 2. Transition energy for the B (top) and A (bottom) transitions of  $CsI_3$  as a function of the Hildebrand  $\delta$  parameter for methanol-water mixtures.

for  $(C_6H_5)_3AsI^+$  and  $(C_2H_5)_4N^+$ , respectively] implies a greater sensitivity of the  $\pi_g \rightarrow \sigma_u^*$  transition to solvent variation. One should note that alcohol-ethers, such as ethylene glycol monomethyl ether or diethylene glycol, despite being highly structured solvents give rise to transition energies typical of ether rather than alcoholic solvents.

Another correlation worth reporting is observed with methanol-water binary mixtures; a linear plot (Figure 2) results if the parameters A or B are expressed against the dielectric constant or the cohesive energy for the mixture, as represented by the Hildebrand  $\delta$  parameter.<sup>14</sup> This points to the importance of solvent cohesion, when the bulky anion  $I_3^-$  is forced into these highly structured solutions; due to Franck-Condon strain, the excited state is more and more destabilized as the medium increases its internal pressure.

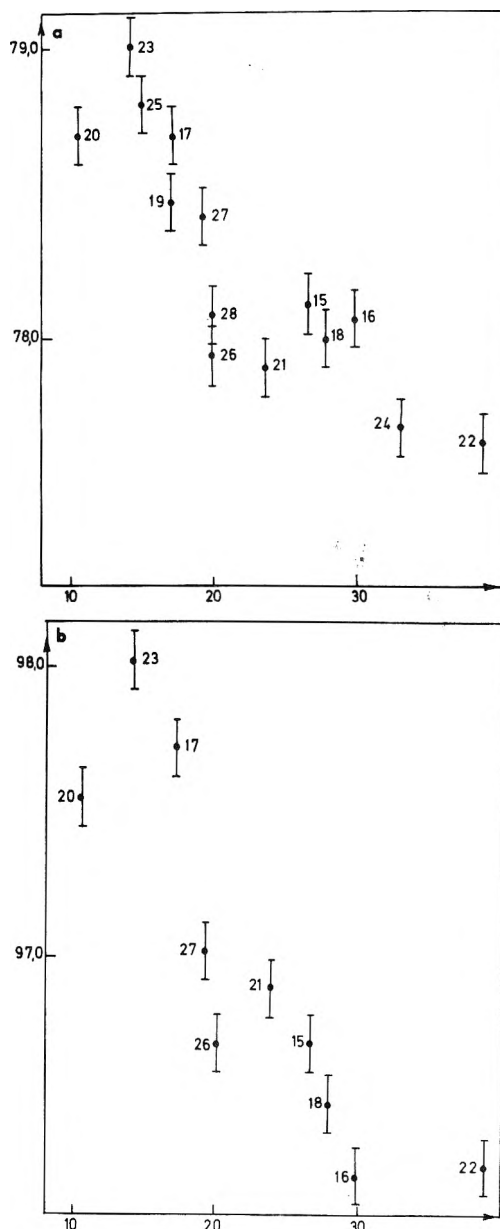


Figure 3. Transition energy for  $CsI_3$  as a function of the Gutmann donicity of the solvent: A transition (a) and B transition (b).

Naturally, we could not resist the urge of correlating the experimental transition energies with the numerous available parameters characteristic of the solvent, its polarity, or polarizability.<sup>15</sup> Just like other investigators,<sup>16</sup> we were graced by success with some parameters, viz. the Gutmann donicity number,<sup>17</sup> or, in a more limited sense (vide infra) the  $(n^2 - 1)/(2n^2 + 1)$ ,<sup>18</sup> and the Hildebrand  $\delta$ <sup>14</sup> parameters. With other parameters, including the Kosower<sup>19</sup> and Dimroth<sup>20</sup> transition energies for betaine systems in the same solvents, correlations are, at best, cloudy. This is not too surprising, considering for instance the ease of deformation of  $I_3^-$  from a linear to a bent structure.

The correlation obtained with the Gutmann donicity number DN<sup>17</sup> is displayed in Figure 3.

The reduction in the transition energies as the solvent becomes a better donor arises either from predominant destabilization of the initial  $\sigma_g$  or  $\pi_g$  state, or from predominant stabilization of the  $\sigma_u^*$  excited state. The normal expectation, based upon the ionic nature of the substrate and its attendant

large solvation, together with the notion of Franck–Condon strain of the excited state, would have been an *increase* of the transition energies with the donicity of the solvent, contrary to what is observed.

One is therefore dealing with an extremely interesting phenomenon. In order to dissect it further, and to distinguish between the two above-mentioned possibilities, we shall now describe the results of a thermochemical comparison between acetonitrile and dimethyl sulfoxide. These two solvents have very similar values of most of their physical parameters, including the cohesive energy or internal pressure if approached through the Hildebrand  $\delta$  (11.9 and 12.0, respectively),<sup>14</sup> the dielectric constants  $\epsilon$  (37.5 and 48.9, respectively), the Dimroth  $E_T$  values<sup>20</sup> (46 and 45, respectively), or the Kosower  $Z$  values (71.3 and 71.1, respectively).<sup>14</sup> Yet, they differ markedly in their polarizabilities, as measured by the  $(n^2 - 1)/(2n^2 + 1)$  term: 0.175 vs. 0.221; and in their Gutmann donicities: 14.1 vs. 29.8. With the usual extrathermodynamic assumptions of equal solvation for  $(C_6H_5)_4As^+$  and  $(C_6H_5)_4B^-$ ,<sup>21</sup> the heat of transfer of tetraethylammonium ion from acetonitrile to dimethyl sulfoxide is +1.3 kcal mol<sup>-1</sup>.<sup>22</sup>

In order to infer from this result the relative stabilization enthalpies for the triiodide  $I_3^-$  anion in acetonitrile and dimethyl sulfoxide, one must take into account the heat associated with the formation in these two solvents of cavities accommodating the  $^+N(C_2H_5)_4I_3^-$  salt. Following numerous investigators<sup>23</sup> we factorize the heat of solvation as follows:

$$H_{sol} = H_{int} + H_{cav}$$

where  $H_{int}$  represents the enthalpy of interaction between solute and solvent molecules, due to van der Waals and electrostatic forces, and where  $H_{cav}$  is the enthalpy required to form a solvent cavity commensurate with the solute molecule. The first term, negative, balances the second, always positive. From the known cohesive energy densities  $\Delta H_{vap}/V$  in these two solvents, viz. 150.22 and 177.27 cal cm<sup>3</sup>,<sup>24</sup> lower limits for the enthalpy of cavity formation around the anion and the cation are calculated on the basis of the corresponding partial ionic volumes (Table II). The greater cohesion of dimethyl sulfoxide corresponds to values of  $\delta\Delta H_{cav}(CH_3CN \rightarrow Me_2SO) = 3.8$  for the tetraethylammonium cation, and +2.4 kcal mol<sup>-1</sup> for the triiodide anion. Since the heats of transfer from acetonitrile to dimethyl sulfoxide are +1.3 kcal mol<sup>-1</sup> for the cation,<sup>22</sup> and -0.9 kcal mol<sup>-1</sup> for the salt, the heat of transfer of the triiodide anion is -2.2 kcal mol<sup>-1</sup>. Hence, the  $I_3^-$  ground state is stabilized by 2.2 + 2.4 = 4.6 kcal mol<sup>-1</sup> in going from acetonitrile to dimethyl sulfoxide, in keeping with the larger polarizability of the latter solvent. The transition at 360 nm connects states such that the  $\sigma_u^*$  excited state is better stabilized by 1.1 kcal mol<sup>-1</sup> relative to the  $\pi_g$  initial state. A similar conclusion is obtained for the 290-nm transition, with an increased stabilization of the excited state by 1.8 kcal mol<sup>-1</sup> relative to the  $\sigma_g$  initial state. The corresponding "absolute" values are ca. 5.7 and 6.4 kcal mol<sup>-1</sup>. The difference of 0.7 kcal mol<sup>-1</sup> points to differential solvation of the  $\sigma_g$  and  $\pi_g$  states in going from acetonitrile to dimethyl sulfoxide. It would indicate better solvation by this amount of the  $\pi_g$  initial state.

However the important finding is the greater solvation of the excited state, as compared to the ground state, for both of the transitions studied. A similar conclusion had been reached by Haberfield<sup>26</sup> for the  $n \rightarrow \pi^*$  transition of ketones; it has been shown<sup>23b</sup> to be invalid because of the neglect of the

TABLE II: Heat of Formation of Cavities

Ion	Volume, ml mol <sup>-1</sup>	Solvent	$\Delta H_{cav}$ , kcal mol <sup>-1</sup>
$^+N(C_2H_5)_4$	142.0 <sup>a</sup>	CH <sub>3</sub> CN	21.3
$^+N(C_2H_5)_4$	142.0 <sup>a</sup>	(CH <sub>3</sub> ) <sub>2</sub> SO	25.2
$I_3^-$	88.0 <sup>b</sup>	CH <sub>3</sub> CN	13.2
$I_3^-$	88.0 <sup>b</sup>	(CH <sub>3</sub> ) <sub>2</sub> SO	15.6

<sup>a</sup> In methanol, ref 25, using 3,3-diethylpentane as a hydrocarbon model, a value of 136 ml mol<sup>-1</sup> was calculated from the expression  $V = 0.79 M/d$ . We are thus assuming the cavity size appropriate for the isolated particle, excluding any free volume associated with the solute. <sup>b</sup> Volume of a cylinder of height 10.1 Å (= molecular length of 5.8 Å + one van der Waals radius for iodine (2.15 Å) at each end), with a circular base whose radius is also 2.15 Å.

cavity term. We submit this eximious instance of the triiodide anion, in which the reduction in charge dispersal in going from the ground to the excited state,<sup>4</sup> translates, we surmise, into better solvation.

*Acknowledgments.* We thank Joaquim Ramos, Marie-Louise Stien, and Professor Jacques Reisse, Université Libre de Bruxelles, for stimulating discussions, and for calorimetric measurements.

## References and Notes

- R. Alexander, E. C. F. Ko, Y. C. Mac, and A. J. Parker, *J. Am. Chem. Soc.*, **89**, 3703 (1967); A. J. Parker and R. Alexander, *ibid.*, **90**, 3313 (1968).
- W. Gabe and D. J. Stufkens, *Spectrochim. Acta, Part A*, **30**, 1835 (1974).
- K. R. Loos and A. C. Jones, *J. Phys. Chem.*, **78**, 2306 (1974).
- G. C. Pimentel, *J. Chem. Phys.*, **19**, 446 (1951).
- A. I. Popov and R. F. Swensen, *J. Am. Chem. Soc.*, **77**, 3724 (1955); M. Smith and M. C. R. Symons, *Trans. Faraday Soc.*, **54**, 338 (1958); N. Mataga and T. Kubota, "Molecular Interactions and Electronic Spectra", Marcel Dekker, New York, N.Y., 1970.
- R. G. Pearson, Ed., "Hard and Soft Acids and Bases", Dowden Hutchinson and Ross, Stroudsburg, Pa., 1973.
- "Ions and Ion Pairs in Organic Reactions", Vol. 1, M. Szwarc, Ed., Wiley-Interscience, New York, N.Y., 1972.
- A. D. Beveridge and G. S. Harris, *J. Chem. Soc.*, 6076 (1964).
- F. D. Chattaway and G. Hoyle, *J. Chem. Soc.*, 654 (1923).
- M. Espeillac and D. Decroocq, *Bull. Soc. Chim. Fr.*, 2418 (1971).
- J. M. Sturvesant, "Techniques of Organic Chemistry", 3d ed, Part I, A. Weissberger, Ed., Interscience, New York, N.Y., 1963, p 541.
- G. R. Hedwig and A. J. Parker, *J. Am. Chem. Soc.*, **96**, 6589 (1974).
- E. M. Arnett and D. R. Kelvey, *J. Am. Chem. Soc.*, **88**, 2598 (1966).
- J. H. Hildebrand, J. M. Prausnitz, and R. L. Scott, "Regular and Related Solutions", Van Nostrand-Reinhold, New York, N.Y., 1970; R. L. Reeves, M. S. Maggio, and L. F. Costa, *J. Am. Chem. Soc.*, **96**, 5917 (1974).
- M. Jauquet and P. Laszlo, "Solutions and Solubilities", I-4, M. R. J. Dack, Ed.; A. Weissberger, Ed., "Techniques of Chemistry", Vol. VIII, Wiley, New York, N.Y., 1975.
- F. W. Fowler, A. R. Katritzky, and R. J. D. Rutherford, *J. Chem. Soc. B*, 460 (1971).
- V. Gutmann and U. Mayer, *Struct. Bonding (Berlin)*, **12**, 113 (1972).
- M. F. Nicol, *Appl. Spectrosc. Rev.*, **8**, 183 (1974); E. G. McRae, *J. Phys. Chem.*, **61**, 562 (1957).
- E. M. Kosower, *J. Am. Chem. Soc.*, **80**, 3253, 3261 (1958).
- C. Reichardt and K. Dimroth, *Fortschr. Chem. Fcscsh.*, **11**, 1 (1968).
- E. Grunwald, G. Baughman, and G. Kohnstam, *J. Am. Chem. Soc.*, **82**, 5801 (1960).
- B. G. Cox, G. R. Hedwig, A. J. Parker, and D. G. Watts, *Austr. J. Chem.*, **27**, 477 (1974).
- Inter alia: (a) J. A. V. Butler, *Trans. Faraday Soc.*, **33**, 229 (1937); O. Sinanoglu in "Molecular Associations in Biology", B. Pullman, Ed., Academic Press, New York, N.Y., 1968, p 427; T. Halicioğlu and O. Sinanoglu, *Ann. N.Y. Acad. Sci.*, **158**, 308 (1969); R. R. Birge, M. J. Sullivan, and B. E. Kohler, *J. Am. Chem. Soc.*, **98**, 358 (1976); (b) J. J. Moura Ramos, M. L. Stein, and J. Reisse, *Chem. Phys. Lett.*, submitted for publication.
- Inter alia: M. R. J. Dack, *Aust. J. Chem.*, **28**, 1643 (1975).
- J. Padova, *J. Chem. Phys.*, **56**, 1606 (1972).
- P. Haberfield, *J. Am. Chem. Soc.*, **96**, 6526 (1974); see also E. M. Arnett, D. Hufford, and D. R. McKelvey, *J. Am. Chem. Soc.*, **88**, 3142 (1966).

# Approximate Molecular Orbital Theory for Positrons and Positronium Atoms Bound to Molecules<sup>†</sup>

D. M. Schrader\* and C. M. Wang

Chemistry Department, Marquette University, Milwaukee, Wisconsin 53233 (Received November 12, 1975)

Publication costs assisted by the Petroleum Research Fund

An approximate molecular orbital theory for bound positrons is presented. The theory is semiempirical and the parameterization scheme is based upon some very sparse data together with plausible interpolation ideas. We follow the CNDO/2 approach for the positron, and use that method also for the purely electronic part of the theory; molecules comprising first-row atoms are considered. The calculations yield fully self-consistent positronic and electronic molecular orbitals, as well as positron and positronium affinities of molecules. Results for over 60 molecules presented, among which are eight studied by Madia et al. who used a combination of ideas to construct a semiempirical approach for the positronic molecular orbitals; we compare our results with theirs for the eight common molecules. General features of positron and positronium binding are discussed. Positronium appears to be stable to split-off in molecules in which it replaces hydrogen; for weak acids, a good correlation is found between acid strength and positron affinity for the anion; however, the positron does not appear to be a typical electrophile in aromatic addition reactions. Some justification of our approach is provided by agreement or consistency of our calculated results with some recent experimental observations: our calculated positronium affinities for toluene and nitrobenzene (0 and  $1.1 \pm 0.8$  eV, respectively) are in excellent relative and fair quantitative agreement with enthalpies of positronium attachment for these molecules observed by Ache and co-workers (0 and  $0.20 \pm 0.01$  eV, respectively) and with the positronium binding energy of nitrobenzene obtained by Goldanskii and co-workers by fitting experimental data to a simple model potential (0.15 to 0.17 eV, depending upon solvent); our calculated positronium affinity for *p*-benzoquinone is in disagreement with observations by these two authors, however. For smaller molecules, positronium bond strengths in  $\text{PsO}_2$ ,  $\text{PsNO}$ , and  $\text{PsNO}_2$  (0, 0, 1.95 eV, respectively) seem to be consistent with relative tendencies of gaseous  $\text{O}_2$ , NO, and  $\text{NC}_2$  molecules to quench triplet positronium by chemical combination as opposed to spin conversion (0, 0, 25%) as reported by Goldanskii and co-workers. Quenching cross sections for these three molecules as reported by Chuang and Tao (0.002 65, 0.008 45, and  $26 \text{ \AA}^2$ , respectively) seem to suggest the stability of  $\text{PsNO}_2$  but not  $\text{PsO}_2$  and  $\text{PsNO}$ , in agreement with our calculations.

## I. Introduction

Positron annihilation in a molecular medium proceeds by a complicated mechanism featuring a number of competing processes.<sup>1</sup> While all these ultimately lead to the same result for the positron, namely, annihilation, the characteristics of the final state of the host molecule, as well as the positron lifetime and angular correlation of annihilation radiation, depend strongly upon the history of the system. In modern experiments, several competing positron decay channels can be distinguished and partly characterized. In order to explain observed positron lifetimes and angular correlation of annihilation radiation, experimentalists have presumed a variety of decay channels: annihilation from bound states of positron-molecule complexes, bound states of positronium-molecule complexes, scattering states, as well as resonance states. The importance of bound states of positronium-molecule complexes has been reviewed recently by Goldanskii and Shantarovich.<sup>2</sup>

<sup>†</sup> Presented in part at the VIII Midwest Theoretical Chemistry Conference, Madison, Wisc., May 1-3, 1975; and at the IV International Conference on Positron Annihilation, Helsingør, Denmark, Aug. 23-26, 1976.

\* Address for 1976-1977 academic year: Mathematics Department, University of Nottingham, Nottingham NG7 2RD, United Kingdom.

It seems worthwhile to supplement these attempts at rationalizing observed results with quantum mechanical calculations on the intermediate complexes. The purpose of this paper is to present a molecular orbital theory for the structure of bound states of positron- and positronium-molecule complexes. In this first attempt, the important short-range electron-positron correlation effects<sup>3</sup> are merely parameterized. The highly empirical CNDO theory<sup>4</sup> is used for the electrons, and the positronic molecular orbital is calculated using a set of assumptions which are similar to the CNDO approach as available data permits.

The CNDO assumptions for electronic systems correspond to approximations which appear to be gross. Yet the method has been highly successful in applications on purely electronic molecules, not so much in absolute predictions as in relative predictions and rationalizations of chemical data for sets of related molecules. The reasons for this success remain something of a mystery. We hope that, by using the same approach for the positron, our calculations will also be useful for relative predictions and rationalizations of results for related molecules. However, we should not expect accurate numerical determination of positron interaction parameters with individual molecules.

A great advantage of a CNDO-type approach is its simplicity: large molecules can be routinely treated. We hope, by looking at a large number of related molecules, to discover

trends in positron binding mechanisms which will give rise to some fundamental understanding of the structure of such systems. We believe that the present work makes some progress in that direction.

It should be noted that recently<sup>5</sup> a theory was proposed for positronic molecular orbital computations. That theory is like our own in that the CNDO/2 approach was used for the electrons; however, a combination of approximate ideas was used for the positron. No empirical information was used to evaluate positronic parameters in that theory. While experimental information on positron binding is very sparse, it is not non-existent; all such information pertaining to atoms and diatomic molecules known to us was used to calibrate the approach described in the present work.

## II. CNDO Theory for Positrons

Ignoring for the moment electron-positron correlation, we can write an approximate molecular orbital wave function for the system consisting of a positron bound to a closed shell electronic system as<sup>6</sup>

$$\begin{aligned} & \Psi(1, 2, \dots, n, p) \\ & = \psi_p(p)\alpha(p)\mathcal{A}[\psi_1(1)\alpha(1)\psi_1(2)\beta(2)\psi_2(3)\alpha(3)\dots\psi_{n/2}(n)\beta(n)] \end{aligned} \quad (1)$$

$\psi_p$  is the molecular orbital for the positron (positronic molecular orbital, PMO),  $\psi_i$  are the electronic molecular orbitals (EMO), and  $\mathcal{A}$  is the  $n$ -electron antisymmetrizer and normalizer. Each molecular orbital is written as a sum of atomic orbitals:

$$\begin{aligned} \psi_i & = \sum_{\mu} c_{\mu i} \phi_{\mu} \\ \psi_p & = \sum_{\mu} c_{\mu p} \phi_{\bar{\mu}} \end{aligned} \quad (2)$$

Each electronic basis function  $\phi_{\mu}$  is a Slater-type atomic orbital characterized by quantum numbers  $n$ ,  $l$ , and  $m$ , and an exponential parameter  $\zeta$ . The functional form for the STO's is familiar to many; it is given, along with values for  $\zeta$ , on pp 23–29 of Pople and Beveridge's book.<sup>4</sup> The basis for the PMO,  $\{\phi_{\bar{\mu}}\}$ , we discuss below. In general, a bar above a subscript or the subscript  $p$  in this work denotes a positronic quantity.

Minimizing the expectation value of the Hamiltonian by varying the coefficients in eq 2 while keeping the MO's normalized and the EMO's orthogonal leads to Roothaan-Hartree-Fock<sup>7</sup> type equations:

$$\begin{aligned} (\mathbf{F} - \epsilon_i \mathbf{S})\mathbf{c}_i & = 0 \quad i = 1, 2, \dots, \\ (\mathbf{F}_p - \epsilon_p \mathbf{S}_p)\mathbf{c}_p & = 0 \end{aligned} \quad (3)$$

which are coupled together and are solved self-consistently.  $\mathbf{c}_i$  and  $\mathbf{c}_p$  are column vectors of coefficients for the  $i$ th EMO and the PMO:

$$\begin{aligned} \mathbf{c}_i & = [c_{1i}c_{2i}c_{3i}\dots]^T \quad i = 1, 2, \dots \\ \mathbf{c}_p & = [c_{1p}c_{2p}c_{3p}\dots]^T \end{aligned} \quad (4)$$

$\epsilon_i$  and  $\epsilon_p$  are the eigenvalues for the  $i$ th EMO and the PMO,  $\mathbf{F}$  and  $\mathbf{S}$  are the electronic Fock and overlap matrices, and  $\mathbf{F}_p$  and  $\mathbf{S}_p$  are the corresponding positronic quantities:

$$\begin{aligned} S_{\mu\nu} & = (\phi_{\mu}|\phi_{\nu}) = \int \phi_{\mu}^* \phi_{\nu} d\bar{\mathbf{r}} \\ S_{\bar{\mu}\bar{\nu}} & = (\phi_{\bar{\mu}}|\phi_{\bar{\nu}}) \end{aligned} \quad (5)$$

$$\begin{aligned} F_{\mu\nu} & = H_{\mu\nu} + \sum_{\lambda} \sum_{\sigma} \left\{ P_{\lambda\sigma} \left[ (\mu\nu|\lambda\sigma) - \frac{1}{2} (\mu\lambda|\nu\sigma) \right] \right. \\ & \quad \left. - P_{\bar{\lambda}\bar{\sigma}} (\bar{\lambda}\bar{\sigma}|\mu\nu) \right\} \\ F_{\bar{\mu}\bar{\nu}} & = H_{\bar{\mu}\bar{\nu}} - \sum_{\lambda} \sum_{\sigma} P_{\lambda\sigma} (\bar{\mu}\bar{\nu}|\lambda\sigma) \end{aligned} \quad (6)$$

where  $\mathbf{H}$  and  $\mathbf{H}_p$  are the matrices of the core Hamiltonian:

$$H_{\mu\nu} = (\phi_{\mu}|H^{\text{core}}|\phi_{\nu}) \quad (7)$$

$$H_{\bar{\mu}\bar{\nu}} = (\phi_{\bar{\mu}}|H_p^{\text{core}}|\phi_{\bar{\nu}})$$

$$H^{\text{core}} = -\frac{1}{2} \nabla^2 - \sum_A V_A(\bar{\mathbf{r}}) \quad (8)$$

$$H_p^{\text{core}} = -\frac{1}{2} \nabla_p^2 + \sum_A V_A(\bar{\mathbf{r}}_p)$$

where  $V_A$  is the potential generated by the nucleus and core electrons of atom  $A$ . (We neglect a very small difference in  $V_A$  for electrons compared to positrons due to exchange.) The matrices  $\mathbf{P}$  and  $\mathbf{P}_p$  in eq 6 are the density matrices

$$\begin{aligned} P_{\mu\nu} & = 2 \sum_i^{\text{occ}} c_{\mu i}^* c_{\nu i} \\ P_{\bar{\mu}\bar{\nu}} & = c_{\bar{\mu}p}^* c_{\bar{\nu}p} \end{aligned} \quad (9)$$

and the symbol  $(\mu\nu|\lambda\sigma)$  denotes the interaction integral

$$(\mu\nu|\lambda\sigma) = \iint \phi_{\mu}^*(1)\phi_{\nu}(1) \frac{1}{r_{12}} \phi_{\lambda}^*(2)\phi_{\sigma}(2) d\bar{\mathbf{r}}_1 d\bar{\mathbf{r}}_2 \quad (10)$$

The symbol  $(\bar{\mu}\bar{\nu}|\lambda\sigma)$  denotes an electron-positron interaction integral; its definition follows from eq 10. In eq 6, the signs attached to these quantities should be noted, along with the absence of an exchange term in the second part of eq 6.

The zero differential overlap approximation is applied to the positron in the same way as to the electrons:

$$\begin{aligned} \phi_{\mu}^* \phi_{\nu} & = |\phi_{\mu}|^2 \delta_{\mu\nu} \\ \phi_{\bar{\mu}}^* \phi_{\bar{\nu}} & = |\phi_{\bar{\mu}}|^2 \delta_{\bar{\mu}\bar{\nu}} \end{aligned} \quad (11)$$

This approximation is applied consistently throughout the CNDO approach except in the evaluation of those matrix elements of  $\mathbf{H}$  and  $\mathbf{H}_p$  (eq 7) which contain a two-center charge distribution in the integrand. These integrals are responsible for most of the chemical bonding effects. Rather than neglecting them, they are set equal to an empirical parameter:

$$\begin{aligned} H_{\mu\nu} & = \beta_{\mu\nu} \quad \left\{ \begin{array}{l} \mu \neq \nu, \mu \text{ on A} \\ \nu \text{ on } \beta, \text{ A} \neq \text{B} \end{array} \right\} \\ H_{\bar{\mu}\bar{\nu}} & = \beta_{\bar{\mu}\bar{\nu}} \end{aligned} \quad (12)$$

Rotational invariance is automatically achieved if all the integrals that appear in the Roothaan-Hartree-Fock equations (eq 3) are evaluated by integration. If some integrals are approximated, as in CNDO theory, rotational invariance must be endowed by subsidiary conditions. Our choice of conditions for the positron is exactly the same as Pople's for the electrons:

$$\begin{aligned} (\phi_{\mu}|V_B|\phi_{\mu}) & = V_{AB}, (\phi_{\bar{\mu}}|V_B|\phi_{\bar{\mu}}) = V_{\bar{A}B}, \mu \text{ on A} \neq \text{B} \\ (\mu\mu|\nu\nu) & = \gamma_{AB}, (\bar{\mu}\bar{\mu}|\nu\nu) = \gamma_{\bar{A}B}, \nu \text{ on B} \\ \phi_{\mu}, \phi_{\nu}, \phi_{\bar{\mu}} & \rightarrow s \text{ type} \end{aligned} \quad (13)$$

The parameters  $\beta_{\mu\nu}$  and  $\beta_{\bar{\mu}\bar{\nu}}$  are set equal to

$$\begin{aligned} \beta_{\mu\nu} & = \frac{1}{2} S_{\mu\nu} (\beta^{\circ}_A + \beta^{\circ}_B) \\ \beta_{\bar{\mu}\bar{\nu}} & = \frac{1}{2} S_{\bar{\mu}\bar{\nu}} (\beta^{\circ}_{\bar{A}} + \beta^{\circ}_{\bar{B}}) \end{aligned} \quad (14)$$

where  $S_{\mu\nu}$  and  $S_{\bar{\mu}\bar{\nu}}$  are calculated, and  $\beta^{\circ}_A$  and  $\beta^{\circ}_{\bar{A}}$  are bonding parameters characteristic of atom A, not the individual orbitals on A.

These approximations render the Roothaan-Hartree-Fock equations (eq 3) as follows:

$$(\mathbf{F} - \epsilon_i \mathbf{1})\mathbf{c}_i = \mathbf{0} \quad i = 1, 2, \dots$$

$$(\mathbf{F}_p - \epsilon_p \mathbf{1})\mathbf{c}_p = \mathbf{0}$$

$$F_{\mu\mu} = U_{\mu\mu} - \sum_{B \neq A} V_{AB} + \sum_B P_{BB} \gamma_{AB} - \frac{1}{2} P_{\mu\mu} \gamma_{AA} - \sum_B P_{B\bar{B}} \gamma_{B\bar{A}}$$

$$F_{\bar{\mu}\bar{\mu}} = U_{\bar{\mu}\bar{\mu}} + \sum_{B \neq A} V_{\bar{A}B} - \sum_B P_{BB} \gamma_{\bar{A}B}$$

$$F_{\mu\nu} = \frac{1}{2} S_{\mu\nu} (\beta^{\circ}_A + \beta^{\circ}_B) - \frac{1}{2} P_{\mu\nu} \gamma_{AB} \quad \mu \neq \nu$$

$$F_{\bar{\mu}\bar{\nu}} = \frac{1}{2} S_{\bar{\mu}\bar{\nu}} (\beta^{\circ}_{\bar{A}} + \beta^{\circ}_{\bar{B}}) \quad \mu \neq \nu \quad (15)$$

where  $\mu$  is on A and  $\nu$  is on B.  $U_{\mu\mu}$  and  $U_{\bar{\mu}\bar{\mu}}$  above are the atomic integrals

$$U_{\mu\mu} = \left( \phi_{\mu} \left| -\frac{1}{2} \nabla^2 - V_A \right| \phi_{\mu} \right)$$

$$U_{\bar{\mu}\bar{\mu}} = \left( \phi_{\bar{\mu}} \left| -\frac{1}{2} \nabla^2 + V_A \right| \phi_{\bar{\mu}} \right) \quad (16)$$

and  $P_{BB}$  ( $P_{B\bar{B}}$ ) is the electronic (positronic) population of atom B:

$$P_{BB} = \sum_{\nu \text{ on B}} P_{\nu\nu} \quad P_{B\bar{B}} = \sum_{\nu \text{ on B}} P_{\bar{\nu}\bar{\nu}} \quad (17)$$

We use Pople's values for the electronic integrals in eq 15, and adhere as closely as possible to his methods for arriving at these in assigning values for the corresponding positronic integrals. For example,  $V_{\bar{A}B}$  is taken to be  $\gamma_{\bar{A}B}$  times the number of valence electrons on atom B,  $Z_B$ :

$$V_{AB} = Z_B \gamma_{AB} \quad V_{\bar{A}B} = Z_B \gamma_{\bar{A}B} \quad A \neq B \quad (18)$$

$\gamma_{\bar{A}B}$  and  $S_{\bar{\mu}\bar{\nu}}$  in eq 15 are evaluated by direct integration, as are their electronic counterparts. Pople chooses values for  $\beta^{\circ}_A$  which cause the CNDO results to mimic those for minimal basis ab initio calculations. No such calculations exist to guide us in choosing values for  $\beta^{\circ}_{\bar{A}}$ , so we resort to a semiempirical determination described below.

The atomic integral  $U_{\mu\mu}$  can be related to the ionization potential  $I_{\mu}$  and to the electron affinity  $A_{\mu}$ . Pople ignored exchange contributions to write an average expression as

$$U_{\mu\mu} = -\frac{1}{2} (I_A + A_{\mu}) - \left( Z_A - \frac{1}{2} \right) \gamma_{AA} \quad (19)$$

$I_{\mu}$  and  $A_{\mu}$  are taken directly from atomic spectral data as averages of atomic term values weighted according to the multiplicity of each term arising from the lowest configuration. A great deal of such data exists for parameterizing the electronic quantities, but positron ionization potentials and affinities are generally unknown. Indeed, the literature shows only five usable numbers of our parameterization! These are: the positronium affinities of H (1.014 eV, ref 8), O ( $2.2 \pm 0.5$  eV), OH (<1.5 eV), and F ( $2.9 \pm 0.5$  eV, ref 9); and the positron affinity of H (<0, ref 10). (Accurate scattering data exists for positrons off hydrogen and helium atoms, but this is of no interest to us in the present application.) Thus we see our task

is quite different from that of Pople: we must fit our five numbers to some orderly and sensible scheme which permits us to interpolate values for lithium through nitrogen. To aid us we must make some assumptions regarding the positron affinities of the first row atoms. These assumptions can be modified later as more experimental and theoretical data become available. At this time, we do not have enough data to enable us to average our positronic parameters over multiplets as Pople did for the electronic calculations. We must be content with what little ground state data on positron-atom binding is presently available.

Let us consider the diagonal matrix elements first. We may write, from eq 15, 16, and 18:

$$F_{\bar{\mu}\bar{\mu}} = (U_{\bar{\mu}\bar{\mu}} - P_{AA} \gamma_{\bar{A}\bar{A}}) + \left( \sum_{B \neq A} Q_B \gamma_{\bar{A}B} \right) \bar{\mu} \text{ on A} \quad (20)$$

The first parenthetical term is purely atomic, and we recognize it as the interaction of a positron in the orbital  $\phi_{\bar{\mu}}$  with atom A. It is the balance of a large repulsive core part  $U_{\bar{\mu}\bar{\mu}}$  and a large attractive part  $P_{AA} \gamma_{\bar{A}\bar{A}}$  due to the valence electrons. Suppose  $P_{AA} = Z_A + 1$ . Then  $U_{\bar{\mu}\bar{\mu}} - P_{AA} \gamma_{\bar{A}\bar{A}}$  is the negative of  $PA_{\bar{\mu}}^-$ , the positron affinity of the ion  $A^-$ :

$$U_{\bar{\mu}\bar{\mu}} = -PA_{\bar{\mu}}^- + (Z_A + 1) \gamma_{\bar{A}\bar{A}} \quad (21)$$

We can relate the positron affinity of  $A^-$ ,  $PA_{\bar{\mu}}^-$ , to the quantity about which we have a little information, the positronium affinity of A,  $PsA_{\bar{\mu}}^-$ , by the equation

$$PsA_{\bar{\mu}}^- = PA_{\bar{\mu}}^- + A_{\mu} - 6.8 \text{ eV} \quad (22)$$

whence

$$U_{\bar{\mu}\bar{\mu}} = (A_{\mu}^- - PsA_{\bar{\mu}}^- - 6.8 \text{ eV}) + (Z_A + 1) \gamma_{\bar{A}\bar{A}} \quad (23)$$

which is the positronic counterpart to eq 19. In order to remain consistently within the CNDO framework, we use the electron affinities averaged over multiplets as calculated by Pople and Segal<sup>11</sup> even though more modern values exist.<sup>12</sup> Also, we note that the electron is going into the lowest empty orbital of the ground state atom. Therefore  $\mu$  in  $A_{\mu}$ , eq 22, is identified as 1s for H, 2s for Li, and 2p for Be through F.

There is a little information on the identification of  $\bar{\mu}$  from theory. Some Hartree-Fock calculations on  $PsH^{13}$  and  $PsCl^{14}$  show that within a shell the positronic eigenvalues are inverted compared to electronic eigenvalues, but that the 1s positronic level is invariably much lower than the 2p.

Cade and co-workers<sup>15</sup> have done some positron-atom Hartree-Fock calculations recently, but report no more than one positronic orbital (1s, 2p) per shell for each atom treated. Hartree-Fock calculations contain no positron-electron correlation, but even if that important effect were included it seems unlikely that the 2p level would fall below the 1s. We therefore, take  $\bar{\mu}$  in eq 23 to denote the positronic 1s orbital. Equation 23 now becomes, for our three known positronium affinities

$$U_{\bar{s}\bar{s}}(H) = 2\gamma_{\bar{H}\bar{H}} - 7.07 \text{ eV} \quad (24)$$

$$U_{\bar{s}\bar{s}}(O) = 7\gamma_{\bar{O}\bar{O}} - 6.63 \text{ eV} \quad (25)$$

$$U_{\bar{s}\bar{s}}(F) = 8\gamma_{\bar{F}\bar{F}} - 6.20 \text{ eV} \quad (26)$$

In order to proceed further, we must decide upon a functional form for the positronic atomic orbitals (PAO),  $\phi_{\bar{\mu}}$ , so that the two particle integral  $\gamma_{\bar{A}\bar{A}}$  above can be calculated.

First we note that  $\phi_{\bar{\mu}}$  should have a small value at the nucleus, owing to positron-nuclear repulsion. 2s and 2p STO's

TABLE I: Positronic Exponential Parameters

A	$r_A,^a \text{ \AA}$	Ratio	$r_A,^b \text{ \AA}$	$\zeta^c$	$\bar{\zeta}^c$
H	0.32		1.54	1.20	0.6265 <sup>d</sup>
Li	1.23		(1.67)	0.65	0.478
Be	0.89	1.382	(1.54)	0.975	0.564
B	0.82	1.085	(1.44)	1.30	0.739
C	0.77	1.065	(1.40)	1.625	0.893
N	0.75	1.027	(1.37)	1.95	1.066
O	0.73	1.027	(1.35)	2.275	1.230
F	0.72	1.014	1.33	2.60	1.405
Ne	0.71	1.014			

<sup>a</sup> From ref 16. <sup>b</sup> Parenthetical values are inferred (see text between eq 26 and 27). <sup>c</sup>  $\zeta$  is the electronic exponential parameter, and  $\bar{\zeta}$  the positronic. <sup>d</sup> The value which gives  $\gamma_{\text{HH}} = 8.25 \text{ eV}$  (see text following eq 33).

are zero at the nucleus, so that feature recommends them as our choice. The symmetries of the PAO's must conform to the full rotation group, as do STO's. Therefore, we choose STO's as our PAO's for the first row atoms. For H, we take the PAO to be 2s rather than 1s in order to keep the positron from the nucleus. It deserves to be emphasized that the positronic orbitals we are trying to describe are either the lowest s (i.e., 1s) or lowest p (i.e., 2p); and that we are choosing a 2s STO to describe this 1s PAO, and a 2p STO for the lowest p PAO. These functions do not satisfy the positron-nucleus cusp value, but neither do the electronic AO's. Their virtue is that they keep the positron away from the repulsive nuclei, and they have the right atomic symmetry. We still have to determine the exponential parameters for the PAO's, to which we now turn. We will consider first the atoms Li to F.

We believe if positronium binds to an atom A, the radius of the complex will be closer than that of  $A^-$  than A, perhaps a little larger than either. This makes sense because the principle source of stability of the complex is resonance between a structure in which positronium orbits A (with due regard being given the indistinguishability of all the electrons involved) and a structure in which the positron orbits  $A^-$ . To facilitate this resonance, the positron will orbit at a radius about equal to that of  $A^-$ . Therefore, the exponential parameter for  $\phi_{\bar{p}}$  should be smaller than that of  $\phi_{\mu}$  by a factor equal to the ratio of the radii of A to  $A^-$ . The radii of the atoms A we take to be Sanderson's "nonpolar covalent" radii.<sup>16</sup> The radius of  $F^-$  is given by Sanderson to be 1.33 Å. Radii of other mononegative first-row ions are unknown, but we estimate them by assuming the shrinking in going from F to Ne to be relatively the same as that in going from  $O^-$  to  $F^-$ , the ratio of the radii of O to F to be the same as  $N^-$  to  $O^-$ , and so on. The ratios and radii obtained in this way are listed in the first three columns of Table I; the last column gives the resulting exponential parameters.

Values obtained for  $\gamma_{\text{AA}}$  from Roothaan's formulas<sup>17</sup> with these exponential parameters are shown in the first column of Table II.  $U_{\text{ss}}$  for O and F can now be calculated from eq 25 and 26; they are listed in the third column.

In the case of hydrogen, had we followed the same procedure, we would have arrived at a value of 0.416 for  $\bar{\zeta}$ . This value is not realistic, because when combined with eq 24 it predicts the positron affinity of H

$$-U_{\text{ss}}(\text{H}) + \gamma_{\text{HH}} \quad (27)$$

to be 1.45 eV; but we know H cannot bind a positron.<sup>10</sup> We will return to this difficulty shortly.

Now we turn to the problem of devising values of  $U_{\text{ss}}$  for the

atoms Li to N. As a guide we use the relationship between  $U_{\text{ss}}$  as used in the electronic CNDO/2 calculations, and those calculated as the energy of an electron in a Slater 2s orbital in the field of the nucleus and two 1s electrons (neglecting exchange):

$$U_{\text{ss}}^{\text{calcd}} = \left( \phi_{2s} \left| -\frac{1}{2} \nabla^2 - \frac{Z}{r} + 2J_{1s}(r) \right| \phi_{2s} \right) \quad (28)$$

The ratio

$$\rho = U_{\text{ss}}^{\text{calcd}}/U_{\text{ss}} \quad (29)$$

varies smoothly and monotonically from 1.106 for Li to 1.091 for O and for F. The corresponding ratio for positrons

$$\bar{\rho} = U_{\text{ss}}^{\text{calcd}}/U_{\text{ss}} \quad (30)$$

can be calculated for O and F, and is seen to be 1.082 and 1.083, respectively. We therefore assume  $\rho$  and  $\bar{\rho}$  to differ by a constant for the first-row atoms.  $\bar{\rho}$  thus obtained for Li through N are given in the second column of Table II, and the values of  $U_{\text{ss}}$  that result from

$$U_{\text{ss}} = U_{\text{ss}}^{\text{calcd}}/\bar{\rho} \quad (31)$$

are given in the third column in parentheses.

Returning now to hydrogen, we seek better values of  $U_{\text{ss}}(\text{H})$  and  $\gamma_{\text{HH}}$  by calculating the positron affinities of each atom Li to F from

$$PA_s = -U_{\text{ss}}(A) + Z_A \gamma_{\text{AA}} \quad (32)$$

using the values of  $U_{\text{ss}}$  and  $\gamma_{\text{AA}}$  already arrived at. The results are in Table II. The correlation between these positron affinities and the electron affinities of 2s holes as averaged over states by Pople (i.e.,  $A_s$  of eq 19) is quite good (and inverse); these two quantities are linearly related. Extrapolating to hydrogen gives  $-1.20 \text{ eV}$  as its positron affinity:

$$-U_{\text{ss}}(\text{H}) + \gamma_{\text{HH}} = -1.20 \text{ eV} \quad (33)$$

A simultaneous solution of eq 24 and 33 gives  $U_{\text{ss}} = 9.45 \text{ eV}$  and  $\gamma_{\text{HH}} = 8.25 \text{ eV}$ . The latter number corresponds to a value for the positronic exponential parameter for hydrogen,  $\bar{\zeta}_{\text{H}}$ , of 0.6265, the value which we hereafter adopt.

It is interesting to compare our calculated positron and positronium affinities with those of other workers. The approximate theory of Goldanskii and Sayasov<sup>18</sup> is not of much help in arriving at positron affinities: using the polarizabilities listed by Sanderson<sup>16</sup> one finds Goldanskii's necessary condition for positron binding is satisfied by H and, to a lesser extent, all the first-row atoms. However, H is known not to bind a positron, as we have noted several times above. Perhaps we might conclude that a fortiori none of the first-row atoms will bind a positron; that conclusion is in accord with our result (Table II).

In Goldanskii's theory, the Schrodinger equation was solved for a positron moving in a Moussa-type potential,  $V(r) = -\alpha/(r^2 + r_A^2)^2$ ,  $\alpha$  being the polarizability. In a newer calculation,<sup>19</sup> Spruch's necessary condition for binding<sup>10</sup> was coupled with the more realistic Morse potential, and Golden and Epstein found that H and N definitely will not bind a positron, but that a bound state for  $e^+O$  could not be ruled out.

The calculations of Cavaliere and Ferrante<sup>20</sup> indicated a positron affinity of 2.80 eV for lithium, in sharp contrast to our result in Table II. These authors used a Hellmann pseudopotential for the electron-core interaction, and a Coulomb potential for the positron which they assumed to be completely shielded from the nucleus by the core electrons. Both

TABLE II: Positronic Integral Parameters<sup>a</sup> for CNDO/2 Calculations

A	$\gamma_{\bar{A}A}$	$\bar{\rho}^b$	$U_{ss}$	PA <sup>c</sup>	PsA <sup>d</sup>	$U_{pp}$ (eq 35)	$q^{\circ}_A$ (eq 34) <sup>e</sup>
H	8.25 <sup>f</sup>		9.45 <sup>f</sup>	-1.20	1.00		0.145
Li	5.382	(1.097)	(6.89) <sup>g</sup>	-1.51	-2.11	9.74	0.280
Be	6.818	(1.086)	(15.47) <sup>g</sup>	-1.83	-2.65	18.54	0.269
B	8.971	(1.084)	(30.13) <sup>g</sup>	-3.22	-1.35	34.79	0.359
C	10.926	(1.083)	(48.24) <sup>g</sup>	-4.54	+0.07	54.86	0.415
N	13.059	(1.083)	(71.75) <sup>g</sup>	-6.46	1.16	80.91	0.494
O	15.105	1.082	99.11 <sup>h</sup>	-8.48	2.20	111.80	0.561
F	17.256	1.083	131.84 <sup>h</sup>	-11.05	2.91	147.52	0.640

<sup>a</sup> All energies in eV. <sup>b</sup> Equation 30. <sup>c</sup> The positron affinity of atom A from eq 32 for Li to F, extrapolated as described in the text (following eq 32) for H. <sup>d</sup> Values for H, O, and F are fitted; others from eq 22. <sup>e</sup>  $q^{\circ}_A$  is the critical electron population for positron binding. <sup>f</sup> Obtained from eq 24 and 33. <sup>g</sup> Equation 31. <sup>h</sup> Equations 25 and 26 with calculated  $\gamma_{\bar{A}A}$ .

these assumptions correspond to rather gross approximations, the validity of which were not investigated. Then the energy was estimated as the expectation value of the resulting model potential, using a very simple trial wave function. We believe the reliability of such a procedure is not any greater than our own extrapolations.

An earlier calculation on e<sup>+</sup>Li by Hoang<sup>21</sup> has some major defects on which we have already commented.<sup>7</sup>

The Hartree-Fock results of Cade<sup>15</sup> indicate a positron affinity of fluoride to be 5.05 eV, for which eq 22 along with an electron affinity of 3.50 eV for fluorine gives a positronium affinity of 1.75 eV. This is in good agreement with the value in Table II, particularly when one considers that Hartree-Fock wave functions do not have any positron-electron correlation. Our value in Table II is, of course, that given by Tao and Green.<sup>9</sup>

Also given in Table II is the quantity

$$q^{\circ}_A = \frac{U_{ss}}{\gamma_{\bar{A}A}} - Z_A \quad (34)$$

which is seen from the discussion following eq 20 to be the critical excess electron population on atom A for binding a positron. There it is seen that, of all atoms considered, hydrogen is the most hospitable to a positron for binding since an excess negative charge of only 0.145 e is sufficient; fluorine is the least hospitable.

We believe our values for positron and positronium affinities are not less realistic than others already reported. We therefore adopt the parameters leading to them as described above; we intend to modify them as more information becomes available.

To determine  $U_{pp}$ , we assume the centrifugal gap,  $U_{pp} - U_{ss} = \langle r^{-2} \rangle_p$ , to be proportional to that for the electrons, for want of a better criterion:

$$U_{pp} = U_{ss} + \frac{U_{ss}}{|U_{ss}|} (U_{pp} - U_{ss}) \quad (35)$$

The resulting values of  $U_{pp}$  are given in Table II. They are larger than  $U_{ss}$ , in agreement with some early atomic calculations.<sup>13,14</sup> The difference between our values for  $U_{ss}$  and  $U_{pp}$  for fluorine (15.68 eV) is considerably greater than Cade and Farazdel's<sup>15</sup> value for the difference in energy between PsF with the positron in its lowest s and p states (2.02 eV); however, these differences are not directly comparable since the interaction integral  $\gamma_{\bar{A}A}$  is constrained to be the same for s and p atomic orbitals in the CNDO method but not in Cade's calculation.

Now our positron problem is fully parameterized except for

the  $\beta^{\circ}_{\bar{A}}$  in eq 14. Our one molecular datum, the positronium affinity of the OH radical<sup>9</sup> is available for this parameterization. For simplicity we take the positronium  $\beta^{\circ}_{\bar{A}}$  to be proportional to its electronic counterpart  $\beta^{\circ}_A$ :

$$\beta^{\circ}_{\bar{A}} = \bar{K} \beta^{\circ}_A \quad (36)$$

where  $\bar{K}$  is atom independent. We seek that value of  $\bar{K}$  which gives the correct positronium affinity of OH, which we take from Tao and Green<sup>9</sup> to be 1.00 eV. That is, we want to find  $\bar{K}$  so that

$$-\epsilon_p = PA^- = PsA - EA + 6.8 \text{ eV} \quad (37)$$

$PA^-$ , the positron affinity of OH<sup>-</sup>, we take to be the negative of the lowest positronic eigenvalue in a calculation on PsOH; the positronium affinity of OH, PsA, is 1.00 eV; and the electron affinity of OH, EA, is 1.825 ± 0.002 eV.<sup>22</sup> This gives -5.97 eV as the desired value of  $\epsilon_p$ .

An artifact of CNDO theory is that  $\epsilon_p$  is independent of the sign of  $\bar{K}$  for PsOH and decreases monotonically as  $|\bar{K}|$  increases. The highest value attainable is therefore that obtained with  $\bar{K} = 0$ . Unfortunately this turns out to be -6.67 eV for PsOH.

As a practical means to extricate ourselves from this dilemma we use for PsOH and in all subsequent calculations of positronium affinities, calculated rather than experimental electron affinities. (The same practice was used by Madia et al.<sup>5</sup>) These we take from Koopmans' theorem to be the negative of the highest electronic eigenvalue for occupied EMO's in a CNDO/2 calculation on the purely electronic negative ion. While this procedure introduces some artificiality and uncertainty into our approach and unquestionably detracts somewhat from its predictive utility, we believe that a consistent use of the procedure gives us positron and positronium affinities which still have relative significance.

Another, lesser important, source of ambiguity has to do with alternate formulas for the positronium affinity PsA: from eq 37

$$PsA = EA + PA^- - 6.8 \text{ eV} \quad (38)$$

but Madia, Schug, Nichols, and Ache<sup>5</sup> used

$$PsA = EA(e^+M) + PA - 6.8 \text{ eV} \quad (39)$$

which are equivalent except when the affinities on the right-hand sides are determined by approximate calculations, as is the case here. For the scores of molecules studied in this work, the two values of PsA are quite close together; only for ozone and benzaldehyde (see below) are the differences greater than

the averages, thus constituting an ambiguity in our predictions of the existence of stable  $\text{PsO}_3$  and  $\text{PsC}_6\text{H}_5\text{CHO}$  complexes. A third estimate of the positronium affinity, the difference in the total energies calculated for A and  $\text{PsA}$ , is much less reliable due to large correlation errors for both systems which do not exactly cancel.

The calculated electron affinity of OH is  $-0.45$  eV. This makes  $-8.25$  eV our desired  $\epsilon_p$ , which is obtained for  $\bar{K} = \pm 0.136$ .

The sign of  $\bar{K}$  has no effect on  $\epsilon_p$  for PsOH but turns out to be very important for most other molecules. We therefore must make a choice. One might reasonably guess that  $\bar{K}$  should be negative on the grounds that the electronic and positronic binding parameters are mostly potential energy, and that the electron and positron charges differ by a sign. We will now see on the basis of a more careful analysis that this is indeed the correct choice for the sign of  $\bar{K}$ .

A calculation on PsOH with each choice for the sign of  $\bar{K}$  gives the coefficients listed in Table III. One intuitively expects the most stable PMO for a diatomic molecule to be one in which the positronic density is small in the repulsive internuclear region and large in the outer regions of the molecule. The positron thus contributes to chemical bonding by pushing atoms together somewhat like a vice, rather than glueing them together as electrons do. These considerations and the results in Table III lead us to the negative sign for  $\bar{K}$  as our choice. They also suggest that when we interpret the positronic bond order matrix, we should associate negative elements with bond strengthening, and positive elements with bond weakening; this is the opposite of the correct interpretation of the electronic bond order matrix. That the analogous interpretation of the diagonal elements of this matrix is manifestly correct [i.e., positive values contribute positively to the atomic charge, opposite to the electronic case] supports our interpretation for the off-diagonal elements.

The other choice for  $\bar{K}$  leads to very deeply bound positronic levels in many molecules.<sup>23</sup> In their parameterization of a PMO theory Madia et al.<sup>5</sup> had large negative off-diagonal Hamiltonian matrix elements (in contrast to our small positive off-diagonal values), which gave calculated positron and positronium binding energies much deeper than ours. We believe these deeply bound levels are spurious. We now consider the approach of these authors in more detail.

*Comparison with the Approach of Madia et al.* Recently Madia, Schug, Nichols, and Ache<sup>5</sup> presented the first semi-empirical PMO theory. As in our own work, CNDO/2 theory was used for the electrons, but the PMO was calculated by combining ideas from a variety of sources. The zero differential overlap assumption and the method of assuring rotational invariance were taken from CNDO theory; thus these authors also solve eq 15 with the matrix elements given there. However, the parameterization scheme used by them is quite different from ours. They took  $\gamma_{AB} = \gamma_{BA}$  and  $S_{\mu\nu} = S_{\nu\mu}$ ; i.e., they assumed the positronic basis  $\{\phi_{\mu}^+\}$  to be identical with that for the electrons,  $\{\phi_{\mu}\}$ . Our  $\gamma_{AB}$  are a little smaller than the corresponding  $\gamma_{AB}$ , and our  $S_{\mu\nu}$  are usually larger (sometimes quite a bit larger, and occasionally smaller; even a few sign changes were observed).

By applying the virial theorem to individual core matrix elements, these authors found  $U_{\mu\mu} = -3U_{\mu\mu}$ . This yields very large (positive) values for  $U_{\mu\mu}$ . Our values for  $U_{\mu\mu}$  were much smaller; most of them are less than the absolute values their electronic counterpart (by an average of about 25%, see Table II).

Madia et al. did not use any empirical data for determining

TABLE III: PMO<sup>a</sup> for e<sup>+</sup>LiH and the Sign of  $\bar{K}$

$\bar{K}$	-0.136	+0.136
$c_{2s}$	0.656	0.656
$c_{2p_o}$	0.021	0.021
$c_H$	-0.754	0.754

<sup>a</sup> Tabulated entrees are  $c_{\mu p}$  in eq 2.

their positronic parameters. If we use their assumptions to calculate positronium affinities, we get from eq 23 with their parameter values

$$\text{PsA(Madia et al.)} = 3U_{\mu\mu} - 6.8 \text{ eV} + (Z_A + 1)\gamma_{AA} + A_{\mu} \quad (40)$$

which gives, for A = H, O, and F the values  $-17.4$ ,  $-294$ , and  $-396$  eV, respectively, quite different from the literature values, namely,  $1.014$ ,<sup>8</sup>  $2.2 \pm 0.5$ ,<sup>9</sup> and  $2.9 \pm 0.5$  eV,<sup>9</sup> respectively.

For the two-center matrix element  $H_{\mu\nu}$ , Madia et al. use the Mulliken approximation, somewhat as in CNDO theory, together with a proportionality constant  $k^{(+)}$

$$H_{\mu\nu}(\text{Madia et al.}) = \frac{1}{2} k^{(+)} S_{\mu\nu} (H_{\mu\mu} + H_{\nu\nu}) \quad (41)$$

Madia et al. state their proportionality constant  $k^{(+)}$  should be in the range  $\frac{2}{3}$  to  $\frac{3}{4}$ . A rough comparison of values for  $F_{\mu\nu}$  is possible by combining the last parts of eq 15 and eq 36 with the value of our proportionality constant  $\bar{K}$ ,  $-0.136$ . We find

$$\frac{F_{\mu\nu}(\text{Madia et al.})}{F_{\mu\nu}(\text{Schrader and Wang})} \approx 15 \frac{U_{\mu\mu}}{\beta_A} \quad (42)$$

This quantity is 30 for H and ranges upward from 8.5 for Li to 75 for F. Thus the off-diagonal Fock matrix elements for the positron are much larger in the approach of Madia et al. than our own. As we stated at the end of the preceding section, these extremely large off-diagonal matrix elements apparently produce very deeply bound PMO's. The lack of atomic parameterization in their approach casts further doubt on its predictive ability, in our opinion.

### III. Results

We give in this section calculated results for a selection of molecules and some discussion of these results. All the molecular geometries were taken from standard tables.<sup>24</sup> The positron affinities reported are the negatives of the lowest positronic eigenvalue,  $\epsilon_p$  in eq 15. A negative affinity means the positron is unbound, i.e., the eigenvalue is positive.<sup>25</sup> Positronium affinities reported are the averages of the two values resulting from eq 38 and 39, and the uncertainty is half the difference; the electron affinity EA is taken to be the negative of the eigenvalue of the highest occupied EMO of the molecular anion (see the discussion in the second paragraph under eq 37), and the positron affinity of the anion  $\text{PA}^-$  is the negative of the lowest positronic eigenvalue obtained in a calculation on positron-plus-anion.

The SCF equations (eq 15) are solved as follows: To get the iterations started, the positron is first ignored and Huckel EMO's are calculated, thus generating an approximate set of electronic atomic populations. These atomic populations are input to the CNDO SCF procedure described in the previous section. Each step in the iteration process consists of two parts: (1) the positronic part of eq 15 is solved with the most recent

**TABLE IV: Calculated Positron and Positronium Affinities<sup>a</sup> for First-Row Hydrides**

	Positron affinity	Positronium affinity	Dipole moment <sup>b</sup>
LiH	0.45	$-1.70 \pm 0.01$	5.88
BeH <sub>2</sub>	-0.02	$-7.00 \pm 0.00$	0
B <sub>2</sub> H <sub>6</sub>	-0.17	$-3.99 \pm 0.14$	0
CH <sub>4</sub>	-0.13	$-5.60 \pm 0.43$	0
NH <sub>3</sub>	-0.06	$-5.52 \pm 0.75$	1.47
H <sub>2</sub> O	-0.09	$-5.90 \pm 0.87$	1.85
HF	-0.84	$-7.00 \pm 0.39$	1.82

<sup>a</sup> In electron volts. <sup>b</sup> In debye; from "Handbook of Chemistry and Physics", 51st ed, R. C. Weast, Ed., The Chemical Rubber Co., Cleveland, Ohio, 1970-1971.

set of electronic atomic populations, thus providing an improved set of positronic atomic populations; (2) these are used in a new solution of the electronic part of eq 15, thus providing an improved set of electronic atomic populations. Our code is not fully optimized for running times, so our execution times are not of great significance. We find that adding a positron to a molecule approximately doubles the computing time. The computing times on our Xerox Sigma 9 computer for C<sub>6</sub>H<sub>6</sub>, e<sup>+</sup>CH<sub>6</sub>, C<sub>6</sub>H<sub>6</sub><sup>-</sup>, and PsC<sub>6</sub>H<sub>6</sub> are 35, 73, 59, and 101 s, respectively. For H<sub>2</sub>O the same sequence of times is 0.6, 1.1, 0.7, and 1.5 s.

a. *First-Row Hydrides.* Calculated positron and positronium affinities for the simplest hydride of each first-row element are displayed in Table IV. There it can be seen that only LiH binds a positron, and positronium is bound by none, according to our calculations.

Our calculations give for the positronic population of the atoms in e<sup>+</sup>LiH ( $P_{LiLi}$  and  $P_{HH}$ , eq 17) the values of 0.25 for lithium and 0.75 for hydrogen. The energy lowering achieved by positronic delocalization is apparently great enough to partly offset the repulsive nature of the positron-lithium ion interaction. Perhaps one should not neglect, as many have, the cation contribution to annihilation probabilities in alkali halides and alkali hydrides.

The electronic populations in e<sup>+</sup>LiH are 2.62 for lithium (counting the core) and 1.38 for hydrogen, compared to 2.73 and 1.27 for LiH. Thus, a slight increase of electronic charge on the already negative hydrogen is induced by the bound positron. Another indication of the relaxation of the electrons is given by the calculated dipole moments: 6.16 D for LiH and 6.40 D for e<sup>+</sup>LiH, counting only nuclei and electrons. The overall dipole moment of e<sup>+</sup>LiH (i.e., counting the positron) is 0.73 D, in the same direction.

The positronic MO coefficients are (-0.429, -0.111, +0.869) for the PAO basis functions (Li(s), Li(p), H). The EMO and PMO along the internuclear axis and its extensions are shown in Figure 1. The appearance of the PMO suggests that, were it an EMO, it would be strongly antibonding; we have already pointed out that this shape contributes to bonding for a PMO. The positronic bond order matrix elements ( $P_{\mu\nu}^+ = c_{\nu p}^* c_{\mu p}$ ; cf. eq 9) for Li(s)-H and Li(p)-H are -0.419 and -0.096, respectively. The corresponding electronic bond order matrix elements are 0.644 and 0.665. Thus, the positron enhances the electronic bond, and constitutes 28% of the total bond order. We did not find the internuclear distance for e<sup>+</sup>LiH which gives the lowest total energy; presumably that distance is less than that of LiH (1.595 Å) and at that lesser distance the positron affinity and the positronic contribution to the total bond order should both be slightly greater.

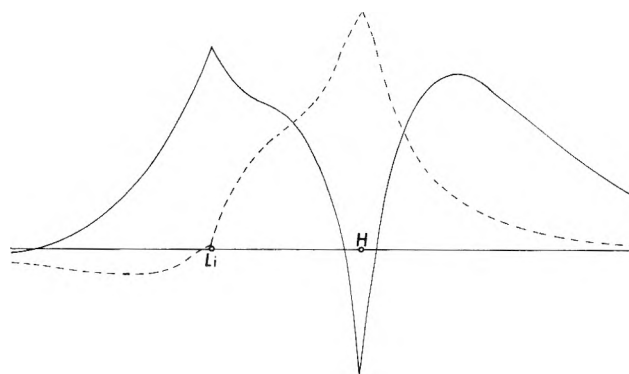


**Figure 1.** Positronic molecular orbital (PMO) in e<sup>+</sup>LiH (full curve), and the electronic molecular orbital (EMO) (dashed curve). The two MO's are drawn to different scales

The detailed shape of the PMO as shown in Figure 1 is probably not very significant. For example, it includes none of the effects of electron-positron correlation. It also suffers from the restricted nature of our positronic basis set: we should have 2p orbitals on the hydrogen in order to be consistent with the other atoms, since there are no positronic cores for any of them. However, we feel that the additional programming required is not worth the return in this initial attempt at a semiempirical approach to positron binding. The additional flexibility endowed by extending the basis set in this way would skew the hydrogen contribution slightly to the right in Figure 1, as the lithium contribution now is. This would reduce the positronic density of lithium from 0.25 to some smaller value.

The shape of the PMO in Figure 1 does not strongly suggest the large density on the hydrogen indicated by our population analysis (0.75). One should realize however that a better visual guide to the atomic populations is given by the square of the PMO times a volume element which, for the appropriate bi-centric coordinate system, is proportional to  $r_{Li}r_H$ . This factor gives a positronic probability distribution which is small everywhere along the line containing the nuclei except to the right of the hydrogen nucleus. Taking this into account, the positronic atomic populations as given by the standard population analysis (eq 17) are seen to be quite reasonable.

From Table IV we see that NH<sub>3</sub> and H<sub>2</sub>O come close to being able to support a bound PMO. Perhaps dimers of these molecules will offer enough delocalization energy to bind a positron; this would be a case of "positrostriction," the analogue of electrostriction. Such a phenomenon might be involved in the anomalous positron lifetimes observed for ammonia and methane by McNutt and co-workers.<sup>26</sup> This matter is under further investigation.

b. *Diatomics and Simple Binary Compounds.* Calculated positron and positronium affinities for a number of simple molecules are given in Table V. None of the homonuclear diatomics studied bind either a positron or a positronium atom. The amount by which a positron fails to be bound parallels the (negative) positron affinities of the isolated atoms (Table II), and is less than this quantity due to the delocalization stabilization. That O<sub>2</sub> fails to bind positronium may be significant in view of its known quenching ability for ortho-positronium by spin conversion but not by chemical combination.<sup>27,28</sup>

Our calculations (Table V) for the molecules LiF, BeO, CO, and NO indicate no positron or positronium binding. In view of Crawford's<sup>29</sup> argument concerning the influence of a permanent dipole moment on electron affinities, one might ex-

TABLE V: Calculated Positron and Positronium Affinities<sup>a</sup> for Diatomics, Simple Binary Compounds, and Ozone

	Positron affinity	Positronium affinity	Dipole moment <sup>b</sup>
H <sub>2</sub>	-0.03	-5.25 ± 0.00	
Li <sub>2</sub>	-0.50	-3.52 ± 0.00	
N <sub>2</sub>	-3.60	-12.40 ± 0.00	
O <sub>2</sub>	-5.35	-9.11 ± 0.00	
F <sub>2</sub>	-8.06	-3.38 ± 0.00	
LiF	-0.81	-2.93 ± 0.00	6.33 <sup>c</sup>
BeO	-1.09	-0.59 ± 0.05	6.19 <sup>d</sup>
CO	-3.07	-11.75 ± 0.03	0.11 <sup>c</sup>
NO	-4.30	-10.83 ± 0.01	0.15 <sup>c</sup>
NO <sub>2</sub>	-4.36	-0.02 ± 0.00	
N <sub>2</sub> O	-3.78	-10.15 ± 0.20	
N <sub>2</sub> O <sub>2</sub>	-4.15	-6.15 ± 0.00	
N <sub>2</sub> O <sub>4</sub>	-4.93	-3.84 ± 0.02	
O <sub>3</sub>	-5.42	0.22 ± 0.43	

<sup>a</sup> In electron volts. <sup>b</sup> In debye. <sup>c</sup> From "Handbook of Chemistry and Physics", 51st ed, R. C. Weast, Ed., The Chemical Rubber Co., Cleveland, Ohio, 1970-1971. <sup>d</sup> Calculated using the CNDO/2 method.

pect LiF and BeO to bind a positron. Perhaps our parameterization scheme described above results in values of  $\gamma_{\text{O}}$  and  $\gamma_{\text{F}}$  which are too small. One should recognize that the calculated positron affinities of the atoms (Table II) are gotten from eq 32, which entails taking the difference of two large and uncertain quantities. Despite a lengthy search for alternant parameterizations, we were unable to find one which gave significantly better results and at the same time was justifiable by acceptable arguments. The basic problem here is a shortage of empirical and theoretical data on positron and positronium affinities of atoms. As more of this information becomes available, an improved parameterization will be constructed.

It should be pointed out here that our negative results for positron binding to highly polar molecules may stem from an inadequacy of the electronic CNDO method itself. CNDO and related methods frequently give a poor account of ionic compounds, perhaps owing to the use of standard atomic exponents in the electronic basis. We believe that this work is not the proper place to experiment with new electronic parameterizations, owing to the novelty of our systems, so we do not pursue this point further.

None of the oxides of nitrogen for which results are given in Table V bind either a positron or a positronium atom, although for NO<sub>2</sub> the calculated positronium affinity is extremely close to the threshold for binding. Below it is seen that positronium affinities are quite geometry dependent, especially that for NO<sub>2</sub>. NO<sub>2</sub> and NO, being radicals and efficient quenchers of orthopositronium, are of special interest here. It should be noted that for ozone, the two formulas for positronium affinity, eq 38 and 39, give results for opposite sign, yielding a difference (0.43 eV) greater than the average (0.22 eV). Thus our method gives ambiguous results in this case.

*c. Ethylene and Its Fluoro Derivatives.* A study of ethylene and its fluoro-substituted analogues is instructive. Our results are given in Table VI. There it is seen that the positron and positronium affinities correlate not at all with dipole moment but very well (negatively) with the number of fluorine atoms. A fluorine atom tends to decrease the electron population of other atoms in a molecule, but in doing so it never acquires enough electron population to equal its critical binding value

TABLE VI: Calculated Positron and Positronium Affinities<sup>a</sup> for Ethylene and Its Fluoro Derivatives

	Positron affinities	Positronium affinities	Dipole moment <sup>b</sup>
C <sub>2</sub> H <sub>4</sub>	-0.01	-2.32 ± 0.65	0
C <sub>2</sub> H <sub>3</sub> F	-0.07	-2.18 ± 0.76	1.43
C <sub>2</sub> H <sub>2</sub> F <sub>2</sub> (1,1)	-0.30	-2.29 ± 0.92	1.38
C <sub>2</sub> H <sub>2</sub> F <sub>2</sub> (trans)	-0.64	-2.49 ± 0.67	0
C <sub>2</sub> H <sub>2</sub> F <sub>2</sub> (cis)	-0.62	-2.47 ± 0.70	2.42
C <sub>2</sub> HF <sub>3</sub>	-0.72	-3.74 ± 0.20	1.40
C <sub>2</sub> F <sub>4</sub>	-2.89	-5.49 ± 0.02	0

<sup>a</sup> In electron volts. <sup>b</sup> In debyes, from "Handbook of Chemistry and Physics", 51st ed, R. C. Weast, Ed., The Chemical Rubber Co., Cleveland, Ohio, 1970-1971.

of 0.64 e (see Table II). The effect of each fluorine atom in a molecule is therefore to discourage positron and positronium binding (except in fluorobenzene, as noted below, for which resonance effects are important), and Table VI shows the effect is approximately additive.

The almost-bound PMO's in ethylene and fluoroethylene are both  $\sigma$  type. In ethylene, the PMO has the maximum number of interatomic nodes, and shows a positron density of 0.00 on each carbon and 0.25 on each hydrogen. In e<sup>+</sup>C<sub>2</sub>H<sub>3</sub>F, the positron populations are given in Figure 2. The repulsive effect of the fluorine atom on the positron is obvious, although more subtle effects are apparently also involved. For example, the two hydrogen atoms farthest from the fluorine have different polarizabilities as is shown by their net charges (not counting the positron) in C<sub>2</sub>H<sub>3</sub>F and e<sup>+</sup>C<sub>2</sub>H<sub>3</sub>F: they are both 0.04 in C<sub>2</sub>H<sub>3</sub>F, but the hydrogen trans to the fluorine goes up to 0.05 in e<sup>+</sup>C<sub>2</sub>H<sub>3</sub>F and the one cis goes down to 0.02, thus becoming relatively more attractive to the positron. Larger relaxation effects occur in the  $\pi$  system: The carbon closest to fluorine loses 0.07 e from its  $\pi$  orbital and the other carbon gains 0.08 e upon the addition of the positron. The relaxations of the other AO's in the molecule are much smaller; apparently the large buildup of positronic charge on the cis hydrogen is due to an intricate interplay of several small forces.

*d. Positronium Anion Compounds.* Next we consider a series of compounds analogous to positronium hydroxide (PsOH) and positronium fluoride (PsF), both of which we used in our parameterization. Geometries used in this section are those of the corresponding acid in the gas phase, with the acidic proton removed and a positron added. Positronium affinities are reported in Table VII as positronium binding energies.

The binding energies of PsNO and PsNO<sub>2</sub> differ from the positronium affinities of NO and NO<sub>2</sub>, respectively reported in Table V because the geometries used there are those of the gas phase radicals. For NO, the N-O distances used are 1.1502 and 1.2116 Å in Tables V and VII, respectively: for NO<sub>2</sub>, the geometry used in Table V is ( $\angle\text{ONO} = 134.25^\circ$ , NO = 1.197 Å; the two O's are equivalent), whereas in Table VII we used ( $\angle\text{ONO}' = 118^\circ$ , NO = 1.20 Å, NO' = 1.40 Å, the hydrogen in HNO<sub>2</sub> is bonded to the primed oxygen). Comparing Table V and VII for PsNO<sub>2</sub> shows the great sensitivity of the calculated positronium affinities of symmetric molecules to small symmetry-reducing geometry changes. Thus it appears that full geometry optimization is called for. This is beyond the scope of the present work, but is now under further study.

In HNO the hydrogen is bonded to the nitrogen, in PsNO

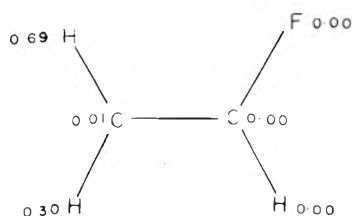


Figure 2. Positron population in  $C_2H_3F$  (but the lowest PMO is not quite bound; see text).

TABLE VII: Calculated Binding Energies<sup>a</sup> of Some Positronium–Anion Compounds

Compound	Binding energy	Compound	Binding energy
PsNO	$-9.97 \pm 0.02$	PsCN	$2.64 \pm 0.01$
PsNO <sub>2</sub>	$1.95 \pm 0.21$	HCOOPs	$3.27 \pm 0.57$
PsNO <sub>3</sub>	$2.83 \pm 0.16$	CH <sub>3</sub> COOPs	$3.79 \pm 0.78$

<sup>a</sup> In electron volts.

the positron populations of N and O are 0.59 and 0.41, respectively. In HNO<sub>2</sub>, the hydrogen is bonded to the primed oxygen (see geometry above), and in PsNO<sub>2</sub> the positron populations of N, O, and O' are 0.48, 0.02, and 0.50, respectively. In PsNO<sub>3</sub>, the positron populations are 0.72 for N, and 0.09, 0.09, 0.11 for the three oxygens, the latter being the one to which the hydrogen is bonded in HNO<sub>3</sub> (gas phase geometry). In e<sup>+</sup>NO and e<sup>+</sup>NO<sub>2</sub> the atomic positron populations are about the same as in the respective positronium compound; but for e<sup>+</sup>NO<sub>3</sub>, the positron populations for N, O, O, and O' are 0.37, 0.01, 0.01, and 0.62, respectively, in marked contrast to the positron population in PsNO<sub>3</sub>.

Thus there is a good correlation between hydrogen positions in acids HA and positron densities in compounds PsA, but only among atoms of the same atomic number within a molecule. A stronger effect seems to be the chemical environment of each atom; specifically, a positron is stabilized on a given atom almost as much by excess electrons on adjacent atoms as by excess electrons on the atom itself. For example, in PsNO<sub>3</sub> the nitrogen has 72% of the positron, but its electron population, 6.68, indicates a loss of 0.32 electrons to the three bonded oxygens. The positron sits mainly on the repulsive nitrogen in order to avail itself of the negative charges on all these oxygens simultaneously. This peculiar behavior is a consequence of the diffusiveness of the PAOs, which was put into our parameterization by means of the small positronic exponential parameters (Table I, last column). We feel this diffusiveness is realistic, and that the resulting positronic distributions are not far off.

The relative binding energies of PsNO and PsNO<sub>2</sub> are consistent with the relative propensities of NO and NO<sub>2</sub> to combine chemically with positronium, as observed by Goldanskii and co-workers,<sup>27</sup> and by Chuang and Tao.<sup>28</sup> The latter report quenching cross sections for O<sub>2</sub>, NO, and NO<sub>2</sub> to be (0.002 65, 0.008 45, and 26 Å<sup>2</sup>, respectively); the geometries used here show positronium affinities of ( $-9.11 \pm 0.00$ ,  $-9.97 \pm 0.02$ ,  $1.95 \pm 0.21$  eV, respectively).

Positronium cyanide, positronium formate, and positronium acetate are all strongly bound, according to our calculations.

As a numerical experiment, we ran formic and acetic acids with a nonacidic proton replaced by a positron. The positronium binding energies obtained are  $1.23 \pm 0.87$  eV for "PsCOOH" and  $2.92 \pm 0.39$  eV for "CH<sub>2</sub>PsCOOH". The total energies computed for these two compounds show that they

TABLE VIII: Proton<sup>a</sup> vs. Positron Affinities and Hydrogen<sup>a</sup> vs. Positronium Affinities of Several Radicals

	Proton affinity <sup>b</sup>	Positron affinity <sup>b</sup>	Hydrogen affinity <sup>b</sup>	Positronium affinity <sup>b</sup>
CH <sub>3</sub>	$5.39 \pm 0.01$	-0.16	$4.68 \pm 0.01$	$2.01 \pm 0.45$
C <sub>2</sub> H <sub>3</sub>	$7.33 \pm 0.05$	-0.01	$4.24 \pm 0.05$	$2.24 \pm 0.44$
C <sub>2</sub> H <sub>5</sub>	6.44	+0.09	4.37	$2.81 \pm 0.37$
C <sub>6</sub> H <sub>5</sub>	$9.33 \pm 0.11$	+0.27	$4.97 \pm 0.11$	$2.71 \pm 0.31$
NH <sub>2</sub>	$8.0 \pm 0.1$	-0.14	$4.6 \pm 0.1$	$1.83 \pm 0.84$
HO	$6.37 \pm 0.12$	-0.78	$5.38 \pm 0.12$	$1.61 \pm 0.74^c$
HO <sub>2</sub>	$6.35 \pm 0.06$	-0.66	$3.84 \pm 0.05$	$2.41 \pm 0.23$

<sup>a</sup> Calculated by the present authors from data listed by J. L. Franklin et al., *Natl. Stand. Ref. Data Ser., Natl. Bur. Stand., No. 26* (1969). <sup>b</sup> In electron volts. <sup>c</sup> Differs from 1.00, the value used in our parameterization, owing to geometry changes. 1.00 eV is presumably for the actual O–H distance in the PsOH species. 1.61 ± 0.74 is for the O–F distance in PsOH the same as in H<sub>2</sub>O.

are 3.01 and 2.83 eV less stable than HCOOPs and CH<sub>3</sub>COOPs, respectively; the stabilization of the latter two compounds compared to the former two comes from a large decrease in core–core repulsions which swamps out a small increase in total light particle energy.

In CH<sub>3</sub>COOPs, only 0.02 of the positron is on the CH<sub>3</sub> group, but in CH<sub>2</sub>PsCOOH the situation is reversed: 0.03 is on the COOH group. In both molecules, one of the carbons has most of the positron (the COOPs carbon in CH<sub>3</sub>COOPs has a positron population of 0.77; the CH<sub>2</sub>Ps carbon in CH<sub>2</sub>PsCOOH has a positron population of 0.58). Thus, the positron tends to stay in the same part of the molecule as the proton it replaced, although not always on the same atom if it can stabilize itself by sharing negative charges of more than one adjacent electronegative atom.

e. *Comparison of Positron and Proton Affinities, and of Positronium and Hydrogen Bond Energies.* In this section we report our results for several species RH; we calculate positron and positronium affinities for R· and compare these with literature values of proton and hydrogen affinities. Table VIII summarizes our results. Of those radicals studied, only the ethyl and phenyl radicals will bind a positron; all will bind a positronium atom. An examination of the values in Table VIII shows there to be no correlation whatever between proton and positron affinities, and between hydrogen and positronium affinities.

In the molecule C<sub>6</sub>H<sub>5</sub>Ps, the carbon from which the proton has been removed has a positron population of 0.75. The adjacent carbons have 0.11 positron each, and their hydrogens have 0.01; no other atom in the molecule has appreciable positron density. However, in e<sup>+</sup>C<sub>6</sub>H<sub>5</sub>, the positron is localized (77%) on the hydrogen across the ring from the carbon from which the proton was removed. In e<sup>+</sup>C<sub>2</sub>H<sub>5</sub> the positron is localized 45% on each hydrogen in the CH<sub>2</sub> group.

f. *Comparison of pK<sub>a</sub> Values and Positron Affinities of Anions of Several Weak Acids.* pK<sub>a</sub>'s for several weak acids are displayed alongside the calculated positron affinities of the anion in Table IX and shown graphically in Figure 3. The correlation is quite strong, except for the molecules phenol, H<sub>2</sub>O<sub>2</sub>, and water (which one might not regard as typically acidic in their other properties), for H<sub>3</sub>BO<sub>3</sub> (the only Lewis acid on our list), and for the one example of second ionization. One can draw a straight line through the four points for phenol, H<sub>2</sub>O<sub>2</sub>, water, and H<sub>3</sub>BO<sub>3</sub> which has a slope approximately equal to that of the larger group.

**TABLE IX:  $pK_a$  vs. Positron Affinity for Several Weak Acids<sup>a</sup>**

Acid, HA	$pK_a$	Positron affinity of $A^-$
1. Oxalic acid (first)	1.42	6.04 eV
2. HF	3.16	6.26 <sup>b</sup>
3. HNO <sub>2</sub>	3.35	6.29
4. HCOOH	3.68	6.58
5. Benzoic acid	4.18	6.85
6. Oxalic acid (second)	4.30	12.40
7. HN <sub>3</sub>	4.72	6.66
8. Acetic acid	4.74	6.65
9. H <sub>3</sub> BO <sub>3</sub> (first)	9.22	7.00
10. HCN	9.4	7.91
11. Phenol	10.0	6.44
12. H <sub>2</sub> O <sub>2</sub>	11.62	6.90
13. Water	15.7	8.31

<sup>a</sup>  $pK_a$ 's from T. R. Hogness, W. C. Johnson, and A. R. Armstrong, "Quantitative Analysis and Chemical Equilibrium", 5th ed, Holt, Rinehart and Winston, New York, N.Y., 1966.

<sup>b</sup> From the positronium affinity of F used in the parameterization of this work (2.91 eV), the electron affinity of F (3.45 eV), and the binding energy of positronium (6.8 eV).

g. *Benzene and Related Compounds.* In this section we present our results for benzene and some of its simple derivatives, and borazole. The results are summarized in Table X. Eight of the eleven compounds studied in this section were also studied by Madia et al.<sup>5</sup> They found the calculated positron and positronium affinities to be very sensitive to the value of  $k^{(+)}$ , and presented calculation on each molecule for two values of  $k^{(+)}$ ,  $\frac{2}{3}$  and  $\frac{3}{4}$ , stating that the actual value should be in that range.

Our results for benzene suggest that the positron is not bound, although the (positive) eigenvalue is very close to zero. The PMO associated with this lowest eigenvalue has virtually all its probability density on the hydrogens (less than 0.2% on the carbons), and is the completely antisymmetric  $\sigma$  orbital ( $B_{1u}$ ) with a node between all bonded atoms as well as between adjacent hydrogens (we have already noted that such nodes are characteristic of bonding PMO's). Madia et al. also found the lowest orbital to be  $\sigma$ , but give no other information except the binding energy, which they report as 0.22 or 7.7 eV depending on the value of  $k^{(+)}$ . Thus Madia et al. predict a bound positron and we do not.

Many workers, including one of us,<sup>30</sup> have assumed the existence of a bound  $\pi$  PMO, but our present calculations show the lowest  $\pi$  PMO is unbound by 8.63 eV; there are 13 lower  $\sigma$  PMO's. This is a consequence principally of the relative values of the atomic integrals  $U_{ss}$  and  $U_{pp}$  for carbon and  $U_{ss}$  for hydrogen, values which we believe are quite reasonable.

Madia et al. report a positronium affinity for benzene of either  $-5.98$  or  $+1.62$  eV, our result is  $-7.62 \pm 0.60$  eV. That is, we predict that benzene will not bind positronium.

The next eight molecules in Table X, numbered 2 through 9, are arranged according to the effect of their substituents on electrophilic substitution, the strong activators leading the list. The first three have activating groups, and the first four have ortho, para directors. Trends in affinities with activating power are weak or nonexistent. Our results indicate that nitrobenzene will bind positronium but not a positron; and the reverse is true for the other seven molecules, although our result for the positronium affinity of benzaldehyde is ambiguous. In contrast, Madia et al. show very much deeper

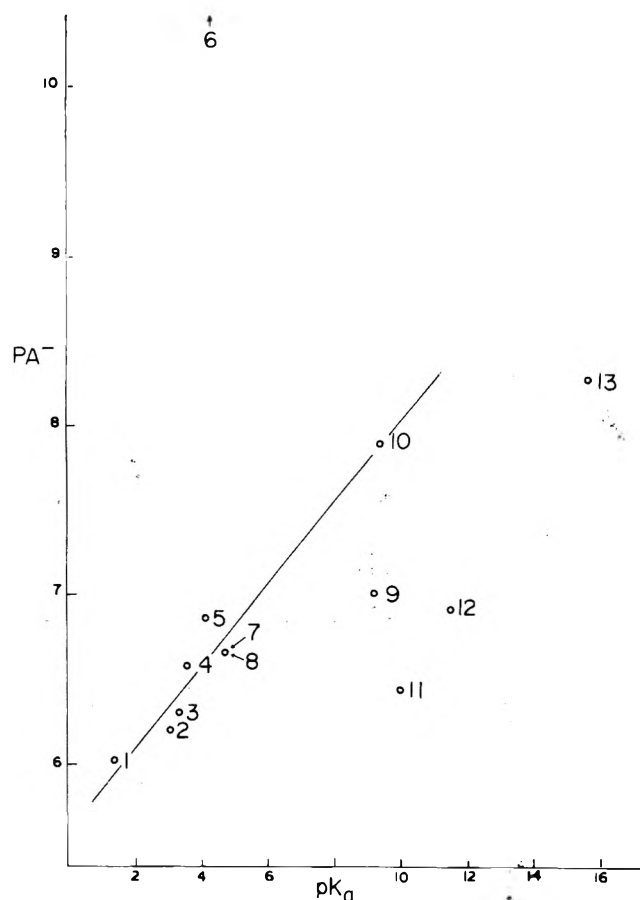


Figure 3. For acids HA, the positron affinity of the anion  $A^-$  (in electron volts, ordinate) vs.  $pK_a$ . See Table IX for the numerical  $k \times y$ .

positronic levels for each of the six molecules they studied in this group. Indeed, these workers report at least one bound PMO for each molecule studied and several bound PMO's for most of them (up to eight, depending upon the value of  $k^{(+)}$ ). We found only three bound excited PMO's for the entire group of eight molecules (one each for aniline, phenol, and toluene), and the deepest of these is bound by only 0.05 eV.

Our results show that, for each of the seven molecules capable of binding a positron, the positron is extremely strongly localized on a single hydrogen atom, as is shown in Table X. In five molecules, the positron is localized on the hydrogen in the para position; in benzoic acid and benzaldehyde, on the ortho hydrogen syn to the acyl oxygen. No other molecules in this group have an acyl oxygen. We are unable to rationalize these results in a simple way. Apparently a delicate balance of several factors determines what part of a molecule will provide the most attractive site for a positron. Relative polarizabilities of atoms in a molecule, as well as the overall electronic distribution before the positron approaches are certain to be significant factors.

Of all the atoms considered here, hydrogen is by far the most hospitable to positrons and fluorine the least (see the last column of Table II). Thus one should probably expect about the same contribution to annihilation rates and angular correlation curves from all bound positron-molecule complexes which contain hydrogen.

Fortunately unbound positrons also contribute to experimental results, perhaps dominantly, and for such positrons totally symmetric representations of the positron wave must

TABLE X: Positron and Positronium Affinities<sup>a</sup> of Benzene and Related Compounds

	This work		Madia et al. <sup>d</sup>		This work
	Positron affinity	Positronium affinity	Positron affinity <sup>c</sup>	Positronium affinity <sup>c</sup>	Positron position in e <sup>+</sup> -molecule
1. C <sub>6</sub> H <sub>6</sub>	-0.06	-7.62 ± 0.60	3.96 ± 3.74	-2.18 ± 3.80	Unbound
2. C <sub>6</sub> H <sub>5</sub> NH <sub>2</sub>	0.51	-2.71 ± 0.37	11.74 ± 4.29	7.51 ± 4.29	<i>p</i> -H (80%)
3. C <sub>6</sub> H <sub>5</sub> OH	0.41	-2.32 ± 0.20			<i>p</i> -H (78%)
4. C <sub>6</sub> H <sub>5</sub> CH <sub>3</sub>	0.46	-2.32 ± 0.19	7.75 ± 3.86	-2.20 ± 3.85	<i>p</i> -H (79%)
5. C <sub>6</sub> H <sub>5</sub> F	0.17	-2.68 ± 0.36	6.10 ± 3.29	1.05 ± 3.25	<i>p</i> -H (77%)
6. C <sub>6</sub> H <sub>5</sub> COOH	0.52	-0.58 ± 0.44			<i>o</i> -H (89%) <sup>b</sup>
7. C <sub>6</sub> H <sub>5</sub> NO <sub>2</sub>	-0.16	1.11 ± 0.81	4.69 ± 4.15	0.31 ± 4.42	Unbound
8. C <sub>6</sub> H <sub>5</sub> CN	0.24	-1.84 ± 0.08	4.85 ± 3.84	-0.21 ± 4.49	<i>p</i> -H (78%)
9. C <sub>6</sub> H <sub>5</sub> CHO	0.44	-0.09 ± 0.47	6.97 ± 3.43	3.44 ± 3.45	<i>o</i> -H (88%) <sup>b</sup>
10. <i>p</i> -C <sub>6</sub> H <sub>4</sub> O <sub>2</sub>	-0.35	-1.88 ± 0.03	4.37 ± 4.02	3.50 ± 4.13	Unbound
11. B <sub>3</sub> N <sub>3</sub> H <sub>6</sub>	-0.02	-8.20 ± 0.23			Unbound

<sup>a</sup> In electron volts. <sup>b</sup> Only the ortho hydrogen nearest the oxygen in the carbonyl group has positron population. <sup>c</sup> Uncertainties are due to an incompletely determined parameter,  $k^{(+)}$ , in their method. <sup>d</sup> Reference 5.

dominate at low scattering energies (in contrast to the completely antisymmetric bound PMO's), thus giving rise to features in the observed results quite different from those arising from annihilation from bound states.

Binding dynamics for positronium atoms are quite different than for positrons. Indeed, our results in Table X show that if a molecule can bind a positron it cannot bind positronium and vice versa.

It is gratifying that nitrobenzene, the only molecule in Table X which our calculations show can bind positronium, has already been found by Ache and co-workers<sup>31</sup> to have a positive positronium binding enthalpy in toluene as a solvent; and that toluene itself, for which we do not find a positive affinity, has been found to have zero binding enthalpy for positronium capture. Our results for benzoquinone differ from those of Ache et al., however.

Good agreement with a model-dependent approach of Goldanskii and co-workers<sup>32</sup> should also be noted. These authors report a positronium binding energy to nitrobenzene of 0.15–0.17 eV (the energy being slightly solvent dependent), which is a good deal smaller than our calculated value. Again our results for benzoquinone are inconsistent with observations: The temperature dependence of the positronium quenching rate for these molecules observed by Goldanskii and co-workers<sup>2,32</sup> indicate nitrobenzene to be a weak quencher and *p*-benzoquinone strong.

We have noted, however, a great sensitivity of calculated positron and positronium affinities of symmetrical molecules to small distortions which reduce the symmetry. A discussion of this point with regard to NO<sub>2</sub> is given above. We observed the same effect for *p*-benzoquinone and borazole. Therefore, the affinities reported for these molecules in Table X are somewhat provisional until geometry optimization can be performed. Perhaps then our calculations will agree even better with experiment.

Positron populations are quite different for positron-molecule complexes than positronium-molecule complexes. In the case of PsC<sub>6</sub>H<sub>5</sub>NO<sub>2</sub>, the extra electron attaches itself to the oxygens and the positron sits on the nearby nitrogen, and not at all on the hydrogens. The special reactivity of nitrobenzene toward positronium has already been observed by Ache and co-workers,<sup>33</sup> who also found that positronium attack is probably at the nitrate group, in agreement with our results.

## Summary

The capacity for binding a positron or a positronium atom seems to be fairly rare for small diamagnetic molecules; the only unambiguous exception among the example in Tables IV and V is LiH, with O<sub>3</sub> as a less certain possibility. Grati-fying concordance was obtained between our results for the positronium affinities of O<sub>2</sub>, NO, and NO<sub>2</sub> and the observed action of these molecules as reacting quenchers.<sup>27,28</sup>

The discrepancy between our results for LiF and BeO and Crawford's condition<sup>29</sup> seems to indicate a defect in our parameterization for the positron or Pople's parameterization for the electron, which somewhat vitiates our results for ionic compounds. Contrary to widespread assumption and reasonable intuition,  $\pi$  systems are inhospitable to positrons and positronium atoms; that result of our calculation appears to be real and, we believe, incontrovertible. Positronium atoms appear to be stable to homolytic cleavage when replacing hydrogen atoms in compounds, but less so than hydrogen. This latter observation is to be expected because of the greater "zero-point vibration" of positronium compared to hydrogen. It should be noted that the positronium atom is usually well localized near to the hydrogen vacancy.

We have discovered a definite correlation between acid strength and the positron affinity of the acid anion, but the expected and related behavior of the positron as a good electrophile in aromatic substitution was not found.

For all aromatic molecules studied in this work (except benzene, benzoquinone, and borazole), each molecule binds either a positron or positronium but not both. This is in contrast to the results of Madia et al.<sup>5</sup> whose calculated positronium affinities were less than calculated positron affinities for each molecule studied. Perhaps our results are consistent with the fact that some molecules are good quenchers (positronium bound states?), others are good inhibitors (positron bound states?), and few are both.

The necessity for using calculated electron affinities in eq 38 and 39 is a defect resulting from our parameterization. That of Madia et al. suffers similarly. A number of alternative parameterizations were investigated including some which treated electron-positron correlation more explicitly. Unfortunately, none of these were found to be superior to that described and used in this work. This problem probably renders our calculated positronium affinities less reliable than

our calculated positron affinities. In view of the great importance of bound states in annihilation,<sup>2,26-28,31</sup> we felt it worthwhile to persist in our work with positronium in spite of this deficiency in our present approach.

Perhaps our inability to obtain a bound state of a positron interacting with LiF or BeO, both of which satisfy Crawford's necessary condition<sup>29</sup> by a large margin, stems from the same defect. Another obvious shortcoming in our approach is the absence of hydrogen-based 2p orbitals in the PMO basis set. This has already been discussed above. Perhaps the present formulation should be dubbed "PMO/1" to emphasize its provisional character.

*Acknowledgments.* We are indebted to Mr. John K. Kim who participated in some of our early discussions on the parameterization problem; we have also benefitted from discussions and correspondence with Professor J. R. Bolton, Professor J. Hinze, and Dr. R. M. Lambrecht. We are indebted to Professor H. Ache for providing us with some important experimental results prior to their publication, and to Professor A. F. Clifford for an illuminating comment. The computations were performed on a Xerox Sigma 9 computer at the Marquette University Computer Services Division. The original CNDO/2 program was obtained from the Quantum Chemistry Program Exchange, Indiana University.

We are grateful to the National Science Foundation and to the Marquette University Committee on Research for Support of this work; acknowledgement is also made to the donors of the Petroleum Research Fund, administered by the American Chemical Society, for support.

## References and Notes

- (1) For recent general reviews see J. H. Green, *MTP Int. Rev. Sci., Inorg. Chem., Ser. One*, **8**, 251 (1972); S. J. Tao, *Appl. Phys.*, **3**, 1 (1974); V. I. Goldanskii and V. P. Shantarovich, *Appl. Phys.*, **3**, 335 (1974); R. N. West, "Positron Studies of Condensed Matter", Taylor and Francis, London, 1974.
- (2) V. I. Goldanskii and V. P. Shantarovich, *Appl. Phys.*, **3**, 335 (1974).
- (3) P. B. Navin, D. M. Schrader, and C. F. Lebeda, *Phys. Rev. A*, **9**, 2248 (1974), and earlier work by the same authors.
- (4) J. A. Pople and D. L. Beveridge, "Approximate Molecular Orbital Theory", McGraw-Hill, New York, N.Y., 1970.
- (5) W. J. Madia, J. C. Schug, A. L. Nichols, and H. J. Ache, *J. Phys. Chem.*, **78**, 2682 (1974).
- (6) D. M. Schrader, *Phys. Rev. A*, **1**, 1070 (1970).
- (7) C. C. J. Roothaan, *Rev. Mod. Phys.*, **23**, 69 (1951); C. G. Hall, *Proc. R. Soc. London, Ser. A*, **205**, 541 (1951).
- (8) B. A. P. Page and P. A. Fraser, *J. Phys. B*, **7**, L389 (1974).
- (9) S. J. Tao and J. H. Green, *J. Phys. Chem.*, **73**, 882 (1969).
- (10) I. Aronson, C. J. Kleinman, and L. Spruch, *Phys. Rev. A*, **4**, 841 (1971).
- (11) J. A. Pople and G. A. Segal, *J. Chem. Phys.*, **44**, 3289 (1966).
- (12) E.g., -I. Schmidt-Bocking and K. Bethge, *J. Chem. Phys.*, **58**, 3244 (1973).
- (13) V. I. Goldanskii, A. V. Ivanova, and E. P. Prokopev, *Zh. Eksp. Teor. Fiz.*, **47**, 659 (1964) [*Sov. Phys.-JETP*, **20**, 440 (1965)]; V. I. Goldanskii, A. V. Ivanova, and E. P. Prokopev in "Yadernaya Khimia", V. I. Goldanskii and A. K. Lavrukina, Ed., Nauka, Moscow, 1965, p 249; A. V. Ivanova and E. P. Prokopev, *Zh. Eksp. Teor. Fiz.*, **48**, 1155 (1965) [*Sov. Phys.-JETP*, **21**, 771 (1965)].
- (14) L. Simons, *Soc. Sci. Fenn., Commentat. Phys.-Math.*, **14** (1948), 2, 9, 12 (1949); *Phys. Rev.*, **90**, 165 (1953).
- (15) P. E. Cade and A. Farazdel, *Solid State Commun.*, **14**, 807 (1974); *Phys. Lett.* **47A**, 179 (1974); P. E. Cade and A. Farazdel, preprint (1976); *Phys. Rev. B*, **9**, 2036 (1974).
- (16) R. T. Sanderson, "Inorganic Chemistry", Reinhold, New York, N.Y., 1967.
- (17) C. C. J. Roothaan, *J. Chem. Phys.*, **19**, 1445 (1951).
- (18) V. I. Goldanskii and Yu. S. Sayasov, *Zh. Eksp. Teor. Fiz.*, **47**, 1995 (1964) [*Sov. Phys.-JETP*, **20**, 1339 (1965)].
- (19) S. Golden and I. R. Epstein, *Phys. Rev. A*, **10**, 761 (1974).
- (20) P. Cavaliere and G. Ferrante, *Phys. Lett.*, **34A**, 297 (1971).
- (21) D. V. Hoang, *Dokl. Akad. Nauk B. SSR*, **9**, 798 (1965).
- (22) R. J. Celotta, R. A. Bennett, and J. L. Hall, *J. Chem. Phys.*, **60**, 1740 (1974); H. Hotop and T. A. Patterson, *ibid.*, **60**, 1806 (1974).
- (23) In a preliminary report of this work at the VIII Midwest Theoretical Chemistry Conference (Madison, Wisc., May, 1-3 1975), results for positive *K* were reported; these are hereby retracted.
- (24) H. J. M. Bowen et al., Ed., *Chem. Soc., Spec. Publ.*, **No. 11** (1958); *ibid.*, **No. 1E** (1965).
- (25) We hesitate to assign any physical meaning to the many negative affinities reported here, although it is possible that some of them correspond to resonant states. We do not make any such claims here; the negative affinities are given merely to show by how much a positron or positronium atom fails to be bound.
- (26) J. D. McNutt, W. W. Kinnison, and A. D. Ray, *J. Chem. Phys.*, **60**, 4730 (1974); J. D. McNutt, V. B. Summerour, A. D. Ray, and P. H. Huang, *ibid.*, **62**, 1777 (1975).
- (27) A. D. Mokrushin and V. I. Goldanskii, *Zh. Eksp. Teor. Fiz.*, **53**, 478 (1967) [*Sov. Phys.-JETP*, **26**, 314 (1968)]; V. I. Goldanskii, A. D. Mokrushin, and A. O. Tatur, *Khim. Vys. Energ.*, **3**, 27 (1969) [*High Energy Chem.*, **3**, 22 (1969)].
- (28) S. Y. Chuang and S. J. Tao, *Phys. Rev. A*, **9**, 989 (1974).
- (29) O. H. Crawford, *Mol. Phys.*, **20**, 585 (1971).
- (30) D. M. Schrader and J. K. Kim, *Appl. Phys.*, **4**, 249 (1974).
- (31) W. J. Madia, A. L. Nichols, and H. J. Ache, *J. Am. Chem. Soc.*, **97**, 5041 (1975).
- (32) V. I. Goldanskii, I. B. Kevdina, V. P. Shantarovich, and K. Petersen, *Dokl. Akad. Nauk. SSSR*, **203**, 870 (1972).
- (33) A. L. Nichols, W. J. Madia, and H. J. Ache, *J. Phys. Chem.*, **78**, 1881 (1974).

Electron Spin Resonance of the Triplet  $\pi\pi^*$  State of Pyrene- $d_{10}$  in Benzophenone

L. J. Noe\* and L. F. Wojdac

Department of Chemistry, University of Wyoming, Laramie, Wyoming 82071 (Received May 5, 1976)

The electron spin resonance absorption spectrum of pyrene- $d_{10}$  in benzophenone has been observed at  $-20^\circ\text{C}$ . The analysis was accomplished by rotating about the laboratory fixed **a**, **b**, and **c** crystallographic axes rather than the molecular axes and using a limited self-consistent procedure. The  $zfs$  parameters are the same as those that have been previously reported for pyrene- $d_{10}$  in fluorene. Though pyrene does not fit perfectly into a benzophenone substitutional site the molecules are nearly coplanar with their long axes differing by  $3^\circ$ .

## Introduction

Since the time when Hutchison and Mangum<sup>1</sup> first observed an ESR signal originating from the triplet state of naphthalene the subject of triplet ESR spectroscopy has been extensively treated experimentally and theoretically. Besides obtaining the molecular parameters  $\pm D$  and  $\mp E$ , the absolute signs of  $D$  and  $E$  and triplet sublevel sequencing and activity (from spin polarization measurements), one also obtains the orientation of the guest molecule in substitutional solid solution experiments. The orientational information and sublevel identification are of particular importance for quantitative and qualitative analysis of low-temperature visible-ultraviolet spectroscopy. Normally in the single crystal ESR method the analysis is accomplished by rotating the crystal about the long, normal, or short molecular axis of the guest, the magnetic field directed perpendicular to the rotation axis. With wedges the crystal is adjusted until the axis of rotation is collinear with a molecular axis as evidenced by maximum and minimum separation between pairs of absorption maxima as a function of angle of rotation. Then from the field dependence of the various resonant field maxima the matrix of direction cosines between the molecular axes (**L**, **M**, **N**) and crystal axes (**a**, **b**, **c**) is obtained along with the relative values of the  $D$  and  $E$  parameters.<sup>1-4</sup>

Although McDowell et al.<sup>5</sup> and Fischer and Denison<sup>6</sup> obtained the relative values of  $D$  and  $E$  and the orientation of pyrene- $d_{10}$  in the host crystals fluorene and biphenyl, respectively, we were interested in obtaining this information in the polar host benzophenone and use of it in the analysis of Stark measurements on the lowest triplet level of pyrene. Additionally we thought that it would be of general interest to report on a slightly different procedure of obtaining the aforementioned molecular parameters and orientation that is of particular value for those conducting ESR single crystal investigations using conventional counter top spectrometers. Our approach is to rotate the crystal about the laboratory fixed crystal frame **a**, **b**, and **c** and to employ a limited self-consistent procedure in obtaining the orientation and relative values of  $D$  and  $E$ .

## Experimental Section

All ESR measurements were carried out using a Varian E-3 x-band spectrometer equipped with a HP Model X523B frequency meter. The magnetic field was calibrated using a proton resonance magnetometer. Frequencies ranged from 9.27 to 9.30 GHz for the measurements.

Two types of crystals were studied; pyrene- $d_{10}$  in fluorene

(orthorhombic  $D_{2h}^{16}$ - $P_{nam}$  with four molecules per unit cell<sup>7</sup>) served as our standard and pyrene- $d_{10}$  in benzophenone (orthorhombic  $D_{2h}^4$ - $P_{212121}$  with four molecules per unit cell<sup>8</sup>) served as our system of interest. The former crystals were grown from the melt while the latter were grown from a superconcentrated ethanol solution. In both cases the concentration of pyrene- $d_{10}$  was  $10^{-10}$  to  $10^{-5}$  M. The experiments were conducted at approximately  $-20^\circ\text{C}$  using a 950-W Ze lamp equipped with a Corning 7-54 band pass filter. The red pyrene phosphorescence was visible at ambient temperature in both hosts. Neither of the neat hosts gave rise to ESR signals. Data points were taken in  $10^\circ$  rotational increments by scanning the region from 2350 to 4350 G. The starting point was chosen so that a crystal axis was coincident with the magnetic field direction.

## Results and Discussion

It is well known that a sample of randomly oriented phosphorescent molecules under certain circumstances can yield the relative values of  $D$  and  $E$  or  $D^2 + 3E^2$ ; the canonical orientation relations yield the values of  $D$  and  $E$  for  $\Delta M_s = \pm 1$  with  $H$  perpendicular to  $H_{rf}$ <sup>1,2</sup> and for  $\Delta M_s = \pm 2$  with  $H$  parallel to  $H_{rf}$ <sup>9</sup> while the relation  $D^2 + 3E^2 = 3(h\nu)^2/4 - 3(g\beta H_{\min})^2$  holds for  $H$  perpendicular to  $H_{rf}$  and  $H$  parallel to  $H_{rf}$ .<sup>10</sup> Provided that the relative values of  $D$  and  $E$  can be obtained using the randomly oriented method(s) then it is only necessary to rotate the host crystal about one of the space fixed crystal axes, **a**, **b**, or **c**, and to use a limited self-consistent procedure based on the  $\Delta M_s = \pm 1$  relations with an initial guess of the molecular orientation to refine the parameters and obtain the molecular orientation.

With the axis of rotation precisely collinear with a crystal axis the angular dependence of the resonant magnetic field is simply a pair of symmetrically related curves. If the axis of rotation is not collinear with a crystal axis then one expects a pair of curves for each translationally nonequivalent molecule in the unit cell located on a specified site. Starting with the free electron  $g$  value, the experimental angular dependent resonant magnetic field points, the  $D$  and  $E$  values, and a guess for the molecular orientation, one can readily make use of a numerical iteration that in effect compares the experimental points with the points as calculated from the eigenvalues of the well-known cubic secular equation.<sup>11</sup> The procedure is to successively generate molecular orientation matrices starting with the initial guess and if necessary artificially tilt the crystal and then to minimize the differences between the calculated and experimental points until self-consistency is achieved within experimental error.

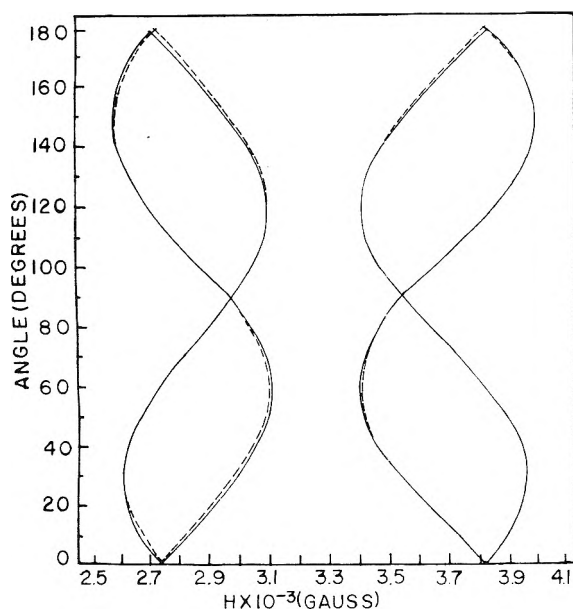


**Figure 1.** Resonant magnetic field vs. angle of rotation for pyrene- $d_{10}$  in fluorene as the crystal is rotated about the  $c$  crystallographic axis. The solid curves are experimental and the dashed curves are calculated. At  $0^\circ$   $H_{app}$  is parallel to  $a$ .

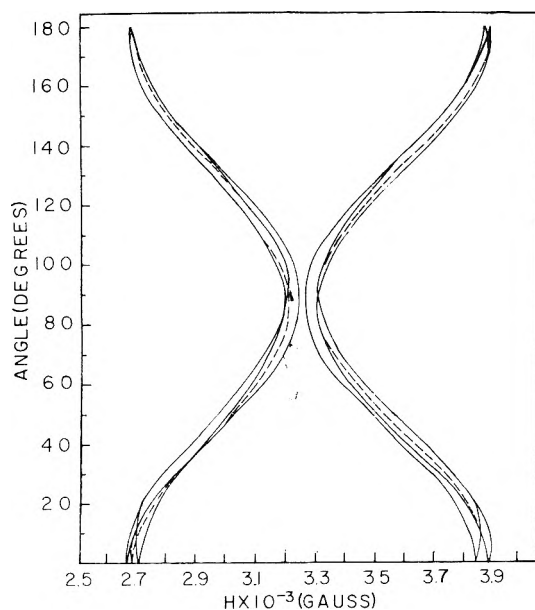


**Figure 2.** Resonant magnetic field vs. angle of rotation for pyrene- $d_{10}$  in benzophenone as the crystal is rotated about the  $a$  crystallographic axis. The solid curves are experimental and the dashed curves are calculated. At  $0^\circ$   $H_{app}$  is parallel to  $c$ .

Using the zfs parameters determined by McDowell et al.<sup>5</sup> for pyrene- $d_{10}$  in fluorene ( $\pm D = 0.06577$ ,  $\pm E = 0.03162$  cm<sup>-1</sup>,  $g_{xx} = 2.0028$ ,  $g_{yy} = 2.0023$ ,  $g_{zz} = 2.0019$ ) we tested this procedure with initial guess of the long axis of pyrene along the  $c$  crystallographic axis and the short and normal axes at  $45^\circ$  to the  $b$  and  $c$  axes. The result for the rotation about  $c$  is typical and is illustrated in Figure 1. The agreement between our orientation matrix and the previously determined one (uncertainty of  $\pm 15^\circ$ ) was within  $1^\circ$  for all matrix elements. Considering the limited nature of the iteration and the uncertainty in our experimental fields ( $\pm 5$  G) we felt that this result demonstrated a reasonable degree of reliability in the

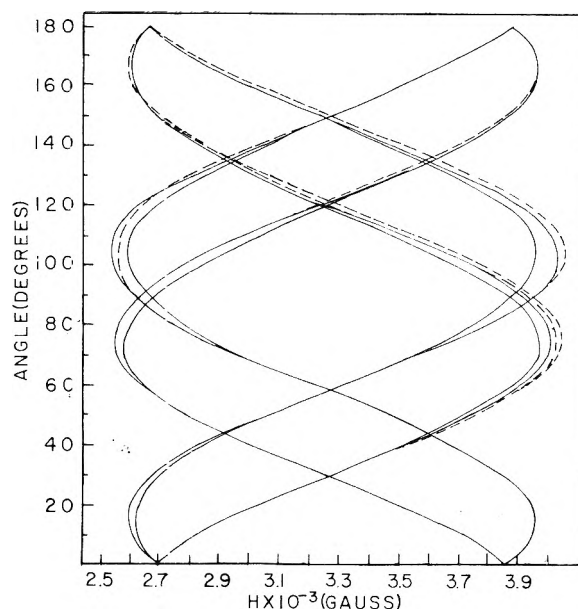


**Figure 3.** Resonant magnetic field vs. angle of rotation for pyrene- $d_{10}$  in benzophenone as the crystal is rotated about the  $b$  crystallographic axis. The solid curves are experimental and the dashed curves are calculated. At  $0^\circ$   $H_{app}$  is parallel to  $c$ .

method. There was exact agreement between the previously determined results<sup>5</sup> and the calculated results using a synthetic rotation (skewed about  $4^\circ$  from  $c$ ) matrix to generate the "experimental" resonant fields.

The field position  $H_{min}$  (1586 G at 9.340 GHz) of the  $\Delta M_s = \pm 2$  transition was found to be the same for a powdered sample of pyrene- $d_{10}$  in either of the host lattices and corresponded exactly with  $D^2 + 3E^2$  as evaluated by the previously determined literature zfs values.<sup>5</sup> We therefore felt justified in using the literature values of  $D$  and  $E$  in our calculations for the fluorene and benzophenone host lattices keeping in mind that our main objective was to determine the orientation of pyrene- $d_{10}$  in benzophenone. The angular dependence of the resonant fields clearly show that pyrene- $d_{10}$  substitutes in the benzophenone lattice in four translationally non-equivalent positions on one site. The degree to which we were able to fit our data for benzophenone host assuming the x-ray determined orientation for benzophenone<sup>8</sup> as a start is shown in Figures 2 and 3 where we have rotated about the  $a$  and  $b$  axes, respectively. The agreement between orientation matrices was within  $1.5^\circ$  per matrix element for these rotations.<sup>12</sup>

We report the molecular orientation matrix for pyrene- $d_{10}$  in benzophenone as

	L	M	N
a	0.9199	-0.2679	0.2863
b	0.3297	0.9236	-0.1954
c	-0.2121	0.2742	0.9380

noting that the pyrene and benzophenone molecules are nearly coplanar based on the previously reported structure of benzophenone;<sup>8</sup>  $L(B) \cdot L(P) \sim 3^\circ$ ,  $M(B) \cdot M(P) \sim 12^\circ$ ,  $N(B) \cdot N(P) \sim 12^\circ$  where B and P symbolize benzophenone and pyrene, respectively, the long axis of benzophenone defined as the line passing through the  $\alpha, \alpha'$ -carbonyl carbons and the short axis defined as the carbonyl axis. Taking our experimental error into account we report the zfs parameters as the same as those previously reported indicating that the polar

host benzophenone does not severely perturb the spin-spin Hamiltonian.<sup>13</sup>

*Acknowledgment.* The authors wish to thank Professor A. Guzzo and the Atomic Energy Commission for the extensive periods they allowed us to use the ESR equipment. We also wish to thank Dr. Barry Garrett for helpful discussion regarding the interpretation of randomly oriented sample spectra.

## References and Notes

- (1) C. A. Hutchison, Jr., and B. W. Mangum, *J. Chem. Phys.*, **29**, 952 (1958).
- (2) R. W. Brandon, R. E. Gerkin, and C. A. Hutchison, Jr., *J. Chem. Phys.*, **41**, 3717 (1964).
- (3) J. S. Vincent and A. H. Maki, *J. Chem. Phys.*, **39**, 3088 (1963).
- (4) M. S. deGroot and J. H. van der Waals, *Mol. Phys.*, **3**, 190 (1960).
- (5) S. W. Charles, P. H. H. Fischer, and C. A. McDowell, *Mol. Phys.*, **9**, 517 (1965).
- (6) P. H. H. Fischer and A. B. Denison, *Mol. Phys.*, **17**, 297 (1969).
- (7) D. M. Burns and J. Iball, *Proc. R. Soc. London, Ser. A*, **227**, 200 (1955).
- (8) E. B. Fleischer, N. Sung, and S. Hawkinson, *J. Phys. Chem.*, **72**, 4311 (1968).
- (9) P. Kottis and R. Lefebvre, *J. Chem. Phys.*, **39**, 393 (1963).
- (10) P. Kottis and R. Lefebvre, *J. Chem. Phys.*, **41**, 379 (1964).
- (11) S. McGlynn, T. Azumi, and M. Kinoshita, "Molecular Spectroscopy of the Triplet State", Prentice-Hall, Englewood Cliffs, N. J., 1969, Chapter 10.
- (12) We also analyzed for the rotation about *c*. The resonant field pattern was very complicated for this rotation and gave a molecular orientation result that differed from the *a* and *b* results by several degrees. This discrepancy was due mainly to an error of  $\pm 5$  G in the measured magnetic field. We report the molecular orientation matrix based on the rotations about *a* and *b* assuming these to be the most accurate.
- (13) Initially we assumed the long axis of pyrene to be collinear with the carbonyl (short) axis of benzophenone, effectively placing the pyrene  $90^\circ$  to the position it actually occupies in the benzophenone crystal. After 12 iterations we obtained the orientation matrix reported above. We have also varied the values of *D* and *E* by as much as 10% and have observed that the calculated values of the resonant fields change by about 3–4 G.

## Infrared Intensities, Polar Tensors, and Atomic Population Densities in Molecules

W. T. King\* and G. B. Mast†

Metcalf Research Laboratory, Brown University, Providence, Rhode Island 02912 (Received April 5, 1976)

The relationship between atomic polar tensors obtained from integrated infrared intensities and the electronic structure of molecules is analyzed. The polar tensor is expressed as a sum of three terms, the net charge and charge "flux" terms of the classical atomic charge model of a molecule, and a quantum-mechanical "interference" term which appears to be at least as important as the classical terms. Calculations are presented which suggest that the effective atomic charges derived from polar tensors are approximately equal to classical net atomic charges and are proportional to Mulliken's atomic population densities. Interpretation of effective charges in terms of population densities is found to account for the magnitude of the effective charges in hydrocarbons, and for the sums of the intensities of the fundamental bands in a wide variety of compounds.

## Introduction

In an earlier paper<sup>1</sup> it was demonstrated that the sums of the integrated intensities of most hydrocarbons were related to one another by a function that depended upon the number of carbon and hydrogen atoms in the molecule, but not upon molecular geometry. It was also demonstrated that the intensities in acetylene presented a most striking exception to this rule. The purpose of this paper is first to develop a framework for the interpretation of infrared intensities and, second, to use this framework to rationalize the above observations on the hydrocarbons.

The sum of integrated intensities of molecules is determined by the effective charges of their atoms,  $\xi_\alpha$ , through the intensity sum rule<sup>2,3</sup>

$$\sum_j \omega_j \Gamma_j = (\pi N_A/3) \sum_\alpha \mu_\alpha \xi_\alpha^2 - \Omega \quad (1)$$

in (1),  $\omega_j \Gamma_j$  denotes the integrated intensity of the *j*th fundamental mode with harmonic frequency  $\omega_j$ .<sup>4,5</sup>

\* Present address: Department of Chemistry, Oregon State University, Corvallis, Oreg.

$$\omega_j \Gamma_j = (1/nl) \int \ln(I_0/I) d\omega$$

$\mu_\alpha$  denotes the reciprocal mass of atom  $\alpha$ , and  $\Omega$  defines a function of the components of the permanent molecular dipole moment **P**, and moments of inertia<sup>2</sup>

$$(\pi N_A/3) \Omega = (P_y^2 + P_z^2)/I_{xx} + (P_x^2 + P_z^2)/I_{yy} + (P_x^2 + P_y^2)/I_{zz} \quad (2)$$

The effective charges in (1) are defined as

$$\xi_\alpha^2 = (\nabla_\alpha \mathbf{P}) \cdot (\nabla_\alpha \mathbf{P})' \quad (3)$$

that is, as the sum of squares of the components of the polar tensor,  $\nabla_\alpha \mathbf{P}$ , for atom  $\alpha$ .<sup>2,6,7</sup>

Clearly, then, to account for the observed behavior of the intensity sums for the hydrocarbons, the dependence of effective charges upon molecular structure must be analyzed. To this end, the dependence of polar tensors upon the electronic structure is examined in the next sections. This investigation suggests that, to a good approximation, the effective charge for an atom is given by the difference between its nuclear charge and its gross electron population density; that is, the net atomic charge defined by Mulliken.<sup>8</sup>

To test this assertion, the effective charges in the hydrocarbons are computed using atomic population densities reported in the literature. The effective charges calculated in this manner were found to be in good agreement with their experimental values, even for acetylene. As an additional test of the relationship between effective charges and atomic population densities, intensity sums were calculated for a variety of molecules using (1) and (2), and were found to compare well with their experimental values.

### Analysis of the Polar Tensor

The relation between integrated intensities and the electronic structure of molecules is a subject of considerable interest.<sup>9</sup> In most of the recent investigations of this problem, the derivatives of the molecular dipole moment have been estimated for specific molecules by numerical differentiation of the computed dipole moments. The majority of these calculations have used electronic wave functions given by the semiempirical CNDO approximation;<sup>10,11</sup> however, a few ab initio calculations have been reported.<sup>9</sup> We are more concerned with a comparison of dipole derivatives for a group of compounds, the hydrocarbons, rather than with the detailed properties of its individual members, and adopt a more formal approach here in order to bring out more clearly the relationship between molecular electronic structure and the polar tensor.

The dipole moment of a neutral molecule is given by

$$\mathbf{P}(\mathbf{R}) = \sum_{\beta} \mathbf{R}_{\beta} Q_{\beta} - \int \mathbf{r} \rho(\mathbf{r}; \mathbf{R}) d^3\mathbf{r} \quad (4)$$

in which  $\mathbf{R}_{\beta}$  denotes the vector defining the position of atom  $\beta$ , with nuclear charge  $Q_{\beta}$ , and  $\rho(\mathbf{r}; \mathbf{R})$  denotes the molecular electron number density function for the nuclear configuration defined by the set of vectors  $\mathbf{R} = \{\mathbf{R}_{\beta}\}$ . For an  $N$ -electron system

$$\rho(\mathbf{r}; \mathbf{R}) = \int |\psi(\mathbf{r}, \mathbf{r}_2, \dots, \mathbf{r}_N)|^2 d^3\mathbf{r}_2 \dots d^3\mathbf{r}_N$$

It is implied by this definition that a natural (atomic) system of units is used in which charge is measured in units of the electron charge,  $e$ . The  $X$ th row of the polar tensor for atom  $\alpha$ , then, is given by the gradient of the  $X$ th component of  $\mathbf{P}$

$$\nabla_{\alpha} P_X = Q_{\alpha} \mathbf{i} - \int x \nabla_{\alpha} \rho(\mathbf{r}; \mathbf{R}) d^3\mathbf{r} \quad (5)$$

The remaining  $Y$ th and  $Z$ th rows of the polar tensor are found analogously.

The two terms in eq 5 clearly give the nuclear and electronic contributions to the polar tensor. The electronic part, in turn, can be conceived of consisting of two parts, a "perfect following" contribution and a "nonperfect following" contribution.<sup>12</sup> The "perfect following" term describes that part of the density function,  $\rho(\mathbf{r}; \mathbf{R})$ , which "follows" a nucleus during a change in nuclear configuration and produces no effect other than to screen the charge on the displaced nucleus, while the "nonperfect following" term describes all remaining contributions and presumably represents the effects of the redistribution of electrons due to nuclear displacement, effects such as, for example, the "charge flux" contribution recently discussed by Decius.<sup>13</sup>

To determine the "perfect following" and "nonperfect following" contributions, it is useful to represent the density function as a multicenter expansion in complete sets or orthonormal atomic orbitals centered on each nucleus<sup>14,15</sup>

$$\rho(\mathbf{r}; \mathbf{R}) = \sum_{\beta, \nu} \sum_{i, j} C_{\beta \nu}^{ij} \psi_i^*(\mathbf{r}_{\beta}) \psi_j(\mathbf{r}_{\nu}) \quad (6)$$

in which, for example,  $\mathbf{r}_{\beta} = \mathbf{r} - \mathbf{R}_{\beta}$  and  $\psi_i(\mathbf{r}_{\nu})$  denotes the  $i$ th orbital centered on nucleus  $\nu$ . The "interference" terms, described by the cross terms in (6), are next partitioned among the other terms by expanding the orbitals centered on one nucleus in terms of orbitals centered on another; that is

$$\psi_j(\mathbf{r}_{\nu}) = \sum_k S_{\nu \beta}^{ik} (R_{\beta \nu}) \psi_k(\mathbf{r}_{\beta})$$

in which  $R_{\beta \nu} = |\mathbf{R}_{\beta} - \mathbf{R}_{\nu}|$  denotes the internuclear distance and  $S_{\nu \beta}^{ik} = \langle \psi_i(\mathbf{r}_{\nu}) | \psi_k(\mathbf{r}_{\beta}) \rangle$  is the overlap integral. Thus (5) may be represented in terms of orbitals centered on one nucleus at a time

$$\rho(\mathbf{r}; \mathbf{R}) = \sum_{\beta} \sum_{i, k} N_{\beta \beta}^{ik} \psi_i^*(\mathbf{r}_{\beta}) \psi_k(\mathbf{r}_{\beta}) \quad (7)$$

in which

$$N_{\beta \beta}^{ik} \equiv \sum_{\nu} \sum_j C_{\beta \nu}^{ij} S_{\nu \beta}^{jk}$$

Integrating (7) over electron coordinates  $r$  yields

$$N = \sum_{\beta} N_{\beta}(\mathbf{R})$$

in which  $N$  is the total number of electrons in the molecule and

$$N_{\beta}(\mathbf{R}) = \sum_i N_{\beta \beta}^{ii}(\mathbf{R}) \quad (8)$$

is the gross electron population density defined by Mulliken.<sup>8</sup>

Substituting (7) into (4) yields the following expression for the dipole moment

$$\mathbf{P}(\mathbf{R}) = \sum_{\beta} \mathbf{R}_{\beta} Q_{\beta} - \sum_{\beta} \sum_{i, k} \langle \psi_i(\mathbf{r}_{\beta}) | \mathbf{r} | \psi_k(\mathbf{r}_{\beta}) \rangle N_{\beta \beta}^{ik}$$

This expression can be further simplified by replacing the spaced-fixed vector,  $\mathbf{r} = \mathbf{r}_{\beta} + \mathbf{R}_{\beta}$ , by the vectors relative to the nuclei in each term in the sum to yield the more familiar form<sup>8</sup>

$$\mathbf{P}(\mathbf{R}) = \sum_{\beta} \mathbf{R}_{\beta} \zeta_{\beta} - \sum_{\beta} \Phi_{\beta \beta}(\mathbf{R}) \quad (9)$$

where, using (8)

$$\zeta_{\beta}(\mathbf{R}) \equiv Q_{\beta} - N_{\beta}(\mathbf{R}) \quad (10)$$

is Mulliken's net atomic charge,<sup>8</sup> and

$$\Phi_{\beta \beta}(\mathbf{R}) \equiv \sum_{i, k} \langle \psi_i(\mathbf{r}_{\beta}) | \mathbf{r}_{\beta} | \psi_k(\mathbf{r}_{\beta}) \rangle N_{\beta \beta}^{ik}(\mathbf{R}) \quad (11)$$

In (11) the terms for which  $i = k$  are not included, for they vanish by symmetry for all  $i$ . Finally, the desired expression for the polar tensor is obtained by computing the gradient of (9)

$$\nabla_{\alpha} \mathbf{P} = \zeta_{\alpha} \mathbf{I} + \sum_{\beta} \mathbf{R}_{\beta} \nabla_{\alpha} \zeta_{\beta} - \sum_{\beta} \nabla_{\alpha} \Phi_{\beta \beta} \quad (12)$$

in which  $\mathbf{I}$  denotes the unit (diagonal) tensor, and since the matrix elements do not depend upon nuclear configuration

$$\nabla_{\alpha} \Phi_{\beta \beta} = \sum_{i, k} \langle \psi_i(\mathbf{r}_{\beta}) | \mathbf{r}_{\beta} | \psi_k(\mathbf{r}_{\beta}) \rangle \nabla_{\alpha} N_{\beta \beta}^{ik}$$

The first two terms in (12) describe the polar tensor obtained from a classical atomic charge model of infrared intensities, in which the  $\Phi_{\beta \beta}$  terms in (9) are ignored. The first term in (12) defines the "perfect following" contribution as the net charge on the atom of interest. The second term de-

scribes that part of the "nonperfect following" contribution that can be attributed to a classical charge model, and represents the "charge flux" contribution to the polar tensor in the model described by Decius,<sup>13</sup> for example.

The third set of terms in (12),  $\nabla_\alpha \Phi_{\beta\beta}$ , cannot be incorporated into a classical atomic charge model, for they do not have a classical analogue.<sup>15</sup> These terms have their origin in the cross terms,  $C_{\beta\alpha}^{ij}$ , in (6) which, in turn, arise from the superposition of basis wave functions describing the quantum mechanical state of a system. The importance of these terms relative to the others in (12), then, determines the value of classical atomic charge models for interpreting infrared intensities.

Although the expression derived for the polar tensor, eq 12, is formally exact within the limitations of the Born–Oppenheimer approximation, it is, nonetheless, model dependent. Since atomic orbitals constitute complete sets of functions in the space in which the number density function for particular nuclear configuration is defined, the number density could, in principle, be represented exactly as a one-center expansion in the orbital products centered on any one nucleus. Because we use complete sets of orbitals on every nucleus, our multicenter representation is overdetermined and, therefore, not unique. Consequently, the extra constraints contained in a model must be impressed upon (6) and therefore (12), to remove ambiguity.

The model adopted here is, of course, the familiar LCAO–MO model. In principle, the atomic orbitals centered on all nuclei are first organized into linear combinations which satisfy the symmetry requirements of the problem, and these linear combinations are then ordered in accordance to their symmetry properties and nodal structure (or energy),<sup>16</sup> so as to correlate, one-to-one, with the one-electron united atom wave functions of the system. In this manner, a complete set of multicenter functions is constructed which are used to obtain an exact "significant"<sup>16</sup> representation of the electron number density. Thus, once the atomic orbital basis set is defined, the terms into which the polar tensor is separated in (12) are specified. Keeping this model dependence in mind, we next use eq 12 as the basis for an initial, rather speculative analysis of experimentally observed polar tensors and effective charges.

So far, polar tensors in only a few, relatively simple systems have been reported.<sup>6,17,18</sup> It is clear from even this limited information that both the "perfect following" and "nonperfect following" terms in (12) are of equal importance. In the absence of "nonperfect following" contributions, a polar tensor would be the constant diagonal tensor, given by the first term in (12). Generally, observed polar tensors contain diagonal elements that differ significantly from one another, some are even of different signs, and when not forbidden by symmetry, they often have non-zero off-diagonal elements. The structure of observed polar tensors, then, suggests that the "following" and "nonfollowing" terms are of the same order of magnitude.

It is not clear from the limited data available that of the two "nonperfect following" terms in (12), one is more important than the other. Approximate (CNDO) calculations on a small, representative sample of systems indicate that the derivatives of the apparent charges,  $|\nabla_\alpha \zeta_\beta|$ , are of the order of  $10^{-2}e$ – $10^{-3}e$ , reflecting a general insensitivity of population densities to changes in nuclear configuration. The first term in (12) has been found to be of the order of  $10^{-4}e$  in the majority of cases described later, so that the "charge flux" contribution might be an order of magnitude smaller than the other terms in (12), and, if so, not the dominant "nonfollowing" contribution.

These speculations about relative magnitude suggest that the quantum mechanical "interference" terms in (12),  $\nabla_\alpha \Phi_{\beta\beta}$ , are too important to ignore, for they may in fact represent the dominant "nonperfect following" contribution to the polar tensor. As more information is accumulated through experimental measurement and through the analysis of accurate molecular wave functions, the relative importance of the "charge flux" and "interference" contributions to polar tensors could be determined in specific cases, and the relevance of interpreting infrared intensities in terms of atomic charge models could be established.

### Effective Charges

The experimentally determined effective charges,  $\xi_\alpha$ , in the hydrocarbons display properties that are not obvious consequences of the properties of the polar tensors from which they are derived. Again, the most striking of these is that, with the exception of acetylene, the effective charge of the hydrogens in the hydrocarbons are independent of structure.<sup>1</sup>

The structural dependence of the polar tensor is largely contained in the two "nonperfect following" terms in (12). It appears explicitly in the "charge flux" contributions,  $\mathbf{R}_\beta \nabla_\alpha \zeta_\beta$ , by way of the set of vectors,  $\mathbf{R}_\beta$ , defining the nuclear configuration and implicitly in the "interference" contributions,  $\nabla_\alpha \Phi_{\beta\beta}(\mathbf{R})$ , because the population matrix elements,  $N_{\beta\beta}^{ik}(\mathbf{R})$ , depend upon structure.

To investigate the dependence of effective charges upon molecular environment, it is helpful to separate the polar tensor into its "following" and "nonfollowing" parts

$$\nabla_\alpha \mathbf{P} = \zeta_\alpha \mathbf{I} + \mathbf{\Pi}_\alpha \quad (13)$$

where, from (12)

$$\mathbf{\Pi}_\alpha = \sum_\beta [\mathbf{R}_\beta \nabla_\alpha \zeta_\beta - \nabla_\alpha \Phi_{\beta\beta}]$$

lumps the two "nonfollowing" contributions together, for convenience. Thus, from eq 3 and 13, the effective charge is given by

$$\xi_\alpha^2 = 3\zeta_\alpha^2 + 2\zeta_\alpha \text{Tr}(\mathbf{\Pi}_\alpha) + \mathbf{\Pi}_\alpha : \mathbf{\Pi}_\alpha' \quad (14)$$

For the reasons given above, it is assumed that the last two terms in (14) containing the "nonfollowing" contributions are more sensitive to differences in molecular structure than the first, "following" term.

The strongest general relationship among the terms in (14) that we have found so far is one deduced using the Cauchy and the "triangle" inequality.<sup>19</sup> Applying the former to eq 3, it follows that

$$\xi_\alpha^2 \equiv (\nabla_\alpha \mathbf{P}) : (\nabla_\alpha \mathbf{P})' \geq (1/3) [\text{Tr}(\nabla_\alpha \mathbf{P})]^2 \quad (15)$$

Here the factor (1/3) is a result of the polar tensors being three-dimensional. Further, since

$$\text{Tr}(\nabla_\alpha \mathbf{P}) = 3\zeta_\alpha + \text{Tr}(\mathbf{\Pi}_\alpha)$$

taking the square root of (15) yields the inequality

$$\xi_\alpha - \sqrt{3}|\zeta_\alpha| \geq -(1/\sqrt{3})|\text{Tr}(\mathbf{\Pi}_\alpha)|$$

thereby establishing one extreme of the differences between effective charges and the "perfect following" net atomic charge,  $\zeta_\alpha$ . Similarly, by applying the triangle inequality<sup>19</sup> to (3) and (13), and combining the result with the above gives

$$[(\mathbf{\Pi}_\alpha) : (\mathbf{\Pi}_\alpha)]^{1/2} \geq \xi_\alpha - \sqrt{3}|\zeta_\alpha| > -1/\sqrt{3}|\text{Tr}(\mathbf{\Pi}_\alpha)| \quad (16)$$

thereby establishing a second extreme value.

TABLE I: Hydrogen Atom Effective Charges in Hydrogen Cyanide and Selected Hydrocarbons, in Units of the Electronic Charge

Molecule	Obsd	Calcd I <sup>a</sup>	Calcd II <sup>b</sup>	Calcd III <sup>c</sup>	Calcd IV <sup>d</sup>	Calcd V <sup>e</sup>
CH <sub>4</sub>	0.167 <sup>f</sup>			0.145	0.031	0.035
C <sub>2</sub> H <sub>6</sub>	0.176 <sup>g</sup>	0.215	0.219	0.135	0.016	0.042
C <sub>3</sub> H <sub>8</sub>	0.181 <sup>g</sup>			0.131		
C <sub>2</sub> H <sub>4</sub>	0.178 <sup>f</sup>	0.242	0.246		0.088	0.068
C <sub>2</sub> H <sub>2</sub>	0.404 <sup>h</sup>	0.326	0.352		0.315	0.300
HCN	0.379 <sup>i</sup>	0.374			0.343	

<sup>a</sup> Reference 20. <sup>b</sup> Reference 21. <sup>c</sup> Reference 22. <sup>d</sup> Reference 23. <sup>e</sup> Reference 24. <sup>f</sup> Reference 2. <sup>g</sup> Reference 25. <sup>h</sup> Reference 1. <sup>i</sup> Reference 26.

These inequalities furnish little insight in the form of necessary conditions as to why effective charges might be insensitive to molecular structure, as has been observed in most of the hydrocarbons. Neither do they provide much useful information on the magnitudes of the "nonfollowing" contribution to polar tensors. What they do suggest, however, is that the dependence of effective charges upon molecular structure and the magnitudes of "nonfollowing" terms in polar tensors are not necessarily correlated. Thus, we feel that we can seek an explanation for effective charges without finding a detailed explanation of polar tensors first.

In order to rationalize the behavior observed for the effective charges in hydrocarbons we invoke a "random phase approximation". This approximation asserts that the dominant, structure-dependent "nonfollowing" terms largely cancel in forming the various sums which constitute the  $\Pi_\alpha$  contribution to (14). Stated more succinctly, we adopt the hypothesis that

$$\xi_\alpha \approx \sqrt{3}|\zeta_\alpha| \quad (17)$$

This hypothesis certainly suppresses the dependence of effective charges upon structure and, in addition, is consistent with one other observation about the effective charge in hydrocarbons. For neutral molecules, the sum of the net atomic charges for all atoms must vanish because of the conservation of charge, that is, from (10)

$$\sum_\alpha \zeta_\alpha = 0$$

For binary compounds consisting of two sets of equivalent atoms,  $N_\beta$  and  $N_\nu$  in number, the above sum may be rearranged to give

$$N_\beta \zeta_\beta = -N_\nu \zeta_\nu$$

so that, from (17)

$$N_\beta \xi_\beta = N_\nu \xi_\nu \quad (18)$$

This last relation (18) has already been shown to express the relationship between the effective charge of the hydrogen and carbon atoms in all the hydrocarbons, except perhaps methane, with useful accuracy.<sup>1</sup>

Thus the "random phase approximation" summarized by eq 17 seems to account qualitatively for the behavior of the effective charge in most hydrocarbons. The remainder of this paper is concerned with how well it accounts for their behavior quantitatively.

### Calculations

The major goal of this paper is to account for the observation that the effective charges for hydrogen are approximately the same in all hydrocarbons except acetylene.<sup>1</sup> According to

the premise of this paper, summarized by eq 10 and 17 only gross electron population densities are needed to explain these facts. Unfortunately, the population densities reported in the literature vary widely, because they depend upon the nature of the approximations made in computing molecular wave functions. To offset this difficulty, then, only population densities for different hydrocarbons derived from wave functions employing the same kinds of approximations are intercompared.

The effective charges derived using five different sets of population densities from the literature are compared in Table I. Because of the simple connection between effective charges and population densities, inclusion of the cited population densities was felt to be unnecessary. Two features are immediately apparent from these calculations. First of all, among the five calculations, there is generally good agreement that the effective charges for the hydrogens are of the same magnitude except for acetylene, where the charge is significantly larger. Second, there is remarkably good agreement between the magnitudes of the calculated and observed effective charges in all calculations except IV and V. In these last two, the effective hydrogen charges in the non-acetylenic compounds are considerably lower and more variable than those given by the other three calculations or by experiment. One feature that distinguishes calculations IV and V from the others is that the population densities were derived from wave functions using Slater-type atomic orbitals approximated by a small number of Gaussian functions (STO-3G or STO-4G).<sup>23,24</sup> The others employed either Slater-type orbitals directly<sup>20,21</sup> or basis sets consisting of a large number of Gaussian functions.<sup>22</sup> Because eq 17 is not sufficiently well tested by these results, it is not valid to draw any firm conclusions about the relative accuracy of the wave function calculations cited.

The good, overall agreement obtained for the hydrocarbons encouraged us to test our hypothesis more thoroughly by considering other systems. Unfortunately isotopic intensity data on most such systems are lacking, and the effective charge for the atoms cannot be computed separately, using (1). As an alternative test we used eq 17 to estimate effective charges, and these parameters were then substituted into (1). The calculated sum of intensities, corrected for the permanent dipole by the term  $\Omega$  defined in (2), was then compared with the observed value.

The results of these comparisons are shown in Figure 1. The intensity sums were computed as described above using a representative sampling of the more recently reported *ab initio* calculations of gross electronic population densities, and the results are given by the abscissa. The observed intensity sums are corrected using observed permanent dipole moments<sup>27</sup> in (2), and these results are given by the ordinate. Once again good agreement between calculation and obser-

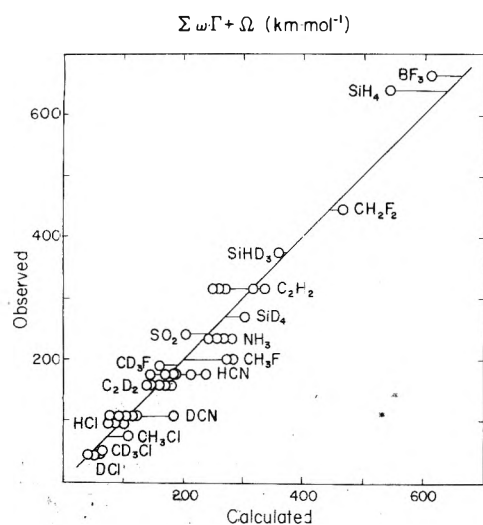


**Figure 1.** Intensity sums calculated from atomic population densities (solid line, theory); HCl, ref 22 (obsd), ref 29–31 (calcd); CH<sub>3</sub>F, ref 32 (obsd), ref 33, 34 (calcd); CH<sub>2</sub>F<sub>2</sub>, ref 35 (obsd), ref 36 (calcd); CH<sub>3</sub>Cl, ref 37 (obsd), ref 38 (calcd); HCN, ref 26 (obsd), ref 20, 23, 39–42 (calcd); C<sub>2</sub>H<sub>2</sub>, ref 1 (obsd), ref 20–24, 31, 43–46 (calcd); NH<sub>3</sub>, ref 47 (obsd), ref 20, 23, 24, 48, 49 (calcd); SO<sub>2</sub>, ref 50 (obsd), ref 51 (calcd); SiH<sub>4</sub>, ref 52 (obsd), ref 30 (calcd); BF<sub>3</sub>, ref 53 (obsd), ref 54 (calcd).

vation is found, for the points defined by the pairs of observed and calculated values generally fall along the diagonal of the graph over a large range of values.

The point of this graph is to demonstrate that the calculated and observed intensity sums are correlated as predicted by our hypothesis, eq 17. Consequently, an extended discussion of errors in either the calculated or observed data seems inappropriate here. Clearly, there is uncertainty in the calculated intensity sums, presumably due to differences in methods of calculation, size of wave-function basis sets, etc. in computing population densities, as indicated by the spread of points parallel to the abscissa. Similarly there is, in many cases, significant error in the observed intensity sums that is not indicated in Figure 1. Inclusion of experimental error in the observed sums (without including new measurements) could only improve the appearance the already good looking correlation displayed in this figure.

## Discussion

The simple connection between atomic effective charges and atomic population densities presented here appears to provide a useful basis for interpreting the sum of integrated intensities in molecules. The behavior of the effective hydrogen charges deduced from the infrared intensities of the hydrocarbons is reflected in the behavior of atomic charges deduced from population analyses. The anomalously large effective charge for the hydrogen atom in acetylene, compared to that in the other hydrocarbons, is rationalized by the significantly lower electron density computed for the (acidic) protons in acetylene, and hydrogen cyanide which was also included in Table I. Indeed, we find it remarkable that infrared intensities might distinguish between the readily ionized protons in C<sub>2</sub>H<sub>2</sub> and HCN, and the tightly bound protons in other hydrocarbons, as these calculations suggest.

In addition, these results provide a basis for at least a tentative analysis of polar tensors into their constituent parts. Effective charges deduced from the intensity sum rule (1) provide an initial estimate of the net atomic charge through (17). Using this estimated value, the "nonperfect following" contribution to polar tensors can, in turn, be estimated

through (12), by subtraction of the "perfect-following" contribution,  $\zeta_{\alpha}I$ . Unfortunately, experimental effective charges only provide a magnitude for the net atomic charge. It seems likely, however, that the sign of the net atomic charge could be deduced more readily using chemical arguments than could, say, a dipole derivative if polar tensors were analyzed in a different manner. Any further analysis of polar tensors into "charge flux" and "interference" contributions seems a much more uncertain problem, one that perhaps can only be accomplished through accurate, quantum mechanical calculation.

## References and Notes

- (1) G. B. Mast and W. T. King, *J. Phys. Chem.*, in press.
- (2) W. T. King, G. B. Mast, and P. P. Blanchette, *J. Chem. Phys.*, **56**, 4440 (1972); **58**, 1272 (1973).
- (3) B. L. Crawford, Jr., *J. Chem. Phys.*, **20**, 977 (1952).
- (4) B. L. Crawford, Jr., *J. Chem. Phys.*, **29**, 1042 (1958).
- (5) I. M. Mills and D. H. Whiffen, *J. Chem. Phys.*, **30**, 1619 (1959).
- (6) W. B. Person and J. H. Newton, *J. Chem. Phys.*, **61**, 1040 (1974).
- (7) J. F. Biarge, J. Herranz, and J. Morcillo, *An. R. Soc. Espan. Fis. Quim. (Madrid)*, **A57**, 81 (1961).
- (8) R. S. Mulliken, *J. Chem. Phys.*, **23**, 1833, 1841, 2338, 2343 (1955); **36**, 3428 (1962).
- (9) See, in particular, the review by W. B. Person and D. Steele, "Molecular Spectroscopy". Specialist Periodical Report of the Chemical Society, Vol. 2, D. A. Long, Ed., London, 1974, No. 29, pp 357–438.
- (10) G. A. Segal and M. L. Klein, *J. Chem. Phys.*, **47**, 4236 (1967).
- (11) R. E. Bruns and W. P. Person, *J. Chem. Phys.*, **58**, 2585 (1973), and references therein.
- (12) A. B. Anderson and R. G. Parr, *J. Chem. Phys.*, **53**, 3375 (1970).
- (13) J. C. Decius, *J. Mol. Spectrosc.*, **57**, 348 (1975).
- (14) W. T. King, *J. Chem. Phys.*, **57**, 4535 (1972).
- (15) K. Rudenberg, *Rev. Mod. Phys.*, **34**, 326 (1962).
- (16) E. B. Wilson, Jr., *J. Chem. Phys.*, **63**, 4870 (1975).
- (17) J. H. Newton and W. B. Person, *J. Chem. Phys.*, **64**, 3036 (1976).
- (18) A. B. M. S. Bassi and R. E. Bruns, *J. Chem. Phys.*, **62**, 3235 (1975).
- (19) See, for example, M. Abramowitz and I. Stegun, "Handbook of Mathematical Functions", Dover Publications, New York, N. Y., 1964.
- (20) W. E. Palke and W. N. Lipscomb, *J. Am. Chem. Soc.*, **88**, 2384 (1966).
- (21) H. A. Germer, *J. Chem. Phys.*, **58**, 3524 (1973).
- (22) G. Kean and S. Fliszar, *Can. J. Chem.*, **52**, 2772 (1974).
- (23) W. J. Hehre and J. A. Pople, *J. Am. Chem. Soc.*, **92**, 2191 (1970).
- (24) K. Jug, *Theor. Chim. Acta*, **31**, 63 (1973).
- (25) S. Kondo and S. Saeki, *Spectrochim. Acta, Part A*, **29**, 735 (1973).
- (26) G. E. Hyde and D. F. Hornig, *J. Chem. Phys.*, **20**, 647 (1952).
- (27) R. D. Nelson, Jr., D. R. Lide, Jr., and A. A. Maryott, *Natl. Stand. Ref. Data Ser., Natl. Bur. Stand. (U.S.)*, No. 10 (1967).
- (28) W. S. Benedict, R. Herman, G. E. Moore, and S. Silverman, *J. Chem. Phys.*, **26**, 1671 (1957).
- (29) S. Rothenberg, R. H. Young, and H. F. Schaefer, *J. Am. Chem. Soc.*, **92**, 3243 (1970).
- (30) H. Johanson, *Chem. Phys. Lett.*, **11**, 466 (1971).
- (31) R. S. Evans and J. E. Huheey, *Chem. Phys. Lett.*, **19**, 114 (1973).
- (32) J. W. Russell, C. D. Needham, and J. Overend, *J. Chim. Phys.*, **45**, 3383 (1966).
- (33) C. A. Naleway and M. E. Schwartz, *Theor. Chim. Acta*, **30**, 347 (1973).
- (34) P. A. Kollman, W. F. Trager, S. Rothenberg, and J. E. Williams, *J. Am. Chem. Soc.*, **95**, 458 (1973).
- (35) J. Morcillo, L. J. Zamorano, and J. M. V. Heredia, *Spectrochim. Acta*, **22**, 1969 (1966).
- (36) M. L. Unland, J. H. Letcher, I. Absor, and J. R. Van Wazer, *J. Chem. Soc. A*, 1328 (1971).
- (37) A. D. Dickson, I. M. Mills, and B. L. Crawford, Jr., *J. Chem. Phys.*, **27**, 445 (1957).
- (38) K. Fukui, H. Fujimoto, and S. Yamabe, *J. Phys. Chem.*, **76**, 232 (1972).
- (39) R. Bonaccorsi, C. Petrongolo, E. Serocco, and J. Tomasi, *J. Chem. Phys.*, **48**, 1500 (1968).
- (40) A. D. McLean, B. J. Ransil, and R. S. Mulliken, *J. Chem. Phys.*, **32**, 1973 (1960).
- (41) A. D. McLean, *J. Chem. Phys.*, **37**, 627 (1962).
- (42) J. Robert, H. Marrmann, I. Absor, and J. R. Van Wazer, *J. Am. Chem. Soc.*, **93**, 3320 (1971).
- (43) J. W. Moskowitz, *J. Chem. Phys.*, **43**, 60 (1965).
- (44) E. Clementi and H. Clementi, *J. Chem. Phys.*, **36**, 2824 (1962).
- (45) I. Fischer-Hjalmars and P. Siegholm, *Theor. Chim. Acta*, **31**, 1 (1973).
- (46) A. Veillard, *J. Chem. Phys.*, **48**, 2012 (1968).
- (47) D. C. McKean and P. N. Schatz, *J. Chem. Phys.*, **24**, 316 (1956).
- (48) J. Krell, Ch. Zuhrt, and L. Zulicke, *Z. Naturforsch. A*, **27**, 1004 (1972).
- (49) D. Renaldi, J. Rivail, and J. Barriol, *Theor. Chim. Acta*, **22**, 291 (1971).
- (50) D. F. Eggers, Jr., and E. D. Schmid, *J. Phys. Chem.*, **64**, 279 (1960).
- (51) M. E. Dyatkina, N. M. Kimeko, and E. L. Rosenberg, *Pure Appl. Chem.*, **38**, 391 (1974).
- (52) I. W. Levin and W. T. King, *J. Chem. Phys.*, **37**, 1375 (1962).
- (53) D. C. McKean, *J. Chem. Phys.*, **24**, 1002 (1956).
- (54) M. E. Schwartz and L. C. Allen, *J. Am. Chem. Soc.*, **92**, 1466 (1970).

## Dielectric Properties of Osmium-Fixed Hemoglobin and Its Water of Hydration

G. T. Koide<sup>1</sup> and E. L. Carstensen\*

Department of Electrical Engineering, College of Engineering and Applied Science, University of Rochester, Rochester, New York 14627  
(Received March 10, 1976)

Publication costs assisted by the National Institutes of Health

A technique originally used in the study of the dielectric properties of the water bound to Sephadex is applied here to hemoglobin. In this case a porous, mechanically stable particle containing hemoglobin at a concentration of roughly 30% is obtained by osmium fixation of erythrocytes. When suspended in water-dioxane mixtures containing 0.14 g of water per gram of fluid, these particles have 0.11 g of bound water/g of hemoglobin. In contrast with Sephadex, the dielectric properties of hemoglobin itself appear to depend upon the amount of water in the environment. Because of uncertainties in properties of the hemoglobin it is only possible to set limits for the dielectric behavior of the bound water. Even so, it is clear that most of the bound water relaxes at frequencies below 1000 MHz.

### Introduction

Recent studies of Sephadex (Pharmacia, Inc.), a porous particle of cross-linked dextrans, have provided us with information about the dielectric behavior<sup>2</sup> of macromolecular solutes and bound water at uhf frequencies. First it is clear that Sephadex itself has a uhf relaxation. Second, it appears that the water tightly bound to Sephadex relaxes at frequencies of the order of 3 to 5 GHz as compared to 20 GHz for free water.

These measurements were possible because the macromolecules were in the form of a porous particle that remained stable in the nonpolar solvent, dioxane, as well as in water. This approach has now been extended to the protein, hemoglobin, by taking advantage of the fact that osmium treatment makes the erythrocyte a porous cell which is stable in almost any environment.<sup>3</sup> The dielectric properties of osmium-fixed hemoglobin are essentially the same as those of normal hemoglobin.<sup>3</sup> Thus, osmium-fixed red blood cells provide a convenient package for studies of partially dehydrated hemoglobin.

### Methods and Materials

Osmium-fixed red blood cells were prepared according to a procedure similar to that described by Glaeser and Mel.<sup>4</sup> Slight modifications of their procedure are described by Carstensen and Smearing.<sup>3</sup> The osmium treatment appears to fix the components of the cell in their normal positions. Sections of osmium-fixed erythrocytes show essentially uniform distribution of hemoglobin throughout the cell. This procedure yielded a mechanically stable red blood cell whose volume is constant over a wide range of osmotic pressures. Even after repeated washings in ethanol or dioxane the cells are stable in size and shape. The membrane resistance drops after fixing leaving a porous particle that is open to small solute molecules as well as water.<sup>5</sup> There was very little loss of hemoglobin from the cells during the measurement procedures. Since the porous membrane had little, if any, effect on the mechanical, chemical, or dielectric properties of the cell, the osmium-fixed erythrocyte for our purposes was much like an ion-exchange or Sephadex particle.

**Dielectric Measurements.** Measurements in the frequency range from 0.5 to 200 MHz were performed with an RX Meter, Type 250A (Boonton Radio Corp., Boonton, N.J.). Measuring

cells and calibration procedures were similar to those of Pauly and Schwan.<sup>6</sup>

Measurements from 300 to 1600 MHz were made with a Rohde and Schwarz (München, West Germany) BN3926/50 coaxial slotted line and BN31319 sample holder. Voltage standing wave ratios were determined either by directly measuring the maximum and minimum of the electric field in the standing wave pattern or by using a 3 dB technique. An iterative method was used to calculate the complex propagation constant from which the complex dielectric constant can be obtained.<sup>7</sup>

### Experimental Results

The study reported here was undertaken (1) to obtain quantitative estimates of the amount of bound water associated with hemoglobin which is exposed to a water-dioxane environment, (2) to determine whether dioxane dehydration has any irreversible effects on the hemoglobin, and (3) to set limits in so far as possible on the dielectric properties of the bound water and hemoglobin.

**Estimation of Bound Water.** The amount of water associated with osmium-fixed hemoglobin can be calculated by the method described by Koide and Carstensen.<sup>2</sup> Figure 1 shows the amount of bound water associated with each gram of hemoglobin as a function of water concentration in the environment (water-dioxane mixture). After repeated washings with dioxane, about 0.05 g of water (at the lowest water concentration in the environment) remain associated with each gram of red blood cells. This value is roughly one fifth of the hydration values commonly assumed for hemoglobin in an aqueous environment.

It should be noted that the procedure used to calculate the amount of bound water assumes that hemoglobin does not bind the organic solvent. If this assumption were in error, the estimates of bound water would have to be revised upward but the qualitative conclusions of the study would not be changed.

**Effects of Dioxane Dehydration on the Dielectric Properties of Hemoglobin.** Previous studies<sup>3</sup> indicate that the dielectric properties of osmium-fixed hemoglobin at vhf frequencies are nearly the same as normal hemoglobin. From the following experiments, it appears that the effects of dioxane dehydration of the osmium-fixed red blood cells are

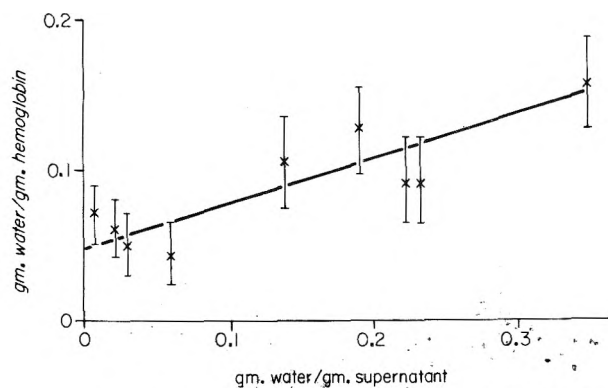


**Figure 1.** Bound water associated with hemoglobin as a function of water content of the environment. Hemoglobin in the form of osmium-fixed erythrocytes is suspended in water-dioxane mixtures. The measuring techniques are described in ref 2.

reversible: (1) After fixation, the cells were washed three times in physiological saline to remove excess osmium. RX Meter measurements of these cells in saline were made. (2) The cells were then washed repeatedly in dioxane until all but about 0.05 g of water/g of hemoglobin had been removed. These cells were then measured in a dioxane environment. (3) The cells were resuspended in saline and dielectric measurements were repeated. The results of these observations are summarized in Figure 2. For purposes of comparison, the data in all three cases are expressed as the effective dielectric constant of hemoglobin without regard to whether water is bound to the protein. In other words, in the Maxwell-Wagner equation<sup>8,9</sup>

$$\frac{\sigma^+ - \sigma_1^+}{\sigma^+ + 2\sigma_1^+} = p \frac{\sigma_2^+ - \sigma_1^+}{\sigma_2^+ + 2\sigma_1^+} \quad (1)$$

where  $\sigma^+$ ,  $\sigma_1^+$ , and  $\sigma_2^+$  are complex conductivities of suspension, suspending medium, and suspended particles, the value used for the volume fraction  $p$  of the suspended phase is just the volume of the hemoglobin as determined from dry weight and density measurements. (The complex conductivity  $\sigma^+ = \sigma + j\omega\kappa\epsilon_0$  where  $\sigma$  is the real conductivity,  $\omega$  is the angular frequency,  $\kappa$  the relative dielectric constant, and  $\epsilon_0$  the permittivity of free space.)

**Dielectric Properties of Partially Dehydrated Osmium-Fixed Hemoglobin.** Osmium-fixed beef red blood cells were washed three times in dioxane. Water was added so that the resulting suspending liquid contained 0.14 g of water/g of liquid. From water determinations by Karl Fischer potentiometric back-titration technique,<sup>10</sup> dry weight analysis, and density measurements, it was found that the resulting hemoglobin had approximately 0.11 g of bound water/g of hemoglobin.<sup>2,7</sup> Again applying the Maxwell-Wagner equation, we can determine the dielectric properties of the protein-bound water complex. Figure 3 gives the complex conductivity  $\sigma^+$  of the suspension; Figure 4 gives the complex conductivity  $\sigma_1^+$  of the suspending medium; then by using for  $p$  the fraction of the total volume occupied by the hemoglobin-bound water as determined above, eq 1 yields the complex conductivity  $\sigma_2^+$  of the protein-bound water as presented in Figure 5.

## Discussion

From dielectric studies of aqueous macromolecular solutions, other investigators<sup>11-13</sup> have reasoned that the relaxation frequency of water bound to the macromolecules is somewhat lower than that of free water. In these studies, there are three unknown quantities: the dielectric properties of the

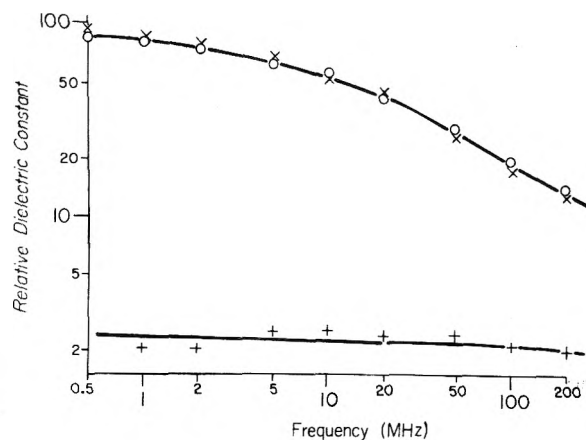


**Figure 2.** Dielectric constant of osmium-fixed hemoglobin in saline (X, O) and dioxane (+). Values presented are those calculated from measurements of suspension and suspending medium using eq 1 where  $p$  is the volume fraction of hemoglobin in the suspension. The fixed cells were first measured in physiological saline (X), washed repeatedly in dioxane and measured in dioxane (+), then resuspended in saline (O). Although hemoglobin becomes essentially irrotational in dioxane, the effect is reversible.  $T = 25^\circ\text{C}$ .

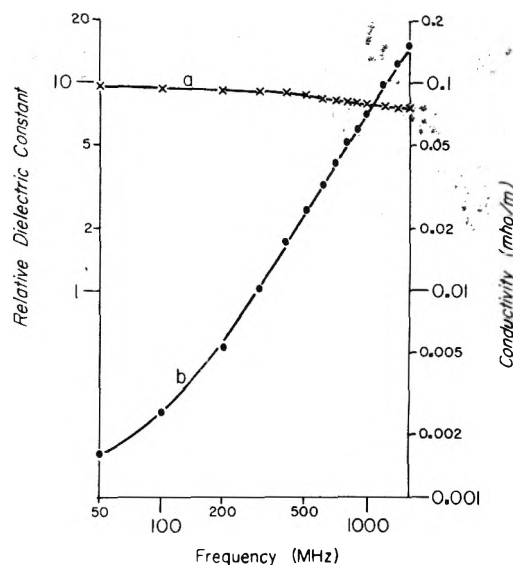


**Figure 3.** Relative dielectric constant (a) and conductivity (b) of a suspension of osmium-fixed red blood cells suspended in a water-dioxane mixture containing 0.14 g of water. Volume fraction of the osmium-fixed hemoglobin with 0.11 g of water/g of hemoglobin is 0.34.  $T = 25^\circ\text{C}$ .

macromolecules themselves, the dielectric properties of the bound water, and the amount of bound water. A number of different but reasonable postulates can be made for these quantities which will be consistent with observed dielectric properties of the macromolecular solutions. Pennock and Schwan,<sup>12</sup> for example, reason that the dispersion observed in hemoglobin solutions below 100 MHz results from rotation of polar side chains of the macromolecules whereas they attribute the relaxation at higher frequencies to bound water.

With Sephadex in water-dioxane mixtures,<sup>2</sup> we were able to determine the quantity of water bound to the macromolecules thus reducing the number of unknowns in the analysis. The Sephadex study was further aided by the fortuitous discovery that the dehydrated macromolecule in the nonpolar solvent, dioxane, remained polar. This permitted an independent measurement of the dielectric properties of the solute. With this information, it became a relatively straight-

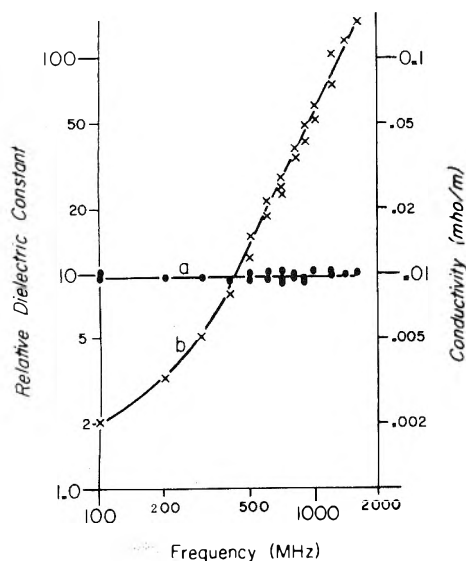


Figure 4. Relative dielectric constant (a) and conductivity (b) of suspending medium in Figure 3.  $T = 25^\circ\text{C}$ .

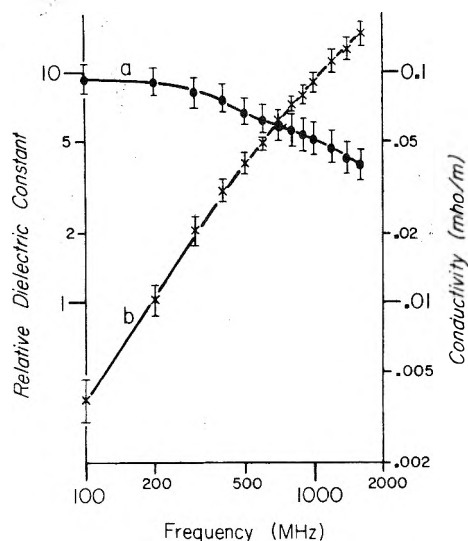


Figure 5. The effective homogeneous dielectric constant (a) and conductivity (b) of hemoglobin with 0.11 g of bound water, calculated from the data of Figures 3 and 4. Vertical bars are estimates of probable errors in the results.  $T = 25^\circ\text{C}$ .

forward process to estimate the dielectric properties of the bound water in hydrated Sephadex. From this analysis it became evident that the Sephadex, itself, has a well-defined relaxation at approximately 300 MHz and that the bound water relaxes above 1000 MHz but somewhat below the relaxation frequency of free water ( $\sim 20$  GHz).

The present study sought to extend to hemoglobin the techniques which were successful with Sephadex. The quantity of bound water could be measured as before but unfortunately the dielectric properties of the hemoglobin itself could not be determined independently. Even so, the data permit us to set some limits on the properties of the bound water associated with the hemoglobin.

Hemoglobin in the fixed form can be conveniently recovered after washing in dioxane. This procedure provides a way of dehydrating the protein. It appears that some of the bound water is removed from the hemoglobin after repeated washings in dioxane but that roughly 0.05 g of water/g of hemo-

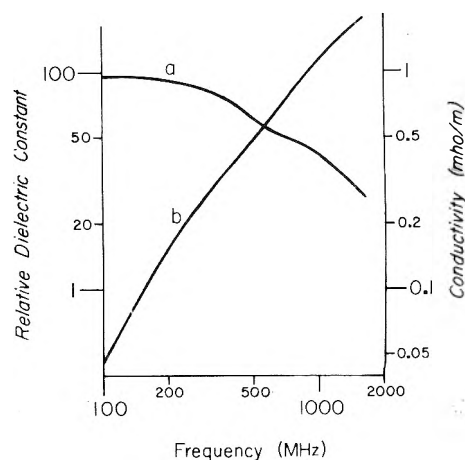


Figure 6. Calculated dielectric constant (a) and conductivity (b) of the bound water in the hemoglobin-bound water complex of Figure 5. The dielectric constant of hemoglobin was assumed to be 2.0.  $T = 25^\circ\text{C}$ .

globin remains. The experiment described in Figure 2 shows that from the dielectric point of view the effects of dioxane treatment are reversible.

Apparently the environment has a profound effect on the polarizability of hemoglobin. In a normal aqueous medium, this macromolecule has a greater dipole moment per unit volume than water. On the other hand, Figure 2 shows that, after dehydration and suspension in dioxane, hemoglobin becomes completely nonpolar. This is in contrast to Sephadex<sup>2</sup> which appears to have very similar dielectric properties (at least at uhf frequencies) in water and in dioxane. Our results with hemoglobin are consistent with a study by Rosen<sup>14</sup> who reported that dehydrated hemoglobin powder is nonpolar.

Partially dehydrated hemoglobin shows some dispersion. The water content corresponding to the data of Figure 3 is high enough to demonstrate this effect yet low enough to permit determination of the amount of bound water with some accuracy. It is a comparatively straightforward procedure to obtain from the data of Figures 3 and 4 the effective, homogeneous dielectric constant and conductivity of the hemoglobin-bound water complex as presented in Figure 5. Certain assumptions relating to the water content of the complex and the shape of the suspended particles are made in applying eq 1 to arrive at this point. However, these assumptions do not enter critically in evaluating the properties of the complex. Although it is clear that either the hemoglobin or the bound water has a dielectric dispersion in the uhf frequency range, it is not possible to take the next step and to determine the properties of protein and bound water separately from these values for the complex. There are, in fact, many combinations of values for the conductivities and dielectric constants of hemoglobin and bound water which will satisfy the observed values of the complex. However, the data do permit an upper limit to be placed on the relaxation frequency of the bound water.

In principle, it is possible to estimate the properties of one of the components of the complex if the other is known. If we assume that the bound water forms a shell of volume  $v_t$  around a protein core with a volume  $v_i$  we can compute the dielectric properties of the shell from the equation<sup>8</sup>

$$\frac{\sigma_2^+ - \sigma_t^+}{\sigma_2^+ + 2\sigma_t^+} = \frac{v_i}{v_i + v_t} \frac{\sigma_i^+ - \sigma_t^+}{\sigma_i^+ + 2\sigma_t^+} \quad (2)$$

where  $\sigma_2^+$  is the complex conductivity of the complex (Figure 5),  $\sigma_i^+$  is the complex conductivity of the protein, and  $\sigma_t^+$  is

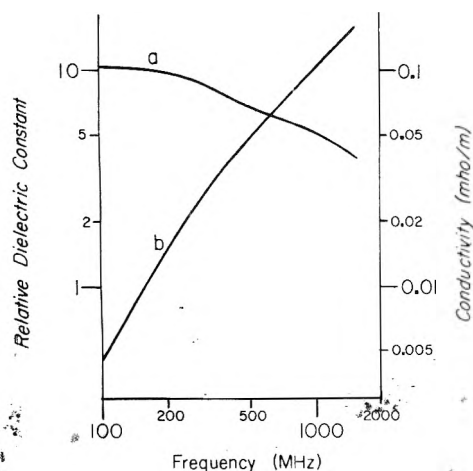


**Figure 7.** Relative dielectric constant (a) and conductivity (b) of hemoglobin in the hemoglobin-bound water complex of Figure 5. In this case the bound water is assumed to be irrotational with a dielectric constant of 5.0.  $T = 25^\circ\text{C}$ .

the complex conductivity of the water. To calculate the dielectric properties of the water in the hemoglobin-bound water complex, it is necessary to assume values for the dielectric properties of the hemoglobin. If we assume that the protein has the minimum reasonable dielectric constant and conductivity, the calculation will give us the upper limit for the dielectric constant and conductivity of the bound water. From the observations of Rosen<sup>14</sup> as well as those in Figure 2, it is unlikely that the dielectric constant of the protein could be less than 2.0. Using this value for the dielectric constant and zero for the protein conductivity together with the data of Figure 5 in eq 2 gives the values for the upper limit of the dielectric constant and conductivity of the bound water shown in Figure 6. Since the values for the dielectric constant are not significantly greater than 80 throughout the range, these measurements do not rule out the possibility that the bound water is responsible for all of the dispersion observed above 100 MHz. Since these values represent upper limits of the dielectric constant of the bound water present in the sample, it is clear that most of the water relaxes at frequencies below 1000 MHz. From the slopes of the dielectric constant and conductivity curves, it appears that a distribution of relaxation frequencies is involved.

This is the only statement which can be made with assurance from the data available at the present time. Of course,

all or part of this bound water may be irrotational. If the bound water is irrotational, then all of the dispersion shown in Figure 5 results from hemoglobin. Using the lowest reasonable value for the dielectric constant of water and zero for its conductivity in eq 2, this gives the values shown in Figure 7 for the dielectric properties of the protein. Effective dielectric constants as high as 10 and relaxation frequencies as high as 850 MHz are not unusual for polymers in aqueous solution. Therefore, it may be that the most tightly bound water in the hemoglobin-bound water complex is irrotational. At lower water concentrations, the effective dielectric constant of the protein approaches 2.5. Thus, if indeed the bound water is irrotational, its presence makes it possible for polar groups on the protein to rotate.

### Conclusion

From these observations it appears that water tightly bound to hemoglobin relaxes below 1000 MHz. It could be completely irrotational. The possibility that hemoglobin itself may relax in the uhf frequency range suggests that care should be exercised in the use of dielectric techniques as a measure of the amount and degree of binding of water in protein solutions and biological material.

*Acknowledgments.* The authors are indebted to Mrs. Sally Child for assistance in the measurements.

This work was supported in part by USPHS Grant No. GM09933.

### References and Notes

- (1) Engineering Department, Hilo College, Hilo, Hawaii 96720.
- (2) G. T. Koide and E. L. Carstensen, *J. Phys. Chem.*, **80**, 55 (1976).
- (3) E. L. Carstensen and R. W. Smearing, *IEEE Trans. Biomed. Eng.*, **14**, 216 (1967).
- (4) R. M. Glaeser and H. C. Mel, *Biochem. Biophys. Acta*, **79** (3), 6061 (1964).
- (5) E. L. Carstensen, A. Coopersmith, M. Ingram, and S. Z. Child, *J. Cell Biol.*, **42**, 565 (1969).
- (6) H. Pauly and H. P. Schwan, *Biophys. J.*, **6**, 621 (1966).
- (7) These and other methods are described in greater detail in an internal report (Electrical Engineering Technical Report No. GM09933-16, "The Dielectric Properties of Structured Water", by G. T. Koide and E. L. Carstensen) which may be made available to the interested reader. This is also available from University Microfilms, Ann Arbor, Mich., order No. 70-2884.
- (8) J. C. Maxwell in "A Treatise on Electricity and Magnetism", 3d ed, Oxford University Press, London, 1832, Art. 310-314.
- (9) K. W. Wagner, *Ann. Phys.*, **40**, 817 (1913).
- (10) J. Mitchell, Jr., and D. M. Smith in "Aquametry", Interscience, New York, N.Y., 1948.
- (11) H. P. Schwan, *Ann. N.Y. Acad. Sci.*, **125**, 344 (1965).
- (12) B. E. Pennock and H. P. Schwan, *J. Phys. Chem.*, **73**, 2600 (1969).
- (13) E. H. Grant, *Ann. N.Y. Acad. Sci.*, **125**, 418 (1965).
- (14) D. Rosen, *Trans. Faraday Soc.*, **59**, 2178 (1963).

## COMMUNICATIONS TO THE EDITOR

### Infrared and Far-Infrared Spectra of Ammonia Adsorbed on Calcium Chloride and Calcium Bromide

*Sir:* The systems  $\text{NH}_3$  and  $\text{ND}_3$  adsorbed on evaporated films of  $\text{CaCl}_2$  and  $\text{CaBr}_2$  at low temperatures were investigated by their ir spectra both in the usual and far regions.

The experimental system was designed and built for this work. It included a special low temperature cell which enabled the preparation of films with large specific area *in situ* at 77 K. The cell served both for adsorption and recording of the spectra at 195 K. The recording of the spectra in both spectral regions could be done either in the same or in separate adsorption experiments. Perkin-Elmer Model 521 spectrophotometer was used in the region  $4000\text{--}250\text{ cm}^{-1}$  and a Grubb-Parsons interferometer was used for the far-infrared region. The experimental procedure was similar to the one described previously.<sup>1</sup>

The results and assignments of the spectra are summarized in Table I.

In the far-infrared  $\text{CaCl}_2$  showed a broad band at  $280\text{ cm}^{-1}$ . When  $\text{NH}_3$  and  $\text{ND}_3$  were adsorbed, this band shifted to  $210\text{ cm}^{-1}$  and two new bands appeared at  $290$  and  $110\text{ cm}^{-1}$ .

From the spectra it was concluded that coordinative linking of  $\text{NH}_3$  to the cation is the dominant mode of adsorption. It is believed that the general form of the complex is  $(\text{NH}_3)_n\text{--Ca}\cdots\text{X}$ . This assumption is based on the spectra in both regions. The internal vibrations show shifts as known in coordinated compounds.<sup>3</sup> The band at  $490\text{ cm}^{-1}$  was assigned to the rocking of H atoms relative to the bound N atom. On adsorption of  $\text{ND}_3$  the band at  $380\text{ cm}^{-1}$  showed the expected isotopic shift for this mode. The rocking mode is typical for coordinated compounds of ammonia.<sup>4</sup>

As mentioned above the spectra in the far-infrared were identical both for  $\text{NH}_3$  and  $\text{ND}_3$ . The band at  $290\text{ cm}^{-1}$  was assigned to the Ca-N stretch and the band at  $110\text{ cm}^{-1}$  to the bending in the complex. The appearance of these bands was accompanied by a shift to lower frequency of the original

TABLE I: Absorption Frequencies of  $\text{NH}_3$  and  $\text{ND}_3$  Adsorbed on  $\text{CaCl}_2$

	$\nu_1, \text{cm}^{-1}$	$\nu_2, \text{cm}^{-1}$	$\nu_3, \text{cm}^{-1}$	$\nu_4, \text{cm}^{-1}$	$\rho_r, \text{cm}^{-1}$
$\text{NH}_3/\text{CaCl}_2$	3260(w)	1150(s)	3360(s)	1595(m)	490(s)
$\Delta\nu = \nu_{\text{ad}} - \nu_{\text{g}}^a$	-76	+200	-54	-32.5	
$\text{ND}_3/\text{CaCl}_2$	2380(w)	905(s)	2500(s)	1170(s)	380(s)
$\Delta\nu = \nu_{\text{ad}} - \nu_{\text{g}}^a$	-39	+156	-55	-21	

<sup>a</sup>  $\Delta\nu$  is the shift of each absorption as compared to the gas phase.<sup>2</sup> (-) red shift, (+) blue shift.

Ca-Cl band, indicating that this bond becomes weaker when the complex is formed.

Additional support for the above assignment was found in the system  $\text{NH}_3/\text{CaBr}_2$ . This adsorbent was chosen because it has a Ca cation in an identical crystallographic structure. As expected, the general behavior in the far-infrared is similar.  $\text{CaBr}_2$  has a broad absorption at  $220\text{ cm}^{-1}$ . On adsorption of  $\text{NH}_3$  this band shifted to a lower frequency ( $140\text{ cm}^{-1}$ ) and the new bands appeared at  $300$  and  $90\text{ cm}^{-1}$ . The relatively small difference in frequency between these two systems are probably due to the presence of different anions in similar crystallographic surroundings.

Further work is being carried out now in order to find more evidence for the above assumptions.

#### References and Notes

- (1) Y. Kozirovski and M. Folman, *Trans. Faraday Soc.*, **62**, 808 (1966).
- (2) Z. Herzberg, "Infrared and Raman Spectra of Polyatomic Molecules", Van Nostrand, New York, N.Y., 1945.
- (3) K. Nakamoto, "Infrared Spectra of Inorganic and Coordination Compounds", Wiley, New York, N.Y., 1963.
- (4) L. Sacconi, A. Sabatini, and P. Gans, *Inorg. Chem.*, **3**, 1772 (1964).

Department of Chemistry  
Technion—Israel Institute of Technology  
Haifa 32000, Israel

O. Marcovitch  
A. Lubetzky  
Y. Kozirovski\*

Received July 1, 1976

# PHYSICAL PHENOMENA

spectroscopy,  
thermodynamics,  
reaction kinetics,  
and other areas  
of experimental  
and theoretical  
physical chemistry  
are covered  
completely in

## THE JOURNAL OF PHYSICAL CHEMISTRY

The biweekly JOURNAL OF PHYSICAL CHEMISTRY includes over 25 papers an issue of original research by many of the world's leading physical chemists. Articles, communications, and symposia cover new concepts, techniques, and interpretations. A "must" for those working in the field or interested in it, the JOURNAL OF PHYSICAL CHEMISTRY is essential for keeping current on this fast moving discipline. Complete and mail the coupon now to start your subscription to this important publication.

**The Journal of Physical Chemistry  
American Chemical Society**

**1976**

1155 Sixteenth Street, N.W.  
Washington, D.C. 20036

Yes, I would like to receive the JOURNAL OF PHYSICAL CHEMISTRY at the one-year rate checked below:

	U.S.	Canada**	Latin America**	Other Nations**
ACS Member One-Year Rate*	<input type="checkbox"/> \$24.00	<input type="checkbox"/> \$30.25	<input type="checkbox"/> \$29.75	<input type="checkbox"/> \$30.25
Nonmember	<input type="checkbox"/> \$96.00	<input type="checkbox"/> \$102.25	<input type="checkbox"/> \$101.75	<input type="checkbox"/> \$102.25

Bill me  Bill company  Payment enclosed

*Air freight rates available on request.*

Name \_\_\_\_\_

Street \_\_\_\_\_

Home   
Business

City \_\_\_\_\_

State \_\_\_\_\_

Zip \_\_\_\_\_

**Journal subscriptions start January '76**

\*NOTE: Subscriptions at ACS member rates are for personal use only. \*\*Payment must be made in U.S. currency, by international money order, UNESCO coupons, U.S. bank draft, or order through your book dealer.

# THEORETICAL CHEMISTRY

## Advances and Perspectives/VOLUME 2

edited by HENRY EYRING and DOUGLAS HENDERSON

From the Preface:

Despite the maturity of theoretical chemistry, there are very few journals or review series devoted to all aspects of this field. It is hoped that this serial publication will fill, in part at least, this gap. Articles concerning all aspects of theoretical chemistry will be published in these volumes. Articles concerning experimental chemistry which pose or answer questions of theoretical interest may also be published from time to time.

CONTENTS: A. T. Amos and R. J. Crispin, Calculations of Intermolecular Interaction Energies. M. L. Glaser, The Electron Gas in a Magnetic Field: Nonrelativistic Ground State Properties. J. Paldus, Many-Electron Correlation Problem. A Group Theoretical Approach.

1976, 312 pp., \$30.00/£ 18.30 ISBN: 0-12-681902-5

# ADVANCES IN PHYSICAL ORGANIC CHEMISTRY, Volumes 12 and 13

edited by V. GOLD

associate editor: D. BETHELL

CONTENTS OF VOLUME 12: L. Ebersson and K. Nyberg, Structure and Mechanism in Organic Electrochemistry. J. F. Ireland and P. A. H. Wyatt, Acid-Base Properties of Electronically Excited States of Organic Molecules. P. Neta, Application of Radiation Techniques to the Study of Organic Radicals.

1976, 324 pp., \$27.25/£ 11.00 ISBN: 0-12-033512-3

CONTENTS OF VOLUME 13: N. L. Allinger, Calculation of Molecular Structure and Energy by Force-Field Methods. E. M. Arnett and G. Scorrano, Protonation and Solvation in Strong Aqueous Acids. A. J. Bard et al., Formation, Properties and Reactions of Cation Radicals in Solution. S. N. Rosenthal and J. H. Fendler, <sup>13</sup>C.N.M.R. Spectroscopy in Macromolecular Systems of Biochemical Interest.

1976, 458 pp., \$34.00/£ 15.60 ISBN: 0-12-033513-1

# IRREDUCIBLE TENSOR METHODS

An Introduction for Chemists

by BRIAN L. SILVER

*Irreducible Tensor Methods* offers chemists the opportunity to learn specialized mathematical techniques and to apply them to atomic and molecular physics. The author has met an important need by offering a unified account of the use of symmetry in atomic and molecular systems at the research level, and in describing the use of irreducible tensors in conjunction with spinor groups and second quantization. In addition, Professor Silver includes a large selection of examples taken from recent

literature and worked through in considerable detail. The simplest possible terms are used in setting out mathematical material, and these terms are consistently allied to the highly technical material of chemical physics. The utility of irreducible tensor operators in atomic and molecular quantum mechanics is the major point, and the main purpose is to illustrate the practical application of the theoretical technique.

1976, 244 pp., \$26.50/£ 16.15 ISBN: 0-12-643650-9

# RELAXATION KINETICS

by CLAUDE F. BERNASCONI

This book deals with the theory and applications of fast reaction techniques commonly referred to as "relaxation kinetics." *Relaxation Kinetics* differs from previous treatments of this subject (e.g., Eigen and DeMaeyer) in its straightforward approach designed to instruct the mathematically unsophisticated readers (e.g., organic chemists) while still dealing comprehensively with all important aspects of relaxation theory. The first part of the book deals with the theory of chemical relaxation

while the second part is devoted to the various experimental techniques and their respective applications. The author has illustrated both the theoretical and experimental aspects with many examples from various branches of chemistry; he has also included a number of problems and exercises to augment the reader's practical understanding of the subject.

1976, 302 pp., \$29.50/£ 18.00 ISBN: 0-12-092950-3

# THE DYNAMIC PROPERTIES OF SUPERCOOLED LIQUIDS

by G. HARRISON

This work, providing as it does a detailed survey of the shear, structural and dielectric relaxational behavior of simple, supercooled liquids, is the first to emphasize the properties of liquids rather than polymers. The early chapters are concerned with the basic equilibrium properties of density and viscosity, and their variation with temperature and pressure. The author introduces the phenomenological theory of linear viscoelasticity and analyzes the propagation of shear and longitudinal waves in liquids. Viscoelastic and ultrasonic behavior is investigated by methods involving the generation of shear and longitudinal

waves in the frequency range  $10^2$  to  $10^9$  Hz, and this range can be extended to  $10^{10}$  Hz by the use of light scattering techniques; the basic theory of these techniques is described together with a great deal of experimental detail. The remainder of the book is devoted to a review of the results obtained from shear wave, longitudinal wave and dielectric measurements on a wide range of liquids, including simple hydrocarbons and benzene derivatives, phosphate, silicate and phthalate esters, phenyl ethers and mineral oils.

1976, 208 pp., \$15.50/£ 6.20 ISBN: 0-12-328150-4

Send payment with order and save postage plus 50¢ handling charge.  
Prices are subject to change without notice.

**ACADEMIC PRESS**

A Subsidiary of Harcourt Brace Jovanovich, Publishers  
111 FIFTH AVENUE, NEW YORK, N.Y. 10003  
24-28 OVAL ROAD, LONDON NW1 7DX